Advanced Microwave Miniature and Lossy Tunable Filters for Wireless Communication Applications

by

Zhou Zhou

A dissertation submitted for the degree of Doctor of Philosophy

Heriot-Watt University

School of Engineering and Physical Sciences

May 2018

Abstract

Microwave filters play very important roles in many RF/microwave applications, which are employed to separate or combine different frequencies. Emerging applications, such as wireless communications, challenge the design of microwave filters with more functionalities and higher performance, such as reconfigurable or tunable, compact size, light weight and lower cost.

In order to meet the increasing challenge requirements, the objective of this dissertation is to develop new multilayer miniaturized filters, compact lossy microstrip filters, and reconfigurable lossy filters. To achieve this, this dissertation is divided into three main parts.

The first part focuses on the design of novel miniature bandpass filter with improved performance. In this aspect, a novel microstrip bandpass filter using slow-wave open-loop resonators is presented, which concentrates on the stopband rejection performance to suppress the harmonic standing wave rather than the passband performance by using multilayer LCP technology. The multilayer open-loop slow-wave resonator has not only very compact size, but also exhibits an excellent wider upper stopband resulting from the dispersion property. Based on this type of resonator, a five-pole bandpass filter has been proposed, which has good stopband rejection and high selectivity as well as compact size and light weight.

The second part is devoted to the design of compact lossy filters with improved performance characteristics. To achieve this, lossy synthesis and extracted-pole technology are combined together to design microstrip filters with flat passband and high selectivity. Two six-pole filters has been analysed from the theoretical circuit model to EM simulations, fabricated to demonstrate the response performance in narrowband and wideband respectively.

The third part concentrates on the designs of novel varactor-tuned microstrip lossy bandpass filters. Firstly, state-of-the-art literature review is given to have a general view of reconfigurable bandpass filter with different tuning centre frequency and bandwidth

characteristics. Then, three types of tunable microstrip bandpass filters with resistor loading under symmetric tuning method are presented to introduce additional loss into the passband to make it flat over the entire tuning range. The first filter is designed to control the bandwidth and selectivity. The second one is designed to control the bandwidth at fixed centre frequency, while the third filter is extended from the first one to combine resistor loading and cross coupling. Finally, microstrip tunable bandpass lossy filters with extracted-pole technology are proposed. Three six-pole filters of this type have been analysed and fabricated. Due to the asymmetric tuning method, the number of tuning components and dc bias schemes are increased, which is a kind of tradeoff with performance.

For all the presented filters, theoretical analyses, implementations and measurements have been given. All of the results achieved in this thesis make the proposed filters attractive for their applications in modern wireless communication systems.

Dedication

To my family, for their ever-lasting love and support.

Acknowledgements

I would like to express sincere gratitude to my supervisor, Prof. Jia-sheng Hong, for his invaluable guidance and support throughout my PhD study. I can fully access to my research under his supervision, which allows me to study in my own way that makes me confident to carry on research independently. I have benefited a lot from his support and passion attitude to the research.

I am particularly thankful for Dr. Ni Jia, for her guidance, assistance and encouragement during the period of my PhD. She helps me a lot not only in theory but also in circuit fabrication at the beginning of my research, which makes me quite confident and enjoyable of my doctoral training.

Special thanks go to Dr. Wenxing Tang for his great help in fabrication procedure and encouragement to my research. He helps me built the patience and confidence on filter fabrications, which I really appreciate.

I would also like to thank all my colleagues and friends for their friendship and generous support. I have unforgettable and invaluable abroad experiences with them.

Finally, I'd like to thank my family, especially my parents, for their ever-lasting support and love.

ACADEMIC REGISTRY

Research Thesis Submission

Name:	ZHOU ZHOU		
School:	EPS/ISSS		
Version: (i.e. First, Resubmission, Final)	Final	Degree Sought:	PhD

Declaration

In accordance with the appropriate regulations I hereby submit my thesis and I declare that:

1) the thesis embodies the results of my own work and has been composed by myself
2) where appropriate, I have made acknowledgement of the work of others and have made reference to work carried out in collaboration with other persons
3) the thesis is the correct version of the thesis for submission and is the same version as any electronic versions submitted*.
4) the thesis contains confidential information.
5) I understand that as a student of the University I am required to abide by the Regulations of the University and to conform to its discipline.
6) I confirm that the thesis has been verified against plagiarism via an approved plagiarism detection application e.g. Turnitin.

* *Please note that it is the responsibility of the candidate to ensure that the correct version of the thesis is submitted.*

Signature of Candidate:		Date:	

Submission

Submitted By (name in capitals):	ZHOU ZHOU
Signature of Individual Submitting:	
Date Submitted:	

For Completion in the Student Service Centre (SSC)

Received in the SSC by (name in capitals):			
Method of Submission (Handed in to SSC; posted through internal/external mail):			
E-thesis Submitted (mandatory for final theses)			
Signature:		Date:	

Table of Contents

List of Figures

List of Tables

Glossary of Terms

RF	Radio Frequency
LCP	Liquid Crystal Polymer
EM	Electromagnetic
SIR	Step-impedance Resonator
LTCC	Low Temperature Co-Fired Ceramic
HTCC	High Temperature Co-Fired Ceramic
LAN	Low Noise Amplifier
UWB	Ultra-Wide Band
LPF	Low-Pass Filter
HPF	High-Pass Filter
BPF	Band-Pass Filter
FBW	Fractional Bandwidth
PCB	Printed Circuit Board
RCC	Resistive Cross Coupling
IMUX	Input Multiplexer
TZ	Transmission Zero
NRN	Non-Resonated Node
MEMS	Micro-Electro-Mechanical System
YIG	Yttrium-Iron-Garnet
BST	Barium Strontium Titanate
CFBW	Constant Fractional Bandwidth
CABW	Constant Absolute Bandwidth

List of Publications by the Candidate

Journal Papers

[1] **Z. Zhou**, J.-S. Hong, "Computer-aided Design of Microstrip Extracted-pole Lossy Filter", Wiley *International Journal of RF and Microwave Computer-Aided Engineering*, 2018; **10**(1002)

[2] **Z. Zhou**, J.-S. Hong, "Asymmetric Microstrip Extracted-Pole Tunable Filter with Reconfigurable Bandwidth and Selectivity Control," (to be submitted).

Conference Papers

[1] **Z. Zhou**, Jia Ni and J.-S. Hong, "Novel Lossy Microstrip Filter with Extracted-pole Technique", *46th Eur. Microw. Conf.*, London, Oct. 2016

[2] **Z. Zhou**, P. M. Iglesias and J.-S. Hong, "Novel Miniature Slow-Wave Resonator Filter Using Multilayer LCP Circuit Technology", *46th Eur. Microw. Conf.*, London, Oct.2016

Book Chapter

Invited Book Chapter **Z Zhou** and J. Hong, "Microstrip Extracted-Pole Lossy Filter", in IET book of Advances in Planar Filters Design (to be published).

CHAPTE 1
Introduction

1.1 Motivation

Microwave filters play very important roles in many RF/microwave applications, which are used to select or confine the RF/microwave signals within assigned spectral limits. Emerging applications, such as wireless communications, challenge the design of microwave filters with more functionalities and higher performance such as reconfigurable or tunable, compact size, light weight and lower cost. In general, most of researches on microwave filters can be classified into one of the following of three groups: 1) structures and materials related to filter design; 2) performance of transmission and rejection related to filter synthesis; 3) issues of size and cost related to manufacture and fabrication.

Highly integration microwave circuit with a compact size and light weight is a major trend and big challenge for modern wireless communication systems. Due to the increasing demand for such miniature and high performance wideband filters operated at low frequencies band, e.g., 0.5-2.0 GHz, for some emerging applications, such as wideband radar. However, conventional planar filters usually have large sizes and are expensive because of the large wavelengths at these frequencies. Many different miniaturized structure filters have been presented, among which include the conventional uses of compact hairpin resonator filters, lumped element filters, miniature fractal filters, miniaturized dual-mode resonator filters, slow-wave distributed resonator filters and multilayer filters. A new microstrip bandpass filter using slow-wave open-loop resonator will be discussed in detail in the thesis.

Conventional microwave lossless synthesis[1]- [4] has been focused for years since it is the fundamental theory to design filters, which can be regarded as “matured” to some extent with any filter transfer function being synthesized to the desired filter topology using exact synthesis procedures. However, these microwave lossless synthesis filters are

designed in the limitation of microwave filter itself without considering from the perspective of the whole system, which can reduce the system compatibility and unnecessary loss. Accepting some additional insertion loss and knowing the fact that the loss can be compensated for by the already-existing microwave amplifiers in the system, the sharp response of the filter transmission can be restored. In the thesis, a new type of microstrip extracted-pole lossy filter is presented. This type of proposed filter has both high selectivity and flat passband not only in narrowband but also in wideband.

The microstrip tunable bandpass filter has been widely used in modern wireless communication systems. Recently many research works focus on controlling the bandwidth, which is because that the centre frequency is easily to be reconfigured by varying the resonators' electrical length by using the commercial tuning components, while the bandwidth tuning depends on both the external quality factor Q_e and coupling coefficients. Moreover, the conventional tunable bandpass filters focus on low-loss insertion loss in the passband, while it is still rare to combine the lossy synthesis in tunable bandpass filter. In the dissertation, tunable bandpass filters have been combined with lossy synthesis to control the centre frequency and bandwidth characteristics. Several types of these filters have been further analysed and fabricated based on symmetric or asymmetric tuning design.

1.2 Objectives

This dissertation focuses on two main types of filter designs:

1. To realize miniaturized microstrip filter based on multilayer LCP technology. The topic is to concentrate on the stopband rejection performance to suppress the harmonic by using the advantage of broadside couplings of multilayer LCP technology rather than focus on the passband performance.

2. To combine microstrip tunable bandpass filter with lossy technology to achieve multi-functions. The goal that needs to be achieved is to control the bandwidth from narrow band to wide band at fixed centre frequency with a flat passband insertion loss and high selectivity at both sides of passband edges in the entire tuning range.

1.3 Organization of Thesis

Following the motivation and the discussion of objectives, the organization of the thesis is given as below:

Chapter 2 focuses on the miniaturized microstrip filter and the topic is to concentrate on the stopband rejection performance to suppress the harmonic standing wave by using the advantage of broadside couplings of multilayer LCP technology rather than focus on the passband performance. A novel microwave bandpass filter using microstrip slow-wave open-loop resonators and multilayer LCP technology is presented.

In Chapter 3, the design of microstrip lossy filters combining lossy synthesis and extracted-pole technique is proposed. This type of proposed filter has both high selectivity and flat passband not only in narrowband but also in wideband. This type of filter is extended to tunable filter in Chapter 6.

In Chapter 4, a literature review of tunable/reconfigurable filter is introduced. This is the preparation for the following tunable filter chapters.

Chapter 5 focuses on symmetric varactor-tuned microstrip bandpass lossy filter. Three types of tunable bandpass lossy filter with resistor loadings are presented and fabricated. The theoretical, full-wave electromagnetic (EM) simulated and measured performances are present.

In Chapter 6, asymmetric high order tunable bandpass lossy filters are proposed. This type of filter can control the bandwidth at fixed centre frequency with flat passband and high selectivity. Through the analysis of the equivalent circuit model and EM simulation model, this type of filter has been investigated step by step.

Finally, a brief summary of the contributions of the presented works and suggestions for future research work are concluded in Chapter 7.

Reference

[1] A. E. Atia, A. E. Williams. ‘Narrow-bandpass waveguide filters’. *IEEE Trans. Microw. Theory Tech*., vol. MTT-20, pp. 258–265, Apr. 1972.

[2] A. E. Atia, A. E. Williams, R. W. Newcomb. ‘Narrow-band multiple-coupled cavity synthesis’. *IEEE Trans. Circuits Syst*., vol. CAS-21, no. 9, pp. 649–655, Sep. 1974.

[3] Cameron, R.J. ‘General coupling matrix synthesis methods for Chebyshev filtering functions’. *IEEE Trans. Microw. Theory Tech.*, vol. 47 (4), pp. 433–442, 1999

[4] Cameron, R.J. ‘Advanced coupling matrix synthesis techniques for microwave filters’. *IEEE Trans. Microw. Theory Tech.*, vol. 51(1), pp. 1–10, 2003

CHAPTER 2

Multilayer Slow-wave Open-loop Resonator Filter

2.1 Overview of Miniaturization Techniques

During the past ten years, with the development of novel multilayer packaging material, miniaturized compact filters have been developed. Many different diversity of miniaturized structure filters have been presented, such as compact hairpin resonator filters, lumped element filters, miniature fractal filters, miniaturized dual-mode resonator filters, multilayer filters and slow-wave distributed resonator filters.

Lumped element filters have been widely applied at lower frequencies, because of its broad spurious frequency bands and small physical size [1]-[5]. Basically, the equivalent circuit model are constructed by capacitors and inductors, which can be designed in different layouts depended on the different required specifications. However, it is critical to use accurate values of these inductors and capacitors to design and model the lumped element filters. Also, the extremely small physical size of lumped element filters may also lead to low power handing capacity and high insertion loss in the passband, especially at higher frequencies.

From resonator structure perspective, some modified topology structures have been presented in order to make a compromise between physical size and response performance. Four different physical structures of microstrip line hairpin resonators have been demonstrated in Figure 2.1. The conventional hairpin resonator shown in Figure 2.1(a) [6], can be miniaturized by adding a lumped element capacitor between both ends of the resonator displayed in Figure 5.2(b) [6], or folding a pair of coupled lines inside the resonator given in Figure 2.1(c) [6], or reshaping into stepped impedance resonator (SIR) with extra advantage of harmonic suppression shown in Figure 2.1(d) [7].

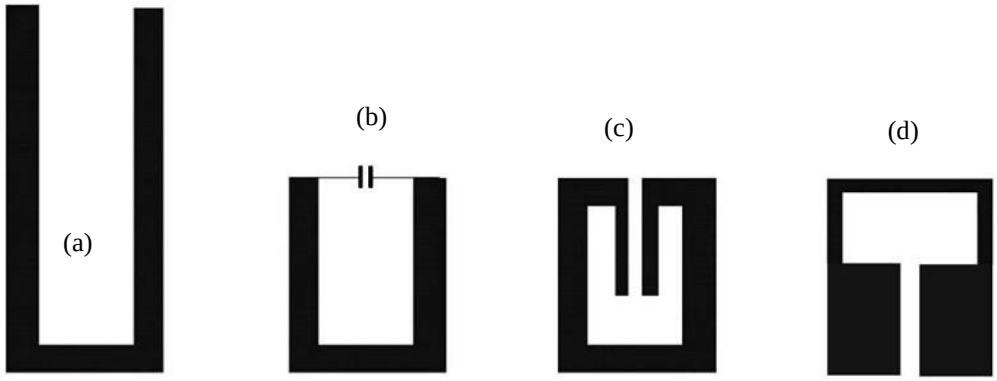

Figure 2.1: Variation structures to miniaturize hairpin resonator.
(a) Conventional hairpin resonator. (b) Miniaturized hairpin resonator with loaded lumped capacitor. (c) Miniaturized hairpin resonator with folded coupled lines.
(d) Miniaturized stepped-impedance hairpin resonator.

For SIR configurations, Figure 2.2 also shows different variation structures. The basic SIR presented in Figure 2.2(a) [7], can be reconfigured as stepped impedance hairpin resonator given in Figure 2.2(b) [7], or miniaturized hairpin resonator with a pair of coupled lines folded inside the resonator shown in Figure 2.3(c) [7].

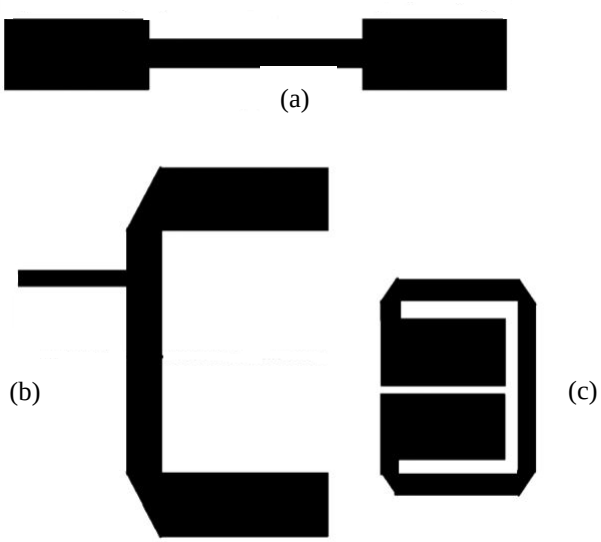

Figure 2.2: Variation SIR configurations. (a) Basic SIR. (b) Stepped impedance hairpin resonator. (c) Miniaturized hairpin SIR.

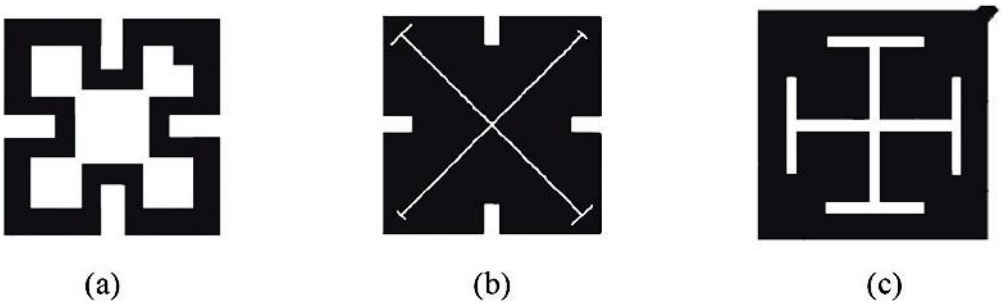

Figure 2.3: Variation dual-mode configurations. (a) Meander loop. (b) Inductively loaded cross-slotted patch. (c) Capacitive stepped-impedance resonator.

Dual-mode resonators, which are featured that each dual-mode resonator can be used as a doubly tuned resonant circuit to reduce the required number of resonator degree to half, have also been widely applied for compact filter configuration. For example, the different reconfigurations of dual-mode resonator are illustrated in Figure 2.3, including meander loop resonator [8], inductively loaded cross-slotted patch resonator [9] and capacitive stepped-impedance resonator [10].

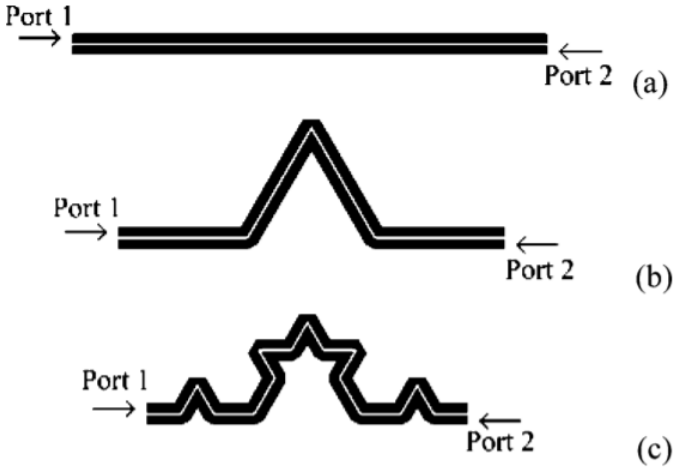

Figure 2.4: Koch curve shaped microstrip coupled line. (a) Koch0: Zeroth iteration. (b) Koch1: First iteration order. (c) Koch2: Second iteration order.

The approach discussed above focus on the symmetrical structure, however, there are always complex situations in filter miniaturization. Another approach in the open literature is to use fractal geometries such as Hilbert curve, Koch curve (exampled in Figure 2.4), Sierpinski gasket to develop compact structures [11]-[12]. Generally, a fractal shape can be filled in a limited area as the order increases and occupies the same area

regardless of the order to reduce the physical dimensions. Fractal filters are basically characterized by two factors: the iteration order and the iteration factor. The iteration order represents how many iteration process are applied and the iteration factor is the construction law of fractal geometry generation [12]. Actually, such space-filling method is not only used to miniature the physical dimension, but also used to control the higher harmonics, since it has a larger effect on the harmonic mode with a shorter electrical length than that of fundamental mode.

What's more, slow-wave resonator, which is normally realized by alternatively loaded inductors and capacitors on a regular transmission line, is also a popular approach to miniature the filter size [13]-[16]. Generally, the transmission propagation variable $\beta = \omega\sqrt{LC}$ increases by using capacitive or inductive loadings. However, the required physical length of the line for a given electrical length is smaller that lead to physical miniaturization. Such slow-wave filters also have good stopbands, which is due to the effect of slow-wave to control the spurious response.

From fabrication perspective, recently, multilayer filters have been widely applied to achieve the challenges of physical size, response performance and cost requirement. Multilayer technology have three dimensions in free space, which can increase the flexibility in filter design and integration with other microwave components and circuits. As illustrated in [7], [17]-[19], various coupled-line resonators and circuit components located at different layers without any direct ground plane insertion between the adjacent layers have been involved in the filter design. In contrast, another type of multilayer filters employed aperture couplings on the common ground between adjacent layers. Defect ground structures formed by pattern ground patch also allows additional filter functions [20]-[22]. In recent advanced packaging materials, the low temperature co-fired ceramic (LTCC) and liquid crystal polymer (LCP) are popular applied in the fabrication of multilayer filters. In the following section, these two multilayer technologies will be briefly introduced.

2.2 Multilayer Technologies

As two very mature and popular technologies in the circuit fabrication, LTCC and LCP have attracted a lot of attention in microwave filter design. These technologies allow the innovation of 3D, monolithic and effective cost microwave circuits/systems package.

2.2.1 LTCC Technology

Low-temperature co-fired ceramic (LTCC) can be defined as a multilayer circuit fabricated by laminating single green sheets (term for unfired tapes; Green TapeTM, Dupont) with printed conductor lines etc. on the surface on top of each other and firing them all together in one step, as illustrated in Figure 2.5 [23]. This procedure is similar to that of high temperature co-fired ceramics (HTCC), but it is possible to use low resistivity conductors like copper, silver, gold and alloys with palladium and platinum instead of molybdenum and tungsten, which is because that the firing temperature operated in LTCC is around $850^{\circ}C$ (mostly 850 to $875^{\circ}C$, what makes it possible to use silver for conductor lines etc.) that is lower than that of HTCC in excess of $1000^{\circ}C$.

The multilayer characteristic of LTCC technology supports good 3D design flexibility. Therefore, many miniaturized LTCC filters, which can't be realized in traditional fabrication technology, have been presented in [24]-[28]. For example, a lumped element two poles bandpass filter for Bluetooth application has been proposed in [27], which overlaps two inductor strips in the 3D-direction to achieve a mutual inductive coupling that obtains a finite transmission zero to improve the selectivity at the image frequency. In [28], strong capacitive couplings between the strips at different layers are easily realized to achieve wide bandwidth up to 60% with much more compact size. Another miniature LTCC bandpass filter for 2.4 GHz wireless low noise amplifier (LAN) applications is also described in [29]. This is a second order filter based on two capacitor-loaded transmission line resonators and three capacitive inverters depicted in Figure 2.6.

However, LTCC also has some disadvantages. Firstly, unpackaged chips with active devices can't survive the lamination temperature of LTCC occurred at $850^{\circ}C$ [23], resulting that they have to be packaged separately with increasing fabrication cost.

Secondly, LTCC is not suitable for antenna applications. In terms of antenna radiation efficiency, the material with a dielectric constant close to the free space is desired, while LTCC has a high relative dielectric constant (around 5.4-9.1). Besides, the cost of LTCC is still expensive compared with some conventional laminate materials. Compared to LTCC, LCP has much lower processing temperature and much cheaper, which will describe in detail in the following section.

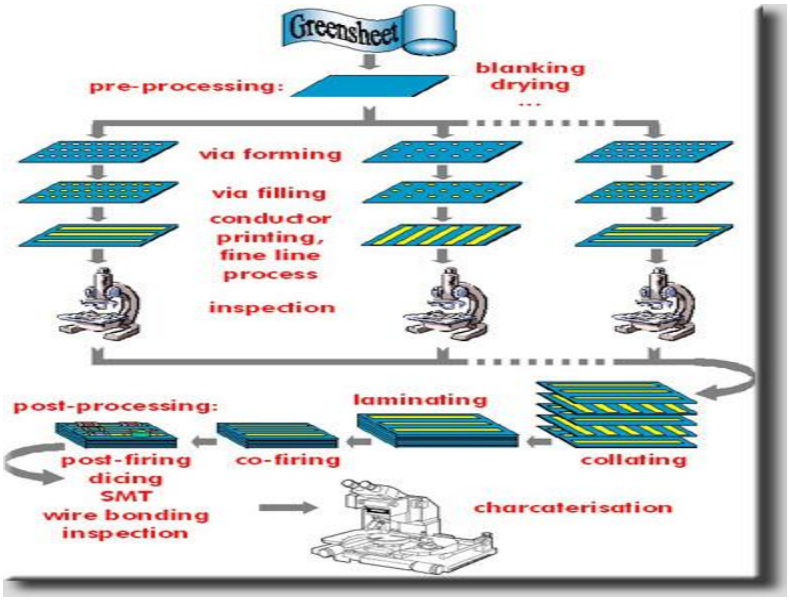

Figure 2.5: LTCC manufacturing process [23].

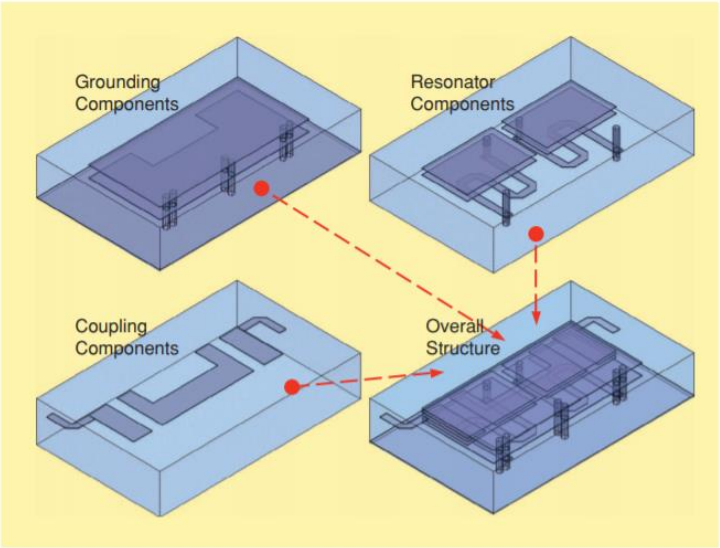

Figure 2.6: Physical structure of a miniature two-pole LTCC filter [28].

2.2.2 LCP Technology

Liquid crystal polymer (LCP) is a new and promising organic thermoplastic material. The typical characteristics of commercially available LCP is shown in Table 2.1. In the table, ULTRALAM 3850 is a core film with $315^{\circ}C$ melting temperature, which is mainly used to support metal circuits and has some available thickness (like 25, 50, 100 μm), whereas ULTRALAM 3908 is a bonding film with $280^{\circ}C$ melting temperature, which is used as a stack inserted between different core films and has a thickness of 25 and 50 μm [30] [31].

In general, LCP has extremely low moisture-absorption character, which can reduce the baking time and maintain stable electrical and mechanical properties in humid environment. It exhibits good dimensional stability and is suitable for the mechanical fabrication. It has extraordinary barrier properties comparable to that of glass and low coefficient of thermal expansion, which are important to packaging applications. What's more, LCP film has excellent electrical characteristics, such as stable low dielectric constant and low dissipation factor, which are desired for the microwave application. It is shown that, from 30 to 110 GHz, the LCP film has a dielectric constant of 3.16 ± 0.05 and a low loss tangent from 0.0028 to 0.0045 [32]. These merits make LCP film an ideal material for millimetre wave application as well.

The cost of liquid crystal polymer is comparable to that of conventional print circuit board material and is cheaper than LTCC. The active and passive devices can be integrated in compact, vertically integrated RF modules by using homogeneous multilayer LCP technology at a low temperature about $290^{\circ}C$, which would be more challenging for LTCC technology because of its much higher processing temperature about $850^{\circ}C$. The unique combination of properties such as lower cost and excellent electrical and mechanical characteristics makes LCP technology ideally suitable for implementing compact high density system-in-package applications. For example, a miniature quasi-lumped-element wideband bandpass filter at 0.5-2 GHz by cascading low pass and high pass filter has been presented in [2]. The ultra-wideband (UWB) filters can ben also reconstructed by using multilayer LCP technology [33]-[36]. With multilayer

capability, not only broadside coupling can easily be realized, but also more functionality can be integrated in a compact structure for UWB filter.

Table 2.1: Typical Characteristics of Liquid Crystal Polymer (LCP) Films [30] [31].

Property		Value		
		ULTRALAM 3850	ULTRALAM 3908	Unit
Mechanical Properties				
Dimensional MD		−0.06	< 0.1	%
Stability CMD		−0.03	< 0.1	
Tensile strength		200	216	MPa
Tensile modules		2255	2450	MPa
Density		1.4		gm/cm3
Thermal Properties				
Coefficient of mhermal expansion, CET (30◦C to 150◦C)	X Y Z	17 17 150	17 17 150	ppm/◦C
Melting temperature		315	280	◦C
Relative thermal index, RTI	Mechanical Electrical	190 240	190 240	◦C
Thermal conductivity		0.5		W/m/◦K
Electrical Properties				
Dielectric constant (10 GHz, 23◦C)		2.9	2.9	
Dissipation factor (10 GHz, 23◦C)		0.0025	0.0025	
Surface resistivity		1.0×10^{10}	1.0×10^{12}	MOhm
Volume resistivity		1.0×10^{12}	2.6×10^{14}	MOhm cm
Dielectric breakdown strength		1378	118	KV/cm
Environment Properties				
Chemical resistance		98.7	98.7	%
Water absorption (23◦C, 24-h)		0.04	0.04	%
Coefficient of hygroscopic expansion, CHE (60◦C)		4	4	ppm /%RH
Flammability		VTM-0	VTM-0	

2.3 Slow-wave Resonator

In order to miniature the physical size of microwave filter, slow-wave resonators are usually employed in filter design [37]-[39]. This is because that the size of microwave filters is proportional to the guided wavelength, which is proportional to the phase velocity. Hence, the size reduction can be achieved by reducing the phase velocity or obtaining slow-wave propagation. On the other hand, it is also very important to reduce interference by keeping out-of-band signals from reaching a sensitive receiver. In general, planar bandpass filters that are comprised of half-wavelength resonators inherently have a spurious passband at $2f_0$. The spurious passband can be suppressed by cascading a lowpass filter or bandstop filter in the cost of larger circuit size and extra insertion loss. The quarter-wavelength resonator filters have the first spurious passband at $3f_0$, but they require short-circuit connection to ground, which may be no desired in planar filter fabrication techniques. Lumped-element filters ideally do not have any spurious response, but suffer from poorer power handling and higher loss. The slow-wave resonator filter is able to control spurious response with a compact filter size.

In theory, the slow-wave resonator can be considered as a capacitively loaded transmission line resonator, shown in Figure 2.7, where C_L, Z_α, β_α and d are the loaded capacitance, the characteristic impedance, the propagation constant and the length of the unloaded line respectively. The electromagnetic wave energy can be stored in the capacitors resulting in a slow-wave effect by employing the loading capacitor. The following section will analyse this type of slow-wave resonator in detail [31].

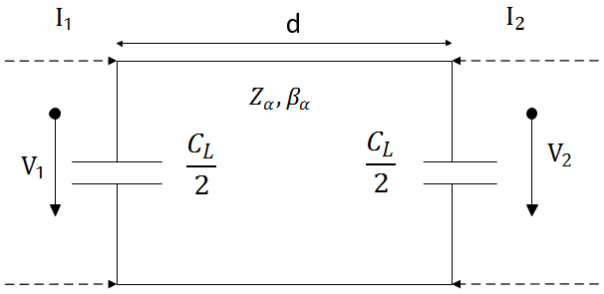

Figure 2.7: Capacitively loaded transmission line resonator.

The circuit response of Figure 2.7 can be determined by using ABCD parameters [38]

$$\begin{bmatrix} V_1 \\ I_1 \end{bmatrix} = \begin{bmatrix} A & B \\ C & D \end{bmatrix} \cdot \begin{bmatrix} V_2 \\ -I_2 \end{bmatrix} \tag{2.1}$$

with

$$A = D = \cos\theta_\alpha - \frac{1}{2}\omega C_L Z_\alpha \sin\theta_\alpha \tag{2.2}$$

$$B = jZ_\alpha \sin\theta_\alpha \tag{2.3}$$

$$C = j(\omega C_L \cos\theta_\alpha + \frac{1}{Z_\alpha}\sin\theta_\alpha - \frac{1}{4}\omega^2 {C_L}^2 Z_\alpha \sin\theta_\alpha) \tag{2.4}$$

where $\theta_\alpha = \beta_\alpha d$ is the electrical length and $\omega = 2\pi f$ is the angular frequency. By applying the boundary conditions $I_1 = I_2 = 0$, we have

$$\frac{C}{A} = \frac{I_1}{V_1}|_{I_2=0} = \frac{I_2}{V_2}|_{I_1=0} = 0 \tag{2.5}$$

Noting that

$$A = \frac{I_1}{V_1}|_{I_2=0} = \begin{cases} -1 & \text{for the fundamental resonance} \\ 1 & \text{for the first spurious resonance} \end{cases} \tag{2.6}$$

Substituting Eq. (2.6) into Eq. (2.2), we can obtain

$$\cos\theta_{a0} - \frac{1}{2}\omega_0 C_L Z_\alpha \sin\theta_{a0} = -1 \tag{2.7}$$

$$\cos\theta_{a1} - \frac{1}{2}\omega_1 C_L Z_\alpha \sin\theta_{a1} = 1 \tag{2.8}$$

where the subscripts 0 and 1 indicate the parameters associated with the fundamental and the first spurious resonance, respectively. Substituting Eq. (2.7) and (2.8) into Eq. (2.4), and letting $C = 0$ based on Eq. (2.5), yields

$$\theta_{a0} = 2\tan^{-1}(\frac{1}{\pi f_0 Z_\alpha C_L}) \tag{2.9}$$

$$\theta_{a1} = 2\pi - 2\tan^{-1}(\pi f_1 Z_\alpha C_L) \tag{2.10}$$

from which the fundamental resonant frequency f_0 and the first spurious resonant frequency f_1 can be determined, shown in Figure 2.8 for different loading capacitance.

It can be seen that when the loading capacitance is increased, in addition to the decrease of both resonant frequencies, the ration of the first spurious resonant frequency to the fundamental one is increased. This is can be explained by calculating the propagation constant or phase velocity of the transmission line. Applying Floquet's theorem [40]

$$V_2 = e^{-j\beta d} V_1 \tag{2.11}$$

$$-I_2 = e^{-j\beta d} I_1 \tag{2.12}$$

to Eq. (2.1) results in

$$\begin{bmatrix} A - e^{-j\beta d} & B \\ C & D - e^{-j\beta d} \end{bmatrix} \cdot \begin{bmatrix} V_2 \\ -I_2 \end{bmatrix} = \begin{bmatrix} 0 \\ 0 \end{bmatrix} \tag{2.13}$$

Since $A = D$ for the symmetry and $AD - BC = 1$for the reciprocity, we have

$$\cos(\beta d) = \cos\theta_\alpha - \frac{1}{2}\omega C_L Z_\alpha \sin\theta_\alpha \tag{2.14}$$

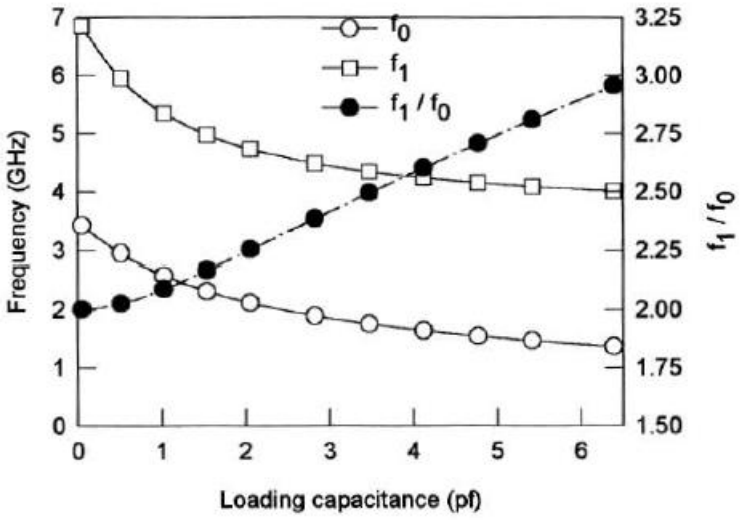

Figure 2.8: Fundamental and first spurious resonant frequencies of a capacitively loaded transmission line resonator, as well as their ratio against loading capacitance [31].

Substituting Eq. (2.9) and (2.10) into Eq. (2.14), it turns out that $\cos\beta_0 d = -1$ for the fundamental resonant frequency and $\cos\beta_1 d = 1$ for the first spurious resonant frequency. As $\beta_0 = {}^{\omega_0}/_{v_{p0}}$ and $\beta_1 = {}^{\omega_1}/_{v_{p1}}$, where v_{p0} and v_{p1} are the phase velocities of the loaded line at the fundamental and the first spurious resonant frequencies respectively. We can obtain

(2.15)

$$\frac{f_1}{f_0} = 2\frac{v_{p1}}{v_{p0}}$$

As can be seen from Eq. (2.15), the dispersion is increased when the ratio of the first spurious resonant frequency to the fundamental one is increased by loading larger capacitance.

Based on this type of slow-wave resonator, a novel microwave bandpass filter using microstrip slow-wave open-loop resonators and multilayer LCP technology will be presented for demonstration in the following section.

2.4 Design of Multilayer Slow-wave Open-loop Resonator Filter

This part presents a novel microwave bandpass filter using microstrip slow-wave open-loop resonators and multilayer LCP technology. The new filter has not only very compact size due to the slow-wave effect, but also exhibits a wider upper stopband resulting from the dispersion property. A five-pole microstrip filter of this type, i.e., a bandpass filter centred at f_c=1.18 GHz with -3dB fractional bandwidth of 17%, has been designed and fabricated. No spurious response, which are at least 30-dB rejection, occurs for the frequency up to 10GHz. Moreover, the fabricated filter also has the compact size of $0.102\lambda_g \times 0.081\lambda_g$ (λ_g is the guided wavelength) and the light weight less than one gram by using multilayer LCP circuit technology. Good agreement can be observed between the simulation and measurement.

2.4.1 Multilayer Slow-wave Open-loop Resonator

The 3D structure of the proposed novel multilayer slow-wave open-loop resonator is shown in Figure 2.9. It consists of three metal layers supported by dielectric substrates with a relative dielectric constant of 3.0 and a total thickness of 0.625mm. The top and middle layer layouts are shown in Figure 2.9(b) and (c). The top layer is a typical stepped impedance open-loop slow-wave resonator, which is broadside coupled with the two patches in the middle layer that compensate the coupling of the top layer resonator itself. The effect of broad side coupling can be only realized in EM simulation, not in the theory

circuit model.

The bottom metal layer serves as solid ground. The resonator has a small footprint of 5mm by 5mm. The floating metal on the middle layer is essential for achieving two desired effects: (i) the slow wave effect to shift the fundamental resonant frequency down for the given footprint; (ii) the dispersion effect to shift the spurious resonances away from the fundamental one.

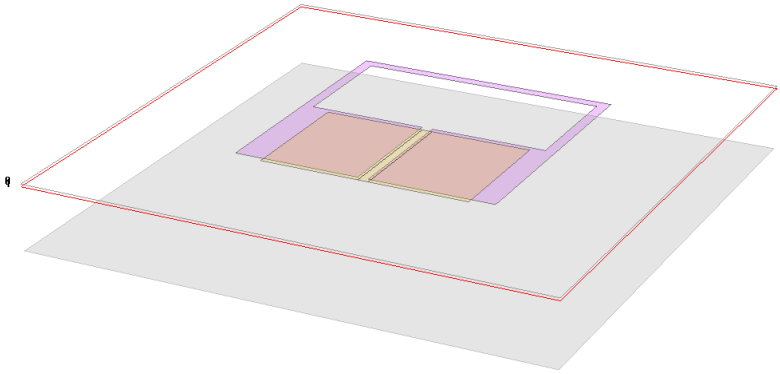

(a)

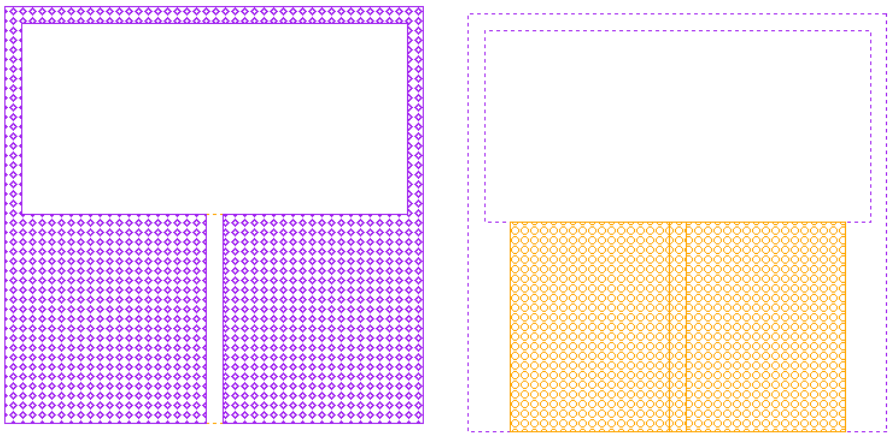

(b) (c)

Figure 2.9: Proposed multilayer slow-wave open-loop resonator. (a) 3D view (b) Top layer (c) Middle layer.

For the fundamental resonant mode, which is an odd mode, the symmetrical plane through the open gap of the top layer is an electrical wall that would virtually makes the floating metal grounded along the symmetrical plane resulting in a typical capacitive loaded lossless transmission line resonator shown in Figure 2.7. Following the theory

analysis in the above section, we can easily understand the structure of multilayer slow-wave resonator, though it has multilayer patches, which use broad-side coupling to compensate coupling of single layer.

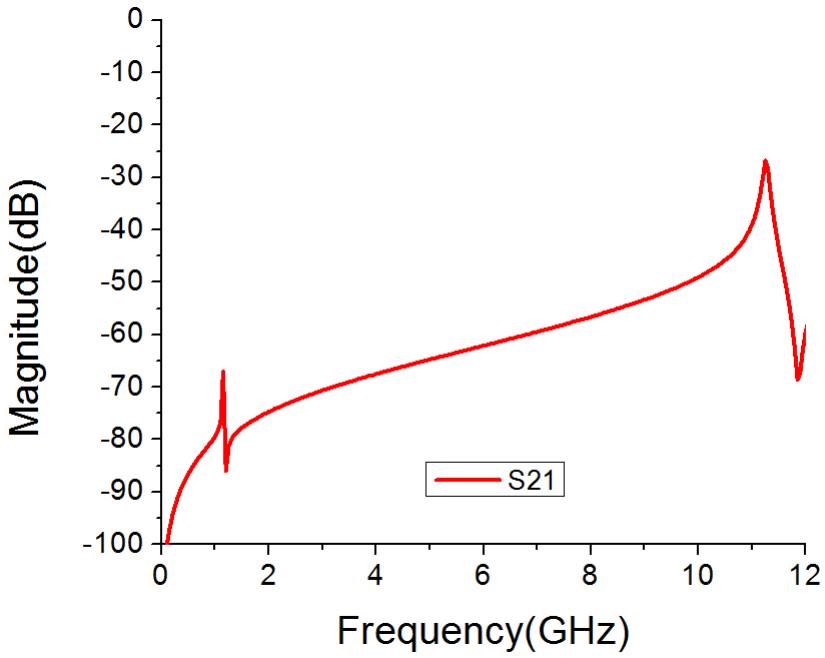

Figure 2.10: Resonant frequency response of proposed multilayer slow-wave resonator.

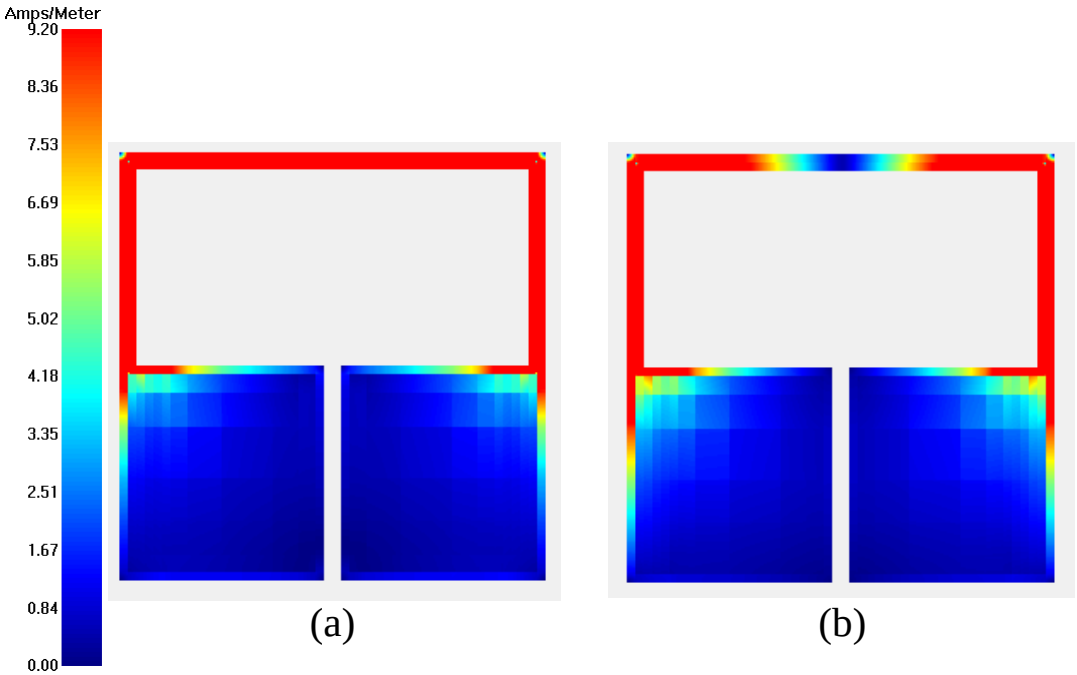

Figure 2.11: (a) Current distribution of the fundamental resonance and (b) Current distribution of the first spurious resonance.

The resonant frequency responses of the multilayer slow-wave resonator is shown in Figure 2.10. The fundamental resonance is at 1.18GHz; the first spurious resonance is at 11.25GHz and the second spurious resonance at 14.95GHz. Note that the free-space wavelength at the fundament resonant frequency of 1.18GHz is about 254mm, which is much larger that the resonator dimensions and the miniaturization of the proposed resonator results from a very low phase velocity or slow-wave associated with the fundamental resonant mode. Another distinct feature of this proposed resonator is that its first spurious resonant frequency is shifted far away from the fundamental one (C_{IF}); in this case, it is about $12 \times C_{IF}$, which is very important for realizing ultra-wide stopband IF filters. The current distribution of the fundamental and the first spurious resonance are shown in Figure 2.11(a) and (b) respectively.

2.4.2 Design of Five-pole Multilayer Slow-wave Open-loop Resonator Filter

For demonstration, a five-pole of this type of resonator filter is designed to meet the following specifications:

Centre frequency	1.18GHz
3-dB bandwidth	180MHz
Min stopband rejection	dc to 1GHz, 45dB
	1.3-2.37GHz, 45dB
	2.37-10GHz, 30dB

2.4.2.1 Theory Circuit Model

The five-pole bandpass filter can be represented by an equivalent circuit shown in Figure 2.12(a), where $M_{12}, M_{23}, \ldots, M_{45}$ are the coupling coefficients among adjacent resonators, and Q_e is the external quality factor denoting the input and output coupling. The coupling coefficients and external quality factor can be synthesized from a low-pass prototype filter shown in Figure 2.12(b), where the rectangular boxes represent frequency invariant immittance inverters defined through a transmission matrix of the form [13]

$$\begin{bmatrix} 0 & j/J \\ jJ & 0 \end{bmatrix}$$

in which J is the characteristic admittance of the inverter, and in our case $J = 1$. The other elements $g_1, g_2, \ldots, g_5$ of the prototype filter could be determined by synthesizing a standard Chebyshev filter. The external quality factor and coupling coefficients can then be found by

$$Q_e = \frac{g_0 g_1}{FBW} \tag{2.16}$$

$$M_{12} = M_{45} = \frac{FBW}{\sqrt{g_1 g_2}} \tag{2.17}$$

$$M_{23} = M_{34} = \frac{FBW}{\sqrt{g_2 g_3}} \tag{2.18}$$

where FBW denotes the fractional bandwidth of bandpass filter.

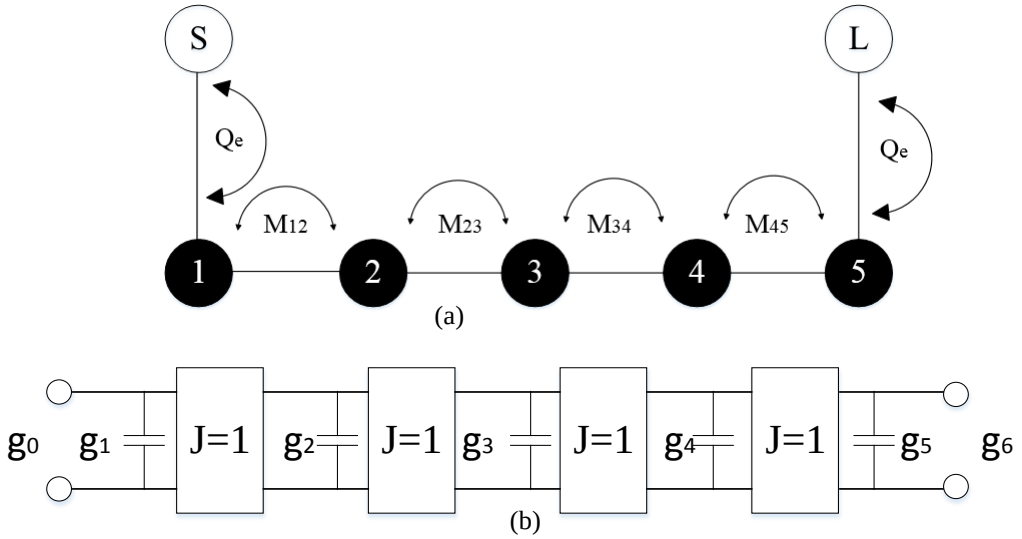

Figure 2.12: (a) An equivalent circuit of the five-pole coupling bandpass filter and (b) an associated low-pass prototype filter.

The calculated design parameters of the five-pole bandpass filter are listed below

$$Q_e = 3.1593$$

$$M_{12} = M_{45} = 0.2407$$

$$M_{23} = M_{34} = 0.1669$$

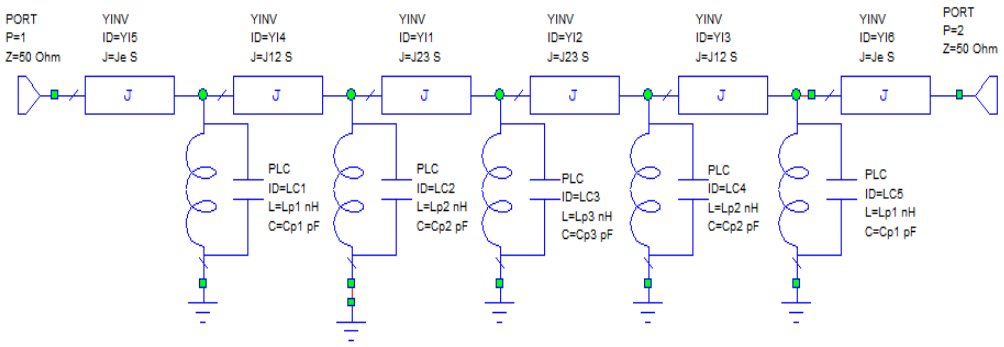

Figure 2.13: The equivalent circuit model of the proposed filter.

According the above discussion, the equivalent circuit model can be built by using Microwave office (AWR) [41], shown in Figure 2.13, where J invert is used to represent the couplings, in which J_e represent the external coupling Q_e and J_{12}, J_{23} represent the coupling coefficients $M_{12}, M_{23}, \ldots, M_{45}$. The parameters value of this circuit model is given in Table 2.2 with slightly optimization [31]. Note that this circuit model is a simplified one, which doesn't include the broadside couplings. Therefore, it can be seen that the response performance only gives a required 16% FBW centred at 1.2GHz without any transmission zeros to improve the selectivity, as illustrated in Figure 2.14.

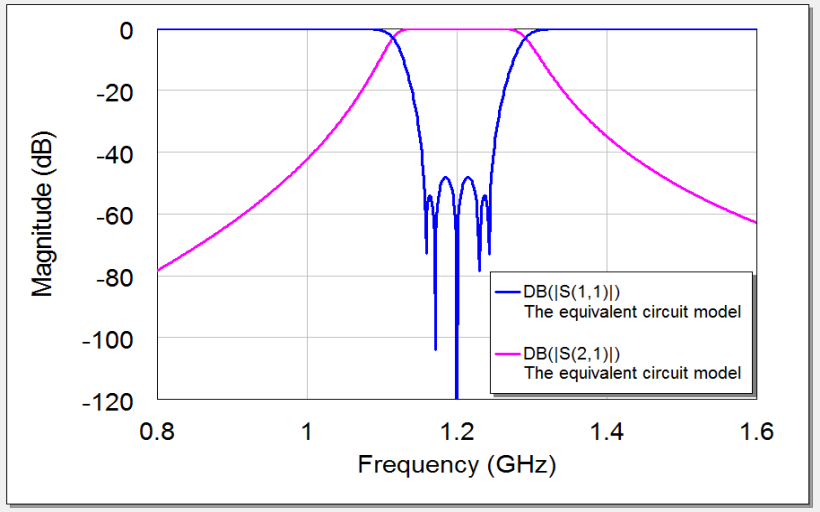

Figure 2.14: The response performance of the proposed filter.

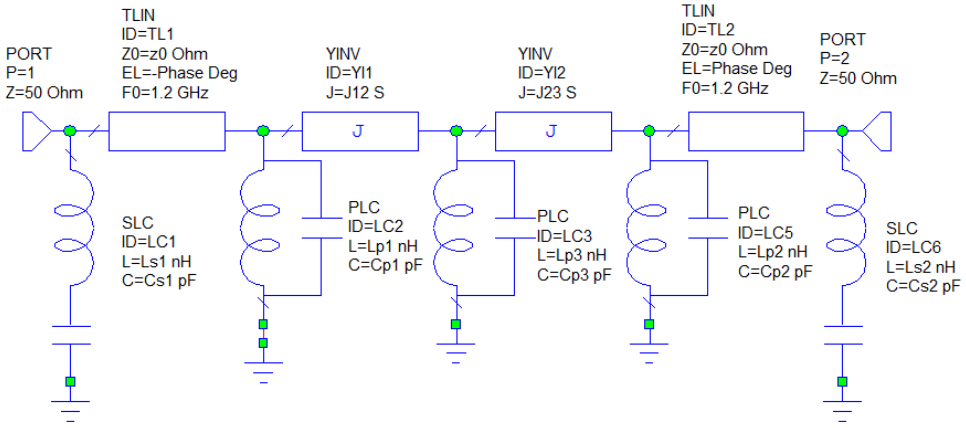

Figure 2.15: The improved equivalent circuit model of the proposed filter.

Table 2.2: Parameters value of the equivalent circuit model.

J_e	0.052 S	L_{p1}	0.2 nH	C_{p1}	88.17 pF
J_{12}	0.089 S	L_{p2}	0.2 nH	C_{p2}	88.17 pF
J_{23}	0.054 S	L_{p3}	0.16 nH	C_{p3}	107 pF

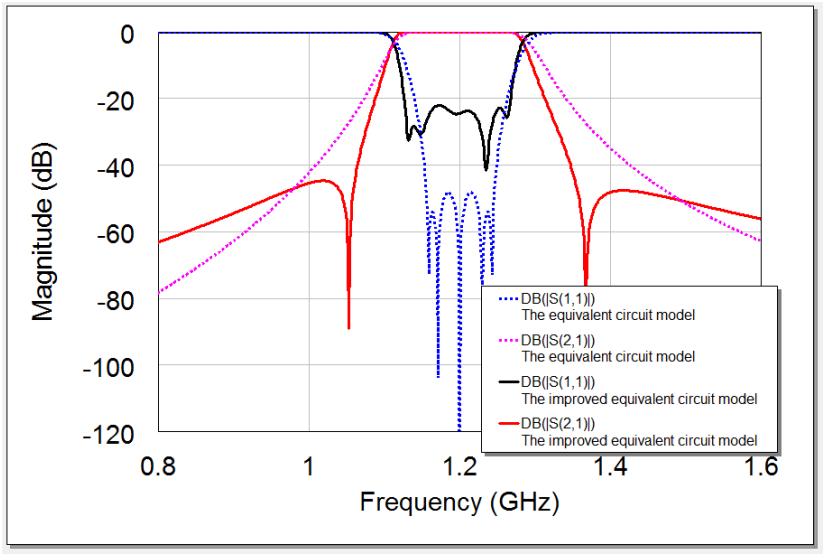

Figure 2.16: The response performance of the improved circuit model.

In order to match the close performance to the actual EM simulations, the equivalent circuit model needs to be improved to be given in Figure 2.15. Two shunt resonators at the source/load are used to replace the series resonators to introduce two transmission zeros to enhance the selectivity, which also contribute the passband as well. The response performance of the improved circuit model is shown in Figure 2.16, in which there are

five poles in the return loss. The parameters value of the improved circuit model are listed in Table 2.3.

Table 2.3: Parameters value of the improved circuit model.

Phase	36.5°	L_{p3}	0.2 nH	L_{s2}	22 nH
J_{12}	0.055 S	C_{p1}	88 pF	C_{s1}	0.79 pF
J_{23}	0.055 S	C_{p2}	84 pF	C_{s2}	1.0 pF
L_{p1}	0.2 nH	C_{p3}	91 pF		
L_{p2}	0.2 nH	L_{s1}	17.2 nH		

2.4.2.2 Filter Implementation

Having characterized the couplings we design the filter with the aid of EM simulator [41]. The method of converting equivalent circuit model to EM simulation can be found in [31].

The general formulation for extracting coupling coefficient k is applicable for synchronously tuned coupled resonators, which can be degenerated to [31]

$$k = \pm \frac{{f_m}^2 - {f_e}^2}{{f_m}^2 + {f_e}^2} \tag{2.19}$$

where f_e and f_m corresponds to the resonant frequency of electric coupling and magnetic coupling respectively.

To demonstrate the application in EM simulation, some instructive numerical examples are included in this section. Two ports are very weakly coupled to the coupled resonator structure and the typical types of coupled microstrip resonator are employed, shown in Figure 2.17. Each of the open-loop resonators is essentially a folded half-wavelength resonator. These coupled structures result from different orientations of a pair of open-loop resonators, which are separated by a spacing s. It is obvious that any coupling in those structures is that of the proximity coupling, which is basically through fringe fields. The nature and the extent of the fringe fields determine the nature and the strength of the coupling [31].

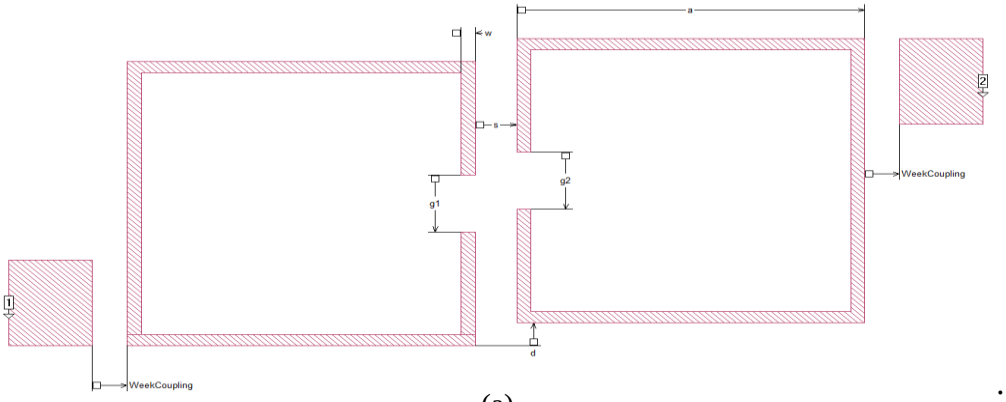

(a)

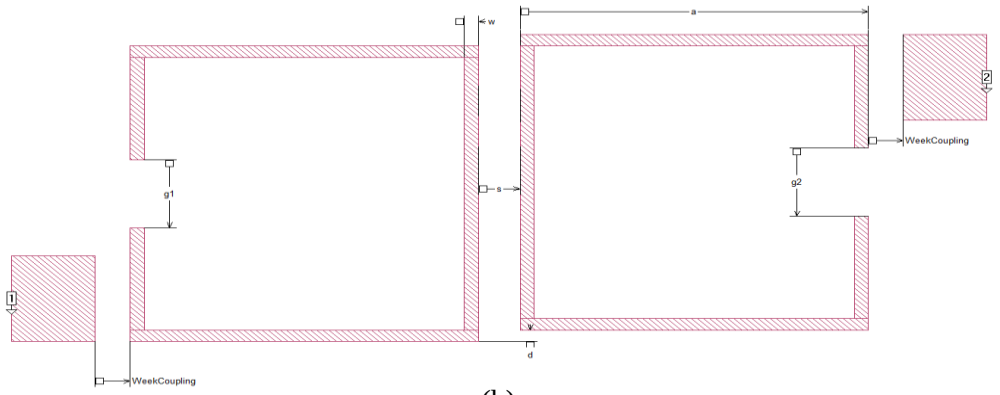

(b)

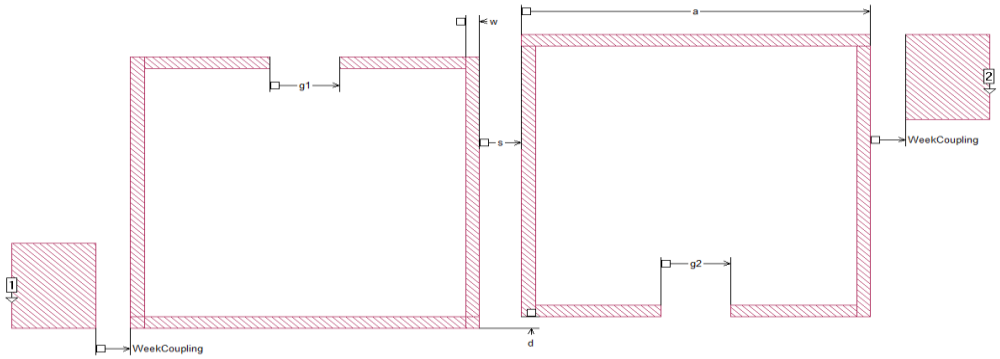

(c)

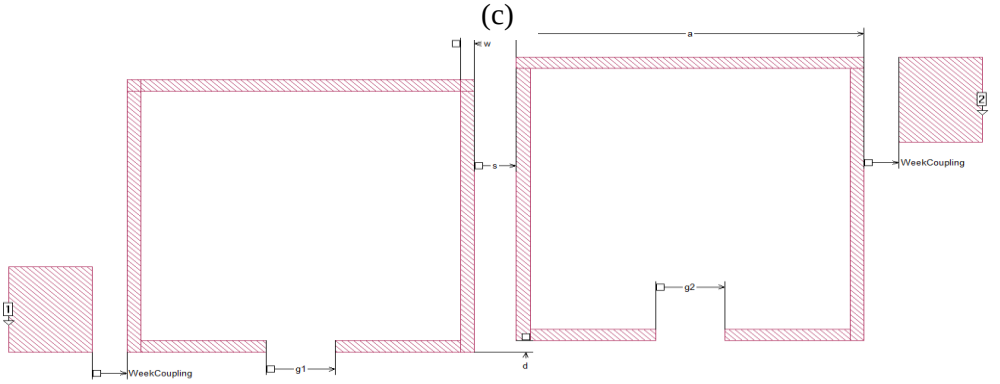

(d)

Figure 2.17: Typical coupling structures of coupled resonators with (a) electric coupling (b) magnetic coupling, and (c-d) mixed coupling.

The electric coupling can be obtained if the open sides of two coupled resonators are proximately placed, as shown in Figure 2.17(a). The magnetic coupling can be obtained if the sides with the maximum magnetic field of two coupled resonators are proximately placed, as seen in Figure 2.17 (b). For the coupling structures in Figure 2.17 (c) and (d), the electric and magnetic fringe fields at the coupled sides may have comparative distributions, so that both electric and magnetic couplings occur. In this case, the coupling may be referred to as a mixed coupling.

The microstrip open-loop resonators have dimensions of a=7.0 mm and w=1.0 mm on a substrate with a relative dielectric constant of 10.8 and thickness of 1.27mm. It is also assumed that g1=g2 for the synchronous tuning and d=0 for a zero offset. Figure 2.18 shows typical simulated resonant frequency response of the coupled resonator structures in Figure 2.17 (a) and (b), respectively, with s=2.0 mm, where S_{21} is the S parameter. Figure 2.18 (a) shows the responses for electric coupling, while Figure 2.18 (b) gives the performance for magnetic coupling. From Figure 2.18 (a), we can find $f_e = 2513$ MHz and $f_m = 2540$ MHz. The coupling coefficient can be extracted by using Eq. (2.19) and is k=0.01084. From Figure 2.18 (b), it can be found that $f_e = 2484$ MHz and $f_m = 2567$ MHz, so the k=0.03313. Hence, with the same coupling space s, the magnetic coupling is stronger than the electric coupling. For the mixed coupling structures shown in Figure 2.17 (c) and (d), coupling coefficients are extracted from the simulated frequency responses, similar to the above, and the results are shown in Figure 2.19.

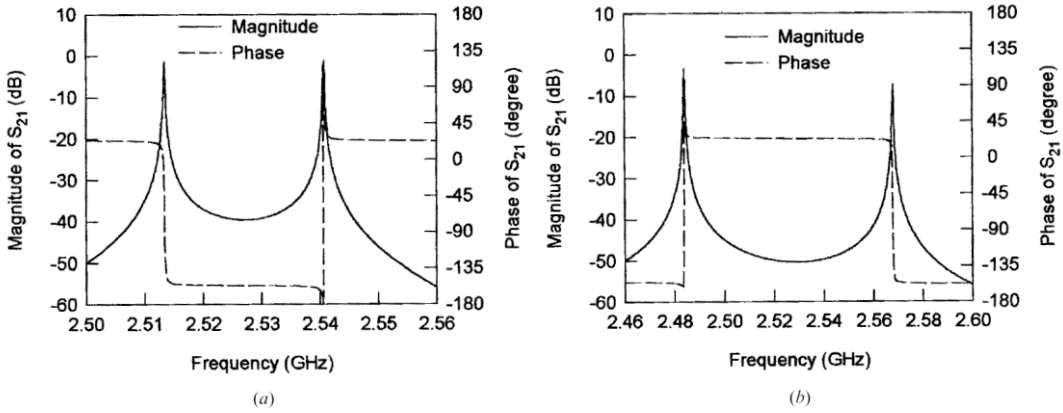

Figure 2.18: Typical resonant response of coupled resonator structure. (a) For the structure in Figure 2.17(a). (b) For the structure in Figure 2.17(b) [31].

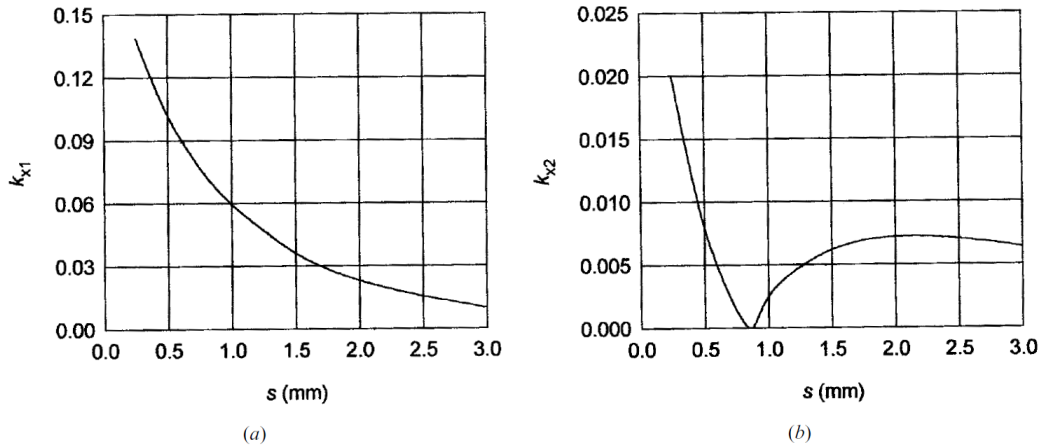

Figure 2.19: (a) Coupling coefficients for the structure in Figure 2.17(c). (b) Coupling coefficients for the structure in Figure 2.17(d) [31].

By following the above procedure, the coupling coefficients between the source/load and resonator (external coupling), resonator and resonator (coupling matrix) can be achieved. The layout of the proposed filter is shown in Figure 2.20. Note that the structure of resonators at two sides are reshaped for better matching with the feeding line. The top layer of Figure 2.20(a) consists of five reshaped slow-wave open loop resonator, while the middle layer has several patches to compensate the couplings by using the broadside couple, which can't be demonstrated by using the theory circuit model. That is the reason why the improved circuit model is used, not the simple equivalent circuit model. The dimensions of the proposed filter is also given in detail by using the unit mm in the layout. The ground layer is the real ground which is not shown. Figure 2.21 shows the current distribution of the fundamental resonance at 1.2GHz and the simulation responses performance compared with the improved circuit model are given in Figure 2.22. There are slight frequency shifts (40 MHz) in the EM simulation

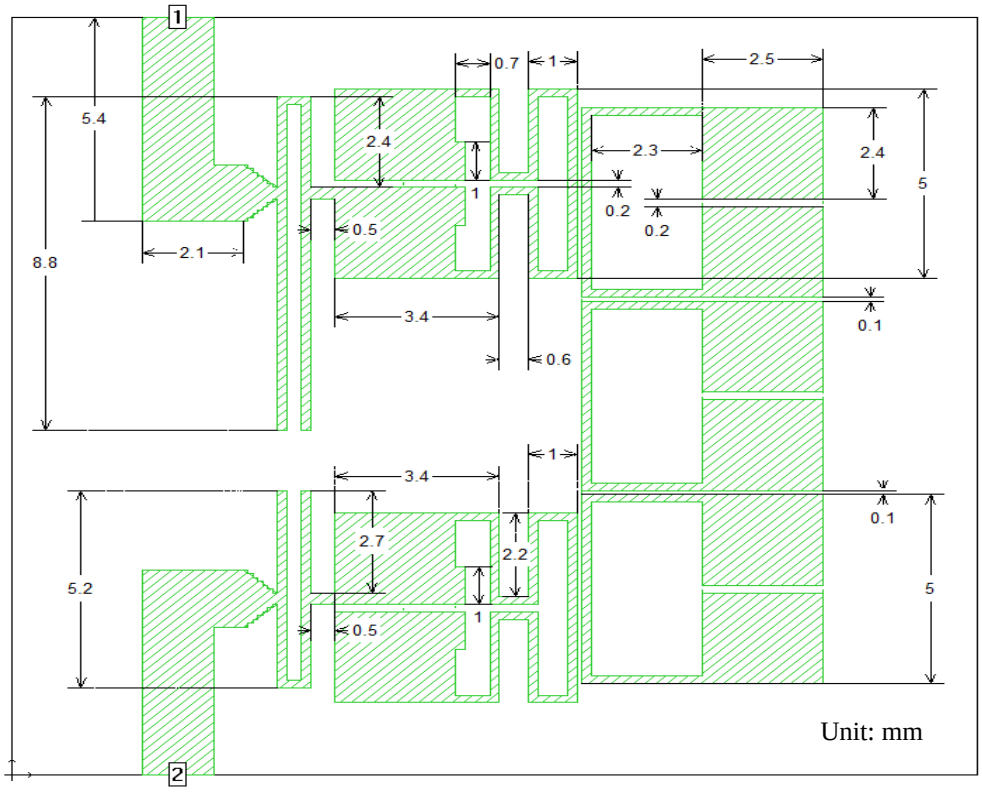

(a)

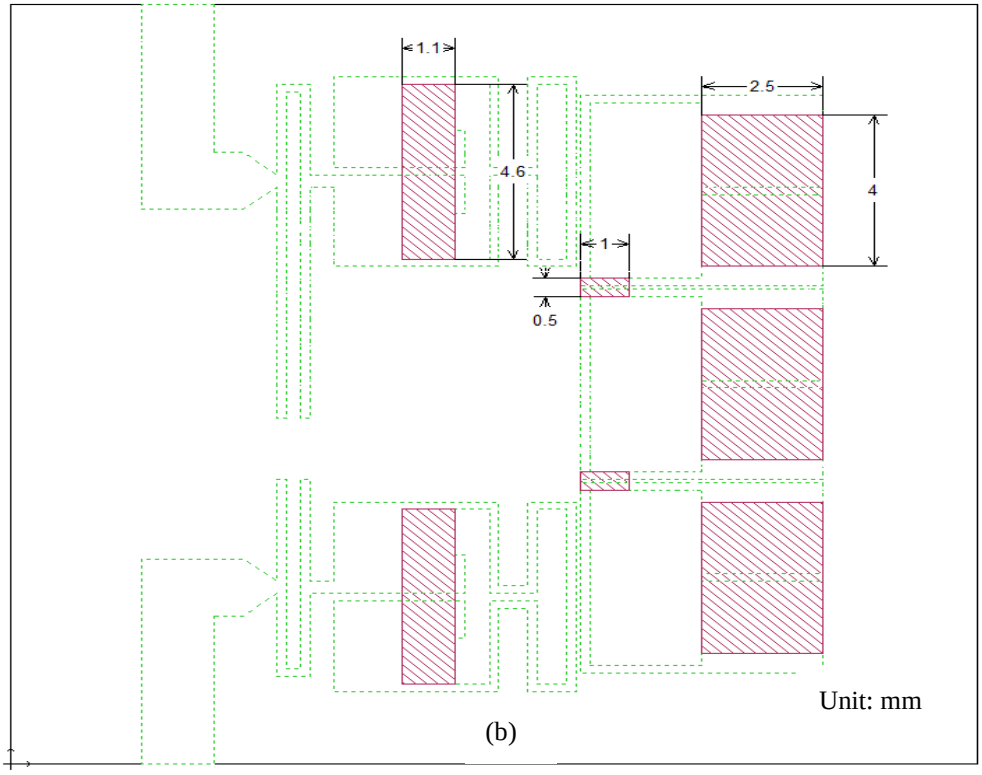

(b)

Figure 2.20: The layout of the proposed filter. (a) The top layer. (b) The middle layer.

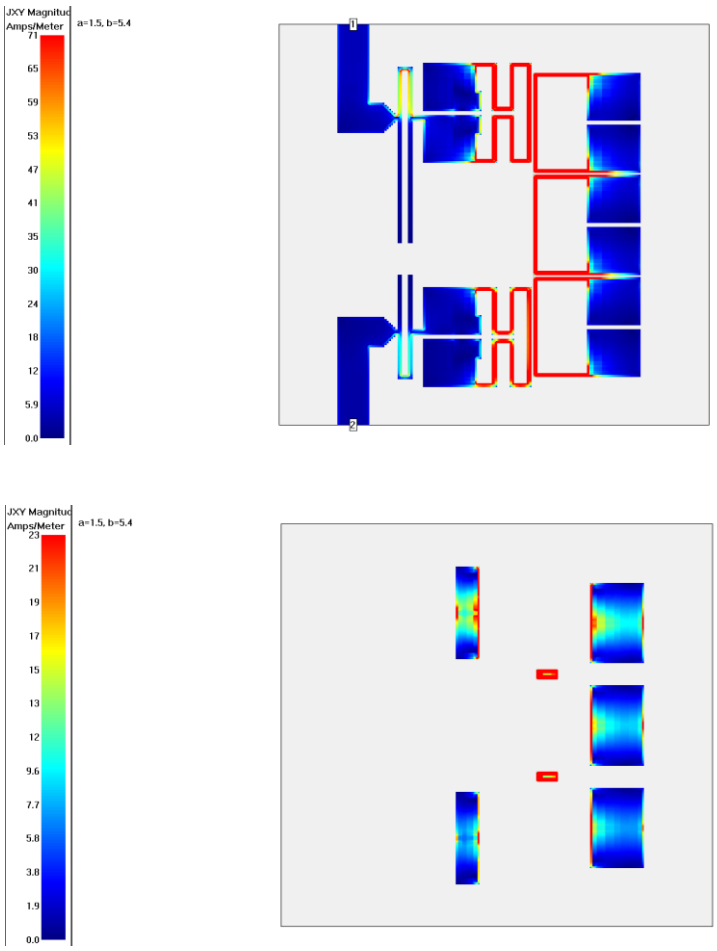

Figure 2.21: Current distribution of the fundamental resonance at 1.2 GHz.

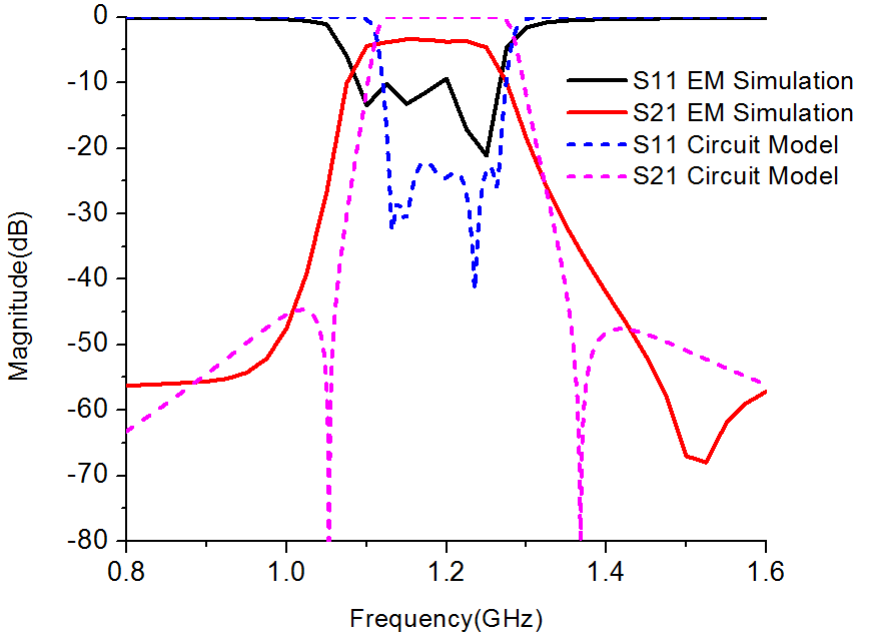

Figure 2.22: The response of EM simulation of five-pole slow-wave open-loop resonator filter.

The filter is fabricated by using multilayer LCP technology. Figure 2.23 shows the fabrication structure of the proposed filter in multilayers. There are nine layers used, in which the first core film layer is etched at two sides with the top layer circuit and the middle layer circuit. The last core film layer is etched at one side to remove all the copper and left the other layer to be the ground.

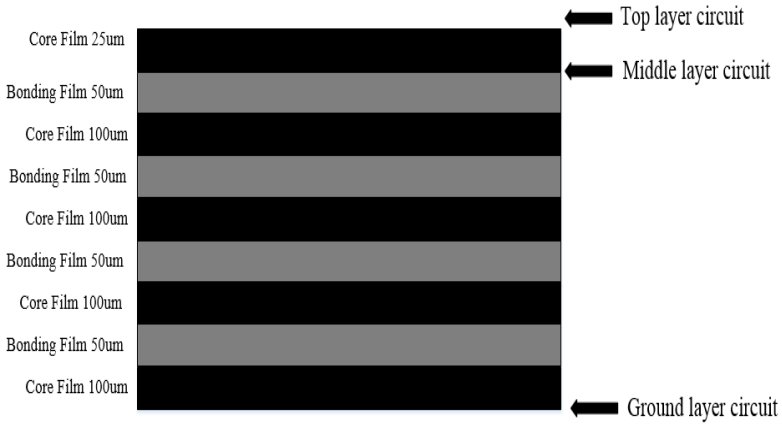

Figure 2.23: Multilayer structures of the proposed filter.

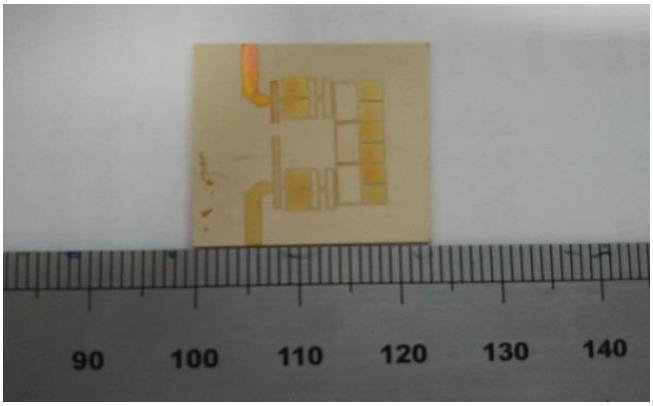

Figure 2.24: A photograph of the fabricated five-pole slow-wave open-loop resonator filter using multilayer LCP technology.

The photo of the fabricated filter is shown in Figure 2.24. The size of circuit area of this filter is about 15mm by 12mm ($0.102\lambda_g \times 0.081\lambda_g$), where λ_g is the guided wavelength of a 50-Ω line on the substrate at the midband frequency. The weight of the filter is less than 1 gram due to the LCP fabricate technologies and the thickness is only 0.625mm, which is very compact size.

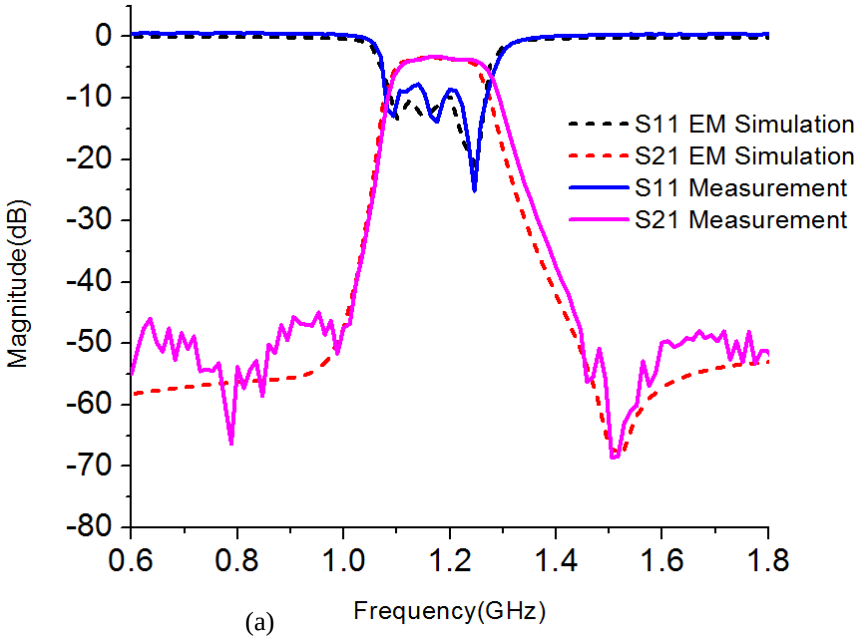

(a)

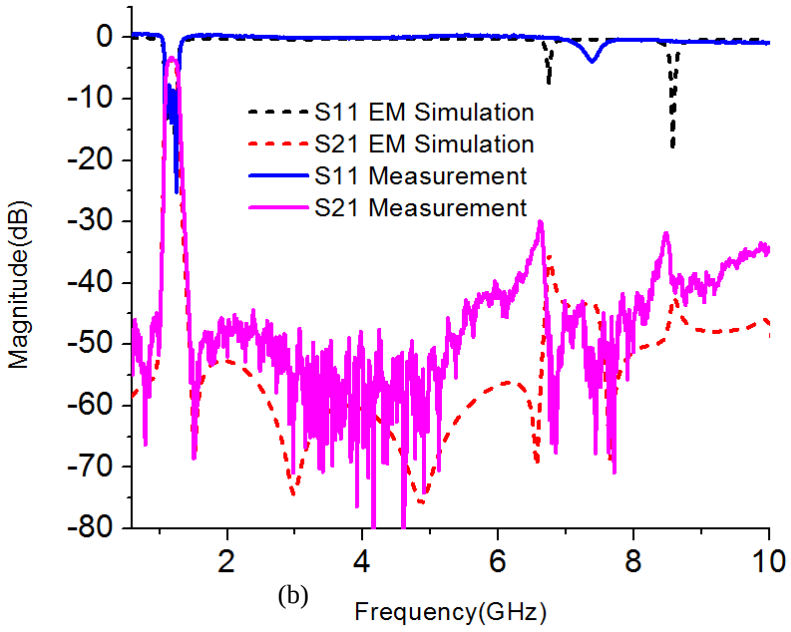

(b)

Figure 2.25: Comparison results between EM simulation and Measurement. (a) Narrowband. (b)Wideband.

The simulated and measured results are shown in Figure 2.25. The measured results have a good agreement with the simulation results. The fabricated filter is centred at 1.18GHz with 3-dB bandwidth of 16%. It has a 30dB rejection upper stopband from $2f_0$ to 10GHz. A performance comparison of the fabricated filter with some reported works is given in Table 2.4.

Table 2.4: Comparison with other publication works.

	Techniques	f_0 (GHz)	Stopband width @rejection (dB)	Selective	Size (mm^2)
[43]	Wiggly-line	2.5	5.6× f_0@30dB	Good	~50 × 20
[44]	Periodic floating metal between coupled lines	2	2.8× f_0@40dB	Poor(3-pole Chebyshev)	~50 × 10
[45]	High/low (radial) impedance (LPF+HPF)	0.9	14× f_0@20dB	Poor(Equivalent to a 3-pole Chebyshev)	~30 × 18
This work	Slow-wave open-loop resonator	1.18	3× f_0@40dB 8.5× f_0@30dB 16.9× f_0@20dB	Good	~15 × 12

2.5 Summary

In this chapter, we have proposed a new microstrip bandpass filter using slow-wave open-loop resonator. It has been shown that the slow-wave effect makes the filter more compact, whereas the dispersion effect results in a wider upper stopband. We have designed and fabricated a five-pole bandpass filter of this type. The measured results show good agreement with the simulation results, which has verified that this filter has not only very compact size, but also a wider upper stopband performance.

Reference

[1] S. Qian, G. Brand, J.-S. Hong and P. Meyer, “The design of miniature multilayer bandpass filter with mixed couplings”, *IEEE Trans. Microw. Theory Tech.*, vol. 61, no. 12, pp. 4072-4078, Dec. 2013.

[2] S. Qian and J.-S. Hong, “Miniature quasi-lumped element wideband bandpass filter at 0.5–2 GHz band using multilayer liquid crystal polymer technology”, *IEEE Trans. Microw. Theory Tech.*, vol. 60, no. 9, pp. 2799–2807, Sep. 2012.

[3] H. Joshi and W. J. Chappell, “Dual-band lumped-element bandpass filter”, *IEEE Trans. Microw. Theory Tech.*, vol. 54, no. 12, pp. 4169–4177, Dec. 2006.

[4] L. K. Yeung and K. L. Wu, “A compact second-order LTCC bandpass filter with two finite transmission zero”, *IEEE Trans. Microw. Theory Tech.*, vol. 51, no. 2, pp. 337–341, Feb. 2003.

[5] C.-W. Tang, C.-W. Shen, and P.-J. Hsieh, “Design of low-temperature co-fired ceramic bandpass filters with modified coupled inductors”, *IEEE Trans. Microw. Theory Tech.*, vol. 57, no. 1, pp. 172–178, Jan. 2009.

[6] M. Sagawa, K. Takahashi, and M. Makimoto, “Miniaturized hairpin resonator filters and their application receiver front-end MIC‘s”, *IEEE Trans. Microw. Theory Tech.*, vol. 37, no. 12, pp. 1991–1997, Dec.1989.

[7] A. Djaiz and T. A. Denidni, “A new compact microstrip two-layer bandpass filter using aperture-coupled SIR-hairpin resonators with transmission zeros”, *IEEE Trans. Microw. Theory Tech.*, vol. 54, no. 5, pp. 1929–1936, May 2006.

[8] J.-S. Hong and M. J. Lancaster, “Microstrip bandpass filter using degenerate modes of a novel meander loop resonator”, *IEEE Microw. Guided Wave Lett.*, vol. 5, no. 11, pp. 371–372, Nov. 1995.

[9] L. Zhu, C. T. Boon and S. J. Quek, “Miniaturized dual-mode bandpass filter using inductively loaded cross-slotted patch resonator”, *IEEE Microw. Wireless Compon. Lett.*, vol. 15, no. 1, pp. 22–24, Jan. 2005.

[10] S.-W. Fok, P. Cheong, K.-W. Tam and R. P. Martins, “A novel microstrip square-loop dual-mode bandpass filter with simultaneous size reduction and spurious response suppression”, *IEEE Trans. Microw. Theory Tech.*, vol. 54, no. 5, pp. 2033–2041, May 2006.

[11] W.-L. Chen and G.-M. Wang, “Effective design of novel compact fractal-shaped microstrip coupled-line bandpass filters for suppression of the second harmonic”, *IEEE Microw. Wireless Compon. Lett.*, vol. 19, no. 2, pp. 74–76, Feb. 2009.

[12] I. Kim, “Fractal-shaped microstrip coupled-line bandpass filters for suppression of second harmonic”, *IEEE Microw. Wireless Compon. Lett.*, vol. 53, no. 9, pp. 2943–2948, Sep. 2005.

[13] J.-S. Hong and M. J. Lancaster, “Theory and experiment of novel microstrip slow-wave open-loop resonator filters”, *IEEE Trans. Microw. Theory Tech.*, vol. 45, no. 12, pp. 2358 – 2365, Dec 1997.

[14] L. H. Hsieh and K. Chang, “Slow-wave bandpass filters using ring or stepped-impedance hairpin resonators”, *IEEE Microw. Wireless Compon. Lett.*, vol. 50, no. 7, pp. 1795–1800, Jul. 2002.

[15] J. Wang, J.-L. Li, J. Ni, S. Zhao, W. Wu, and D. Fang, “Design of miniaturized microstrip dual-mode filter with source-load coupling”, *IEEE Microw. Wireless Compon. Lett.*, vol. 20, no. 6, pp. 319–321,Jun. 2010.

[16] J. P. Wang, B. Z. Wang, Y. X. Guo, L. C. Ong, and S. Q. Xiao, “A compact slow-wave microstrip branch-line coupler with high performance”, *IEEE Microw. Wireless Compon. Lett.*, vol. 17, no. 7, pp. 501–503, Jul. 2007.

[17] J.-S. Hong and M. J. Lancaster, “Aperture-coupled microstrip open loop resonators and their applications to the design of novel microstrip bandpass filter”, *IEEE Trans. Microw. Theory Tech.*, vol. 47, no. 9, pp. 1848–1855, Sep. 1999.

[18] W. Schwab and W. Menzel, “Compact bandpass filters with improved stop-band characteristics using planar multilayer structures”, *IEEE Int. Microw. Symp. MTT-S.*, 1992, Albuquerque, pp. 1207-1209.

[19] C. Cho and K. C. Gupta, “Design methodology for multilayer coupled line filters”, *IEEE Int. Microw. Symp. MTT-S.*, June 1997, pp. 785–788.

[20] N. Karmakar, S. M. Roy, and I. Balbin, “Quasi-static modeling of defected ground structure”, *IEEE Trans. Microw. Theory Tech.*, vol. 54, no. 5, pp. 2160–2168, May 2006.

[21] D. Ahn, J. S. Park, C. S. Kim, J. N. Kin, Y. Qian, and T. Itoh, “A design of the low-pass filter using the novel microstrip defected ground structure”, *IEEE Trans. Microw. Theory Tech.*, vol. 49, no. 1, pp. 86–93, Jan. 2001.

[22] C. Caloz, H. Okabe, T. Twai and T. Itoh, “A simple and accurate model for microstrip structures with slotted ground plane”, *IEEE Microw. Wireless Compon. Lett.*, vol. 14, no. 4, pp. 133–135, Apr. 2004.

[23] LTCC consulting, http://www.ltcc-consulting.com/What_is_the_LTCC.

[24] W. Tung, Y. Chiang and J. Cheng, “A new compact LTCC bandpass filter using

negative coupling", *IEEE Microw. Wireless Compon. Lett*., vol. 15, no. 10, pp. 641–643, Oct. 2005.

[25] G. Brzezina, L. Roy and L. MacEachern, "A miniature LTCC filter using novel resonators for GPS applications", *in Eur. Microw. Conf*., Oct. 2007, pp. 536–539.

[26] C. W. Tang, Y. C. Lin and C.Y. Chang, "Realization of transmission zeros in combine filters using an auxiliary inductively coupled ground plane", *IEEE Trans. Microw. Theory Tech.*, vol. 51, no. 10, pp. 2112–2118, Oct. 2003.

[27] A. Sutono, J. Laskar, and W. R. Smith, "Development of three dimensional integrated Bluetooth image reject filter", *IEEE Int. Microw. Symp. MTT-S.*, Boston, May, 2000, pp. 339–342.

[28] Y. C. Zhang and A. Kantar., "LTCC multi-layer coupled strip-resonator filters", *IEEE Int. Microw. Symp. MTT-S.*, pp. 1039-1042, June 2007.

[29] Dane Thompson, "Characterization and design of liquid crystal polymer (LCP) based multilayer RF components and packages", Doctor of Philosophy thesis, University of Georgia Institute of Technology, 2006.

[30] L. K. Yeung, K.-L. Wu, and Y. E. Wang, "Lowtemperature cofired ceramic LC filters for RF applications," *IEEE Microw. Mag.*, vol. 9, no. 5, pp. 118 –128, Oct. 2008.

[31] J.-S. Hong, "Microstrip Filters for RF/Microwave Application," *Second Edition, Wiley*, 2010.

[32]D. Thompson, O. Tantot, H. Jallageas, G. Ponchak, M. Tentzeris, and J. Papapolymerou, "Characterization of liquid crystal polymer (LCP) material and transmission lines on LCP substrates from 30 to 110 GHz," *IEEE Trans. on Micro. Theory and Tech.*, vol. 52, no. 4, pp. 1343–1352, Apr. 2004.

[33] Z.-C. Hao and J.-S. Hong, "Ultra-wideband bandpass filter using multilayer liquid-crystal-polymer technology", *IEEE Trans. Microw. Theory Tech.*, vol. 56, no. 9, pp. 2095–2100, Sep. 2008.

[34] Z.-C. Hao and J.-S. Hong, "Ultra wideband bandpass filter using embedded stepped impedance resonators on multilayer liquid crystal polymer substrate", *IEEE Microw. Wireless Compon. Lett.*, vol. 18, no. 9, pp. 581–583, Sep. 2008.

[35] Z.-C. Hao and J.-S. Hong, "Compact wide stopband ultra wideband bandpass filter using multilayer liquid crystal polymer technology", *IEEE Microw. Wireless Compon. Lett.*, vol. 19, no. 5, pp. 290–292, May 2009.

[36] Z.-C. Hao and J.-S. Hong, "UWB bandpass filter using cascaded miniature high-pass

and low-pass filters with multilayer liquid crystal polymer technology", *IEEE Trans. Microw. Theory Tech.*, vol. 58, no. 4, pp. 941–948, Apr. 2010.

[37] M. Makimoto and S. Yamashita, "Bandpass Filters Using Parallel Coupled Stripline Stepped Impedance Resonators", Microwave Theory and Techniques, IEEE Transactions on, vol. 28, pp. 1413-1417, 1980.

[38] J.-S. Hong and M. J. Lancaster, "End-coupled microstrip slow-wave resonator filter", Electronics Letters, vol. 32, pp. 1494-1496, 1996.

[39] J.-S. Hong and M. J. Lancaster, "Theory and experiment of novel microstrip slow-wave open-loop resonator filters", Microwave Theory and Techniques, IEEE Transactions on, vol. 45, pp. 2358-2365, 1997.

[40] A. F. Harvey, "Periodic and Guiding Structures at Microwave Frequencies", Microwave Theory and Techniques, IRE Transactions on, vol. 8, pp. 30-61, 1960.

[41] Microwave office AWR.

[42] Sonnet software.

[43]T. Lopetegi, M.A.G. Laso, F. Falcone, F. Martin, J. Bonache, J. Garcia, L. Perez-Cuevas, M. Sorolla, and M. Guglielmi, "Microstrip "wiggly-line" bandpass filters with multispurious rejection," *IEEE Microwave and Wireless Components Letters*, vol. 14, no. 11, pp.531 – 533, Nov. 2004.

[44] T. Yamaguchi, T. Fujii, T. Kawai, and I. Ohta, "Parallel-coupled microstrip filters with periodic floating-conductors on coupled-edges for spurious suppression," in *IEEE MTT-S International Microwave Symposium Digest*, 2008.

[45] J. Xu, Y.-X. Ji, W. Wu, and C. Miao, "Design of miniaturized microstrip LPF and wideband BPF with ultra-wide stopband," *IEEE Microw. Wireless Compon. Lett*, vol. 23, no. 8, pp. 397–399, Aug. 2013.

CHAPTER 3
Microstrip Extracted-Pole Lossy Filter

3.1 Introduction

There are increasing demands for advanced RF/microwave filters other than conventional lossless synthesis filters in modern wireless communications systems. Conventional lossless filter synthesis has been focused for years, which can be regarded as "matured" to some extent that any filter transfer function being synthesized to the desired filter topology using exact synthesis procedures [1]-[3]. However, the lossless synthesis filter is designed in the limitation of microwave filter itself without considering from the perspective of the whole system, which can reduce the system compatibility and unnecessary loss.

The rapid development of mobile and wireless communications has stimulated increasing requirements for compact and high performance microstrip bandpass filter [4]. Normally, for microstrip line filters, the quality factor can achieve no more than 250 (this value is got by my own testing) using conventional conductors and dielectric substrates, which means that taking the limited resonators quality factor (Q) into consideration in filter design is desired. This is because that higher Q often suffers from bigger resonator sizes to make the overall size larger, while lower Q usually leads to degraded insertion loss performance in the passband and rounding passband edges, especially in narrowband filters [5], [6]. Accepting some additional insertion loss and knowing the fact that the loss can be compensated for by the already-existing microwave amplifiers in the system [7], [8], the sharp response of the filter transmission can be restored. The lossy circuit extraction techniques can be used to improve the return loss by using non-uniform dissipation and modified topologies with additional loss.

In this chapter, a new type of microstrip extracted-pole lossy filter is presented [9]. The new type of lossy filter is realized by introducing resistive cross couplings into a microstrip extracted-pole filter to achieve a flat passband. The high selectivity is

achieved by introducing two transmission zeros using two extracted poles, which can be adjusted. It is also found that the additional loss introduced by the resistive cross couplings is independent with the selectivity controlled by the two extracted poles, which means the selectivity can be adjusted as the fractional bandwidth (FBW) changes without affecting the flat passband insertion loss.

In this chapter, microwave filter design from a system perspective is presented and discussed. After that, Microwave lossy technology is discussed in more detail and the conventional approaches to realize in microstrip filter are also described following by some examples. Moreover, the extracted-pole method is introduced with a design example. Two microstrip extracted-pole lossy filters operating at 2 GHz with fractional bandwidth (FBW) 6% and 20% are analysed. These two filter performance will be compared. Simulation tools [10] [11] have been used for theory circuit model and full-wave electromagnetic (EM) simulations. These two filters have been fabricated in standard printed circuit board (PCB) technology. Experimental results, together with a theoretical comparison between different FBWs are also presented.

3.2 Filter Design from System Perspective

Consider microwave filters being used in the receive side cascaded with the low noise amplifier (LNA) for interference filtering and signal channelization. For a conventional filter and amplifier cascade structure shown in Figure 3.1(a), a low-loss filter (Filter 1) is often placed before the LNA. The absolute insertion loss of the filter 1, also known as the preselect filter, can result in more negative effect on the overall noise figure of the receiver. Although higher Q resonators such as cavity or coaxial resonators may be used in the preselect filter design to achieve a lower insertion loss and sharper band edge roll-off, mass and volume are also very critical considerations from a physical perspective. The absolute insertion loss in the passband is often a secondary parameter that can be traded for size reduction. Alternatively, to reduce the insertion loss of the preselect filter, the other requirements of the first filter can be relaxed by moving, for instance, some selectivity and out-of-band rejection requirements to the second filter

(Filter 2). In this case, the absolute insertion loss value of the filter 2 is no longer critical since the LNA can easily make up the loss of the filter by setting the gain to a higher value, while the most critical electrical parameters are in band performance such as the insertion loss variation and the sharper band edge rolloff. Another approach has emerged to split the amplifier into two stages with a filter in between as shown in Figure 3.1(b), which makes it also possible to enhance the performance or at least maintain similar performance by using lower Q resonators for the filter design.

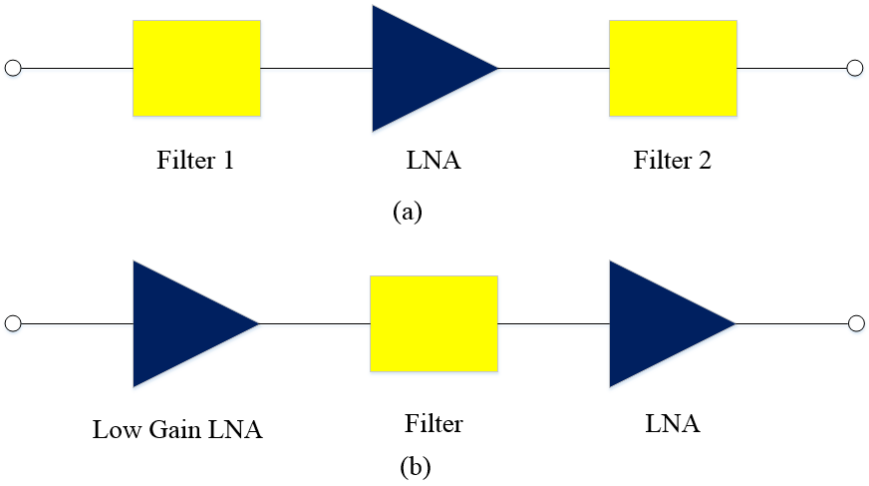

Figure 3.1: Distributed filter with (a) two filter and (b) two LNAs.

The most promising approaches are adaptive pre-distortion and lossy circuit techniques by trading the absolute insertion loss to improve the passband performance. Before further discussion of these two technologies, the effect of loss on filter performance is described below.

Losses can shift the poles and zeros of the transfer function to the left on the complex plane [5] [6]. The effects become more significant at frequencies where the group delay is large, which can be seen as a rounding passband edges and a decrease in maximum stopband attenuation. As group delay is inversely proportional to the bandwidth, these effects become more obvious in narrowband filters.

The adaptive pre-distortion technique [13]-[16] assumes no change to the filter topology resulted in degraded return loss performance. With this technique, the poles of the transfer function are shifted to the right of the complex plane. A lossless filter is then

synthesized. The addition of uniform dissipation loss results in S_{12} of the network having an ideal response other than for increased absolute insertion loss. This technique is useful for applications where the increased passband insertion loss can tolerated. The disadvantage of pre-distortion is that the selectivity increase is realized by reflecting power in the passband, which results in decreased in-band return loss. As a result to compensate for the return loss performance, in practice, pre-distorted filters are usually connected with nonreciprocal devices such as isolators and circulators. It should be noted that since the dissipation loss of a network with uniform dissipation (i.e., constant resonator Q) is proportional to its group delay, then the only way to compensate for losses in such a network is to differentially reflect energy at certain frequencies.

An alternative approach to improve the response is using lossy circuit techniques [5]-[8]. These methods use non-uniform dissipation and modified topologies with additional loss to improve return loss. The main aim of lossy technology is to accept additional insertion loss and/or return loss without changing the passband shape of the filter function knowing that the added loss level can be adjusted using amplifiers in the communication system without affecting the system performance. Compared with pre-distortion, this lossy synthesis is based on the absorption rather than the reflection of power, which can improve return loss. The principle of microwave lossy synthesis consists of adding and distributing losses into the coupled resonators network based on a lossless-like transfer function. There are two normal ways to realizing microwave lossy filter: one is using resistive cross couplings (RCCs) to introduce losses in inline network and the other is using non-uniform Q resonators in transversal network. These two methods can be also mixed in some complex designs.

In the following section, the microwave lossy technology will be discussed in detail presenting physical insights for lossy filter design to create filters with finite Q resonators and resistive cross couplings.

3.3 Microwave Lossy Technology

3.3.1 Lossy Transfer Function

Design methods are needed to help design filters that meet the increasingly stringent demands of modern communication systems. In order to realize optimum performance, resonator losses can't be ignored. Unfortunately, most conventional design techniques do not take losses into account.

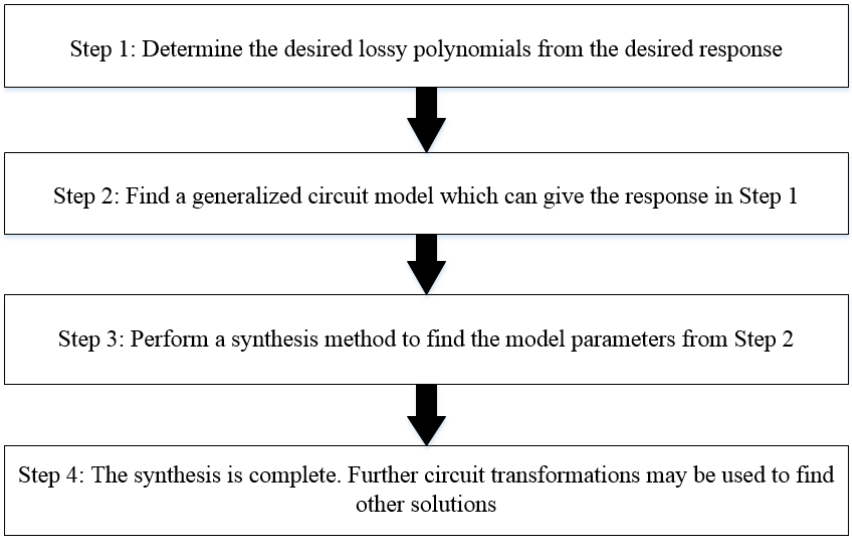

Figure 3.2: Generalized steps for direct synthesis of lossy filters.

The lossy synthesis of microwave filters has recently attracted a lot of attention with promising experimental results. The method starts with a given transfer function. Dissipations included in filter networks introduce rounding at band edge and thus deteriorate the filter's performance. The synthesis of lossy filters is composed of different steps starting from the design requirements to a possible circuit design. Figure 3.2 shows a stepwise approach for a generalized synthesis technique. Based on these steps, two types of synthesis are necessary: polynomial synthesis (Step 1) and circuit synthesis (Step 3). The circuit model is a coupling matrix with complex entries (Step 2). The focus of the theoretical synthesis here is on the circuit synthesis rather than polynomial synthesis.

The theoretical progress for the direct synthesis of lossy polynomials in the literature [7] have been so far limited to multiplying both reflection and transmission polynomials of a lossless function by a constant attenuation factor of $K < 1$ as

$$S_{11\_lossy} = KS_{11\_lossless}$$
$$S_{21\_lossy} = KS_{21\_lossless} \tag{3.1}$$

This is the simplest lossy scattering polynomial resulting in same-order admittance polynomials and thus is most commonly used. From the network perspective, this special case is equivalent to placing two identical matched attenuators at input and output ports of a lossless filter with attenuation factors of $\sqrt{K}$, as in Figure 3.3.

The two identical matched attenuators can then be made using different kinds of resistive networks. By doing some network transformations, the resistive sections can be placed as two shunt resistors at source/load as well as the first/last resonator of the lossless filter. This method is also suitable for an initial lossy coupling matrix synthesis for cases, where both reflection and transmission coefficients are multiplied by K.

Figure 3.3: Equivalent lossy filter network with same attenuation.

This case, however, is not the most general form of lossy polynomials. The shape of these functions may be different from standard filtering functions but still satisfy the design specifications. In some other practical cases, different loss levels for reflection and transmission functions may be required if a lossy filter is to be realized, such as the channel-dropping input multiplexers (IMUX), where a 0-dB out-of-band reflection is crucial. These types of lossy circuits can't be universally synthesized using the attenuator configuration in Figure 3.3.

This new class of microwave filters has been proposed in [17]-[29], and can be realized and divided into two families. Additional losses are introduced either in

individual resonators, forming a network with non-uniform Q resonators [17]-[19], or distributed through resistive cross couplings (RCCs) [6], [19], [20]. In the following section, the two approaches are described with theory design examples.

3.3.2 Resistive Cross Coupling in Inline Network

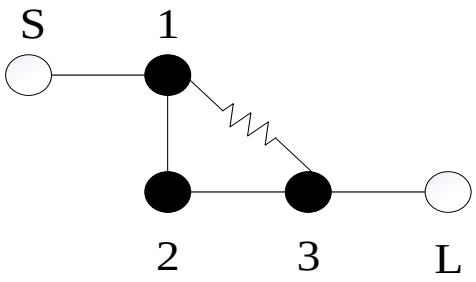

(a)

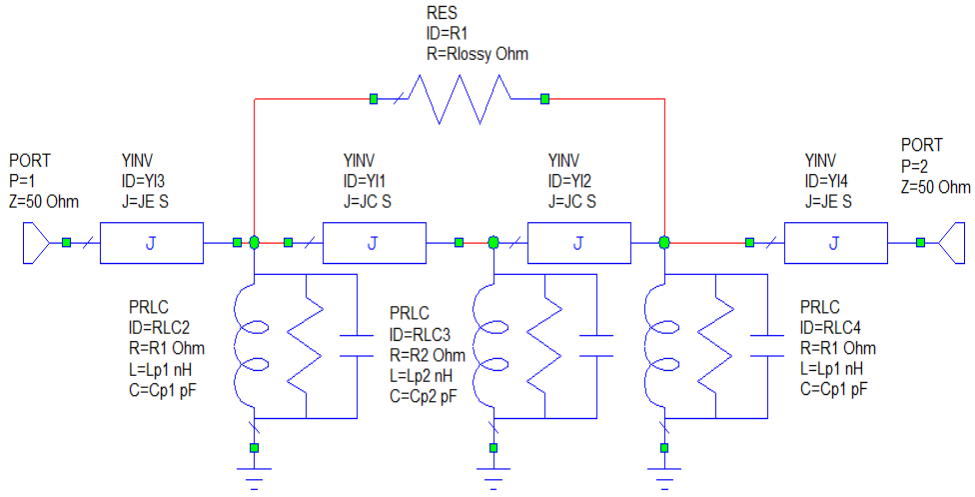

(b)

Figure 3.4: Three-pole lossy filter (a) coupling diagram and (b) equivalent circuit model.

The introduction of RCCs in the network allows adjusting the flatness in the passband. For example, a three pole lossy filter with RCC centred at 1 GHz with a fractional bandwidth (FBW) of 10% is demonstrated. The coupling diagram is given in Figure 3.4 (a). Node 1, 2, 3 are resonators in the inline network with a RCC between node 1 and 3. The equivalent circuit model is shown in Figure 3.4(b) with all units for each parameters. The couplings between resonators (coupling coefficient), represented by JC , and couplings between the resonators and feed lines (the external Q factor), represented by JE , need to be extracted to achieve a desired response. Based on the method described in [4], the initial circuit elements values can be calculated shown in Table I.

The comparison of response with/without RCC is presented in Figure 3.5. It can be seen that the introduction of RCC makes the passband insertion loss flat and the FBW is a little bit smaller due to the increase of the absolute insertion loss and the change of the coupling coefficient affected by the RCC. At the meantime, because of the loss of RCC is more sensitive than the coupling coefficient, there are only two poles shown in the return loss while there are three poles observable without RCC.

Table 3.1: Elements value for lossy synthesis

JE	0.0342 S	Cp2	55.96 pF	R1	100 Ω
JC	0.0334 S	Lp1	0.2199 nH	R2	100 Ω
Cp1	115.2 pF	Lp2	0.4527 nH	Rlossy	100 Ω

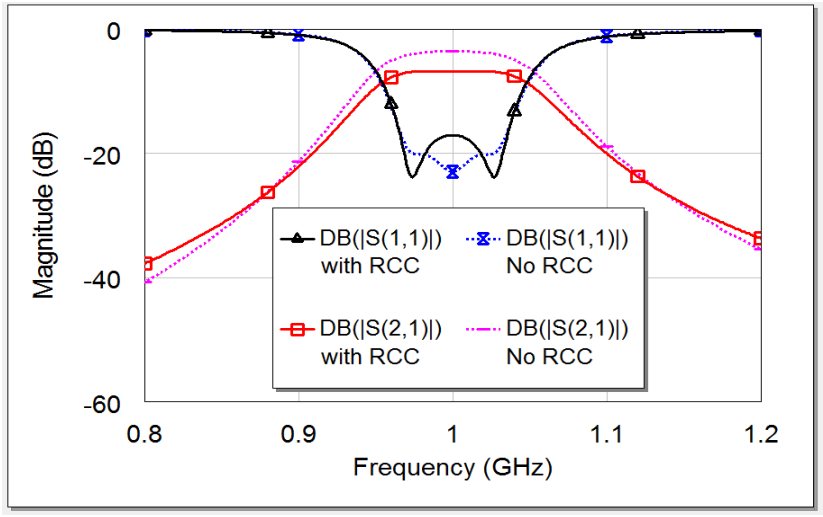

(a)

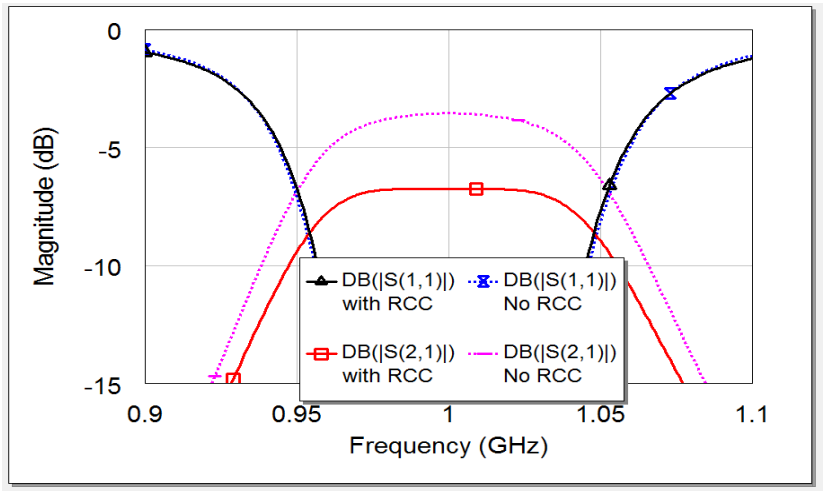

(b)

Figure 3.5: (a) Lossy synthesis performance with/without RCC and (b) zoom in passband.

The comparison of response with/without RCC is presented in Figure 3.5. It can been seen that the introduction of RCC makes the passband insertion loss flat and the FBW is a little bit smaller due to the increase of the absolute insertion loss and the change of the coupling coefficient affected by the RCC. At the meantime, because of the loss of RCC is more sensitive than the coupling coefficient, there are only two poles shown in the return loss while there are three poles observable without RCC.

Another clear way to verify that the RCC can adjust the flatness in the passband is displayed in Figure 3.6, which demonstrates how the different resistor values of RCC can change insertion loss performance. There are also some mismatching. As we can see, the passband performance has a quite different change as the resistor value changes, and attains a good flatness when resistor value is 100 Ω. When the resistor value is 500 Ω, the insertion loss in the passband is upper round, which means the loss introduced by the RCC to the mid-band is not sufficient to flat the passband. On the other hand, when the resistor value is 50 Ω, the insertion loss in the passband is lower round, indicating too much loss being introduced to the mid-band by the RCC. The group delay performance against different values of RCC is illustrated in Figure 3.7. It is clear to see that the larger the resistive loss introduced by the RCC, the larger the group delay across the passband.

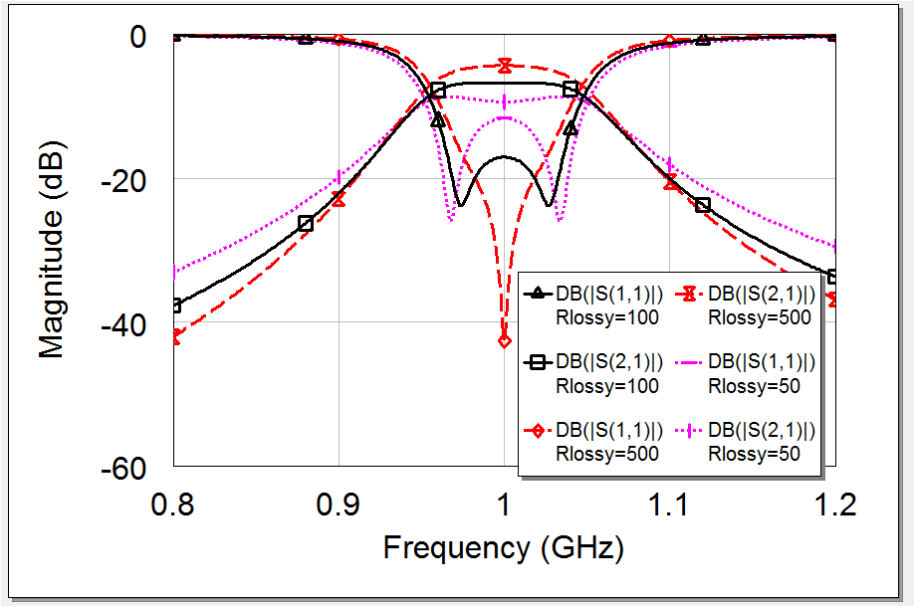

Figure 3.6: Lossy synthesis performance with different values of RCC.

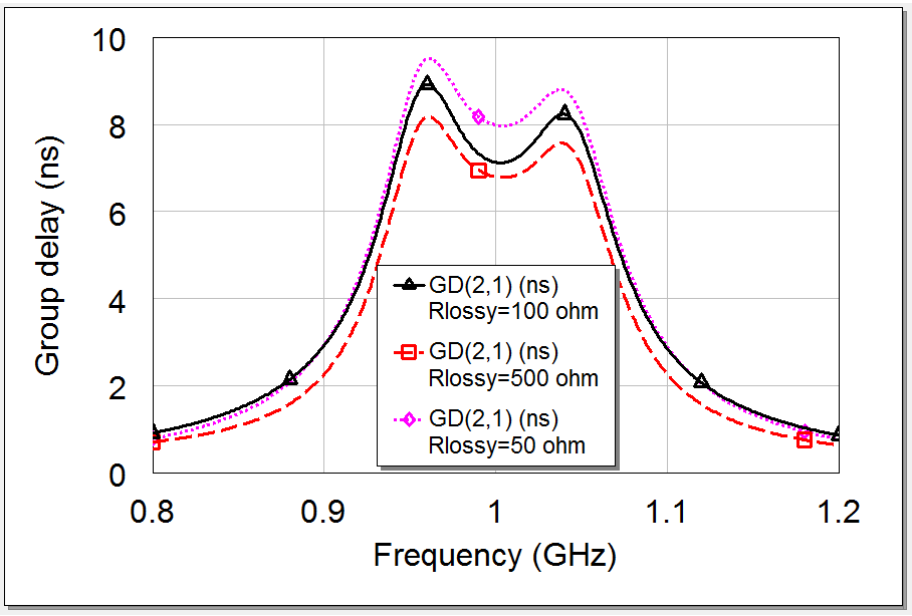

Figure 3.7: Group delay performance against different value of RCC.

3.3.3 Non-Uniform Q Resonators for Transversal Network

In the case of a transversal network, the signal follows multiple paths so that each path contributes in the filter response almost independently. Using a transversal pair network, the path comprising the stronger coupled resonators mainly contributes to insertion loss in the passband edges. For these resonators, the higher the Q, the higher the selectivity. Moreover, the insertion loss is also maximized in the passband edges; consequently these resonators need to be high Q. Other paths, i.e., with weakly coupled resonators, contribute to insertion loss in the middle of the passband. As a result, the quality factor of such resonators can be degraded for increasing the insertion loss in the middle of the passband, reducing by this way the insertion loss variation in the bandpass filter response.

The transversal pair network presented in Figure 3.8 can be synthesized as a lossy filter network by optimizing a coupling matrix obtained from a general Chebyshev filtering function. There are two transversal paths between the source and the load: one has two low Q coupled resonators (path 1) and the other path has two high Q coupled resonators (path 2). Therefore, the path 1 contributes the insertion loss in the middle of the passband, while path 2 affects the passband edges performance. With the compensation of these two paths, the passband insertion loss can be adjusted to be flat.

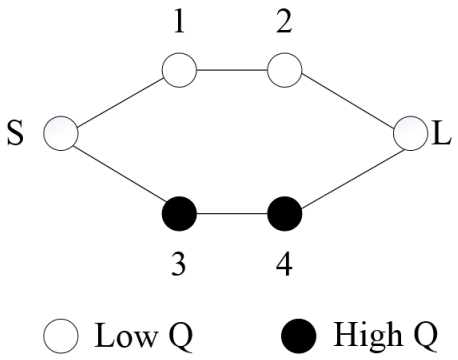

Figure 3.8: Four-pole transversal network with non-uniform Q resonators.

Initially, a coupling matrix with uniform Q resonators is considered. The synthesis consists of optimizing the couplings and the Q of each pair for achieving the desired performances. Figure 3.9 shows the equivalent lump circuit model of this topology defined with microwave office AWR [10], where L_m, C_m (m = 1 and 2) are the circuit parameters of resonators with R_m representing the resonator loss. The J-inverter has been used to represent the coupling between two uniform Q resonators in each path. The synthesis parameters value are given in Table II when the low Q and high Q are 530 and 590 respectively.

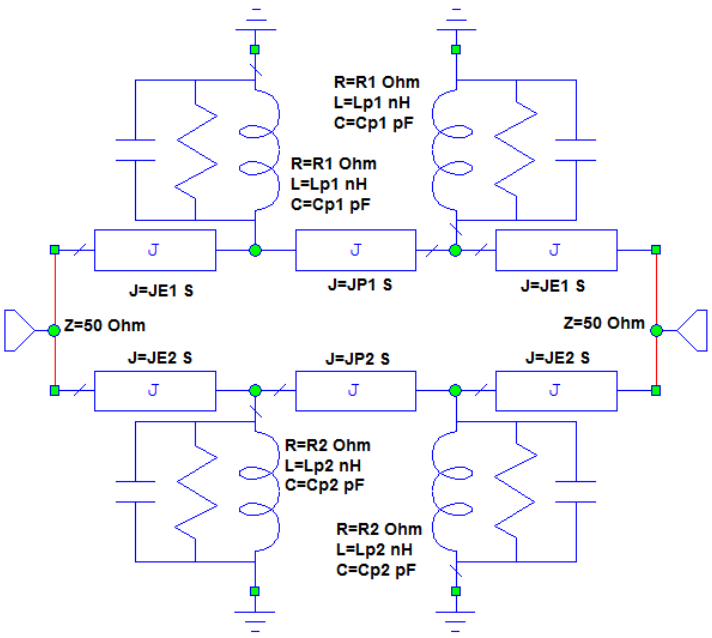

Figure 3.9: The equivalent circuit model of four-pole transversal network with non-uniform Q resonators.

Table 3.2: Elements value for four-pole transversal network.

JE1	0.031 S	Lp1	0.3568 nH	Lp2	0.3654 nH
JE2	0.0247 S	Cp1	70.98 pF	Cp2	69.33 pF
JP1	-0.035 S	Q1	530	Q2	590
JP2	0.0784 S	R1	1188 Ω	R2	1354 Ω

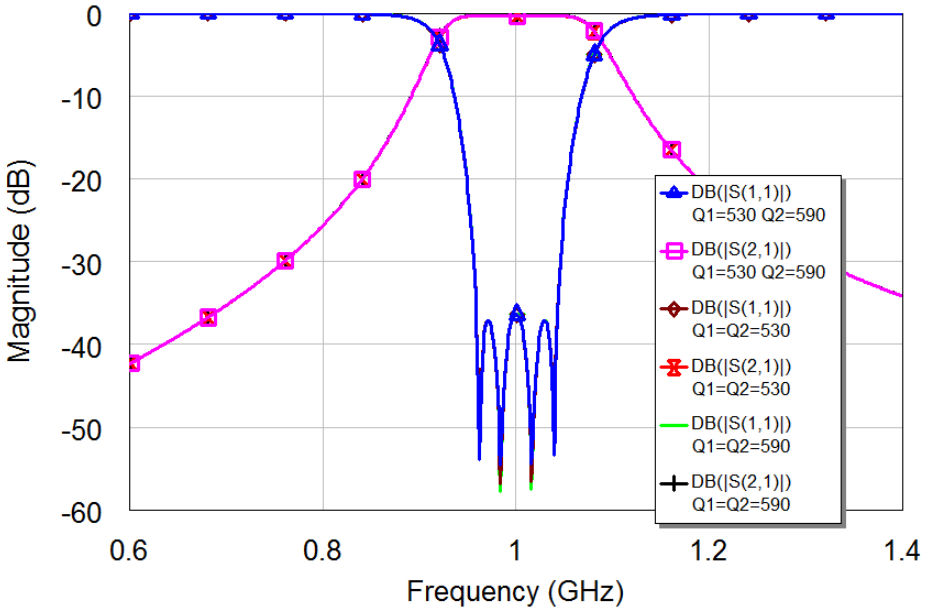

(a)

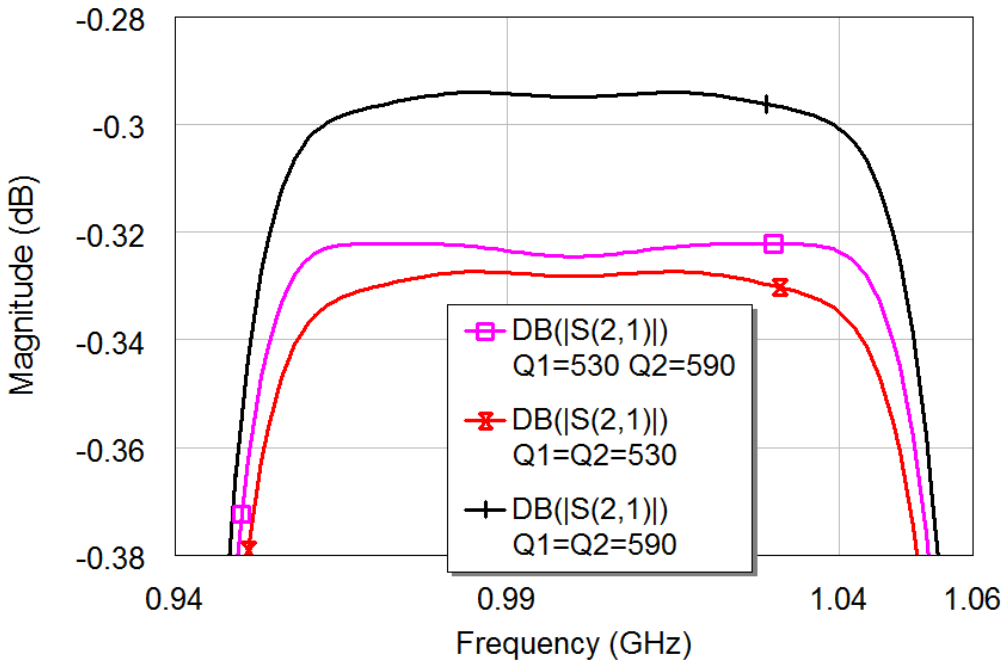

（b）

Figure 3.10: (a) Circuit response of four-pole transversal network with uniform/ non-uniform Q resonators and (b) zoom in passband.

The circuit responses of this four-pole transversal network with uniform/non-uniform Q resonators are compared in Figure. 3.10. Note that only Q1 and Q2 are changed in the circuit model for plotting these responses. It can be seen that the transversal network with non-uniform Q has improved performance in terms of flatness while maintaining a similar selectivity and return loss level.

3.4 Extracted-pole Technology

Extracted pole filters [30]-[32] are well known to generate the transmission zeros (Tzs) by dangling resonators rather than cross couplings [33] in a specified topology. Benefiting from this feature, filter design with extracted pole techniques can have a very flexible layout. It is useful for many applications, especially when a cross-coupled topology can't be realized because of the restricted mechanical configuration. Furthermore, every Tz is uniquely linked to the resonant frequency of the dangling resonator, so it can be controlled independently. Because of this, a less sensitive network can be obtained.

The basic idea of extracted pole synthesis theory was first developed in [30] and the complete description of the synthesis procedure can be found in [31]. Additional corrections are proposed in [34] for fully canonical cases. References [35]-[38] developed the non-resonating node (NRN) synthesis technique, which is indicated that extracted pole and NRN synthesis techniques are mathematically equivalent by [31]. Recently, [39] presented an approach to synthesize the cross-coupled network with both resonator nodes and NRN nodes.

The NRN synthesis combines extracted pole and coupling matrix theory. Although this technique has been used, there is no explicit design procedure because it is hard to find a physical structure to accurately link with the extracted poles in the synthesized prototype.

3.4.1 Synthesis Procedure

Different from the coupling matrix prototype, the extracted pole technique introduce the pole producing elements to generate the finite transmission zeros rather than using cross coupling [4]. There are two types of extraction cycles required in the synthesis procedure. The initial cycle involve extracting a conjugate pair of finite j-axis zeros from the remaining cross-coupled network in a cascaded manner. This cycle may be repeated until either all or desired finite j-axis zeros have been extracted. After this, the second type of extraction cycle, which aims to synthesize the remaining network as a cross-coupled network with complex conjugate symmetry is performed and repeated until the network has been completely synthesized. The synthesis procedure will be detail here.

The equivalent network for extracting the phase shifters is presented in Figure 3.11(a). The remaining network is denoted by N', from which a phase shifter of angle $-\theta$ has been extracted from the input and a phase shifter of angle of θ has been extracted from the output in Figure 3.11(b). When the network N is represented by a frequency invariant matrix $\begin{bmatrix} a & b \\ c & d \end{bmatrix}$, the remaining network N' has a new normalized ABCD matrix of the form

$$\begin{bmatrix} a' & b' \\ c' & d' \end{bmatrix} = \begin{bmatrix} \cos\theta & j\sin\theta \\ j\sin\theta & \cos\theta \end{bmatrix} \cdot \begin{bmatrix} a & b \\ c & d \end{bmatrix} \cdot \begin{bmatrix} \cos\theta & -j\sin\theta \\ -j\sin\theta & \cos\theta \end{bmatrix} \tag{3.2}$$

$$= \begin{bmatrix} a\cos^2\theta + d\sin^2\theta + j\sin\theta\cdot\cos\theta\cdot(c-b) & b\cos^2\theta + c\sin^2\theta + j\sin\theta\cdot\cos\theta\cdot(d-a) \\ c\cos^2\theta + b\sin^2\theta + j\sin\theta\cdot\cos\theta\cdot(a-d) & d\cos^2\theta + a\sin^2\theta + j\sin\theta\cdot\cos\theta\cdot(b-c) \end{bmatrix}$$

In order to extract the frequency invariant admittances from the input and output of the remaining network N', we need to perform a detail equivalent transformations of Figure 3.11 (b), which is shown in Figure 3.12. A shunt admittance of Y_1 and Y_2 have been further extracted from the input and output respectively. Therefore, the normalized ABCD matrix of the remaining network denoted by $N''$is

$$\begin{bmatrix} a'' & b'' \\ c'' & d'' \end{bmatrix} = \begin{bmatrix} 1 & 0 \\ -Y_1 & 1 \end{bmatrix} \cdot \begin{bmatrix} a' & b' \\ c' & d' \end{bmatrix} \cdot \begin{bmatrix} 1 & 0 \\ -Y_2 & 1 \end{bmatrix} = \begin{bmatrix} a' - b'Y_2 & b' \\ c' - a'Y_1 - d'Y_2 + b'Y_1Y_2 & d' - b'Y_1 \end{bmatrix} \tag{3.3}$$

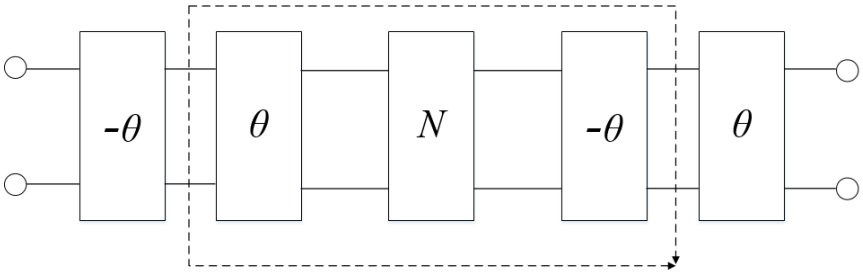

(a)

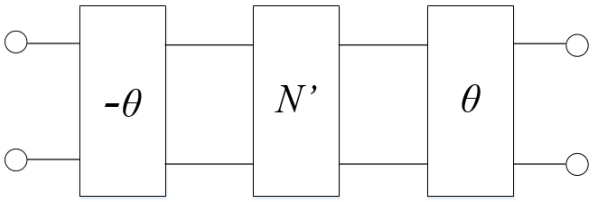

(b)

Figure 3.11: Equivalent networks to extract the phase shifters.

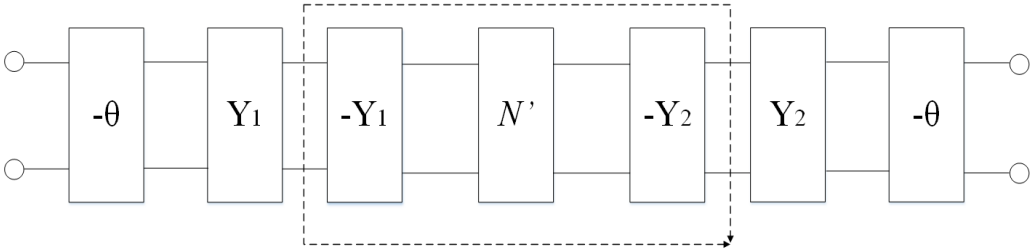

(a)

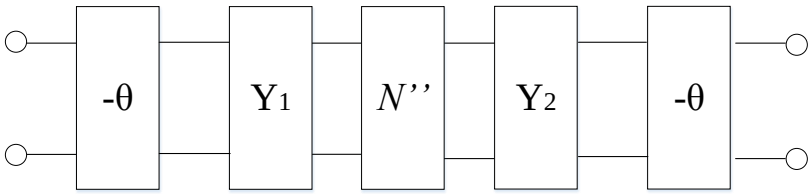

(b)

Figure 3.12: Equivalent networks to extract the frequency invariant admittances.

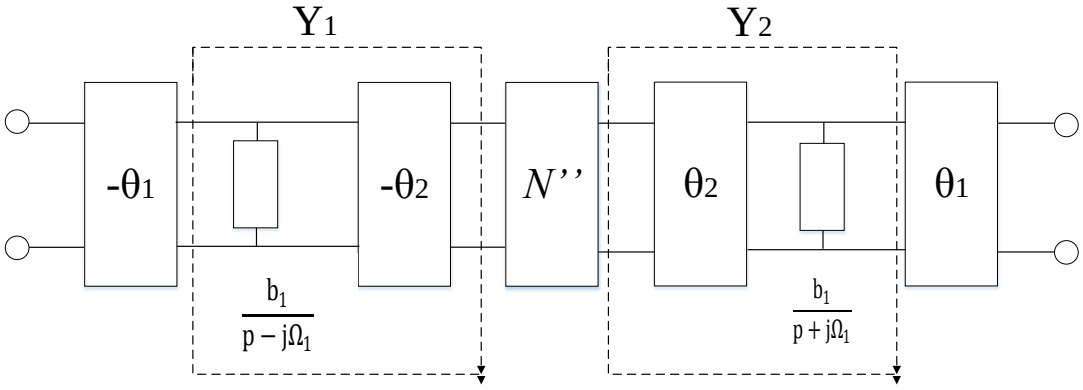

Figure 3.13: Equivalent network of Figure 3.13(b).

When the pair of transmission zeros is at $p = \pm j\Omega_1$ for the first cycle extraction, they can be extracted by the shunt admittances shown in Figure 3.13.

$$Y_1 = \frac{b_1}{p - j\Omega_1}$$
$$Y_2 = \frac{b_1}{p + j\Omega_1} \tag{3.4}$$

where b_1 is a constant, which will be determined later, p is the location of transmission zero and Ω_1 is the cutoff frequency transferred from the lowpass prototype. In Eq. (3.3), because b'' is supposed to be analytical at $p = \pm j\Omega_1$, b' must possess a solution to be 0 when $p = \pm j\Omega_1$. Hence, to find a solution θ_1 for θ , we have

$$b\cos^2\theta_1 + c\sin^2\theta_1 + j\sin\theta_1 \cdot \cos\theta_1 \cdot (d - a)_{|p=\pm j\Omega_1} = 0 \tag{3.5}$$

Dividing by $\cos^2\theta$ at both sides yields

$$b + c\tan^2\theta_1 + j\tan\theta_1 \cdot (d - a)_{|p=\pm j\Omega_1} = 0 \tag{3.6}$$

Since $\mathrm{ad} = \mathrm{bc}$ for the reciprocity from Eq. (3.6), we can obtain a useful solution

$$\tan\theta_1 = \frac{b}{ja}_{|p=-j\Omega_1} \tag{3.7}$$

In this case, $b' = 0$. At the same time, from Eq. (3.3)

$$d'' = d' - b'Y_1 = d' \tag{3.8}$$

Because d'' is also supposed to be analytical under this useful solution at $p = -j\Omega_1$, i.e., this solution results in d'' having a factor of $p = +j\Omega_1$. From Eq. (3.3) and Eq. (3.4), we can have

$$d''(p^2 + {\Omega_1}^2) = d' - b'\frac{b_1}{p - j\Omega_1} \tag{3.9}$$

so that $\lim_{p \to j\Omega_1} d''\left(p^2 + {\Omega_1}^2\right) = 0$, the constant $b_1$is actually a residue given by

$$b_1 = \lim_{p \to j\Omega_1} (p - j\Omega_1)\frac{d'}{b'} \tag{3.10}$$

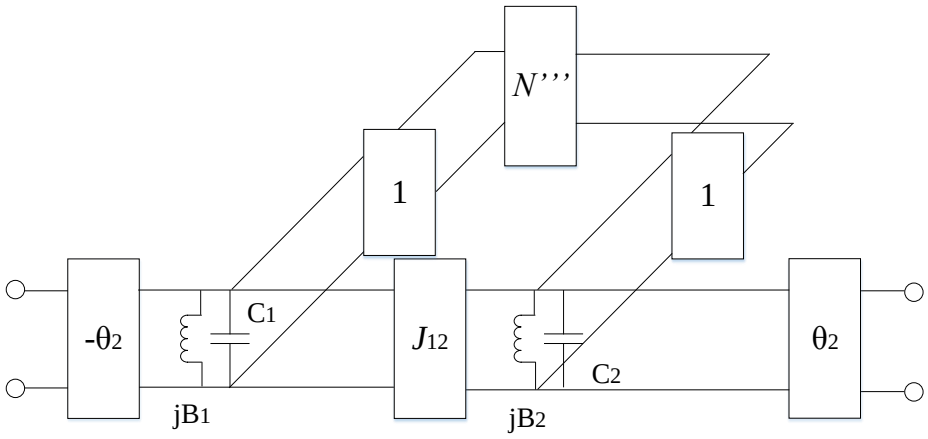

Figure 3.14: Detail equivalent network of N'' in Figure 3.13.

A complete cycle of the extraction of a pair of finite j-axis zeros has now been completed with a determined ABCD matrix of Eq. (3.3) for the remaining network. This basic cycle may now be repeated until either all or the desired pairs of finite j-axis zeros have been extracted in this manner. Afterward, the remaining network is to be synthesized as a cross-coupled double array with complex conjugate symmetry. Assume that there is at least a pair of transmission zeros at $p = \pm j\infty$, which will be extracted in the second kind of extraction cycle, shown in Figure 3.14.

From Eq. (3.7), the desired phase shifter θ_2 is

$$\tan\theta_2 = \frac{b}{ja}_{|p=-j\infty} \tag{3.11}$$

Compared with Figure 3.13(a) and Figure 3.14, we can see that the second kind of extraction cycle starts with the extraction of a pair of admittances

$$\begin{aligned} Y_1 &= pC_1 + jB_1 \\ Y_2 &= pC_1 - jB_1 \end{aligned} \tag{3.12}$$

where C_1 and B_1 are the capacitance and frequency invariant susceptance of inline resonator respectively. Substituting Eq. (3.4) and Eq. (3.10) to Eq. (3.12), we can obtain

$$C_1 = \frac{a' + d'}{2b'p}_{|p=j\infty} \tag{3.13}$$

$$B_1 = \frac{d' - a'}{2jb'}_{|p=j\infty}$$

The immittance inverter of characteristic admittance J_{12} must be extracted in parallel with the network, which means the remaining network possesses another pair of transmission zeros at infinity. This results in

$$J_{12} = \frac{1}{jb''}_{|p=j\infty} \tag{3.14}$$

The second kind of extraction of extraction cycle is then repeated until the filter network is completely synthesized. It should be noted that when mapping the prototype to the physical structure, the frequency shift to the resonators can be easily controlled by adjusting the resonator's dimensions, but the junction susceptance can't be modified freely unless a special T junction is used. The synthesis starts from the low-pass quasi-elliptic transfer function and it can only be performed on a complex conjugate symmetrical network which means that it will only work on an even-order transfer function with a fourth-order minimum.

As shown in Figure 3.15, the distribution of the pole elements in a filter topology have combination of the following three types: 1) the pole node is located between two resonator nodes; 2) two pole elements are arranged next to each other; and 3) the pole element is located next to the input/output port.

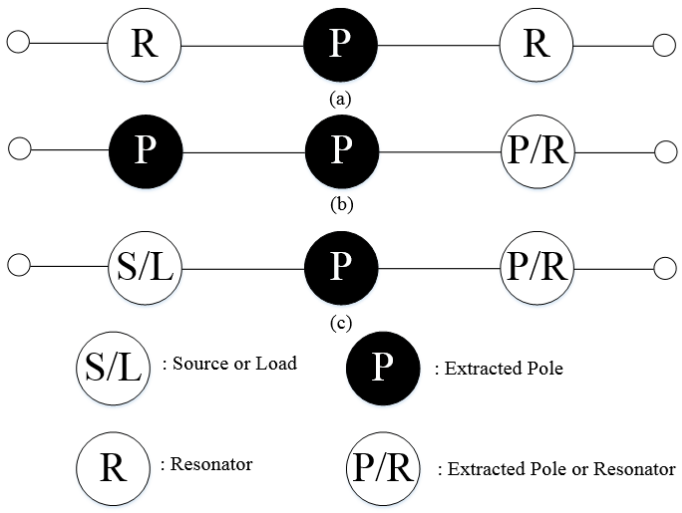

Figure 3.15: Possible configuration of extracted pole elements.

With these three types of reconfiguration processes, parameters b_1 can be set to the predefined values relating to the EM structure during the synthesis procedure. After applying the synthesis procedure, the designer only needs to calculate the physical dimensions of the remaining elements.

3.4.2 Design Example

A five-pole filter centred at 3GHz with 10% FBW, 20 dB return loss and two extracted poles, which have a single pair of TZs at $p = \pm j2.0$, is designed as a demonstration. The lossless coupling topology is shown in Figure 3.16. Node 1 and 5 are two extracted-poles connected to the NRN nodes, while node 2, 3, 4 are resonators in the inline network.

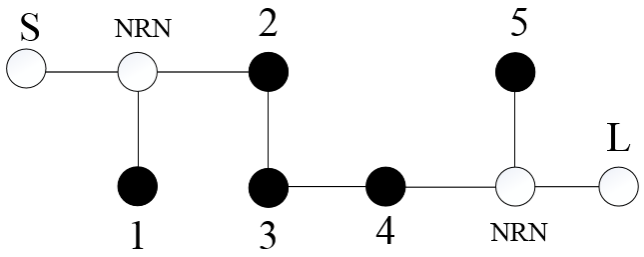

Figure 3.16: Lossless coupling topology of five-pole extracted-pole filter.

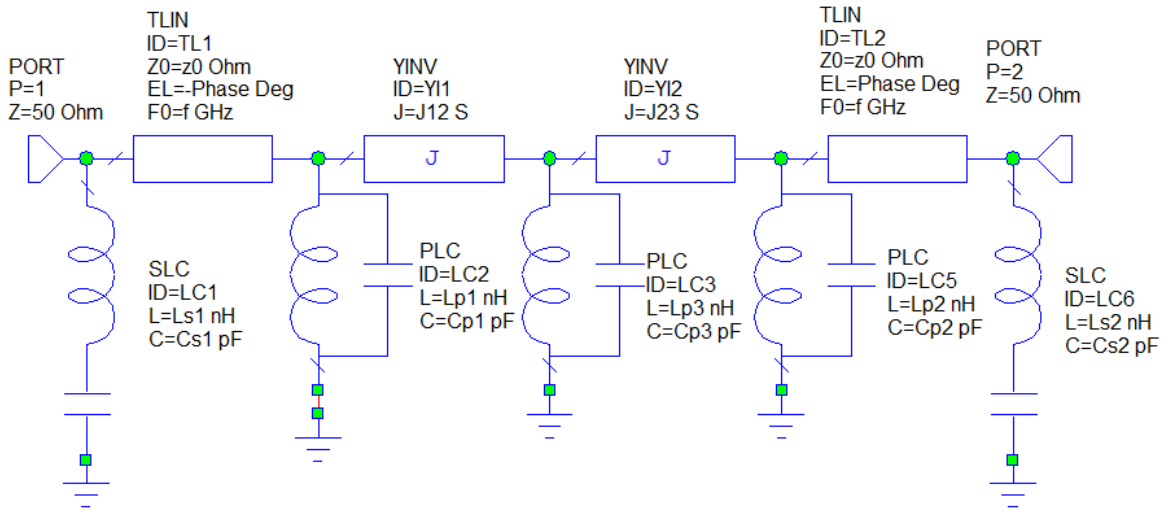

Figure 3.17: The equivalent circuit model of five-pole extracted-pole filter.

Figure 3.17 shows the equivalent circuit model. Firstly, the lowpass quasi-elliptic function prototype is designed to convert to bandpass. Since the five poles are odd

numbers, which is not standard even symmetric model, we can easily start to extract from four poles symmetric model and extract the last pole of middle-band with optimization, because the last pole will only contribute the middle passband performance. The element values of the four pole lowpass cross-couple filter, which can be obtain from [4], are

$$\mathrm{g}_1 = 0.95449 \qquad \mathrm{J}_1 = 0.95449$$

$$\mathrm{g}_2 = 1.38235 \qquad \mathrm{J}_2 = 0.95449$$

Having obtained the design parameters of bandpass filter, we may use the general formulation for cross-coupled resonator filters to analyse the filter frequency response. Alternatively, the frequency response can be calculated by

$$S_{21}(\Omega) = \frac{Y_o(\Omega) - Y_e(\Omega)}{(1 + Y_e(\Omega)) \cdot (1 + Y_o(\Omega))} \qquad (3.15)$$

$$S_{11}(\Omega) = \frac{1 - Y_o(\Omega) \cdot Y_e(\Omega)}{(1 + Y_e(\Omega)) \cdot (1 + Y_o(\Omega))}$$

Where Y_e and Y_o are the even- and odd- mode input admittance. Therefore, the Y_e and Y_o can easily be expressed in terms of the elements in a ladder structure such as

$$Y_e(\Omega) = j(\Omega \mathrm{g}_1 - J_1) + \frac{1}{j(\Omega \mathrm{g}_2 - J_2)} \qquad (3.16)$$

$$Y_o(\Omega) = j(\Omega \mathrm{g}_1 + J_1) + \frac{1}{j(\Omega \mathrm{g}_2 + J_2)}$$

The initial ABCD matrix of the filter can be determined by

$$\begin{bmatrix} a & b \\ c & d \end{bmatrix} = \frac{1}{Y_o - Y_e} \begin{bmatrix} Y_e + Y_o & 2 \\ 2Y_e\, Y_o & Y_e + Y_o \end{bmatrix} \qquad (3.17)$$

Using Eq. (3.7) with $\Omega = 2.0$ yields

$$\theta_1 = 33.96^{\circ}$$

From Eq. (3.10) with $\theta = \theta_1$, the residue b_1 is then found

$$b_1 = 2.58$$

By applying the frequency transformation and equating slope reactances as well as slope

susceptances, we can obtain

$$C_{s1} = \frac{b_1}{\omega_0}\left(\frac{1}{FBW} + \frac{\Omega}{2}\right)^{-1} \qquad L_{s1} = \frac{1}{\omega_0 b_1}\left(\frac{1}{FBW} - \frac{\Omega}{2}\right)$$

$$C_{s2} = \frac{b_1}{\omega_0}\left(\frac{1}{FBW} - \frac{\Omega}{2}\right)^{-1} \qquad L_{s2} = \frac{1}{\omega_0 b_1}\left(\frac{1}{FBW} + \frac{\Omega}{2}\right)$$

$$C_{p1} = \frac{1}{\omega_0}\left(\frac{C_1}{FBW} + \frac{B_1}{2}\right) \qquad L_{p1} = \frac{1}{\omega_0}\left(\frac{C_1}{FBW} - \frac{B_1}{2}\right)^{-1}$$

$$C_{p2} = \frac{1}{\omega_0}\left(\frac{C_1}{FBW} - \frac{B_1}{2}\right) \qquad L_{p2} = \frac{1}{\omega_0}\left(\frac{C_1}{FBW} + \frac{B_1}{2}\right)^{-1}$$

$$C_{p3} = \frac{1}{\omega_0}\left(\frac{C_2}{FBW} + \frac{B_2}{2}\right) \qquad L_{p3} = \frac{1}{\omega_0}\left(\frac{C_2}{FBW} - \frac{B_2}{2}\right)^{-1}$$

where ω_0 is the angular frequency, f_0 is the centre frequency and FBW is the fractional bandwidth. The symbol b_1 is a residue constant of the extracted pole, B_1, B_2 and C_1, C_2 are the frequency invariant susceptance and capacitance respectively. The synthesis parameters value with optimization are given in Table III. The responses of lossless synthesizes is presented in Figure 3.18. It can be seen that the two extracted poles introduce two transmission zeros for the selectivity enhancement and contribute the passband, which can be clearly seen that five transmission poles from the passband return loss response in the lossless synthesis.

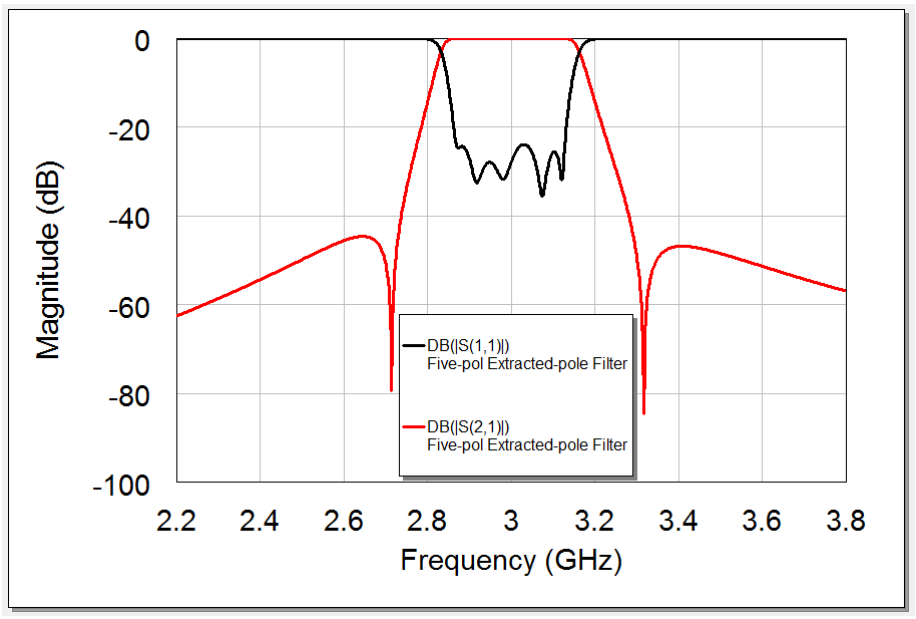

Figure 3.18: Responses of lossless synthesis of five-pole extracted-pole filter.

Table 3.3: Elements value for five-pole extracted-pole filter.

z_0	50 Ω	Cs1	0.253 pF	Ls1	9.12 nH
f	3.0 GHz	Cs2	0.3 pF	Ls2	11.14 nH
phase	36.4°	Cp1	43.85 pF	Lp1	0.067 nH
J12	0.053 S	Cp2	42.27 pF	Lp2	0.064 nH
J23	0.054 S	Cp3	46.98 pF	Lp3	0.06 nH

3.5 Microstrip Extracted-Pole Lossy Filter

3.5.1 Design of Five-pole Extracted-pole Lossy Filter

In the previous section, a lossless synthesis of five-pole extracted pole filter is described to design in detail. For this section, we convert it to the lossy synthesis to introduce additional loss to make the passband flat with the same selectivity. The easy way is to introduce one RCC between resonator 2 and 4, shown in Figure 3.19. Following the procedure discussed above, the equivalent circuit model can be set up given in Figure 3.20 and the element values are displayed in Table IV with the uniform resonators $Q = 160$. The simulation response and group delay performance are illustrated in Figure 3.21 and 3.22 respectively, which can be told that the passband is very flat.

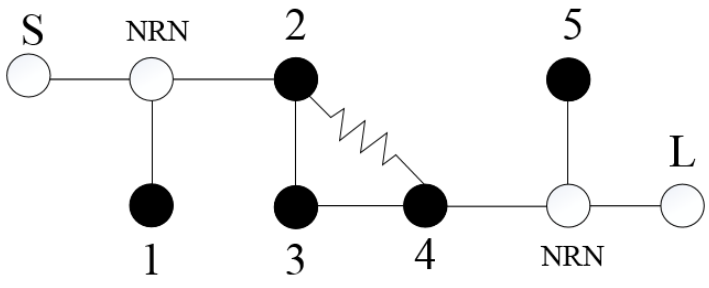

Figure 3.19: Lossy synthesis topology of five-pole extracted-pole filter.

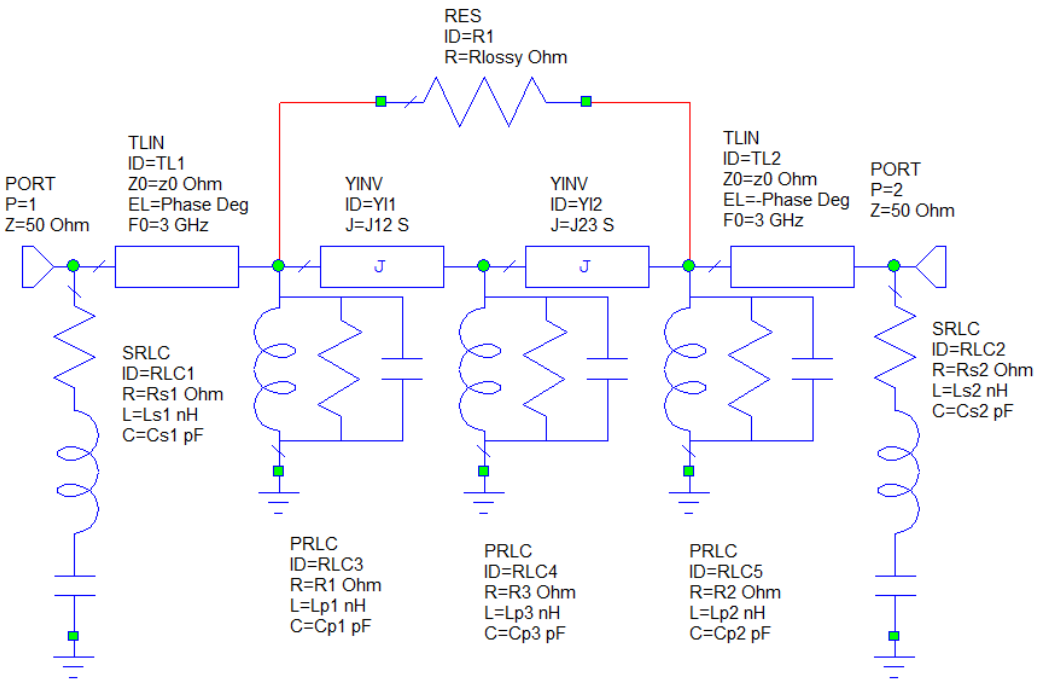

Figure 3.20: Equivalent circuit model of lossy synthesis of five-pole extracted-pole filter.

Table 3.4: Elements value for five-pole extracted-pole lossy filter.

z_0	50 Ω	Cp1	54.22 pF	Lp3	0.054 nH
f_0	3.0 GHz	Cp2	52.69 pF	Rs1	0.74 Ω
phase	36.4°	Cp3	52.29 pF	Rs2	0.9 Ω
J12	0.0527 S	Ls1	9.36 nH	Rp1	235 Ω
J23	0.05412 S	Ls2	11.45 nH	Rp2	242 Ω
Cs1	0.246 pF	Lp1	0.053 nH	Rp3	244 Ω
Cs2	0.3 pF	Lp2	0.052 nH	Rlossy	320 Ω

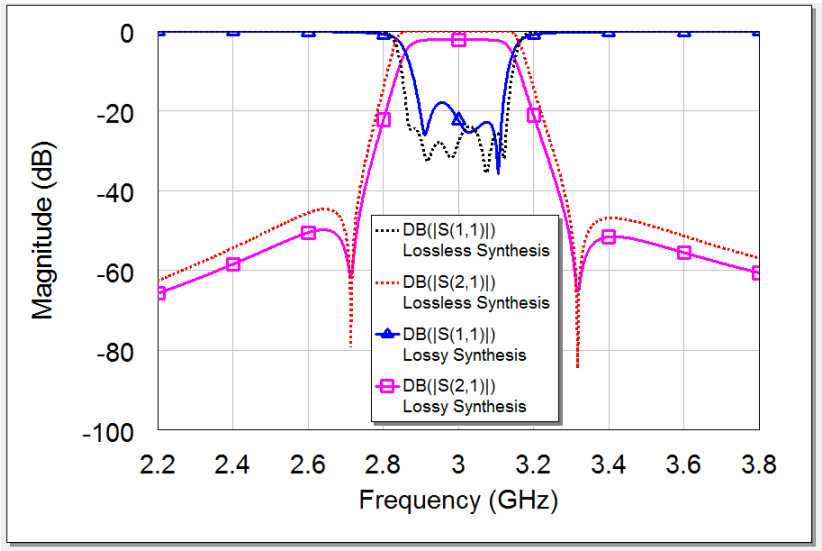

Figure 3.21: Response comparison of lossy and lossless synthesis of five-pole extracted-pole filter.

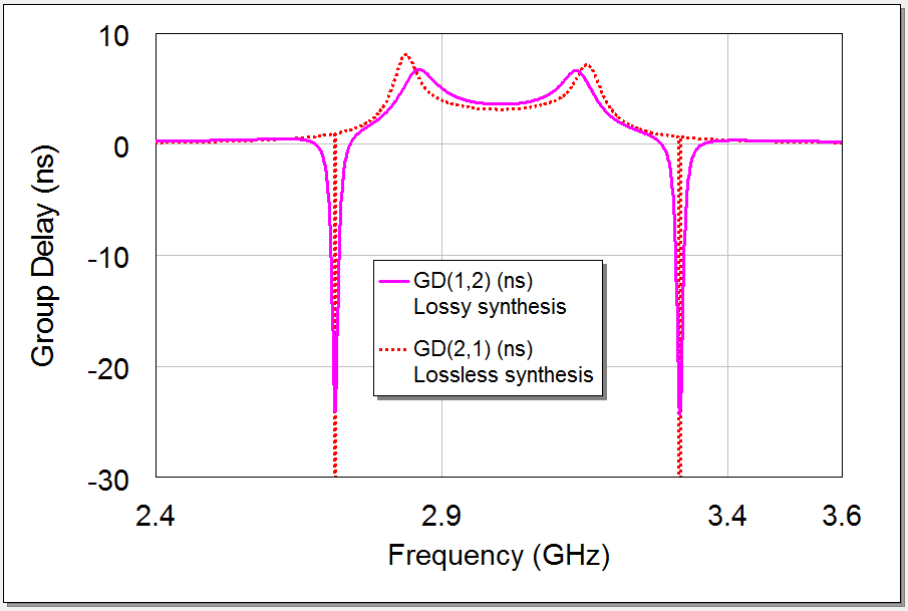

Figure 3.22: Group delay of lossy synthesis of five-pole extracted-pole filter.

3.5.2 Design of Six-pole Extracted-pole Lossy Filter

Last section just give a quite simple example to combine the lossy synthesis and extracted-pole to have a flatness insertion loss with high selectivity at the same time. In this section, two six-pole microstrip extracted-pole lossy bandpass filters, operating at 2GHz with different FBWs 6% and 20% will be presented [40]. These two filters have been demonstrated to analysis from the theoretical circuit model to EM simulations,

fabricated and measured. All necessary design equations and information can be used for the design of higher-order extracted pole lossy bandpass filter as well. In addition, the proposed filters will be compared to other state-of-the-art lossy filters.

3.5.2.1 Theoretical Circuit Model

The lossless and lossy coupling topology of proposed filter is shown in Figure 3.23(a) and (b) respectively. Node 1 and 6 are two extracted-poles connected to the non-resonated nodes (NRNs), while node 2, 3, 4 and 5 are resonators in the inline network. Two RCCs are added between node 2 and node4, node 3 and node 5 respectively. The minimum required number of resonators for applying two RCCs is four in the inline network.

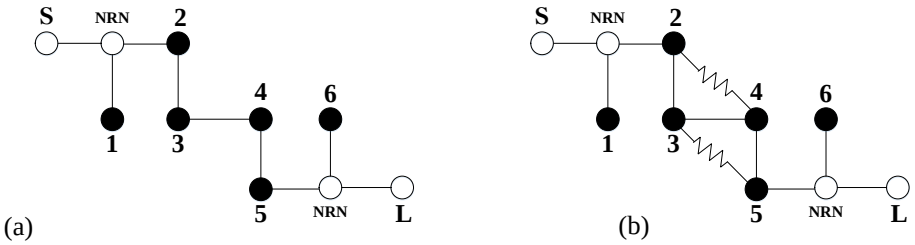

Figure 3.23: (a) Lossless coupling diagram and (b) Lossy coupling topology.

For computer-aided modelling and design, an equivalent circuit model of extracted-pole lossy filter topology used by AWR [10] is given in Figure 3.24(b), where L_{sm}, C_{sm} and R_{sm}, (m=1 and 2) are the circuit parameters of the two extracted-pole resonators with R_{sm} representing the resonator losses while L_{pm}, C_{pm} and R_{pm} $(m = 1\ to\ 4)$ are the circuit parameters of the four parallel resonators with R_{pm} representing the resonator losses; J inverters are used to represent the couplings and R_{lossy} represents the resistive coupling introduced for the lossy technique. The coupling between the resonator and feed line (the external Q-factor) and the coupling between resonators (coupling coefficient) have to be determined to achieve a desired response. The initial circuit element values were first calculated based on the method described in [4] for the lossless circuit model of Figure 3. 24(a).

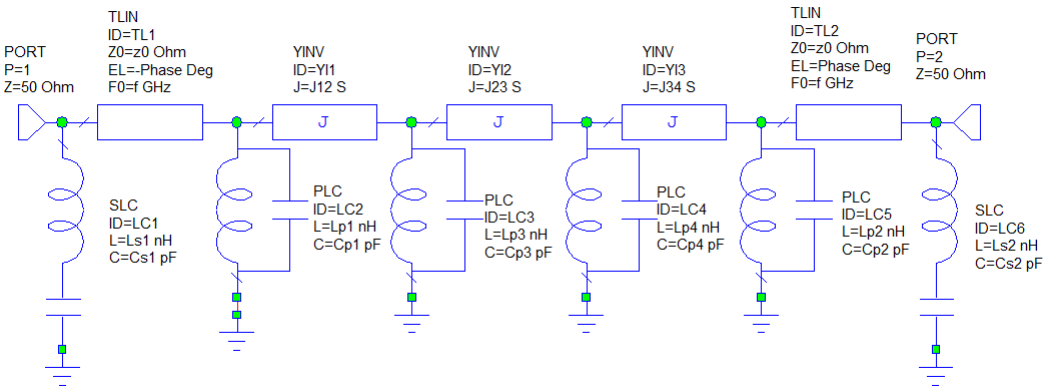

(a)

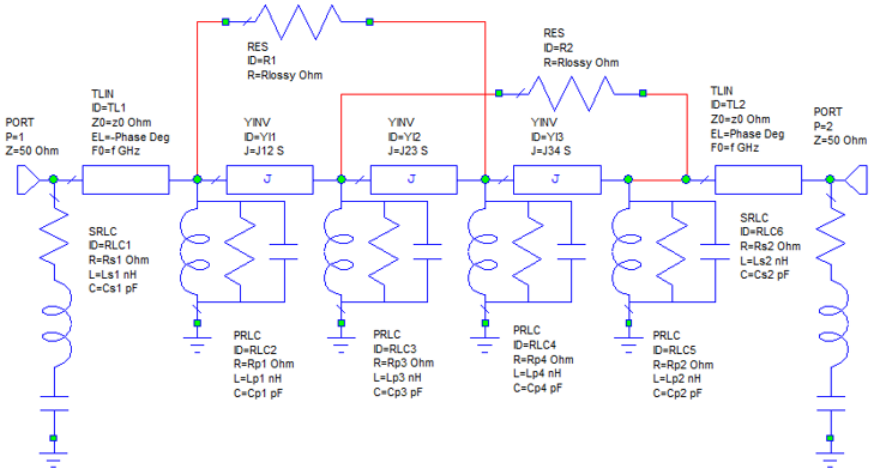

(b)

Figure 3.24: (a) Lossless circuit model and (b) Circuit model of lossy synthesis.

By applying the frequency transformation and equating slope reactances as well as slope susceptances, we can obtain:

$$
\begin{aligned}
C_{s1} &= \frac{b_1}{\omega_0}\left(\frac{1}{FBW}+\frac{f_0}{2}\right)^{-1} & L_{s1} &= \frac{1}{\omega_0 b_1}\left(\frac{1}{FBW}-\frac{f_0}{2}\right)\\
C_{s2} &= \frac{b_1}{\omega_0}\left(\frac{1}{FBW}-\frac{f_0}{2}\right)^{-1} & L_{s2} &= \frac{1}{\omega_0 b_1}\left(\frac{1}{FBW}+\frac{f_0}{2}\right)\\
C_{p1} &= \frac{1}{\omega_0}\left(\frac{C_1}{FBW}+\frac{B_1}{2}\right) & L_{p1} &= \frac{1}{\omega_0}\left(\frac{C_1}{FBW}-\frac{B_1}{2}\right)^{-1}\\
C_{p2} &= \frac{1}{\omega_0}\left(\frac{C_1}{FBW}-\frac{B_1}{2}\right) & L_{p2} &= \frac{1}{\omega_0}\left(\frac{C_1}{FBW}+\frac{B_1}{2}\right)^{-1}\\
C_{p3} &= \frac{1}{\omega_0}\left(\frac{C_2}{FBW}+\frac{B_2}{2}\right) & L_{p3} &= \frac{1}{\omega_0}\left(\frac{C_2}{FBW}-\frac{B_2}{2}\right)^{-1}\\
C_{p4} &= \frac{1}{\omega_0}\left(\frac{C_2}{FBW}-\frac{B_2}{2}\right) & L_{p4} &= \frac{1}{\omega_0}\left(\frac{C_2}{FBW}+\frac{B_2}{2}\right)^{-1}
\end{aligned}
\tag{3.19}
$$

where ω_0 is the angular frequency, f_0 is the centre frequency and FBW is the fractional bandwidth. The symbol b_1 is a residue constant of the extracted pole, B_1, B_2

and C_1, C_2 are the frequency invariant susceptance and capacitance respectively. From Eq. (3.7) to Eq. (3.13), as an example, given $b_1 = 2.5489, B_1 = 1.476, B_2 = 0.21, C_1 = 3.838$ and $C_2 = 4.398$, Table V shows the element values of Figure 3.24(a) for a lossless extracted-pole filter with a FBW of 6% centred at $f_0 = 2GHz$.

To extend to the lossy synthesis, two resistive cross couplings (RCCs) are added as shown with R_{lossy} in Figure 3.24(b). The loss in the resonators themselves is also needed to consider, which are related to the Q factor of the resonators themselves given in Eq. (3.20) and (3.21), for series and parallel resonators respectively:

$$R_{s_m} = \frac{\omega_{sm} L_{s_m}}{Q_{s_m}} \quad m = 1,2 \tag{3.20}$$

$$R_{p_m} = \frac{Q_{p_m}}{\omega_{p_m} C_{p_m}} \quad m = 1,2,3,4 \tag{3.21}$$

where ω_{sm} and ω_{p_m} are the angular resonant frequencies of the series and parallel resonators, respectively. Assuming an equal Q of 163 for the microstrip resonators to be used, the parameters values in Table VI are extracted from this procedure with a slight optimization to adjust the better response for the circuit model of Figure 3.24(b) for an extracted-pole lossy filter with a FBW of 6% centred at $f_0 = 2GHz$.

Table 3.5: Elements Value for Lossless Synthesis.

z_0	50 Ω	Cp2	121 pF
f_0	2 GHz	Cp3	140.2 pF
phase	36.4°	Cp4	139.8 pF
J12	0.0533S	Ls1	29.66 nH
J23	0.0527 S	Ls2	32.78 nH
J34	0.0535 S	Lp1	0.0523 nH
Cs1	0.193 pF	Lp2	0.0513 nH
Cs2	0.213 pF	Lp3	0.0453 nH
Cp1	123.3 pF	Lp4	0.0452 nH

Table 3.6: Elements Value for Lossy Synthesis.

z_0	50 Ω	Cp2	129 pF	Rs1	3 Ω
f_0	2.0 GHz	Cp3	160 pF	Rs2	3.3 Ω
phase	37.2°	Cp4	160 pF	R1	99.2 Ω
J12	0.0489 S	Ls1	31 nH	R2	100.8 Ω
J23	0.0549 S	Ls2	34.3 nH	R3	100 Ω
J34	0.0497 S	Lp1	0.049 nH	R4	100 Ω
Cs1	0.185 pF	Lp2	0.0483 nH	Rlossy	220 Ω
Cs2	0.204 pF	Lp3	0.0396 nH		
Cp1	131.1 pF	Lp4	0.0396 nH		

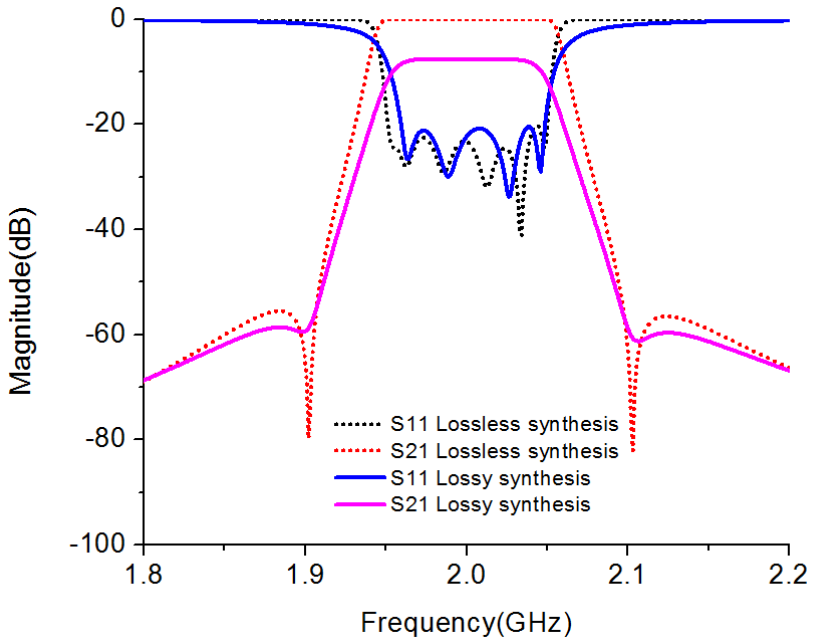

Figure 3.25: Responses of lossless and lossy synthesis.

The responses of lossless and lossy synthesizes are also compared in Figure 3.25. It can be seen that the two extracted poles introduce two transmission zeros for the selectivity enhancement. It can also be clearly seen that 6 transmission poles from the passband return loss response in the lossless synthesis. However, as the resonator losses are large in the lossy synthesis assuming the unloaded Q (Qu) of 163 for each resonator, only 4 transmission poles observable in the return loss ripple. Even with the low-Q resonators, the insertion loss is also very flat indicating that the two RCCs work well.

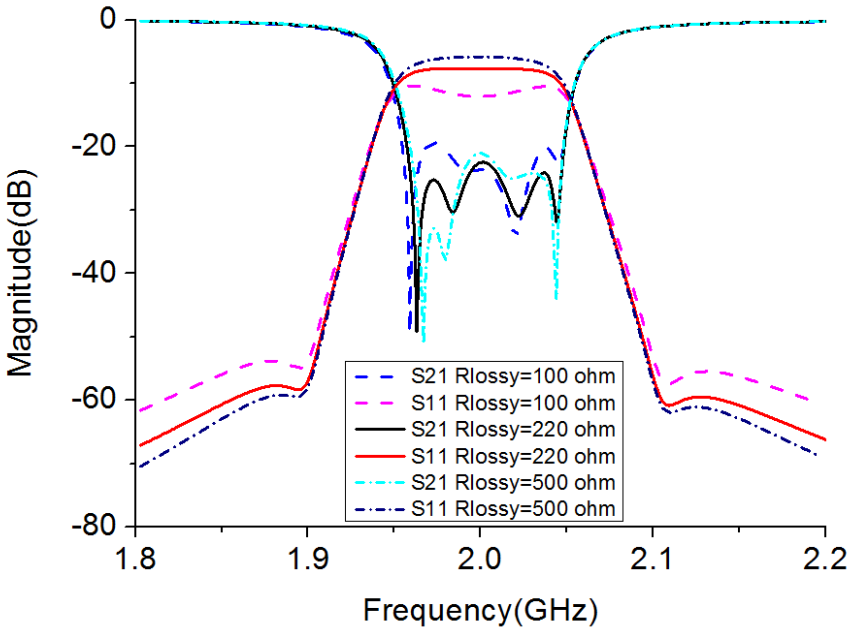

Figure 3.26: Lossy synthesis performance with different values of RCCs.

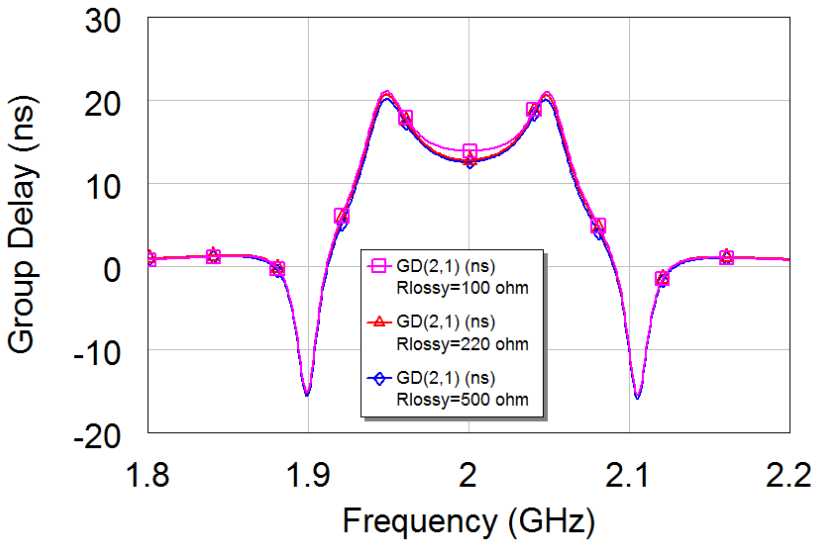

Figure 3.27: Group delay performance against different values of RCCs.

To see the effect of the RCCs clearly, Figure 3.26 shows the passband performance of 6% FBW with different values of resistors in the RCCs. The group delay performance against different values of RCCs is illustrated in Figure 3.27. In this example circuit model, the best value of resistor in RCCs is 220 ohm. For our investigation, the value of resistor in the RCCs can mainly affect the passband flatness rather than the positions of these two transmission zeros. Therefore, the RCCs in lossy synthesis can not only achieve a flat insertion loss, but also improve extracted-pole technique to better control the selectivity, compared with normal lossless synthesis.

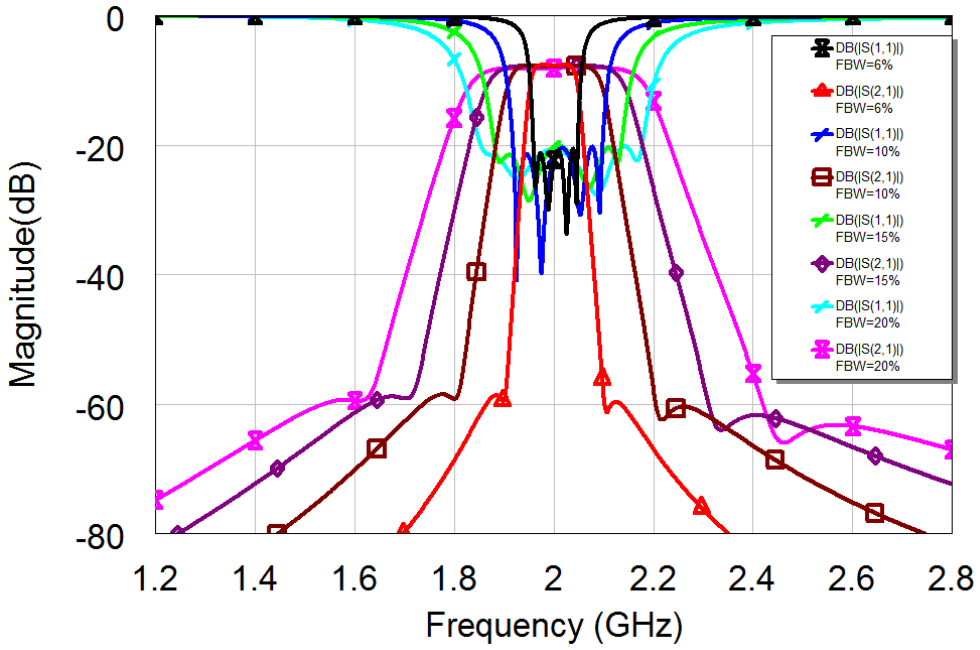

Figure 3.28: Lossy synthesis performance with different FBWs.

The lossy synthesis performance with different FBWs is shown in Figure 3.28 and the group delay comparison with different FBWs is also given in Figure 3.29. As we can see, the circuit model responses are good with flat passband and high selectivity in different FBWs from narrowband to wideband. The positions of two transmission zeros in different FBWs' response are the same in lossy synthesis, in which p=2.0, where p is the position of transmission zero in lossy synthesis method. However, the slope of the passband edges are much sharp as the FBW decreases. It's also more obvious to achieve a flat passband when RCCs are applied in narrowband.

For a given FBW of this proposed filter, the selectivity can also be improved by adjusting the extracted poles, i.e. varying the parameter p, with slightly affecting the passband insertion loss and return loss ripple, which can be ignored. An example response of 20% FBW is illustrated in Figure 3.30. The group delay comparison with different selectivity in this example is shown in Figure 3.31. When the positions of two transmission zeros change, the group delays only change a little at passband edge, while they are almost same in the passband, which verify again that the extracted pole technique can be use independently with RCCs in lossy synthesis method.

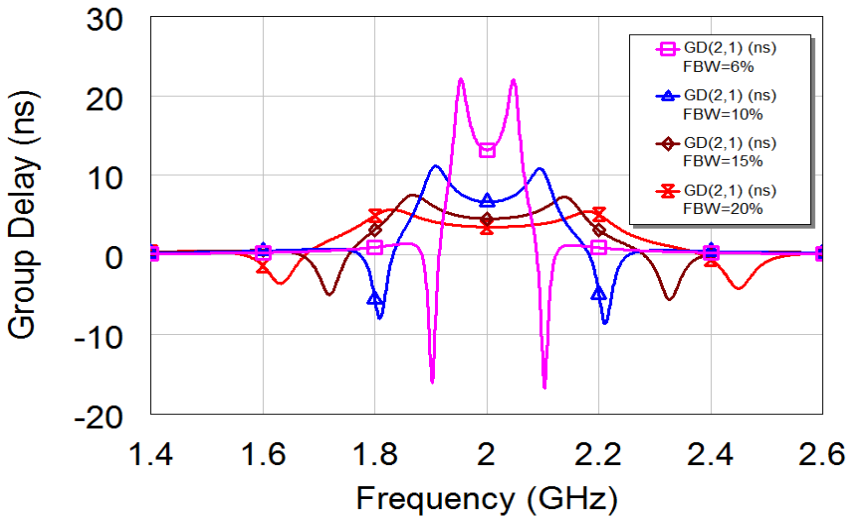

Figure 3.29: Group delay comparison with different FBWs.

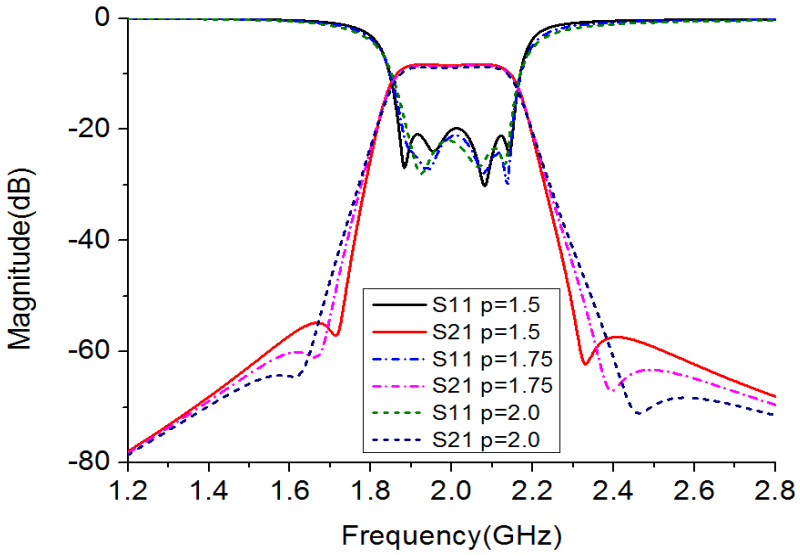

Figure 3.30: Lossy synthesis performance at 20% FBW with different selectivity.

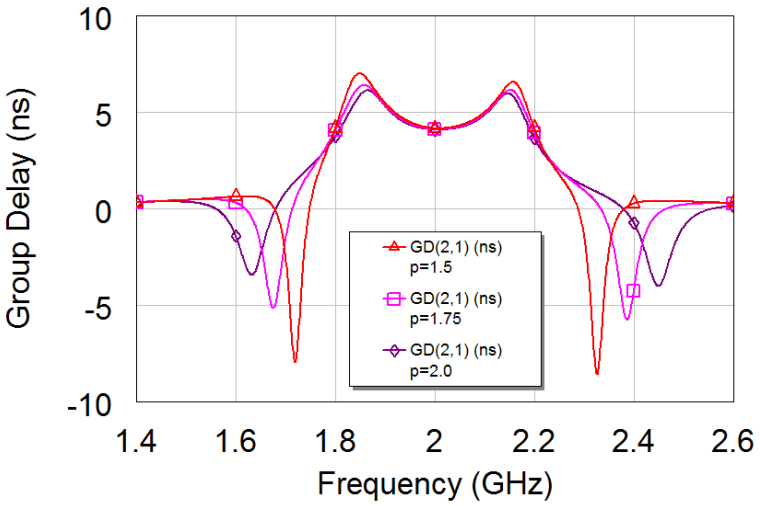

Figure 3.31: Group delay comparison with different selectivity.

3.5.2.2 Filter Example Implementations

For the implementation of microstrip extracted-pole filter, a new set of design parameters, i.e. the external Q-factor $Q_{ext,m}$ and the coupling coefficients$M_{m,m+1}$, is derived as follows [4]

$$Q_{ext,sm} = \frac{\omega_{\mathrm{sm}} L_{s_m}}{Z_0}, \qquad m = 1,2 \tag{3.22}$$

$$Q_{ext,pm} = \omega_{pm} C_{pm} Z_0, \qquad m = 1,4 \tag{3.23}$$

$$M_{m,m+1} = \frac{J_{m,m+1}}{\sqrt{\omega_{p_m} C_{p_m} * \omega_{p_{m+1}} C_{p_{m+1}}}}, \quad m = 1,2,3 \tag{3.24}$$

where $\omega_m = 2\pi f_m$, and f_m is the resonance frequency of the mth resonator. Z0 = 50 ohms is the terminal impedance.

For examples, the external Q-factors and coupling coefficients based on the lossless synthesis of Table I and the lossy synthesis of Table II can then be determined by (4)-(6), and their values are given as:

Lossless synthesis from Table I	Lossy synthesis from Table II
$Q_{ext,s1} = Q_{ext,s2} = 7.837$	$Q_{est1} = Q_{est6} = 8.19$
$Q_{ext,p1} = Q_{ext,p4} = 76.76$	$Q_{est2} = Q_{est5} = 81.76$
$M_{12} = 0.033$	$M_{23} = 0.027$
$M_{23} = 0.03$	$M_{34} = 0.027$
$M_{34} = 0.033$	$M_{45} = 0.027$

To realize the RCCs in the microstrip line, two cross couplings with surface mount resistors are introduced between resonator 2 and resonator 4, resonator 3 and resonator 5 respectively.

Based on the above discussion, a novel microstrip lossy bandpass filter with controlled flat insertion loss and high selectivity can be implemented by combining lossy synthesis and extracted pole technique in both narrowband and wideband. The RCCs are used to introduce the additional loss to make the passband insertion loss flat, which also improve the equivalent Q factor of resonator. The step-impedance resonator is also

applied to make the circuit size compact and achieve a better out-of-band response, compared with conventional hairpin-line resonator. For demonstrations, two six-pole filters centred at 2GHz with 6% and 20% FBWs are implemented. Details of the implementation will be described in the following filter examples.

Filter Example A

The first microstrip lossy filter example to be described exhibits the response performance in narrowband with 6% FBW. The equivalent circuit element values have been listed in Table II.

Following the design equations of (4) to (6), we then carry out full-wave EM simulations to extract the external Q and coupling coefficient against the physical dimensions based on the theory in [4].

Figure 3.32 shows the designed filter layout on a 1.27-mm-thick dielectric substrate with a relative dielectric constant of 10.2. The layout size is 56 mm by 40 mm. The filter is designed in the light of EM simulation. The simulated responses are plotted in Figure 3.33 and 3.34. The designed filter is then fabricated, as displayed in Figure 3.35, and tested with a microwave network analyser. The measured results are plotted in Figure 3.36 and 3.37.

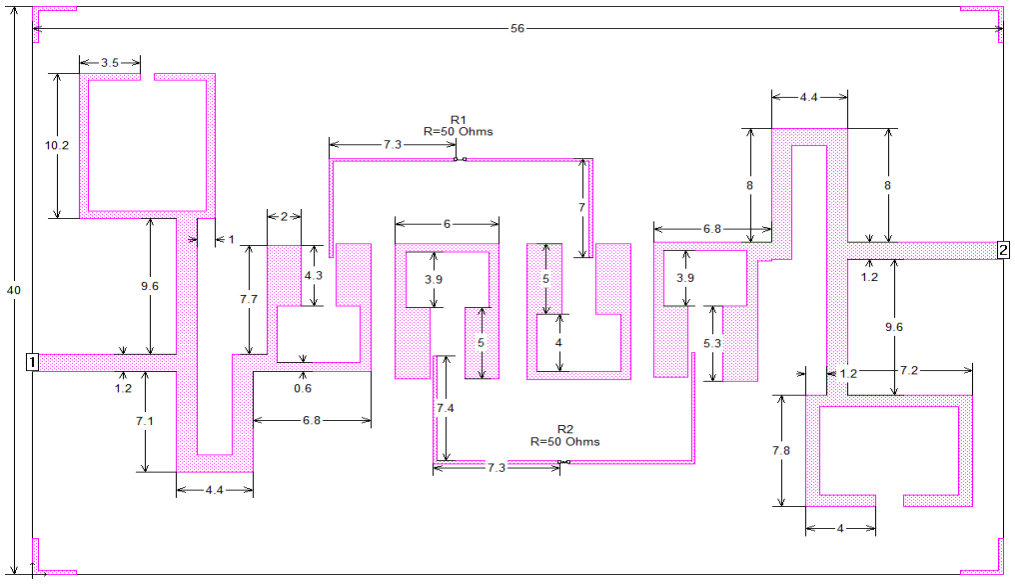

Unit (mm)

Figure 3.32: Layout of filter A.

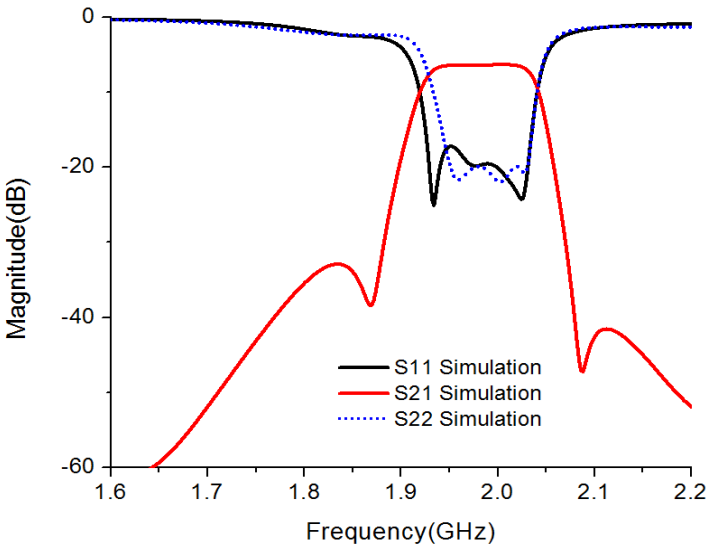

Figure 3.33: Simulated passband response.

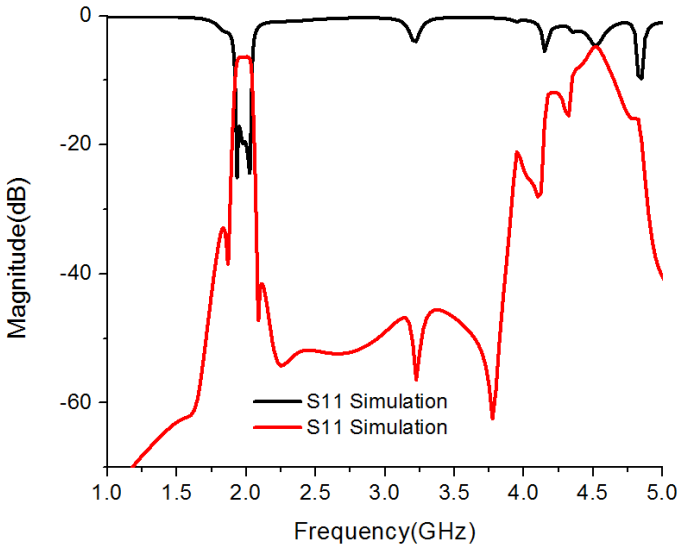

Figure 3.34: Simulated wideband response.

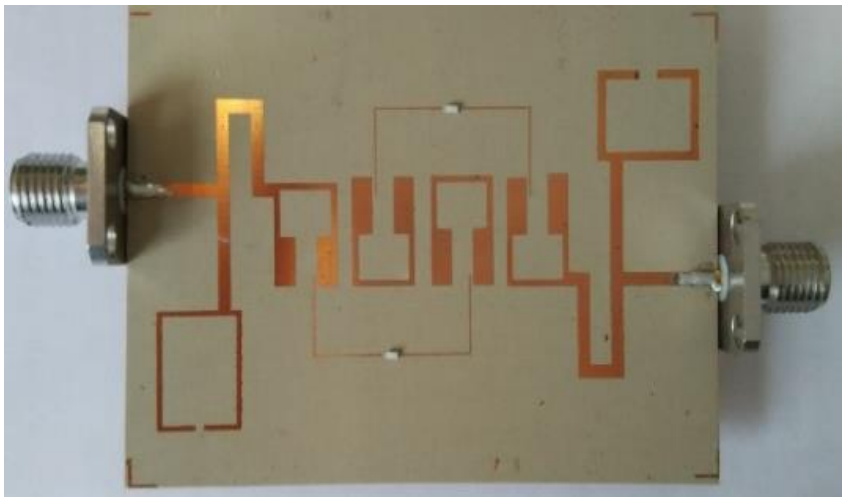

Figure 3.35: Fabrication photo of filter A.

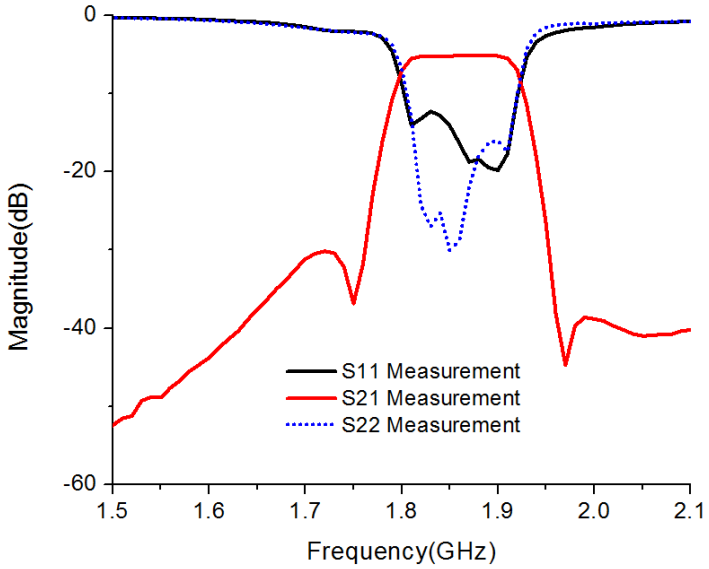

Figure 3.36: Measured passband response.

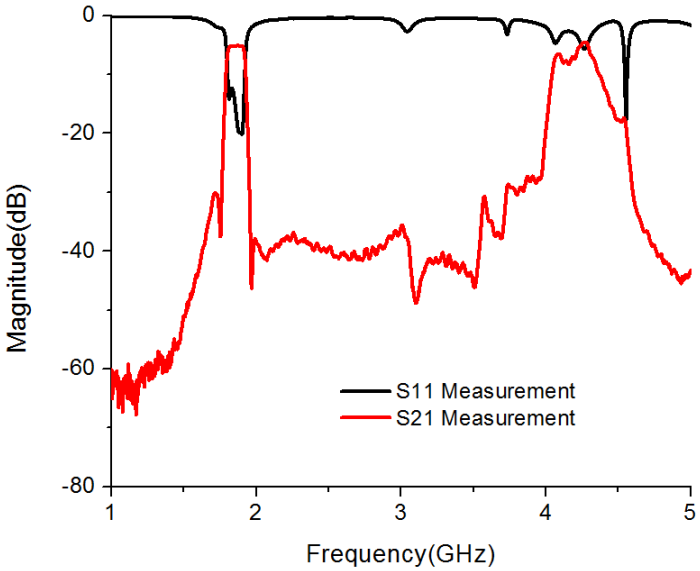

Figure 3.37: Measured wideband response.

Note that, owing to the tolerance in the fabrication, the centre frequency is measured to be 1.86 GHz, which is lower than the simulated one and is mainly because of the dielectric constant and thickness tolerances of the used substrate. Nevertheless, the measured and simulated filtering responses have good agreement in general. The measured filter has high selectivity with two transmission zeros: the lower side is located at 1.75 GHz while 1.97 GHz at high side. The passband is quite flat with a variation only around 0.3 dB, though the absolute insertion loss of the passband is 6.5dB. Such a passband flatness and selectivity would be equivalent to that of a conventional 6-pole

filter with a uniform Q of 600, which means this type of lossy filter can increase the equivalent Q to achieve a higher performance in terms of passband flatness and selectivity.

The measured wideband response of the filter can be seen more clearly in Figure 3.37. The first spurious occurs at 2.25 times the centre frequency. This is a wider upper stopband as compared with a filter using conventional half-wavelength hairpin resonators.

Filter Example B

Filter B demonstrates another example of microstrip extract-pole lossy filter with a wider FBW of 20%. Table VII shows the units values of its lossy synthesis. Following the same procedure in filter A to convert the lossy synthesis to physical dimensions, EM simulation can be carried out to extract the external Q and coupling coefficient against the physical dimensions.

Table 3.7: Elements Value for Lossy Synthesis.

z_0	50 Ω	Cp2	36.21 pF	Rs1	2.039 Ω
f_0	2.0 GHz	Cp3	40.57 pF	Rs2	2.759 Ω
phase	36.9°	Cp4	40.57 pF	R1	97.31 Ω
J12	0.044 S	Ls1	9.947 nH	R2	102.8 Ω
J23	0.042 S	Ls2	13.46 nH	R3	100 Ω
J34	0.044 S	Lp1	0.175 nH	R4	100 Ω
Cs1	0.47 pF	Lp2	0.166 nH	Rlossy	206 Ω
Cs2	0.64 pF	Lp3	0.156 nH		
Cp1	38.24 pF	Lp4	0.156 nH		

Figure 3.38 illustrates the designed layout of the microstrip lossy filter on a layout size of about 68 mm by 45 mm. The filter also uses the same structure as Filter A, but an additional resistor loading is applied in the lower side extracted pole to improve the upper stopband. The simulated responses are plotted in Figure 3.39 and 3.40. The designed filter is then fabricated, as displayed in Figure 3.41 and the measured results are plotted in Figure 3.42 and 3.43.

Again, owing to the tolerance, the measured centre frequency of 1.83 GHz is lower than the simulated one. Nevertheless, it can be seen that the measured frequency characteristic is very similar to the simulated one. The measured filter has two transmission zeros (TZs) located at 1.48 GHz and 2.2 GHz respectively to achieve a good

selectivity. The insertion loss is 2.2 dB, which is lower than that of filter A because of a wider FBW. The flatness of insertion loss is 0.3dB, which is almost the same with filter A.

The measured wideband response of the filter is also shown in Figure 3.43 with the first spurious occurring at 2.18 times centre frequency benefited by deploying the step-impedance half-wavelength resonators, but being suppressed or absorbed to some extend by the additional loading resistor.

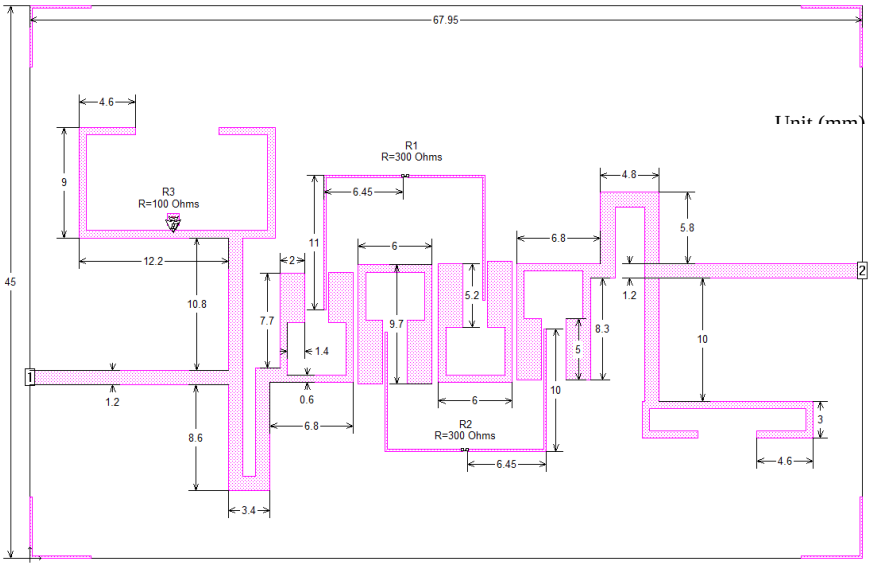

Figure 3.38: (a) Layout of filter B.

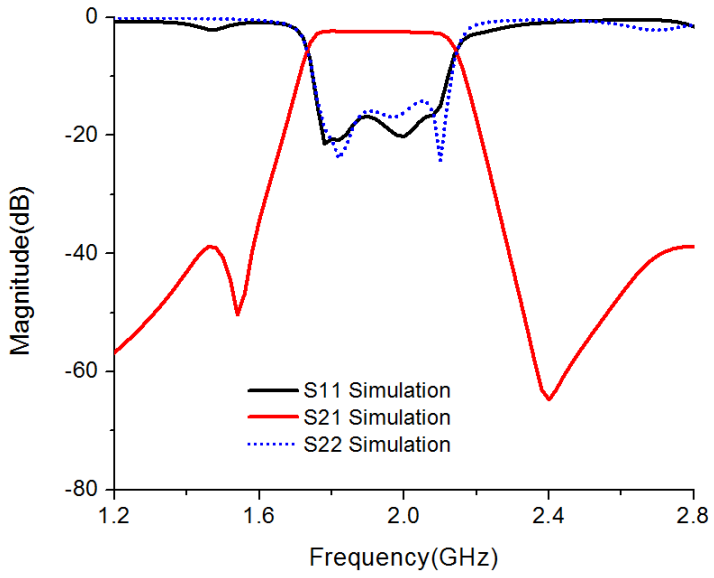

Figure 3.39: Simulated passband response.

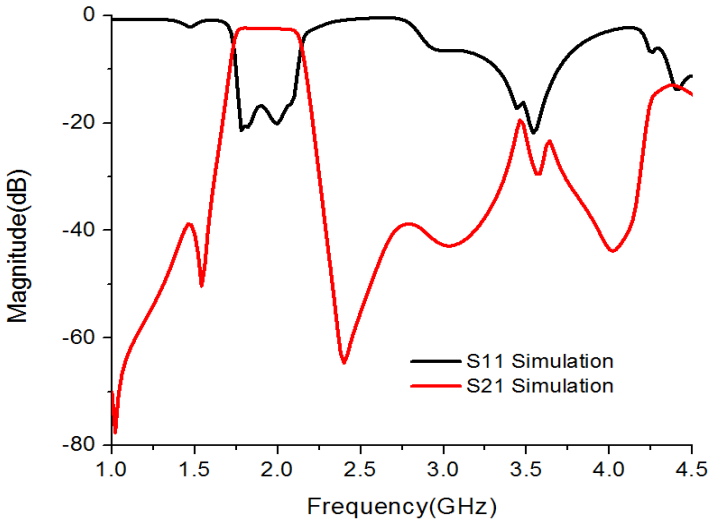

Figure 3.40: Simulated wideband response.

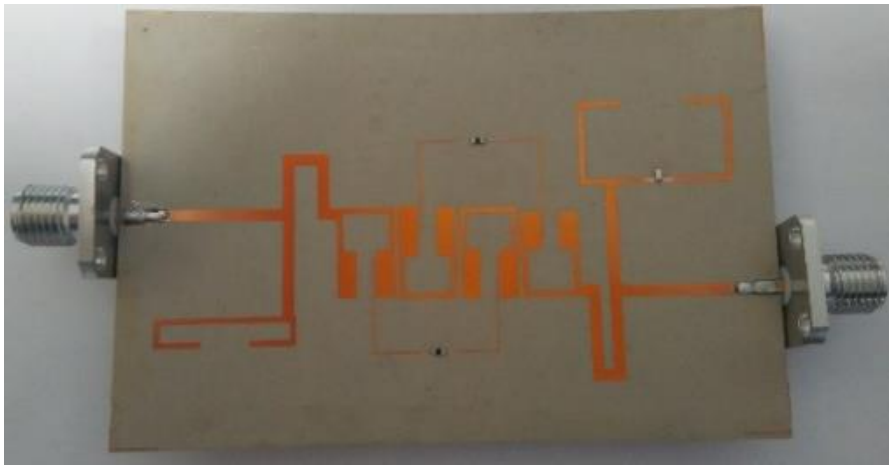

Figure 3.41: Fabrication photo of filter B.

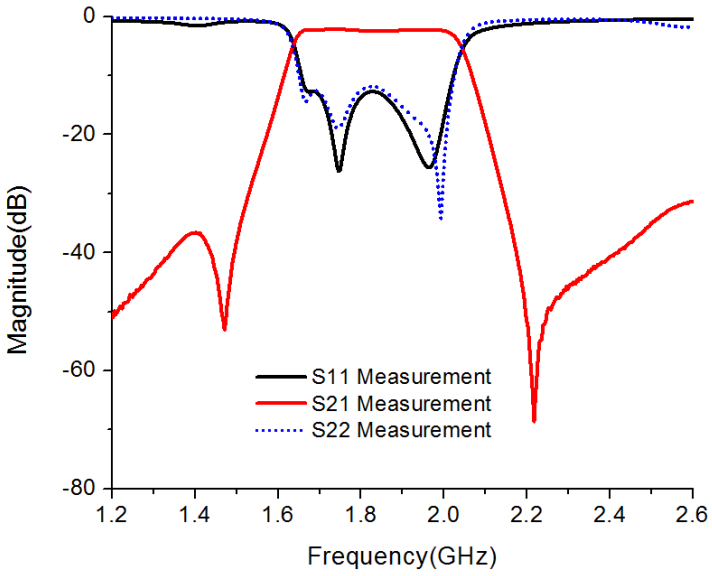

Figure 3.42: Comparison between experimental and theoretical results.

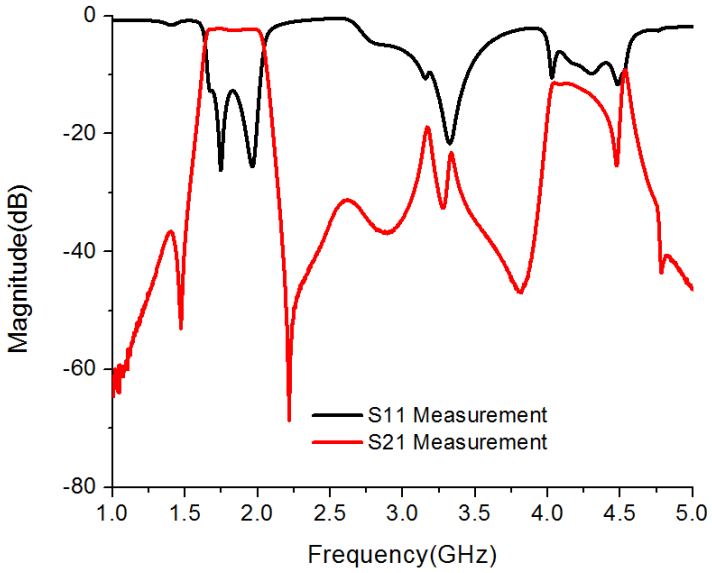

Figure 3.43: Measured wideband response.

3.5.2.3 Comparison to other published results

The comparison between the proposed filters with other relevant published works have been given in Table VIII.

Table 3.8: Comparison of Microstrip Lossy Filter.

Ref.	**Topology**	**TZs enhancing selectivity**	**Lossy Techniques**	f_0**(GHz)/ FBW**	**Absolute IL (dB)**	**Stopband width @rejection(dB)**
[21]	3-pole transversal	Yes	Non-uniform Q	2.48/ 10%	1.5	~1.2 x f_0@20dB
[28]	6-pole inline and transversal hairpin	No	RCCs	3.8/2 1%	3.4/4.2	~1.9 x f_0@30dB
		No	Non-uniform Q		2.5	~1.3 x f_0@30dB
[41]	4-pole inline hairpins	No	RCCs	1/11. 5%	3	N/A
[42]	4-pole dual-mode	Yes	Non-uniform Q	2.01/ 5.4%	6.7	N/A
This work	6-pole Extracted-pole	Yes	RCCs	1.86/ 6%	6.5	~2.2 x f_0@30dB
				1.83/ 20%	2.2	~2.2 x f_0@20dB

3.6 Summary

In this chapter, the design of microstrip lossy filters combining lossy synthesis and extracted-pole technique has been proposed. This type of proposed filter has both of high selectivity and flat passband not only in narrowband but also in wideband. The high selectivity is contributed by using extracted-pole technique and the flat passband is achieved by introducing RCCs in the inline network. Two six-pole filters has been fabricated and analysed to demonstrate the response performance in narrowband and wideband respectively. Good agreements between experimental and theoretical results have been achieved. This proposed filter also has a good upper stopband rejection. This kind of proposed lossy microstrip filter is promising to increase to high order and extend to the tunable filter.

References

[1] A. E. Atia, A. E. Williams. ‘Narrow-bandpass waveguide filters’. *IEEE Trans. Microw. Theory Tech.*, vol. MTT-20, pp. 258–265, Apr. 1972.

[2] A. E. Atia, A. E. Williams, R. W. Newcomb. ‘Narrow-band multiple-coupled cavity synthesis’. *IEEE Trans. Circuits Syst.*, vol. CAS-21, no. 9, pp. 649–655, Sep. 1974.

[3] R. J. Cameron, C. Kudsia, R. Mansour. *Microwave Filters for Communication Systems*, 1st ed. Hoboken, NJ: Wiley; 2007.

[4] J.-S. Hong, M. J. Lancaster. *Microstrip Filters for RF/Microwave Applications*. New York: Wiley; 2001

[5] V. Miraftab, M. Yu. ‘Generalized lossy microwave filter coupling matrix synthesis and design’. *in IEEE MTT-S Int. Microw. Symp. Dig.*, Atlanta, GA; pp. 627–630, Jun. 2008.

[6] V. Miraftab, M. Yu. ‘Generalized lossy microwave filter coupling matrix synthesis and design using mixed technologies’. *IEEE Trans. Microw. Theory Tech.*, vol. 56(12), pp. 3016–3027, Dec. 2008.

[7] A. Guyette, I. Hunter, R. Pollard. ‘The design of microwave bandpass filters using resonators with non-uniform Q’. *IEEE Trans. Microw. Theory Tech.*, vol. 54(11), pp. 3914–3922, Nov. 2006.

[8] A. Guyette, I. Hunter, R. Pollard. ‘Exact synthesis of microwave filters with non-uniform dissipation,” *in IEEE MTT-S Int. Microw. Symp. Dig.*, Hawaii, HI, pp. 537–540, Jun. 2007.

[9] Z. Zhou, J.-S. Hong. ‘Novel lossy microstrip filter with extracted-pole technique’. *46th Eur. Microw. Conf.*, London, pp. 120-123, Oct. 2016.

[10] AWR Microwave Office ver.11

[11] Sonnet ver.13

[12] G. Matthaei, L. Young, E. M. T. Jones. *Microwave Filters, Impedance-Matching Networks, and Coupling Structures*. Norwood, MA: Artech House; p. 152, 1980.

[13] R. M. Livingston. ‘Predistorted waveguide filters’. *in IEEE MTT-S Int. Microwave Symp. Dig.*, pp. 291–297, 1969.

[14] A. E. Williams, W. G. Bush, R. R. Bonetti. ‘Predistortion technique for multicoupled resonator filters’ *IEEE Trans. Microwave Theory Tech.*, vol. MTT-33, pp. 402–407, May 1985.

[15] M. Yu, V. Dokas, W.-C. Tang, R. Cameron. ‘Novel adaptive predistortion technique for cross coupled filters’. *in IEEE MTT-S Int. Microwave Symp. Dig.*, Philadelphia, PA, pp. 929–932, June 8–13, 2003.

[16] M. Yu, W.-C. Tang, A. Malarky, V. Dokas, R. Cameron, and Y. Wang. ‘Novel

adaptive predistortion technique for cross coupled filters and its application to satellite communication systems'. *IEEE Trans. Microwave Theory Tech*., vol. 51(12), pp. 2505–2514, Dec. 2003.

[17] M. Meng, I. C. Hunter. 'The design of parallel connected filter networks with non-uniform resonators'. *in IEEE MTT-S Int. Microw. Symp. Dig.*, Montreal, QC, Canada, pp. 1–3, Jun. 2012.

[18] M. Meng, I. C. Hunter, J. D. Rhodes. 'The design of parallel connected filter networks with non-uniform Q resonators'. *IEEE Trans. Microw. Theory Tech*., vol. 61(1), pp. 372–381, 2013.

[19] V. Miraftab, M. Yu. 'Advanced coupling matrix and admittance function synthesis techniques for dissipative microwave filters'. *IEEE Trans. Microw. Theory Tech*., 57(10), pp. 2429–2438, 2009.

[20] L. Szydlowski, A. Lamecki, M. Mrozowski. 'Design of microwave lossy filter based on substrate integrated waveguide (SIW)'. *IEEE Microw. Wireless Compon. Lett.* vol. 21(5), pp. 249–251, May 201.

[21] I. C. Hunter, A. Guyette, R. Pollard. 'Passive microwave receive filter networks using low- resonators'. *IEEE Microw. Mag*., vol. 6(3), pp. 1959–1962, Sep. 2005.

[22] C.-K. Liao, C.-Y. Chang, J. Lin. 'A vector-fitting formulation for parameter extraction of lossy microwave filters'. *IEEE Microw. Wireless Compon. Lett*. vol. 17(4), pp. 277–279, Apr. 2007.

[23] M. Yu, V. Miraftab. 'Shrinking microwave filters'. *IEEE Microw. Mag.*, vol. 9(5), pp. 40–54, Oct. 2008.

[24] L. Szydlowski, A. Lamecki, M. Mrozowski. 'Synthesis of coupled lossy resonator filters'. *IEEE Microw. Wireless Compon. Lett.* vol. 20(7), pp. 366–368, Jul. 2010.

[25] A. Padilla, J. Mateu, C. Collado, C. Ernst, J. M. Rius, J. M. Tamayo, J. M. O'Callaghan. 'Comparison of lossy filters and predistorted filters using novel software'. *in IEEE MTT-S Int. Microw. Symp. Dig.*, Anaheim, CA, USA, pp. 1720–1723, May 2010.

[26] M. Oldoni, G. Macchiarella, G. Gentili, C. Ernst. 'A new approach to the synthesis of microwave lossy filters'. *IEEE Trans. Microw. Theory Tech*., vol. 58(5), pp. 1222–1229, May 2010.

[27] Jia Ni, W. Xing Tang, J.-S. Hong, Geschke, R.H. 'Design of Microstrip Lossy Filter Using an Extended Doublet Topology'. *Microwave and Wireless Components Letters, IEEE*, 24, (5), pp. 318 – 320, 2014.

[28] A. Basti, A. perigaud, S. Bila, S. Verdeyme, L. Estagerie, and H. Leblond. 'Design of microstrip lossy filters for receivers in satellite transponders'. *IEEE Trans. Microw, Theory Tech*., vol. 62(9), pp. 0018-9480, Sep. 2014.

[29] M. Meng, K.-L. Wu. 'An analytical approach to computer-aided diagnosis and tuning of lossy microwave coupled resonator filters'. *IEEE Trans. Microw. Theory Tech*., vol.

57(12), pp. 3188–3195, Dec. 2009.

[30] R. J. Cameron, C.Kudsia, R. Mansour. *Microwave Filters for Communication Systems*, 1st ed. Hoboken, NJ: Wiley; 2007

[31] J. D. Rhodes, R. J. Cameron. 'General extracted pole synthesis technique with applications to low-loss TE011 mode filters'. *IEEE Trans. Microw. Theory Tech.*, vol. MTT-28, pp. 1018–1028, Sep. 1980.

[32] R. J. Cameron, H. Gregg, C. J. Radcliffe, J. D. Rhodes. 'Extracted pole filter manifold multiplexing'. *IEEE Trans. Microw. Theory Tech.*, vol. MTT-30, pp. 1041–1050, Jul. 1982.

[33] R. J. Cameron. 'General coupling matrix synthesis methods for Chebyshev filtering functions'. *IEEE Trans. Microw. Theory Tech.*, vol. 47(4), pp. 433–442, Apr. 1999.

[34] J. R. Montejo-Garai, J. A. Ruiz-Cruz, J. M. Rebollar, M. J. Padilla-Cruz, A. Oñoro-Navarro, I. Hidalgo-Carpintero. 'Synthesis and design of in-line N-order filters with N real transmission zeros by means of extracted poles implemented in low-cost rectangular H-plane waveguide'. *IEEE Trans. Microw. Theory Tech.*, vol. 53(5), pp. 1636–1642, May 2005.

[35] S. Amari, U. Rosenberg. 'New in-line dual- and triple-mode cavity filters with nonresonating nodes'. *IEEE Trans. Microw. Theory Tech.*, vol. 53(4), pp. 1272–1279, Apr. 2005.

[36] S. Amari, G. Macchiarella. 'Synthesis of inline filters with arbitrarily placed attenuation poles by using nonresonating nodes'. *IEEE Trans. Microw. Theory Tech.*, vol. 53(10), pp. 3075–3081, Oct. 2005.

[37] A. E. Atia, A. E. Williams. 'General TE011-mode waveguide bandpass filters'. *IEEE Trans. Microw. Theory Tech.*, vol. MTT-24, pp. 640–648, Oct. 1976.

[38] S. Amari, U. Rosenberg. 'New building blocks for modular design of elliptic and self-equalized filters'. *IEEE Trans. Microw. Theory Tech.*, vol. 52(2), pp. 721–736, Feb. 2004.

[39] S. Tamiazzo, G. Macchiarella. 'Synthesis of cross-coupled prototype filters including resonant and non-resonant nodes'. *IEEE Trans. Microw. Theory Tech.*, vol. 63(10), pp. 3408–3415, Oct. 2015.

[40] Zhou Zhou, Jia-sheng Hong. 'Computer-aided design of microstrip extracted-pole lossy filter'. *International Journal of RF and Microwave Computer-Aided Engineering*, **10**(1002), 2018.

[41] J. Mateu, A. Padilla, C. Collado, M. Martinez-Mendoza, E. Rocas, C. Ernst, J. M. O'Callaghan. 'Synthesis of 4th order lossy filters with uniform Q distribution'. *in 2010 IEEE MTT-S Int. Microw. Symp. Dig.*, Anaheim (CA), p. 568-571, May 2010.

[42] L.F.Qiu, L.S. Wu, W.Y.Yin, J.F.Mao. ‘A flat-passband microstrip filter with nonuniform-Q dual-mode resonators’. *IEEE Microw. Wireless Compon. Lett*. vol. 26(3), pp.183-185, March 2016.

CHAPTER 4

Introduction to Microwave Tunable Bandpass Filter

4.1 Background

The future wireless communication systems require not only breaking through the traditional microwave standard of the fixed pattern, including carrier frequency, bandwidth, polarization, but also building multimode links to improve anti-interference ability, increase spectrum utilization and expand communication capacity and service quality. Electronically reconfigurable or tunable microwave filters, which are keys to improve the capability of current and future wireless communication systems, have attracted a lot attention for research and development [1].

For example, the frequency spectrum, which is a very limited and expensive resource, has always been used for certain purposes that make it full of unwanted signals when an operation is concerned [1]. This may result in the interference between the operation signal range with the undesired narrow band radio signals, which vary from time to time and place to place. An electronically tunable narrow band rejection can be introduced in the passband of operation signal to provide a good solution for this interference issue. Moreover, the linearity specifications of low noise amplifier (LNA) can be also relax, which is because the interference signal has been attenuated enough that any noise signals produced by the LNA don't have enough power to interfere with the operation signal.

In general, the applied tunable components can increase the complexity of the filter, but the advantages of using tunable filter can still make this drawback to be ignored. These advantages can be summarized in Table 4.1.

In the open literature, current research in the microwave reconfigurable filter are can be divided in two groups: one is the negative effects reduction of the used tuning components on their electrical performance when compared to their fixed frequency

counterparts regarding very critical parameters such as insertion loss, selectivity, power handling capability and the linearity deterioration with tuning; The other is the achievement of increased levels of tunable in filter transfer function in terms of centre frequency, bandwidth and filtering type, like controllable single/multiband operations or switchable bandpass/bandstop response. Therefore, in the following sections, these two categories will be focused in detail: the tuning elements are introduced to cover the first category and the second category will be described in different types of tunable bandpass filters.

Table 4.1: The advantages of using tunable filter.

1. The complexity of system can be reduced;
2. The size and cost of system are reduced;
3. The efficiency and flexibility in spectrum usage are enhanced;
4. RF component count is reduced;
5. The capacity of system is increased;
6. System performance can be optimized;
7. Software control can be applied;
8. The specifications of other devices in the system can be relax.

4.2 Tuning technologies

Generally speaking, microwave tunable filters can be achieved in many different ways. In order to realize a continuous tuning, mechanical tuning elements (like piezoelectric transducers/actuators), MEMS capacitors, varactor diodes, ferroelectric or ferromagnetic materials can be employed. While to achieve a discrete tuning ability, MEMS switches or PIN diodes are normally used.

Mechanically tunable filters aim to move tuning mechanical screws to change the resonant frequency of cavity, coaxial or waveguide resonators. This type of tunable filter always have very high Q and good power handling capabilities, while suffer from low tuning speed and bulky size. For example, in references [2]-[4], piezoelectric transducers are used in a dielectric slab, which can be used to deform a conductive film to tune evanescent mode cavity filters or dielectric resonator filters.

Yttrium-iron-garnet (YIG) filters are often used in the magnetically tunable filters [5]. The effective permeability of the ferromagnetic material can be affected by employing an external DC magnetic field. This kind of filters have low insertion loss and high power handling capability, however, it also suffers from complex bias circuit, big physical circuit size and low tuning speed.

Barium Strontium Titanate (BST) is a popular ferroelectric material, which have a large dielectric constant that can be affected by using a DC electric filed. BST tunable filters can be easily fabricated and have a good tuning speed in ns. However, it has relatively high loss in room temperature. Although this need further investigation to improve the quality factors of BST varactors, good researches [6] [7] have shown that BST tunable filters have promising future.

RF micro-electro-mechanical system (MEMS) switches or varactors are always employed in tunable filters with continuous and discrete tuning [8]-[11]. They use micro meter level movement to achieve switch function or a required capacitance with certain DC voltage. These RF MEMS reconfigurable filters have high integration level, small physical size, low loss, high linearity with low signal distortion and good power handling ability. But they are limited by the requirement of high voltage bias circuit and hermetic packaging.

Varactor-diode-based tunable filters recently attract many attentions with promising results, compact sizes, fast tuning speed and high tunability [12]- [15]. The capacitance of varactor diode can be tuned by the applied reverse voltage across its PN junction. They have been widely employed in designing tunable filters, even though they suffer from low quality factor and poor linearity. In this thesis, varactor diodes have been applied as the

tuning components to design novel tunable filters and tunable lossy filters in the following sections.

Table 4.2 lists the performance comparison among these different tunable technologies. Obviously, none of them is perfect and chosen according to the particular specifications, which always need to do some trade-offs including response performance, physical size and cost, filter complexity, ease of integration.

Table 4.2: Comparison of different tunable technologies [1]-[12].

Tuning Technology	Mech.	YIG	PIN diode	Vacator diode	BST	RF MEMS
Unload Q	> 1000	> 500	R_s=1- 4Ω	30-50[b]	30-150[b]	50-400
Tuning Speed	> 10μs	ns	ns	ns	ns	μs
Bias	> 100V	N/A	10-40mA	< 30V	< 30V	20-100V
Linearity (IIP3: dBm)	high	< 30	> 33	10-35	10-35	> 60
Power handling	high	2W	~ mW	~ mW	~ mW	1-2W
Power Consumption	high	high	medium	low	negligible	negligible
Size	large	large	small	small	small	small
Cost	high	high	low	low	low	medium
Integration	difficult	difficult	good	good	good	good

4.3 Varactor-Diode-Based Tunable Bandpass Filter

To develop a varactor-diode-based tunable bandpass filter, the fix resonator need to be reconstruct with varactor diode to change its electrical length, which can achieve the shift of its resonant frequency. Depended on different required specifications, the couplings between resonators may also need to be controlled by the varcator diodes to meet different bandwidth requirements. In general, most of published reconfigurable filters can be classified into three categories: (1) Controlling the centre frequency; (2)

Controlling the bandwidth at a fixed centre frequency; (3) Simultaneously controlling centre frequency and bandwidth. Another novel type to tune the number of resonators has also been investigated in recent years.

In this part, typical tunable resonator and coupling structures will be described firstly, which gives a general idea about how to achieve tunable resonator and reconfigure the coupling coefficients compared to that of conventional fix resonator structures. Secondly, based on different functions of tunable filters, a featured literature review is given to show the development of varactor-tuned tunable filter in recent years. Finally, a summary is given to summarize the development of tunable filters and give a brief view of my following tunable filter works.

4.3.1 Tunable Resonator and Coupling Structures

In the open literature, many varactor-tuned microwave bandpass filters have been presented with various structures and different tunability degrees [12]-[32]. Among these various structures, varactor-loaded $\lambda/4$ [13]-[15] and $\lambda/2$ [16] resonators and dual-mode resonator [20] [21], shown in Figure 4.1, are widely used because they have very compact structures and are easily to be tuned.

In terms of $\lambda/4$ resonator, Hunter et al. [12] demonstrated a two-pole strip-line tunable combline filter at 3.5-4.5 GHz with a 3-5 dB insertion loss and a 200 ± 20 MHz absolute bandwidth. The analysis shows that the constant absolute bandwidth filters can be achieved for resonator, which have 53° electrical length at the mid-band frequency. This method has been extended in varactor-tuned stepped-impedance combline filter of [13]. A varactor-tuned microstrip combline bandpass filter loaded with lumped series resonator instead of the short-circuited end of combline is proposed [14]. This configuration enhances the tunability, which leads to a wide tuning range with a small capacitance ration of the varactor. In [15], a tunable combline filter using variable coupling reducers between resonators to tune the bandwidth has been presented. The coupling reducers, which are designed as detuned resonators made up of a line segment ending in a variable capacitor, can be regarded as bandwidth control subnetworks,

displayed in Figure 4.2. A two-pole varactor-diode tunable filters operated at 0.85-1.4 GHz with three different predefined bandwidth characteristics (constant absolute bandwidth, constant fractional bandwidth and decreasing fractional bandwidth) has been proposed by using an independent electric and magnetic coupling [16]. The independent electric and magnetic couplings, shown in Figure 4.3, make it possible to manipulate the frequency-dependent coupling coefficient variation, which results in different predefined bandwidth variations versus frequency.

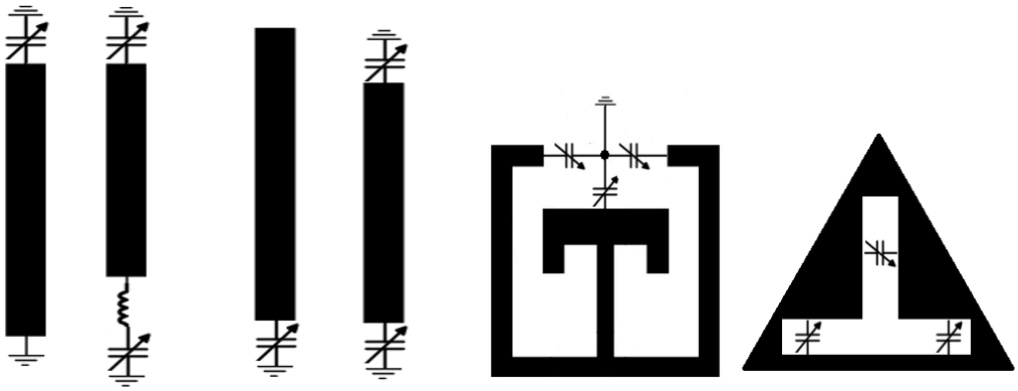

Figure 4.1: Conventional tunable resonator structures. (a) varactor-loaded $\lambda/4$ resonator [14]. (b) varactor-loaded $\lambda/2$ resonator [17]. (c) varactor-loaded dual-mode resonators [19].

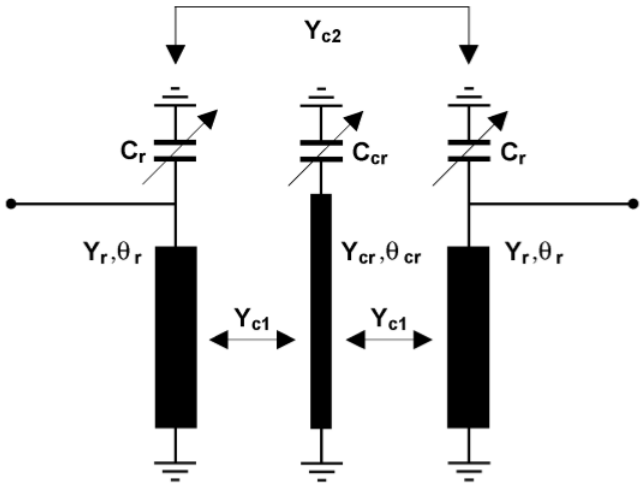

Figure 4.2: Tunable combline filter with coupling reducer [15].

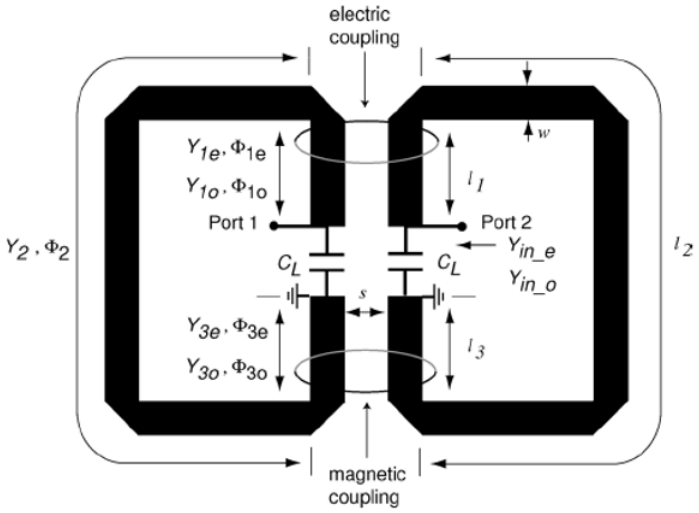

Figure 4.3: Independent electric and magnetic couplings based on varactor-tuned $\lambda/4$ resonator [16].

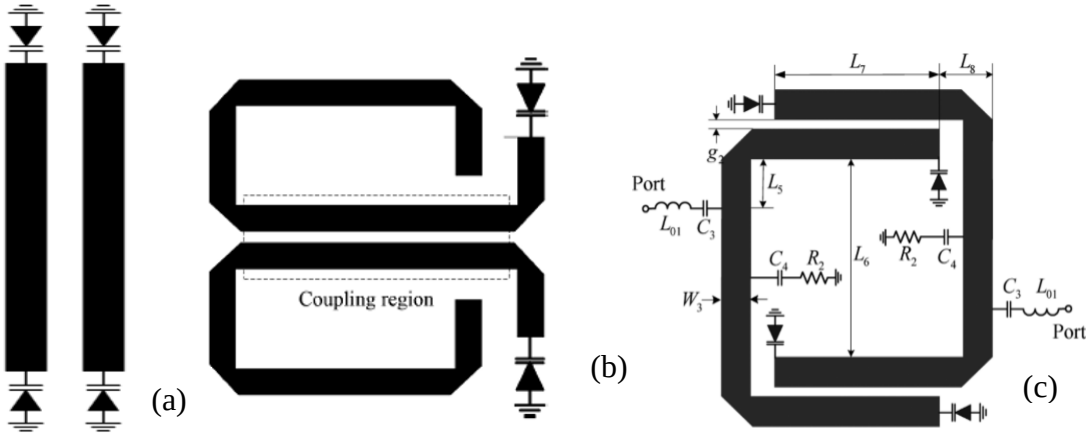

Figure 4.4: Coupling structure based on varactor-tuned $\lambda/2$ resonator.

(a) Conventional coupling. (b) Inter-stage coupling [17].
(c) Harmonic suppressed coupling [19].

As for $\lambda/2$ resonator, compared with conventional varactor-tuned $\lambda/2$ resonator couplings, a novel mixed electric and magnetic coupling scheme to control the coupling coefficients variation is presented in [17], displayed in Figure 4.4. This proposed resonator has higher Q and the coupling coefficient becomes lower as the centre frequency is tuned upward, to meet the requirement of constant absolute bandwidth. This mixed couplings is also applied to design a two-pole tunable filter with frequency tuning from 1.32 to 1.89 GHz in [18]. Moreover, based on this mixed couplings, a harmonic

suppressed tunable bandpass filter with two moveable transmission zeros is purposed in [19]. The harmonic suppressed coupling structure is given in Figure 4.4(c).

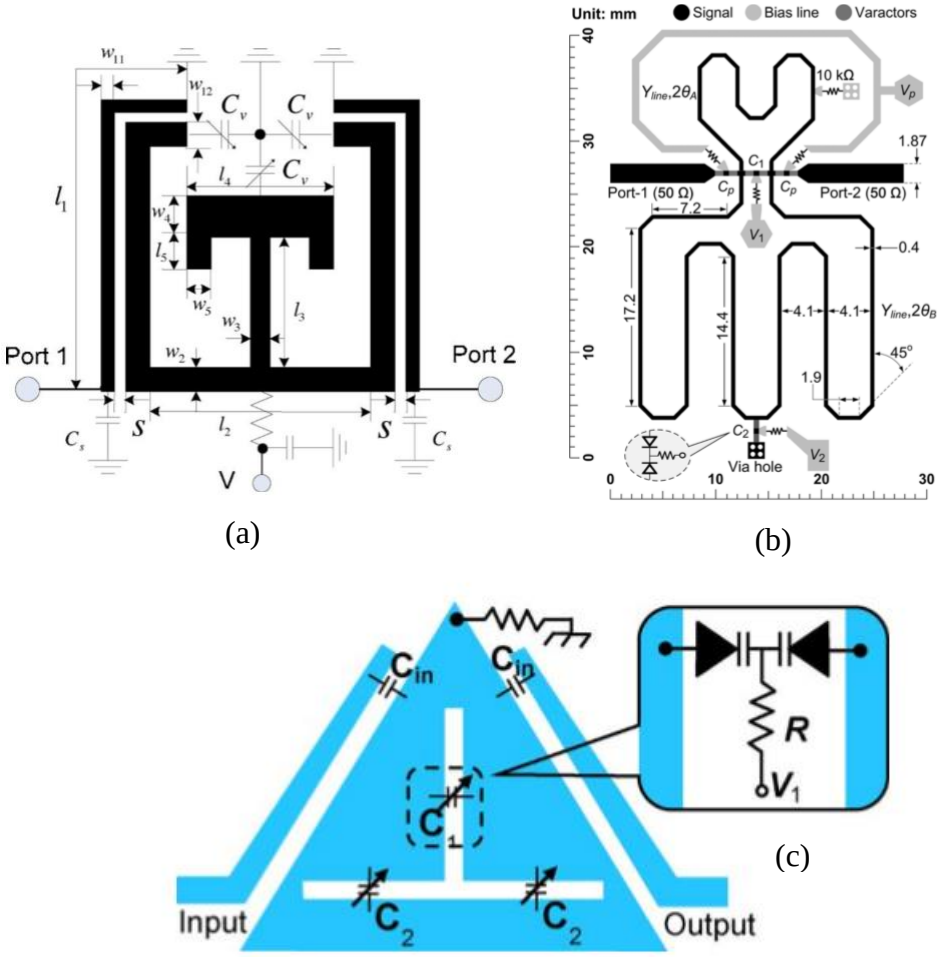

Figure 4.5: Various structures of tunable dual-mode resonators.
(a) Dual-mode open loop resonator [20]. (b) Dual-mode ring resonator [21].
(c) Dual-mode triangular patch resonator [22].

As presented in [20]- [22], various types of varactor-tuned dual-mode resonators, such as dual-mode open loop resonator [20], dual-mode ring resonator [21] and dual-mode triangular patch resonator [22] are also popular to realize reconfigure filters, which is because that these dual-mode resonators have uncoupled degenerate modes that the varactor diodes can tune each mode individually. The layout of these dual-mode resonator structures is shown in Figure 4.5.

Based on the development of reconfigurable filters discussed above, the following sections will introduce the main function categories of tunable filters, i.e., (1) Controlling the centre frequency; (2) Controlling the bandwidth at a fixed centre frequency; (3)

Simultaneously controlling bandwidth and centre frequency; (4) Controlling the number of resonators.

4.3.2 Controlling the Centre Frequency

In the tunable bandpass filter design, the characteristic of passband bandwidth variation as the tuning of centre frequency is an important issue. With the tuning of resonant frequency by using the loading varactors, the slope parameter and the coupling coefficient of the resonators are also changed. The coupling coefficient variation determines the passband bandwidth variation. For instance, a constant coupling coefficient between resonators will result in a constant fractional bandwidth when the centre frequency is tuned. However, in most practical applications, a constant absolute bandwidth (CABW) (effectively a decreasing fractional bandwidth) is desired, independent of tuned frequency. To assure constant filter response shape and absolute bandwidth, coupling coefficients must vary inversely with the tuning frequency. Sometimes, a constant fractional bandwidth (CFBW) is also important, which means the coupling coefficients remain the same while tuning the centre frequency. As to how to realize microstrip tunable bandpass filter, several recently developed typical works are described in the following [12]-[20], [23]-[32].

In [14], unlike the conventional tunable combline resonator, the centre frequency tuning can also be obtained by the additional varactors loaded on the short-circuited end of the transmission line section, as shown in Figure 4.1(a). Since the connected series resonator looks like zero impedance at the resonant frequency, it would not change the characteristic of the initial bandpass filter in the passband. The detail layout of the proposed tunable bandpass filter with active bias circuit is shown in Figure 4.6. The simulated and measured results are given in Figure 4.7. The proposed tunable bandpass filter has a nearly constant 1-dB bandwidth (91-105MHz) over the entire centre frequency tuning range from 1.7 to 2.2 GHz.

As discussed above about [17], a novel mixed electric and magnetic coupling is presented to control the coupling coefficient variation to achieve constant absolute

bandwidth and suppress the second harmonic. The layout of this filter is shown in Figure 4.8 and the simulated and measured results are illustrated in Figure 4.9. This frequency-agile filter with 60 MHz constant absolute bandwidth can be tuned from 0.68 to 1.0 GHz.

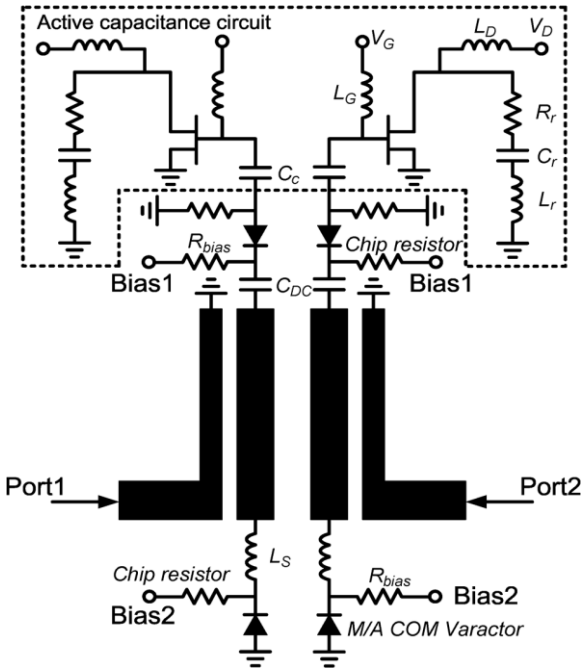

Figure 4.6: The layout of the proposed tunable BPF with active capacitance circuits [14].

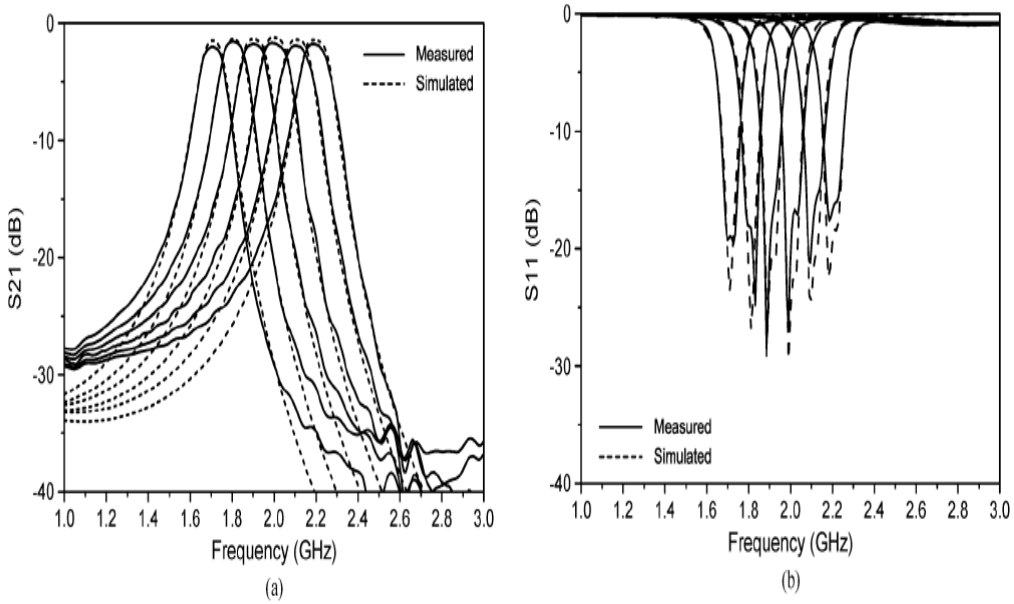

Figure 4.7: Measured and simulated results of the proposed tunable BPF: (a) S_{21} (b) S_{11} [14].

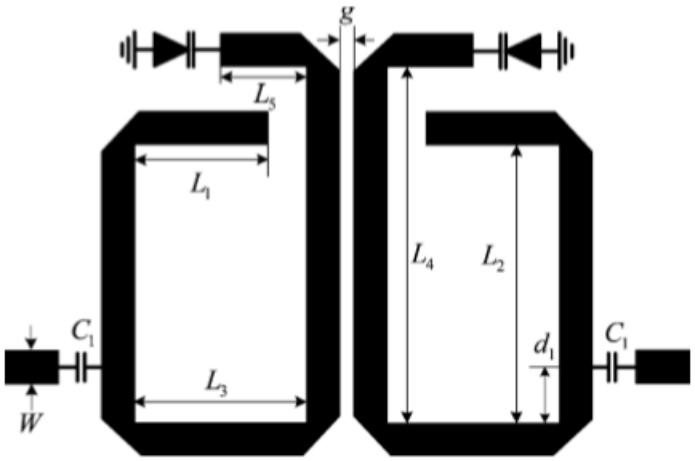

Figure 4.8: Layout of the tunable filter with constant absolute bandwidth [17].

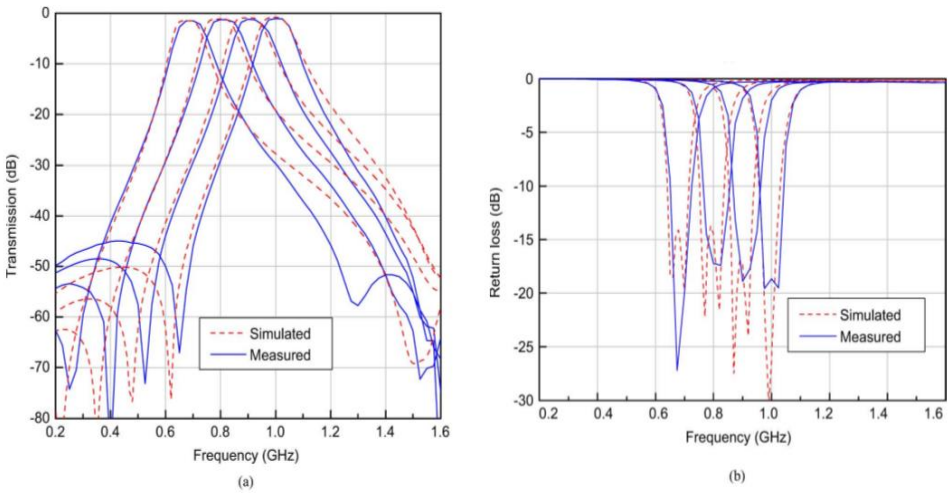

Figure 4.9: Simulated and measured responses. (a) Insertion loss. (b) Return loss [17].

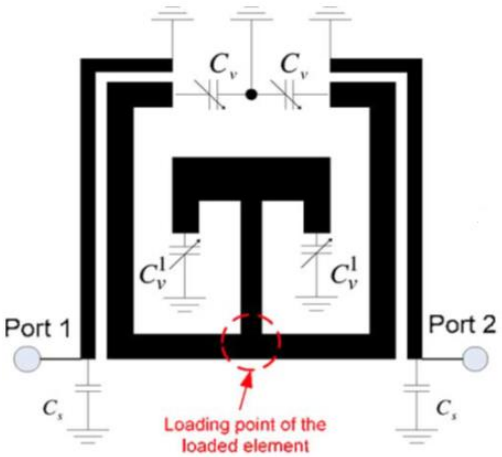

Figure 4.10: Layout of dual-mode open loop tunable bandpass filter [20].

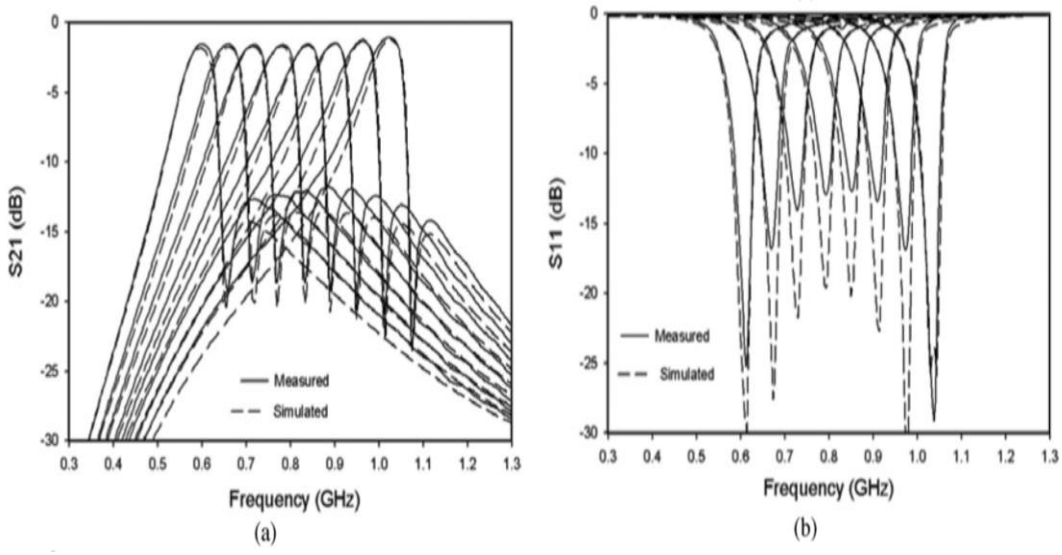

Figure 4.11: Simulated and measured response of the dual-mode tunable filter [20].

A novel type of varactor-tuned bandpass filter using dual-mode open loop resonator has been presented in [20]. By changing the two operating modes (even- and odd-mode) frequencies proportionally, the passband frequency can be easily tuned. Each dual-mode resonator can be regarded as a doubly tuned resonant circuit so that the number of resonators required for a given degree of filter can be reduced to half, which results in a compact filter configuration. What's more, its selectivity also can be tuned to exhibit a high selectivity with a finite frequency transmission zero at each side of the passband. The layout of the proposed dual-mode tunable filter is shown in Figure 4.10. Figure 4.11 illustrates the measured and EM simulated results.

Comparison of tunable filter with controlling centre frequency among recently published works is given in Table 4.3.

Table 4.3: Comparison of recent published tunable filter with controlling the centre frequency.

Ref.	Centre frequency Tuning range (GHz)	Bandwidth (MHz)	Techniques	Selective	Size (mm^2)
[13]	1.85~2.15	-3dB: 100	Varactor-tuned combline BPF with step-impedance resonators	Poor (4-pole Chebyshev)	35 x 35
[14]	1.7 ~ 2.2	-1dB: 91~105	Varactor-tuned combline BPF loaded with lumped series	Poor (4-pole Chebyshev)	60 x 70

			resonators		
[16]	0.85~1.4	-1dB: 40-45	Varactor-tuned microstrip BPF with independent odd- and even-mode	Poor (2-pole Chebyshev)	25 x 15
		-1dB: 4.3%-6.3%			25 x 15
[24]		-1dB: 5.4%±0.3%			24.7 x 13.6
[17]	0.65~0.96	-1dB: 80±3.5	Varactor-tuned microstrip BPF with novel half-wavelength resonators	Normal	50 x 34
	0.63~0.93	-1dB: 60±3			50 x 34
[19]	0.94~1.44	-3dB: 9.3%-9.8%	Varactor-tuned BPF with novel structure resonators	High	20 x 25
[20]	0.57~0.98	-1dB: 91±6	Varactor-tuned dual-mode BPF	High	12 x 18
[25]	0.6~1.07	-1dB: 80±5			12 x 18
[23]	2.1~2.7	-3dB: 90	Varactor-tuned microstrip BPF with step-impedance resonators	Poor (2-pole Chebyshev)	110 x 30
[26]	2.303~2.721	-3dB: 8%-8.5%	Varactor-tuned microstrip LC resonators BPF 0.6~1.07	Poor	20 x 20
	2.415~2.732	-3dB: 200.6-219.1			20 x 20
	2.19~2.55	-3dB: 6.2%-6.8%			20 x 20
	2.25~2.555	-3dB: 183.4-195			20 x 20
[27]	0.75~0.9	-3dB: 66	Varactor-tuned combline filter with source/load-multi-resonator coupling	High	25 x 45
[28]	0.78~1.35	-3dB: 5.8%	Varactor-tuned BPF with two-path mixed coupling	High	20 x 16
[18]	1.32~1.89	-1dB: 70±4	Varactor-tuned corrugated microstrip coupled lines BPF RF-MEMS corrugated tunable BPF	High	10 x 15
[29]	1.5~2.5	-1dB: 72±3		High	15 x 20
	1.5~2.5	-1dB: 115±10		High	15 x 20
[30]	1.4~2.0	-3dB: 5%	Varactor-tuned BPF with back-to back diodes	High	8 x 15
[31]	1.45~1.96	-3dB: 210	Varactor-tuned dual-mode BPF	High	40 x 25
[32]	2.91~3.795	-3dB: 40%	Substrate-integrated evanescent-mode cavity BPF	Poor (2-pole Butterworth)	35 x 20

4.3.3 Controlling the Bandwidth at a Fixed Centre Frequency

Many tunable filters have been investigated in the past which control the centre frequency. The tunability of centre frequency is accomplished by simply varying the electrical lengths of filter resonators. Much less effort has been devoted to design reconfigurable bandwidth bandpass filters [33]-[42]. This is owing to the difficulty involved in finding efficient mechanism to control the inter-resonator couplings, as a main goal to attain passband width variation.

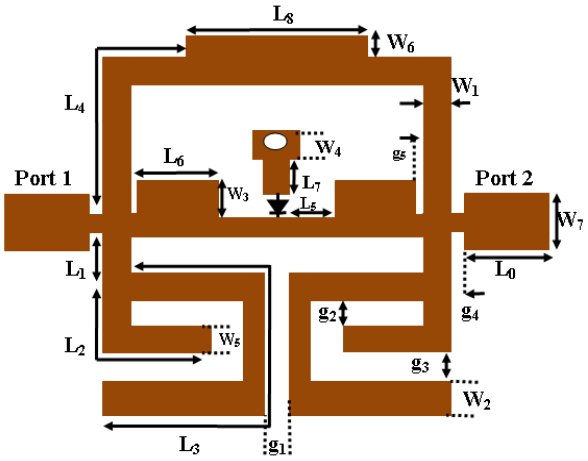

Figure 4.12: Layout of the proposed filter with a reconfigurable bandwidth [33].

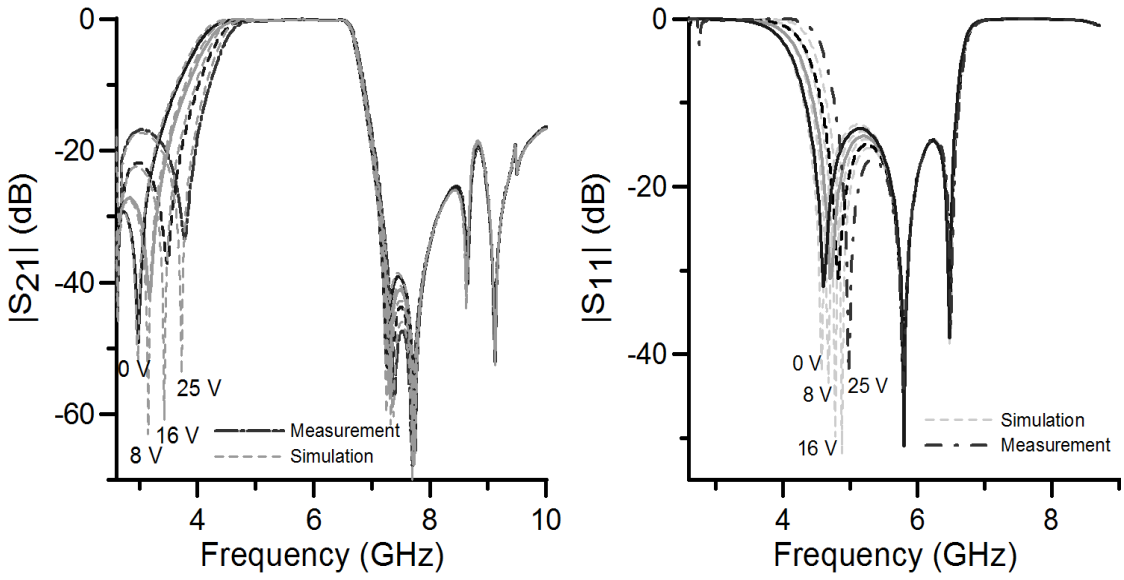

Figure 4.13: Simulated and measured S-parameter of the bandwidth tunable filter [33].

In [33], a novel compact and highly selective microstrip bandpass filter with bandwidth re-configurability for ultra-wideband application is proposed. The design uses stepped impedance resonator for realization of bandpass filter and employs a single

varactor diode for the purpose of reconfiguring bandwidth. Additionally, to improve the selectivity between passband edges, a cross-coupling between I/O feed lines is introduced which generated pairs of attenuation poles at each side of the passband. However, it can only adjust the low side of the passband to achieve the bandwidth reconfiguring. Figure 4.12 shows the layout of the presented filter. The measured response is given in Figure 4.13.

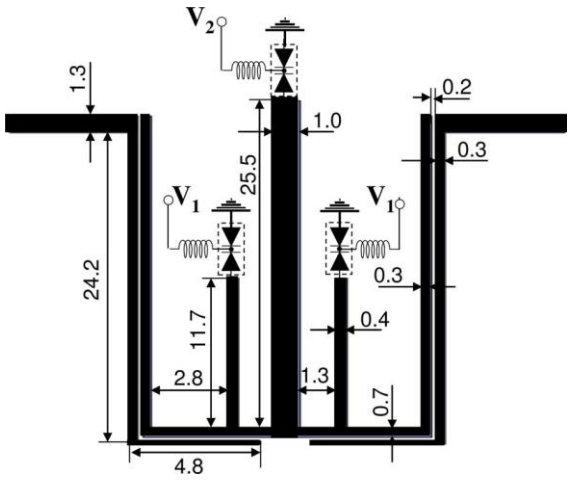

Figure 4.14: Layout of quadruple-mode stub-loaded resonator tunable filter [39].

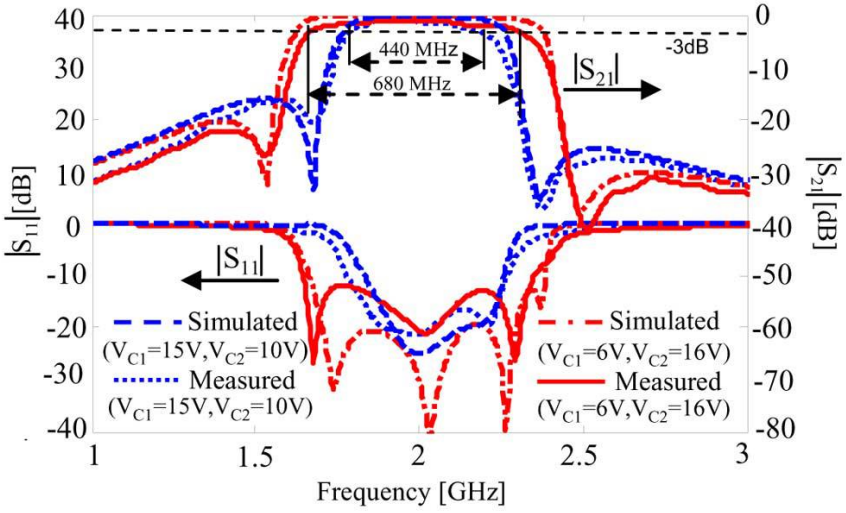

Figure 4.15: Simulated and measured results of the proposed tunable filter [39].

In [39], a new varactor-tuned quadruple-mode stub-loaded resonator is proposed. This resonator can introduce two even-modes, two odd-modes and two transmission zeros at the lower and upper side band edges. The four modes resonant frequencies and two transmission zeros can be tuned individually by tuning the stub's loads. The layout of this

type filter is shown in Figure 4.14. Figure 4.15 illustrates the simulated and measured results of this bandwidth tunable bandpass filter.

A summary of recent published tunable bandwidth filters has been demonstrated in Table 4.4.

Table 4.4: Summary of recent tunable bandwidth filters.

Ref.	Bandwidth * Tuning	Centre frequency (GHz)	Techniques	Selective	Size (mm2)
[33]	-3dB: 3.1-6.1 GHz	4.85	Varactor-tuned SIR BPF	High	18 x 20
[34] [35]	-3dB: 16.3%-35%	1.9	PIN diodes tuned short circuit coupled lines BPF with switchable stubs	Poor (2 and 3-pole Chebyshev)	40 x 25
	-3dB: 27.8%-37.4%	1.98			
[36]	-3dB: 26%-50%	2.0	PIN diodes tuned Multilayer cascaded couple line BPF	Poor	92 x 60
[37] [38]	-3dB: 13%-22%	2.5	PIN diodes tuned ring resonator BPF with stepped-impedance stubs	High	50 x 30
[39]	-3dB: 22%-34%	2.0	Varactor-tuned BPF with quadruple-mode stub-loaded resonator	High	35 x 45
[40]	-3dB: 12.6%-54.3%	0.58-0.91	Varactor-tuned half-wavelength resonator BPF with a centre-tapped open-stub.	High	100 x 50
[41]	-3dB: 200 MHz	1.25-2.1	Varactor-tuned combline BPF	High	40 x 20
[42]	-3dB: 4%-5.3%	2.16	Hybrid resonator microstrip BPF	High	30 x 15

4.3.4 Simultaneously Controlling Bandwidth and Centre Frequency

To realize tunable filters with simultaneously controlling centre frequency and bandwidth, both of the resonant frequencies and the coupling coefficient are required to be tuned. This type of tunable filter has been investigated in [22], [43]-[53].

In [22], a tunable dual-mode patch resonator filter with independent control of centre frequency and bandwidth is presented. The bandpass tunable filter uses a triangular resonator with two etched slots that split the fundamental degenerate modes to form the passband. Varactor diodes are put across the slot to change the frequency of each degenerate fundamental mode independently, which exhibits a good tuning range of bandwidth and centre frequency. The configuration of the proposed tunable triangular resonator filter is displayed in Figure 4.16. Figure 4.17 and 4.18 present the measured frequency response with centre frequency tuning, bandwidth control and transmission zeros control.

In [47], a tunable bandpass filter using cross-shaped multiple mode resonators and N:1 transformer based external quality factor tuning structures is presented. The use of a cross-shaped multiple mode resonators simplifies inter-resonators control while two external quality factor tuning structures are incorporated with the multiple mode resonators to implement simultaneous centre frequency agility and bandwidth tuning. Figure 4.19 shows the configuration of Filter A and Filter B. The measured responses of these two filter with centre frequency and bandwidth tuning are illustrated in Figure 4.20 and Figure 4.21 respectively.

Recent research works of tunable filters with centre frequency and bandwidth control, have been summarized and compared in Table 4.5.

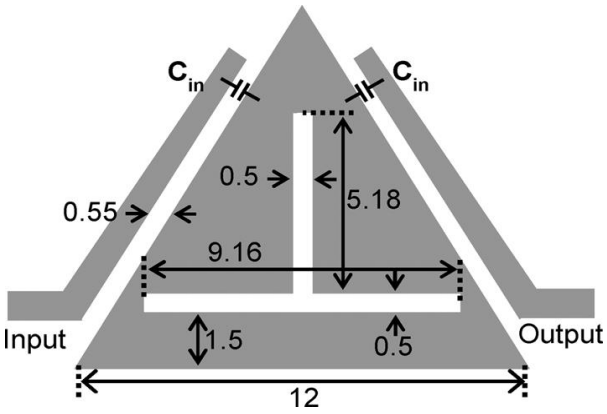

Figure 4.16: Layout of the proposed triangular resonator filter [22].

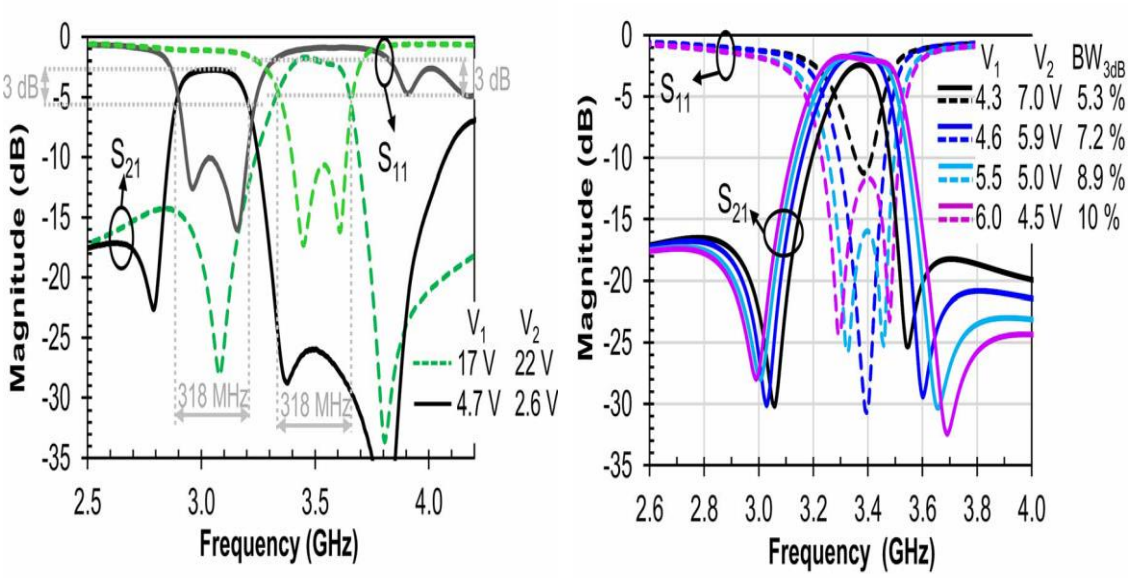

Figure 4.17: Measured response with centre frequency and bandwidth control [22].

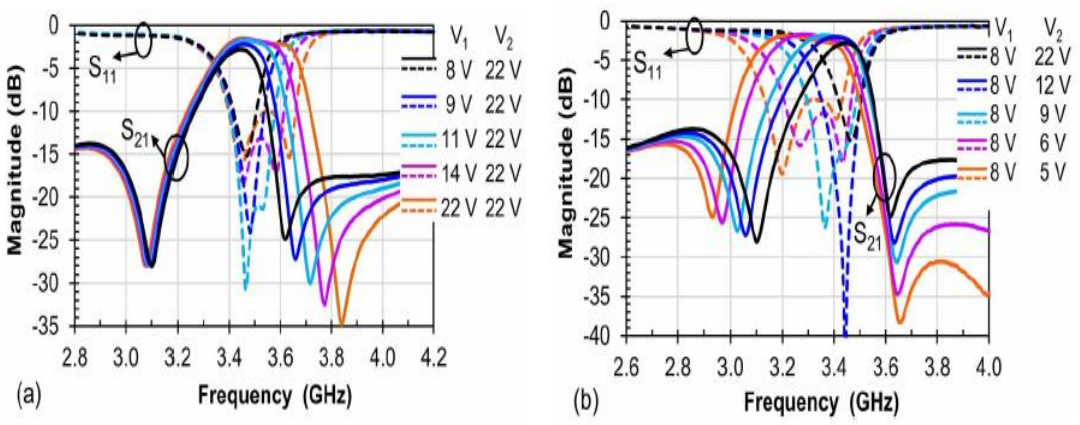

Figure 4.18: Measured response with trasmission zeros control [22].

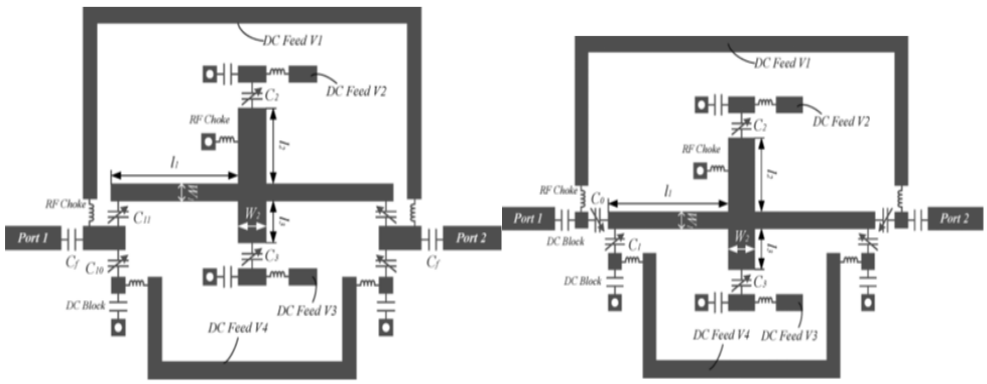

Figure 4.19: Configuration of the proposed filter A and filter B [47].

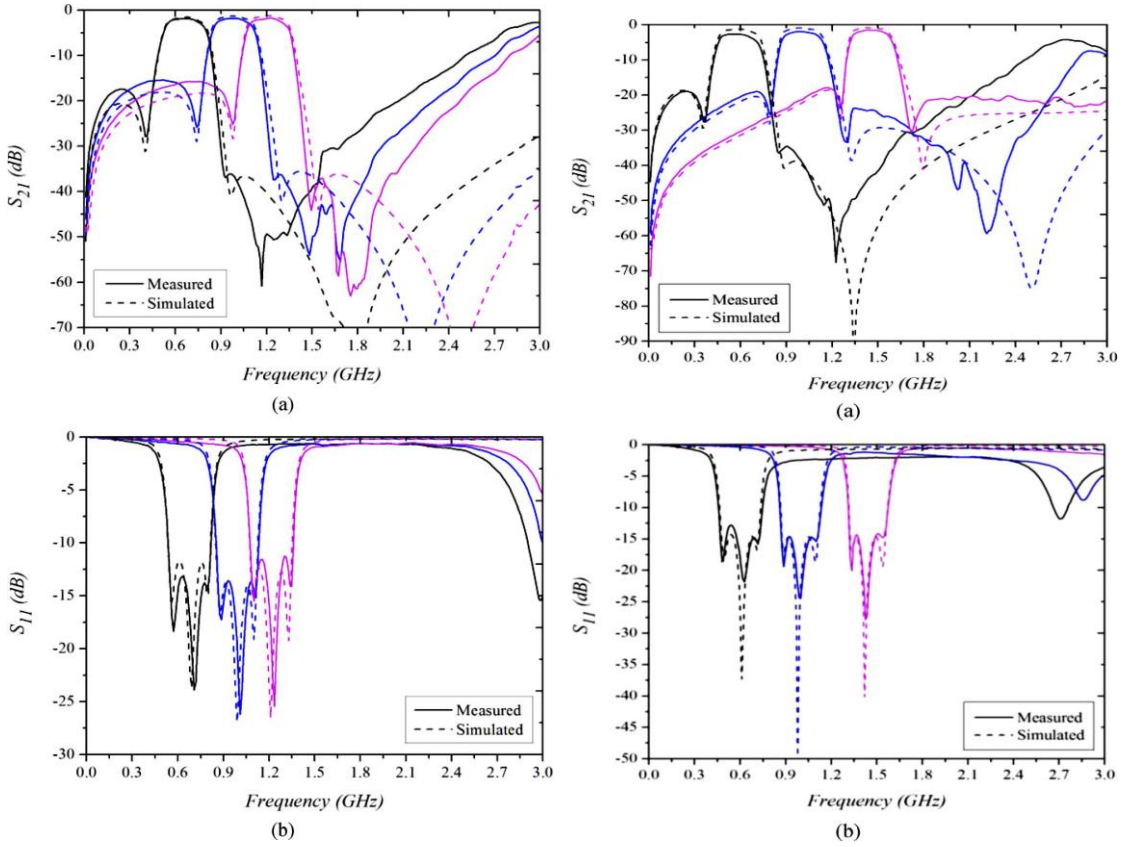

Figure 4.20: Simulated and measured S-parameter of filter A and filter B with centre frequency tuning [47].

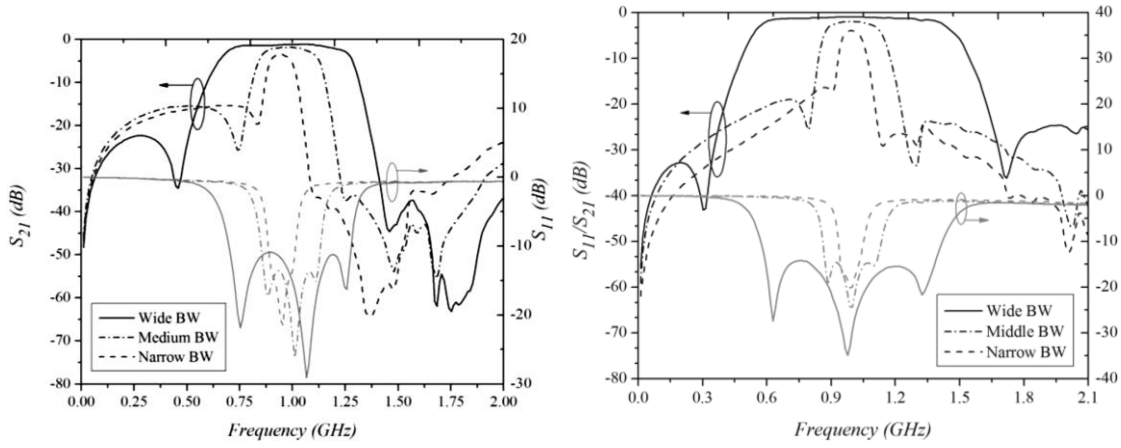

Figure 4.21: Measured S-parameter of filter A and filter B with bandwidth tuning [47].

Table 4.5: Summary of tunable filters with centre frequency and bandwidth control.

Ref.	Centre frequency tuning range (GHz)	Bandwidth tuning (MHz)	Techniques	Selective	Size (mm^2)
[22]	2.56-3.84	-3dB: 4%-12%	Varactor-tuned triangular resonator BPF	High	30 x 15
[43]	1.5-2.2	-3dB: 2.2%-11.2%	Varactor-tuned combline BPF	High	40 x 25
[44]	1.75-2.25	-1dB: 70-100	Varactor-tuned combline BPF	High	40 x 25
[45]	1.55-2.1	-1dB: 40-120	GaAs diodes-tuned combline BPF	High	25 x 15
[46]	0.43-0.6	-1dB: 0-50	Varactor-tuned microstrip BPF with loop-shaped dual-mode resonator	High	30 x 40
[47]	0.71-1.29	-3dB: 14%-64.4%	Varactor-tuned BPF with multimode resonators	High	50 x 30
	0.59-1.414	-3dB: 95%			50 x 30
[48]	1.37-1.77	-3dB: 1.7%-7.4%	Varactor-tuned multi-pole BPF	High	None
[49]	1.7~2.7	-1dB: 50-110	Varactor-tuned combline BPF	High	20 x 30
[50] [51]	0.574~0.826	-3dB: 50-78	Varactor-tuned BPF with slow-wave resonator	Poor (3-pole Chebyshev)	15 x 100
[52]	0.78~1.1	-1dB: 68-120	Varactor-tuned bandpass to bandstop filter asymmetrically loaded microstrip resonator	Poor (2-and 4-pole Chebyshev)	100 x 70
	0.76~1.08	-1dB: 64-115			
[53]	1.8~2.5	-1dB: 2%-11%	Varactor-tuned coaxial step-impedance resonator BPF	High	9 x 12

4.3.5 Controlling the Filter Order

Different from three typical types of tunable filter discussed above, tunable bandpass filter with a reconfigurable filter order is quite new with very few published works [54] [55], which highly rely on the current packaging technology.

In [54], a tunable bandpass filter with a reconfigurable-pole response was presented. 2-, 3- and 4-pole states can be obtained based on employing series resonators with RF switches. The tuning for the centre frequency is done using Schottky diodes and the selection of the filter poles is achieved using RF microelectromechanical systems switches. The insertion loss, bandwidth, rejection level and linearity can be controlled by selecting a 2-, 3-, or 4-pole state. The Layout of the tunable filter is shown in Figure 4.22. Figure 4.23, 4.24 and 4.25 present the measured results of 2-, 3- and 4- pole state respectively.

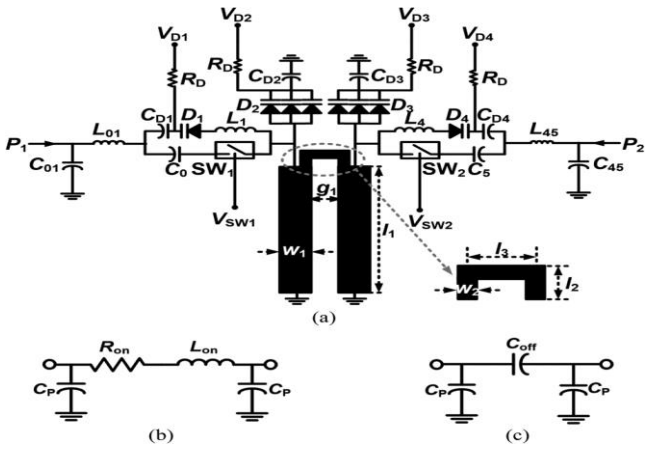

Figure 4.22: Layout of the proposed tunable bandpass Filter with reconfigurable filter order [54].

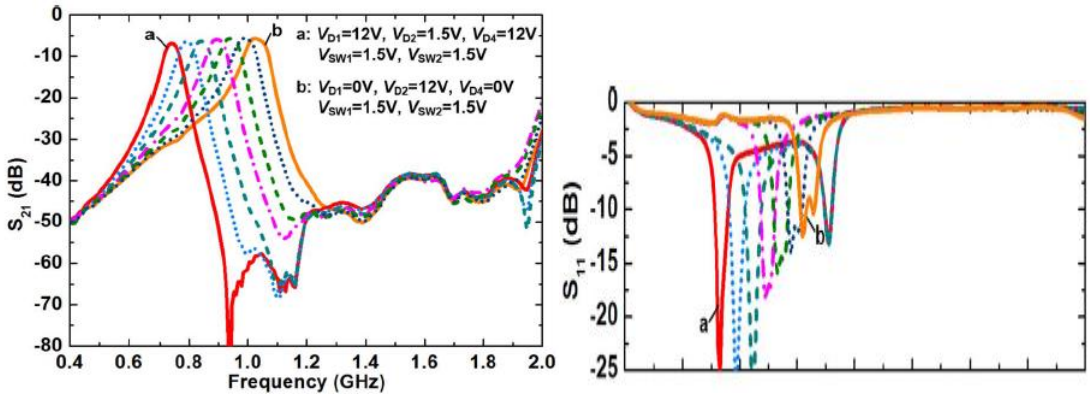

Figure 4.23: Measured S-parameter for 2-pole [54].

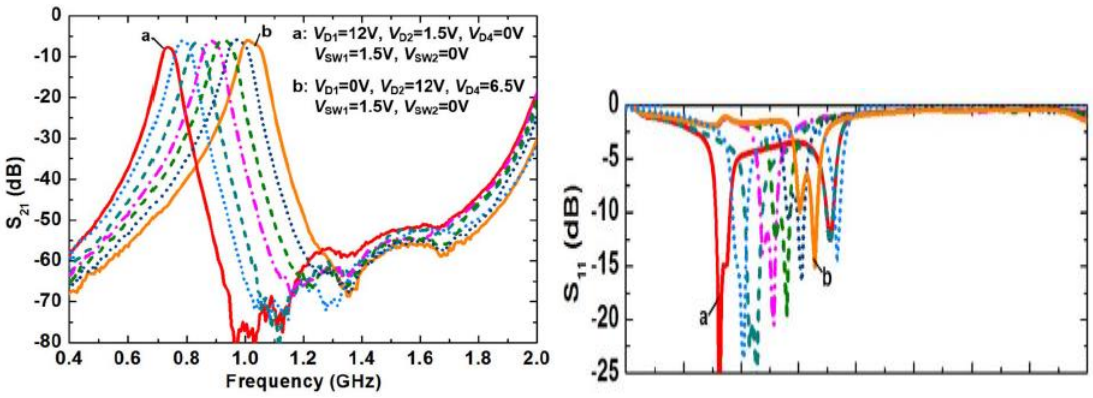

Figure 4.24: Measured S-parameter for 3-pole [54].

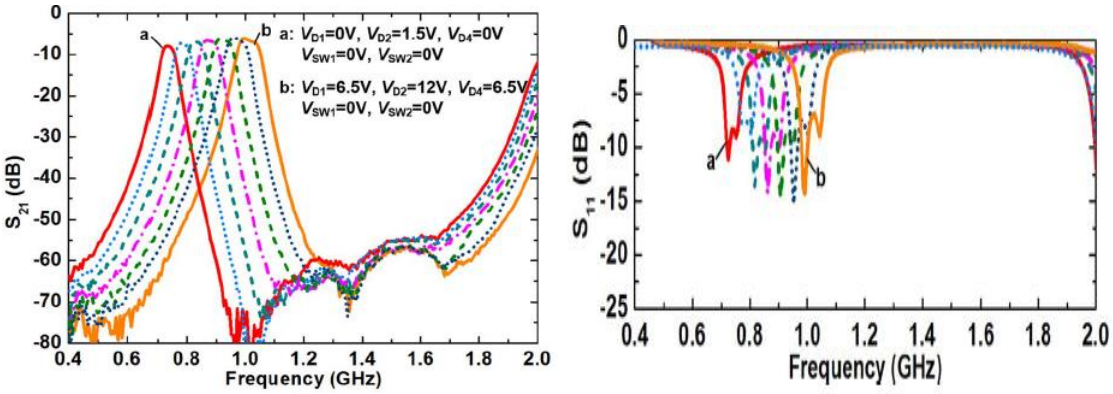

Figure 4.25: Measured S-parameter for 4-pole [54].

Recent research works of tunable filters with reconfigurable filter order, have been summarized in Table 4.6.

Table 4.6: Research works summary for tunable bandpass filter with configurable filter order.

Ref.	Centre frequency Tuning range (GHz)	Number of poles Tuning	Techniques	Selective	Size (mm^2)
[54]	0.73~1.03	2-,3-,4-pole	Tunable BPF using RF MEMS switch	Poor	None
[55]	2.77~3.55	2-,3-,4-pole	Varactor-tuned BPF with evanescent-mode cavity resonators	Poor	50 x 4

4.4 Summary

In this chapter, a literature review of tunable/reconfigurable filter from tuning technologies, conventional tuning structures to recent related tunable works has been given. Different tuning technologies can be used to realize tunable filters, such as mechanically tunable filters, YIG filters, BST filters, RF MEMS switches filters, and Varactor-diode-based filters. Since tunable bandpass filter is the main topic in this thesis, conventional tuning resonator structures, like varactor-loaded $\lambda/4$ and $\lambda/2$ resonators and dual-mode resonators, have been described. Moreover, three classical types of tunable bandpass filter (controlling centre frequency, controlling bandwidth at fixed centre frequency and simultaneously controlling bandwidth and centre frequency) with a new type (controlling filter order) have been introduced in detail with typical research works comparisons. In the following chapters, based on this literature review, my own tunable filter works with lossy technology will be presented.

Reference

[1] J.-S. Hong, “Reconfigurable planar filters,” *Microwave Magazine, IEEE*, vol.10, pp. 73-83, 2009.

[2] F. Huang and R.R. Mansour, “Tunable compact dielectric resonator filters,” *Proceedings of the 42st European Microwave Conference*, pp 559-562, Oct. 2009.

[3] T.-Y. Yun and K. Chang, “Piezoelectric-transducer-controlled tunable microwave circuits,” *IEEE Trans. Microw. Theory Tech*., vol. 50, no. 5, pp. 1303-1310, May. 2002.

[4] E. J. Naglich, J. Lee, D. Peroulis and W. J. Chappell., “Extended passband bandstop filter cascade with continuous 0.856.6-GHz coverage,” *IEEE Trans. Microw. Theory Tech*., vol. 60, no. 1, pp. 21–30, Jan. 2012.

[5] R. E. Tohkeim, C. K. Greene, J. C. Hoover, and R. W. Peter, “Nonreciprocal YIG filters,” *IEEE Trans. Magn.*, vol. MAG-3, PP. 383-392, -Sept. 1967.

[6] J. Nath, D. Ghosh, J. P. Maria, A.I. Kingon, W. Fathelbab, P. D. Franzon, and M. B. Steer, “An electronically tunable microstrip bandpass filter using thin-film barium-strontium-titanate (BST) varactors,” *IEEE Trans. Microw. Theory Tech*., vol. 53, no. 9, pp. 2707–2712, Sep. 2005.

[7] Y.-H. Chun, J. S. Hong, P. Bao, T. J. Jackson and M. J. Lancaster., “BST-Varactor tunable dual-mode filter using variable ZC transmission line,” *IEEE Microw. Wireless Compon. Lett.*, vol. 18, no. 3, pp.167-169, Sep. 2008.

[8] A. Abbaspour-Tamijani, L. Dussopt, and G. M. Rebeiz, “Miniature and tunable filters using MEMS capacitors,” *IEEE Trans. Microw. Theory Tech*., vol. 51, no. 7, pp. 1878-1885, July. 2003.

[9] L. Dussopt and G.M. Rebeiz, “Intermodulation distortion and power handling in RF MEMS switches, varators, and tunable filters,” *IEEE Trans. Microw. Theory Tech*., vol. 51, no. 4, pp. 1247 – 1256, Apr. 2003.

[10] S. Park, M. A. El-Tanani, I. Reines, and G. M. Rebeiz, “Low-loss 4-6 GHz tunable filter with 3-bit high-Q orthogonal bias RF-MEMS capacitance network,” *IEEE Trans. Microw. Theory Tech*., vol. 56, no. 10, pp. 2348 – 2388, Oct. 2008.

[11] M. El-Tanani, “High linearity 1.5-2.5 GHz RF-MEMS and varactor diod based tunable filters for wireless applications,” *Doctor of Philosophy thesis*, The University of California, San Diego, 2009.

[12] I. C. Hunter and J. D. Rhodes, “Electronically tunable microwave bandpass filters,” *IEEE Trans. Microw. Theory Tech.*, vol. 30, no. 9, pp. 1354 – 1360, Sep. 1982.

[13] B. W. Kim and S. W. Yun, "Varactor-tuned combline bandpass filter using step-impedance microstrip lines," *IEEE Trans. Microw. Theory Tech.*, vol. 52, no. 4, pp. 1279 – 1283, Apr. 2004.

[14] X. G. Wang, Y. H. Cho, and S. W. Yun, "A tunable combline bandpass filter loaded with series resonator," *IEEE Trans. Microw. Theory Tech.*, vol. 60, no. 6, pp. 1569 – 1576, Jun. 2012.

[15] M. Sanchez-Rendo, R. Gomez-Garcia, J. I. Alonso, and C. Briso-Rodriguez, "Tunable combline filter with continuous control of centre frequency and bandwidth," *IEEE Trans. Microw. Theory Tech.*, vol. 53, no. 1, pp. 191 – 199, Jan. 2005.

[16] S. Park and G. M. Rebeiz, "Low-loss two-pole tunable filters with three different predefined bandwidth characteristics," *IEEE Trans. Microw. Theory Tech*., vol. 56, no. 5, pp. 1137 – 1148, May 2008.

[17] X. Y. Zhang, Q. Xue, C. H. Chan, and B. J. Hu, "Low-loss frequency-agile bandpass filters with controllable bandwidth and suppressed second harmonic," *IEEE Trans. Microw. Theory Tech.*, vol. 58, no. 6, pp. 1557 – 1564, Jun. 2010.

[18] M. A. El-Tanani and G. M. Rebeiz, "Corrugated microstrip coupled lines for constant absolute bandwidth tunable filters," *IEEE Trans. Microw. Theory Tech*., vol. 58, no. 4, pp. 956 – 963, Apr. 2010.

[19] X. Y. Zhang and Q. Xue, "High-selectivity tunable bandpass filters with harmonic suppression," *IEEE Trans. Microw. Theory Tech*., vol. 58, no. 4, pp. 964–969, Apr. 2010.

[20] W. Tang and J.-S. Hong, "Varactor-tuned dual-mode bandpass filters," *IEEE Trans. Microw. Theory Tech.*, vol. 58, no. 8, pp. 2213-2219, Aug. 2010.

[21] H.-J. Tsai, N.-W. Chen and S.-K. Jeng, "Centre frequency and bandwidth controllable microstrip bandpass filter design using loop-shaped dual-mode resontor," *IEEE Trans. Microw. Theory Tech.*, vol. 61, no.10, pp. 3590-3600, Oct. 2013.

[22] A. L. C. Serrano, F. S. Correra, T.-P. Vuong, and P. Ferrari, "Synthesis methodology applied to a tunable patch filter with independent frequency and bandwidth control," *IEEE Trans. Microw. Theory Tech.*, vol. 60, no.3, pp. 484-493.

[23] J. Lee and K. Sarabandi, "An analytic design method for microstrip tunable filters," *IEEE Trans. Microw. Theory Tech.*, vol. 56, no. 7, pp. 1699–1706, Jul. 2008.

[24] S.-J. Park, K. Van Caekenberghe, and G. M. Rebeiz, "A miniature 2.1-GHz low loss microstrip filter with independent electric and magnetic coupling," *IEEE Microw. Wireless Compon. Lett.*, vol. 14, no. 10, pp. 496–498, Oct. 2004.

[25] Y.-H. Chun and J.-S. Hong, “Electronically reconfigurable dual-mode microstrip open-loop resonator filter,” *IEEE Microw. Wireless Compon. Lett.*, vol. 18, no. 7, pp. 449–451, July 2008.

[26] Q. Y. Xiang, Q. Y. Feng, X. G. Huang, and D. H. Jia, “Electrical tunable microstrip LC bandpass filters with constant bandwidth*,” IEEE Trans. Microw. Theory Tech*., vol. 61, no. 3, pp. 1124–1130, Mar. 2013.

[27] M. Sanchez-Renedo, “High-selectivity tunable planar combline filter with source/load-multiresonators coupling,” *IEEE Microw. Wireless Compon. Lett*., vol. 17, no. 7, pp. 513–515, Jul. 2007.

[28] C. Ge and X.-W. Zhu, “Highly-selective tunable bandpass filter with two-path mixed coupling,” *IEEE Microw. Wireless Compon. Lett.*, vol. 24, no. 7, pp. 451–453, Jul. 2014.

[29] M. A. El-Tanani and G. M. Rebeiz, “High performance 1.5–2.5 GHz RF MEMS tunable filters for wireless applications,” *IEEE Trans. Microw. Theory Tech*., vol. 58, no. 6, pp. 1629–1637, Jun. 2010.

[30] M. A. El-Tanani and G. M. Rebeiz, “A two-pole two-zero tunable filter with improved lineraity,” *IEEE Trans. Microw. Theory Tech*., vol. 57, no. 4, pp. 830–839, Apr. 2009.

[31] L. Athukorola and D. Budimir, “Compact second-order highly linear varactor-tuned dual-mode filters with constant bandwidth,” *IEEE Trans. Microw. Theory Tech*., vol. 59, no. 9, pp. 2214–2220, Sep. 2011.

[32] S. Saeedi, J. Lee, and H. H. Sigmarsson, “Broadband implementation of tunable, substrate-integrated, evanescent-mode, cavity bandpass filters,” *in IEEE 44th Eur. Microw. Conf*., 2014, pp. 849–852.

[33] K. Rabbi and D. Budimir, “Miniaturised sharp rejection bandpass filter with reconfigurable bandwidth for UWB applications”, *43th European Microwave Conference*, EuMC2013.

[34] A. Miller and J. Hong, “Wideband bandpass filter with multiple reconfigurable bandwidth states,” *in Proc. Eur. Microw. Conf.*, Sep. 2010.

[35] A. Miller, J. Hong “Wideband Bandpass Filter with Reconfigurable Bandwidth,” *IEEE Microwave and Wireless Components Letters,* Vol 19, no. 12, pp. XX - XX, Jan. 2010.

[36] A. Miller and J.-S. Hong, “Cascaded coupled line filter with reconfigurable bandwidths using LCP multilayer circuit technology,” *IEEE Trans. Microw. Theory*

Techn., vol. 60, no. 6, pp. 1557–1586, Jun. 2012.

[37] C. H. Kim and K. Chang, "Wideband ring resonator bandpass filter with dual stepped impedance stubs," *in Proc. IEEE MTT-S Int. Microw. Symp. Dig.*, 2010, pp. 229–232.

[38] C. H. Kim and K. Chang, "Ring resonator bandpass filter with switchable bandwidth using stepped-impedance stubs," *IEEE Trans. Microw. Theory Tech.*, vol. 58, no. 12, pp. 3936–3944, Dec. 2010.

[39] X. Huang et al., "Bandpass filter with tunable bandwidth using quadruple-mode stub-loaded resonator," *IEEE Microw. Wireless Compon. Lett.*, vol. 22, no. 4, pp. 176–178, Apr. 2012.

[40] X. Luo, S. Sun and R. B. Staszewski, "Tunable bandpass filter with two adjustable transmission poles and compensable coupling", *IEEE Trans. Microw Theory Tech*., vol.62, no.9, Sep 2014.

[41] T. Yang and G. M. Rebeiz, "Tunable 1.25-2.1-GHz 4-pole bandpass filter with intrinsic transmission zero tuning", *IEEE Trans. Microw Theory Tech*., vol.63, no.5, May 2015.

[42] B-F. Zong, G-M. Wang, J-G. Liang and C. Zhou, "Compact bandpass filter with two tunable transmission zeros using hybrid resonators", *IEEE Microw. Wireless Compon. Lett*., vol. 25, no. 2, Feb 2015.

[43] Y.-C. Chiou and G. M. Rebeiz, "A tunable 3-Pole 1.5–2.2 GHz bandpass filter with bandwidth and transmission zero control," *IEEE Trans. Microw. Theory Tech.*, vol. 59, no. 11, pp. 2872–2878, Nov. 2011.

[44] Y.-C. Chiou and G. M. Rebeiz, "A quasi elliptic function 1.75–2.25 GHz 3-pole bandpass filter with bandwidth control," *IEEE Trans. Microw. Theory Tech*., vol. 60, no. 2, pp. 244–249, Feb. 2012.

[45] Y.-C. Chiou and G. M. Rebeiz, "Tunable 1.55–2.1 GHz 4-pole elliptic bandpass filter with bandwidth control and 50 dB rejection for wireless systems," *IEEE Trans. Microw. Theory Techn*., vol. 61, no. 1, pp. 117–124, Jan. 2013.

[46] H.-J. Tsai, N.-W. Chen, and S.-K. Jeng, "Centre frequency and bandwidth controllable microstrip bandpass filter design using loop-shaped dual-mode resonator," *IEEE Trans. Microw. Theory Tech*., vol. 61, no. 10, pp. 3590–3600, Oct. 2013.

[47] J.-R. Mao, W.-W. Choi, and K.-W. Tam, "Tunable bandpass filter design based on external quality factor tuning and multiple mode resonators for wideband applications," *IEEE Trans. Microw. Theory Tech*, vol. 61, no. 7, pp. 2574–2584, Jul. 2013.

[48] K. Kawai, H. Okazaki, and S. Narahashi, “Centre frequency and bandwidth tunable filter employing MEMS digitally tunable capacitors,” *in Proc. Asia Pacific Microwave Conference*, Seoul, 2013, pp. 188-190.

[49] P-L. Chi, T. Yang and T-Y. Tsai, “A fully tunable two-pole bandpass filter”, *IEEE Microw. Wireless Compon. Lett.*, vol. 25, no. 5, MAY 2015.

[50] E. Pistono, P. Ferrari, L. Duvillaret, J.-M. Duchamp, and A. Vilcot, “A compact tune-all bandpass filter based on coupled slow-wave resonators,” *in Proc. 35th Eur. Microwave Conf., Paris, France*, Oct. 2005, pp. 1243–1246.

[51] E. Pistono, M. Robert, L. Duvillaret, J.-M. Duchamp, A. Vilcot, and P. Ferrari, “Compact fixed and tune-all bandpass filters based on coupled slow-wave resonators,” *IEEE Trans. Microw. Theory Tech*., vol. 54, no. 6, pp. 2790–2799, Jun. 2006.

[52] Y.-H. Cho and G. Rebeiz, “Two- and four-pole tunable 0.7–1.1-GHz bandpass-to-bandstop filters with bandwidth control,” *IEEE Trans. Microw. Theory Techn*., vol. 62, no. 3, pp. 457–463, Mar. 2014.

[53] T. Yang, K. Ho, and G. M. Rebeiz, “Compact self-shielded 2–3 GHz high-Q coaxial fixed and tunable filters,” *IEEE Trans. Microw. Theory Techn.*, vol. 62, no. 12, pp. 3370–3379, Dec. 2014.

[54] Y.-H. Cho and G. M. Rebeiz, “0.73–1.03-GHz tunable bandpass filter with a reconfigurable 2/3/4-pole response,” *IEEE Trans. Microw. Theory Techn.*, vol. 62, no. 2, pp. 290–296, Feb. 2014.

[55] H. H. Sigmarsson, J. Lee, D. Peroulis, and W. J. Chappell, "Reconfigurable-order bandpass filter for frequency agile systems," *IEEE MTT-S Int. Microwave Symp. Dig*., pp.1756-1759, 23-28 May 2010.

CHAPTER 5

Symmetric Varactor-tuned Microstrip Bandpass Lossy Filter

5.1 Introduction

Microstrip tunable bandpass filter has been widely used in modern wireless communication systems. Recently many research works focus on controlling the bandwidth, which is because that the centre frequency is easily to be reconfigured by varying the resonators' electrical length by using the commercial tuning components, while the bandwidth tuning depends on both the external quality factor Q_e and coupling coefficients. For example, the tunable bandpass filter proposed in [1] can easily tuned its centre frequency from 0.7GHz to 1.33 GHz, but difficulty maintain the bandwidth in the tuning range due to the change of external quality factor and coupling matrix. Various filters designed to have a good control of bandwidth have been achieved in [6]-[13]. In [6], a wideband ring bandpass filter with switchable bandwidth ratio 1.22:1.13:1 centred at 2.5GHz is demonstrated by using multiple stepped open stubs and interdigital coupled feed lines. In [7] [8], a cascaded coupled line tunable filter with four bandwidth states from 20 to 50% 3dB FBW centred at 2GHz is described and extended to fabricate by using LCP multilayer circuit technology. A multilayer parallel-coupled lines with short-circuited stubs tunable filter is presented in [9]. In [10], a microstrip bandpass tunable filter is built with two adjustable transmission poles based on a half-wavelength resonator with a centre-tapped open-stub. A four-pole tunable bandpass filter is demonstrated with adjustable transmission zeros (TZs) and bandwidth in [11]. In [12], two compact hybrid resonators tunable filter are presented with a mixed electric/ magnetic (EM) coupling to introduce a tunable transmission zero. In [13], a tunable bandpass filter using cross-shaped multiple mode resonators (MMRs) based on external quality factor tuning structures is proposed. Moreover, the tunable filters with good bandwidth control at varied centre frequency are also investigated in [14]-[20].

The tunable bandpass filters discussed above focus on low-loss insertion loss in the

passband, while it is still rare to combine the lossy synthesis in tunable bandpass filter. The lossy synthesis，which has been discussed in Chapter 3, aims to accept additional insertion loss and/or return loss without changing the passband shape of the filter function, knowing that the added loss level can be compensated by the LNA amplifiers in the communication system without affecting the system performance.

In this chapter, microstrip tunable bandpass filter combining lossy technology will be presented. The presented work in this chapter is based on the patent of European Space Agency [21]. For better demonstration, a symmetric three-pole microstrip tunable bandpass lossy filter with resistor loading to control the bandwidth and selectivity is given firstly. Then extending this filter by tuning the resonators, a three-pole tunable bandpass lossy filter with controlling the bandwidth at fixed centre frequency is achieved. What's more, by changing the method to introduce the loss, a five-pole tunable bandpass lossy filter with combining resistor loading and cross coupling is demonstrated.

5.2 Tunable Lossy Filter with Controlling Bandwidth and Selectivity

In this section, a symmetric three-pole tunable bandpass lossy filter with resistor loading to control bandwidth and selectivity is designed. This filter has a centre frequency tuning range from 0.93 to 1.2 GHz with 3dB FBW tuning range from 77.3% to 9.3% at the same time, by moving the lower side transmission zero at fixed high side transmission zero.

5.2.1 Filter Design and Analysis

The symmetric structure of this proposed filter is shown in Figure 5.1, which has three half-wavelength step-impedance resonator in the inline network. The external couplings can be tuned with varactor C_e, while the coupling coefficient can be tuned with varactor C. A resistor R is loaded in the second resonator and connected to the ground at the other side.

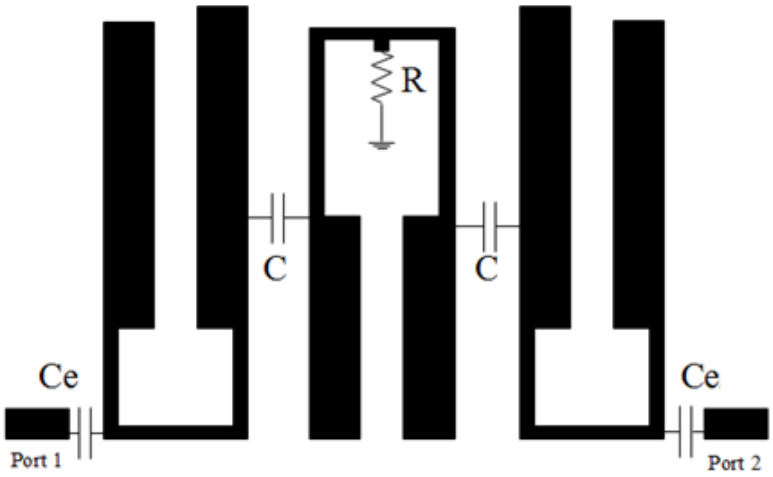

Figure 5.1: Layout of the proposed tunable bandpass filter.

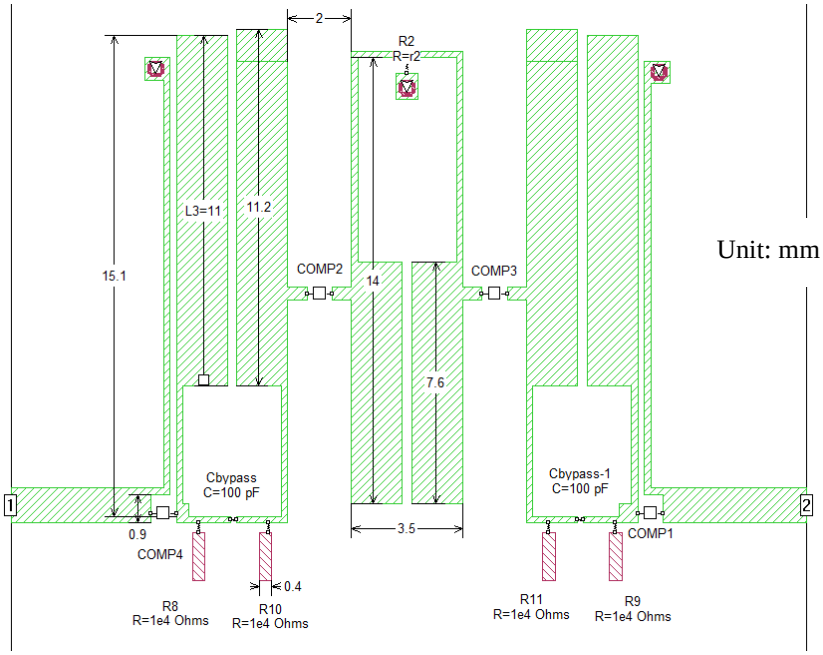

Figure 5.2: Layout of EM simulation with dimensions.

By following the filter implementation method mentioned in Chapter 3, this circuit model can be converted to EM simulation. The layout of EM simulation with dimensions is illustrated in Figure 5.2. The varactors are represented by COMP1, COMP2, COMP3 and COMP4. COMP1 and COMP4 are used to tune the external couplings, while COMP2 and COMP3 are applied to tune the coupling coefficients. Due to the symmetric tuning, COMP1 and COMP4 can be connected to a same dc voltage. Another dc voltage can be used in COMP2 and COMP3 as well, which makes this tunable bandpass filter easy to be tuned with only two dc bias voltages.

5.2.2 Filter Implementation and Measurement

The proposed 3-pole tunable bandpass lossy filter is fabricated on the RT/Duriod 6010 substrate with 1.27 mm thickness and dielectric constant 10.2 (loss $\tan\delta = 0.0023$). The detail fabrication photograph of the filter with bias scheme is shown in Figure 5.3. As we can see, the filter size is $25\text{ mm} \times 20\text{ mm}$ ($0.26\lambda_g \times 0.21\lambda_g$ at fix centre frequency 1.0 GHz), where λ_g is the guided wavelength. Silicon abrupt junction diodes SMV2020-079LF are used for tuning varactors COMP1, COMP2, COMP3 and COMP4 mentioned in Figure 5.2. The Panasonic resistor 10k ohm resistors are used to reduce the RF signal leakage in the dc bias circuits and the Murata 0402 GRM 100pF capacitors are used to block the dc voltages. Because the varactor are drove by the reverse voltages, voltage values are used to represent different states instead of specific capacitance value of the varactors. The SMV2020-079LF capacitance vs reverse voltages is plotted in Figure 5.4.

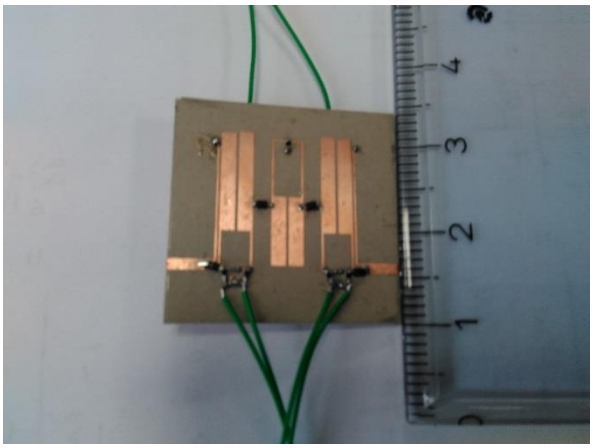

Figure 5.3: Fabrication photo of 3-pole tunable bandpass lossy filter.

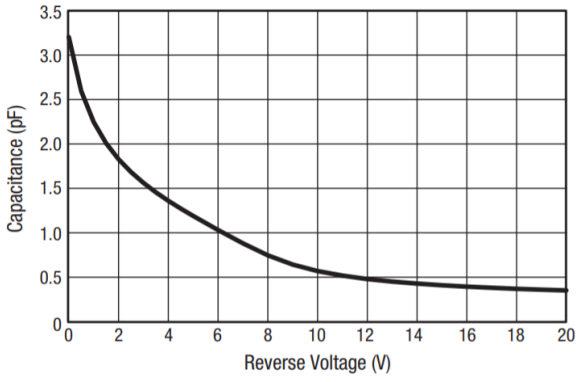

Figure 5.4: SMV2020-079LF capacitance vs reverse voltage [22].

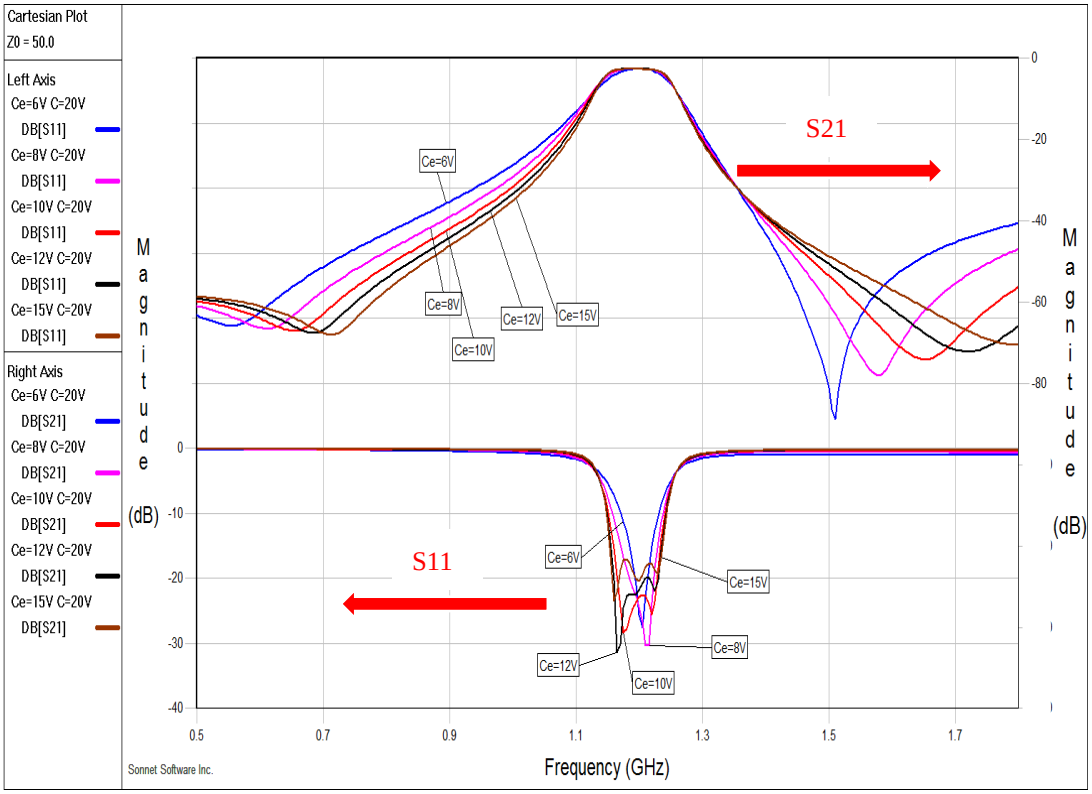

(a)

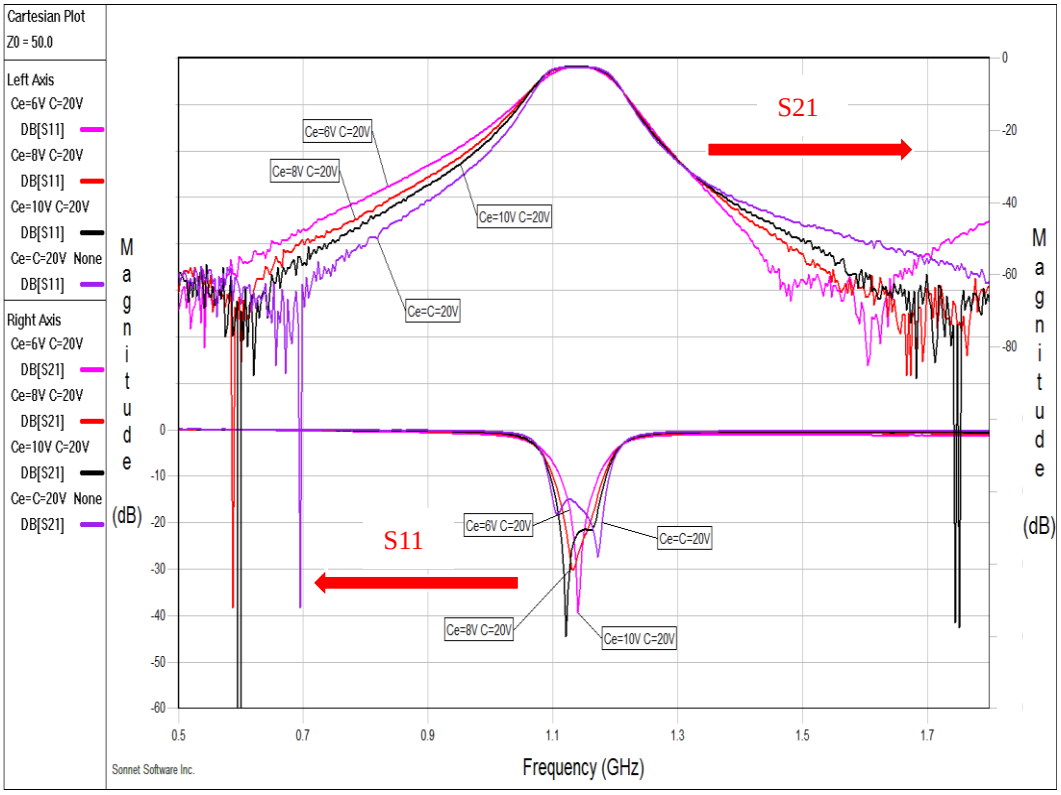

(b)

Figure 5.5: Response performance with variable external coupling Ce and constant coupling coefficients C. (a) Simulation. (b) Measurement.

The response performance of the fabricated filter with variable external coupling Ce and constant coupling coefficients is shown in Figure 5.5. It can be seen from the simulation results that it has a constant 10.5% 3dB FBW due to the constant coupling coefficients and a flat passband with 0.5 dB passband variation (insertion loss varying from -2.5 to -3.0 dB) centred at 1.2 GHz among different states. This fabricated filter has two transmission zeros at each band edge, which is because of the external coupling structure. By varying the external coupling, these two transmission zeros also shift with slightly affecting the insertion loss, which can be ignored. When the reverse voltage of varactors controlling external coupling increases, their capacitances reduce and the two transmission zeros shift to the higher side frequency domain. The measurement results show a good agreement with the simulation results. The fabricated filter has a constant 10.6% 3dB FBW centred at 1.15 GHz with 0.4 dB passband variation (insertion loss varying from -2.7 to -3.1 dB) among different tuning states. There are some noises around the transmission zeros in the measurement results, which can be improved by calibration.

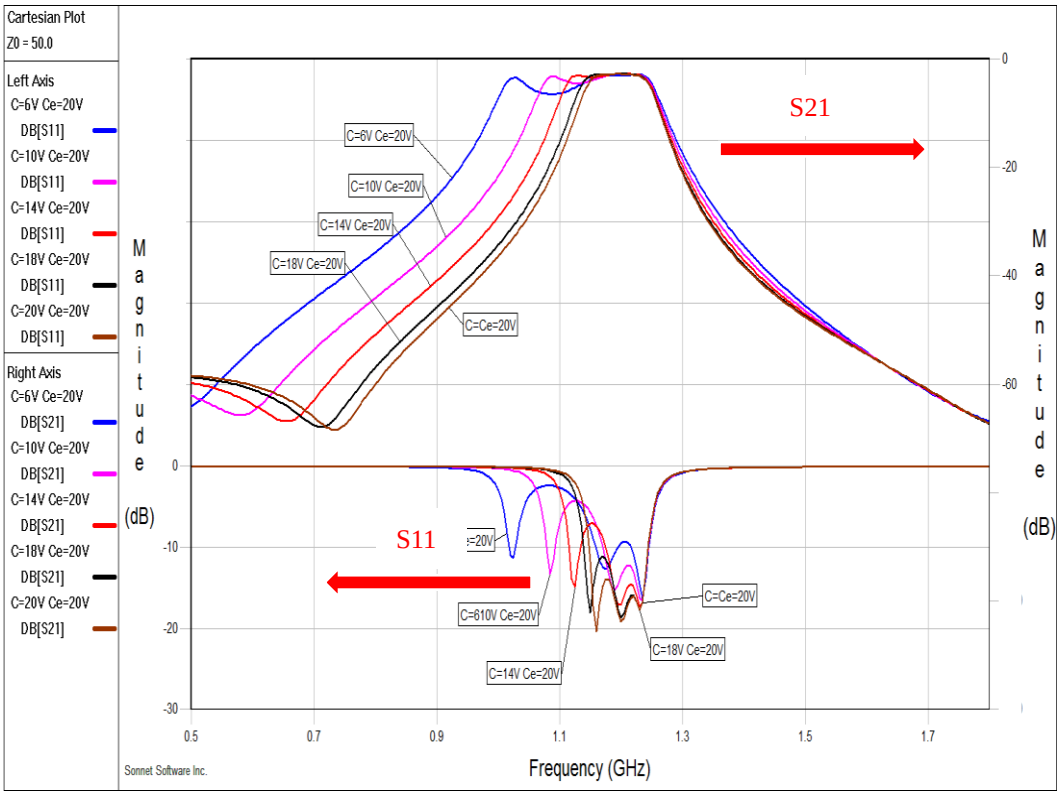

(a)

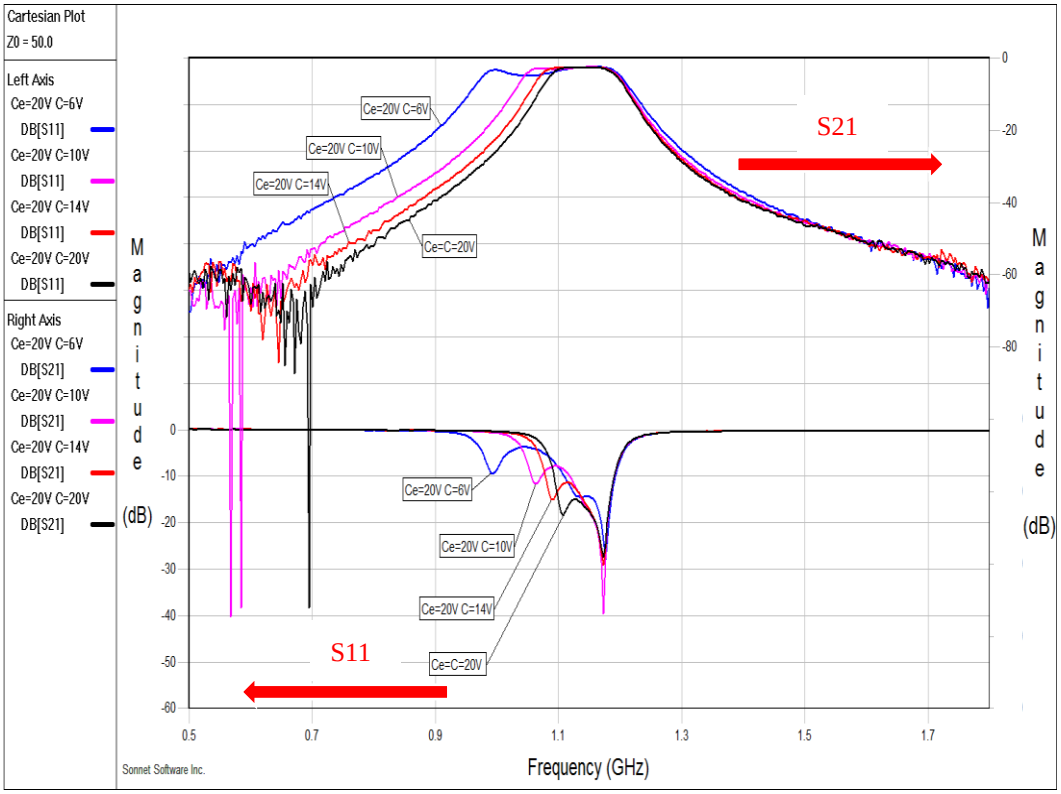

(b)

Figure 5.6: Response performance with variable coupling coefficients C and constant external coupling Ce. (a) Simulation. (b) Measurement.

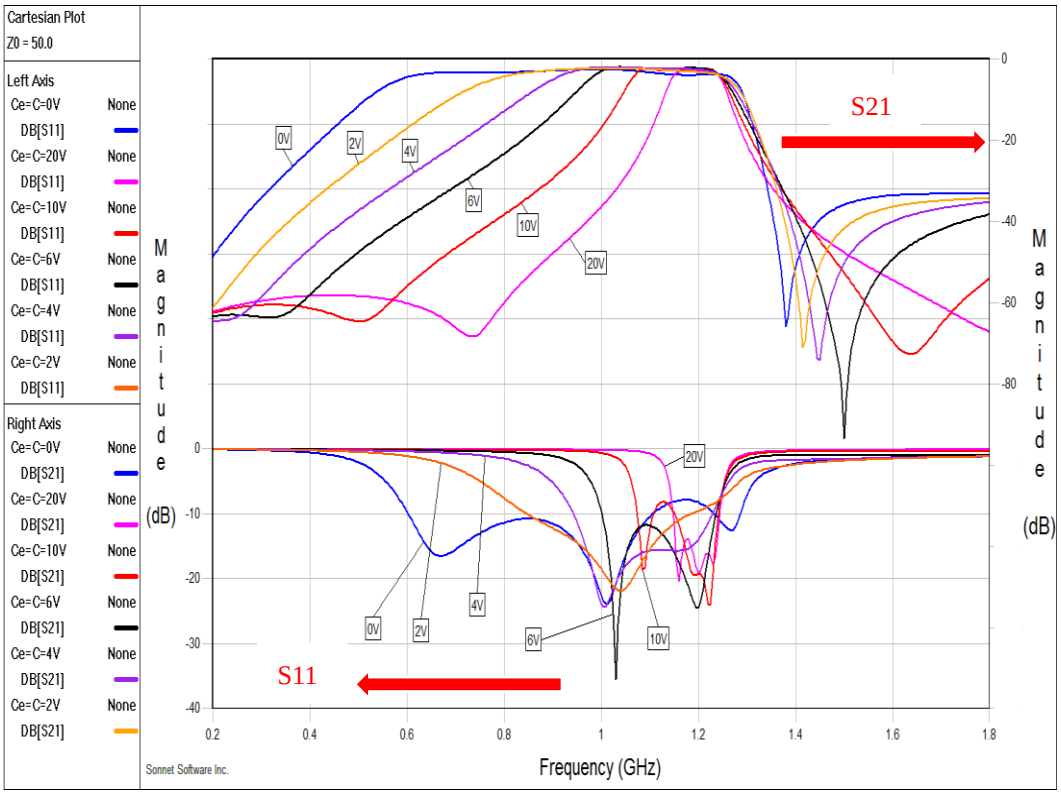

(a)

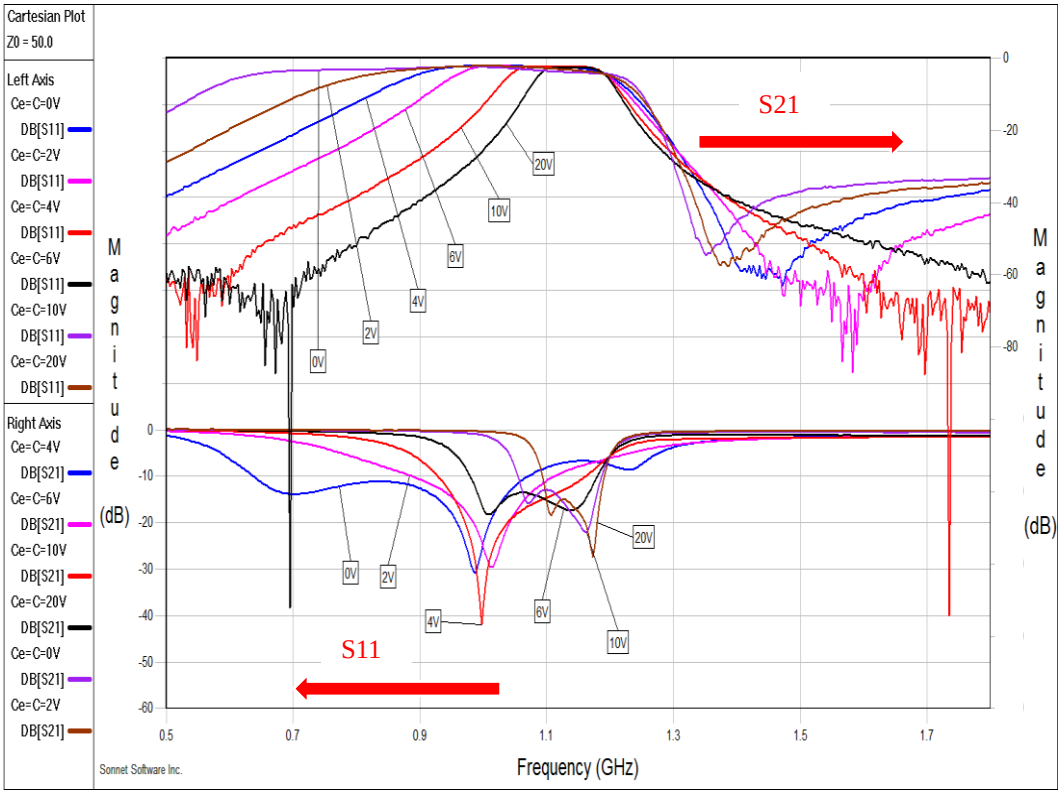

(b)

Figure 5.7: Response performance with controlling bandwidth and selectivity. (a) Simulation. (b) Measurement.

The response performance of the fabricated filter with variable coupling coefficients C and constant external coupling Ce is shown in Figure 5.6. As the varying of coupling coefficients, the FBWs of the filter also change. When the reverse voltage of C reduces, the FBW increases. However, the higher side transmission zero is missing because of mismatching and the lower side transmission zero shift as the FBW. At the same time, the passband can't stay flat and this happens at lower side band edge, which is also because the external couplings mismatch between the input/output and the remaining filter circuit. The measurement results are similar with the simulation results.

The response performance with controlling bandwidth and selectivity is shown in Figure 5.7. The comparison of different tuning states between simulation results and measurement results is summarized in Table 5.1. Due to the fabrication tolerance, the measurement results have 60 MHz phase shift to the lower side frequency domain, but still have a good agreement with the simulation results. This proposed filter has a wide bandwidth tuning range (3dB FBW: from 12.9% to 66% operated at from 1.14 to 0.9 GHz)

with good controlling selectivity introduced by the bias external coupling structure. Moreover, it has good flatness passband in each tuning state with insertion loss variation from 0.2 to 1.62dB. From the comparison of FBWs in the same state, it can be seen that this fabrication filter is over etched, which makes the coupling coefficients of the fix structure weak to result in smaller bandwidth. It can be also seen that the lossy technology has better result in narrow band compared with wide band, from the comparison of passband variations.

The proposed tunable bandpass lossy filter tunes the external couplings and coupling coefficients to control the bandwidth and selectivity without tuning the resonators' resonated frequencies. In the next section, the resonators' frequencies will be also tuned to enhance the performance to control the bandwidth at fixed centre frequency with a flatness passband.

Table 5.1: comparison of different tuning states between simulation results and measurement results.

States	Simulation			Measurement		
	Centre frequency (GHz)	3dB FBW	Passband variation (dB)	Centre frequency (GHz)	3dB FBW	Passband variation (dB)
State 1	1.2	9%	0.17	1.14	12.9%	0.2
State 2	1.16	18.8%	0.27	1.12	15%	0.42
State 3	1.11	29%	0.3	1.07	24%	0.6
State 4	1.07	34%	0.75	1.04	31%	1.2
State 5	1.0	56%	0.88	1.0	42%	1.42
State 6	0.92	82%	1.0	0.9	66%	1.62

5.3 Tunable Lossy Filter with Controlling Bandwidth at Fixed Centre Frequency

As discussed in the above section, to enhance the performance, filter resonators' frequencies should also be tuned to control the bandwidth at fixed centre frequency with a flat passband. With some modifications of tuning scheme, the EM simulation layout of

this filter with a detail of resonator tuning scheme is shown in Figure 5.8. To tune the resonator, 100 pF capacitor is employed to block the dc and 10K ohm resistor is used to reduce the RF signal leakage. A variable capacitance value cf2 and resistor rf2 are utilized to be regarded as tuning varactor. The red patches are connected the dc voltages.

The simulation responses of the proposed filter are shown in Figure 5.9. As we can see, the presented tunable bandpass lossy filter has three 3dB bandwidth states (12%, 30% and 57%) operated at 1.02 GHz with flat passband. By tuning the resonators' resonated frequencies, the different bandwidths states of last section tunable bandpass lossy filter move to have a same fixed centre frequency 1.02 GHz with keeping the insertion loss flat.

The fabrication photograph of the proposed filter is displayed in Figure 5.10. The filter is fabricated on the RT/Duriod 6010 with dielectric constant 10.2 and 1.27mm thickness (loss tan $\delta = 0.0023$). SMV1800-079LF varactors are used to tune the external couplings and SMV2020-079LF varactors are employed to tune the coupling coefficients and resonators' resonated frequencies. The physical size of the filter is 25 mm × 20 mm ($0.26\lambda_g \times 0.21\lambda_g$ at fix centre frequency 1.02 GHz).

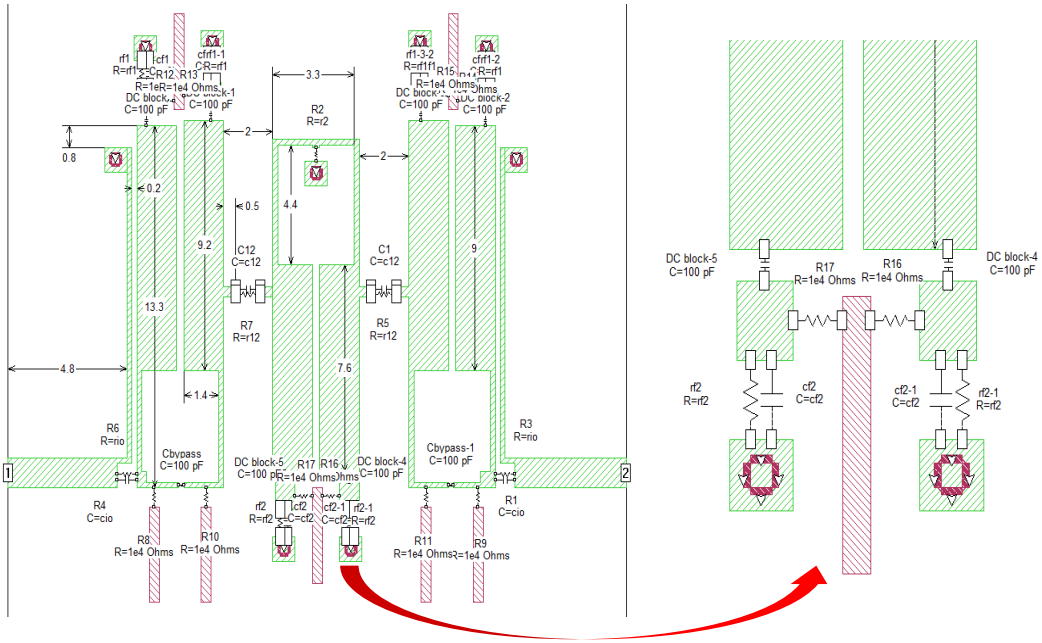

Figure 5.8: EM simulation layout of the proposed filter with resonator tuning scheme.

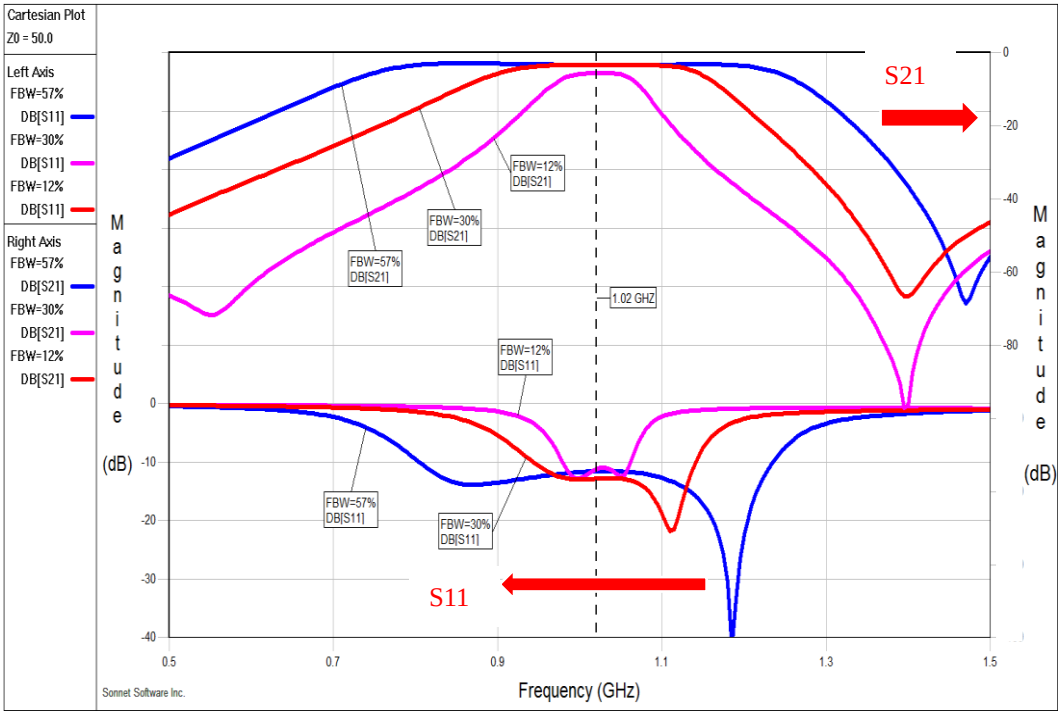

Figure 5.9: Simulation responses of the proposed filter.

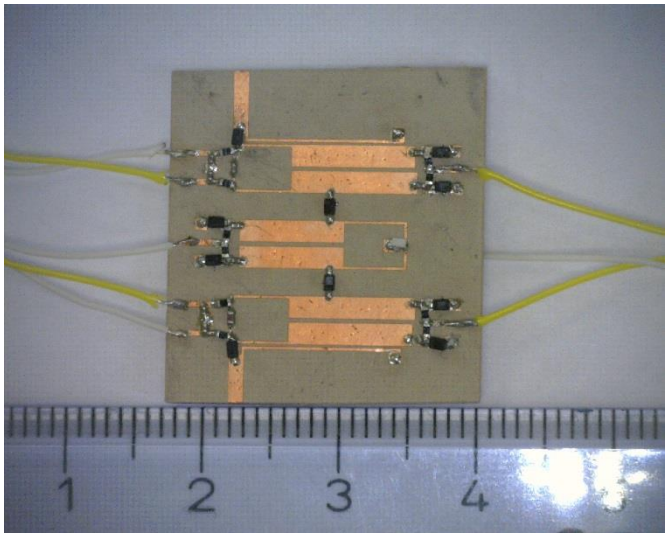

Figure 5.10: Fabrication photograph of the proposed filter.

Table 5.2: Values of tuning varactors for each state.

Tuning values	External Coupling	Coupling Coefficients	Resonators
Varactor type	SMV1800-079LF	SMV2020-079LF	SMV2020-079LF
FBW=53.7%	7.0pf (2.5V)	2.59pf (0.5V)	0.52pf (11V)
FBW=36.4%	4.85pf (4V)	2.01pf (1.5V)	0.75pf (8V)
FBW=24.0%	3.2pf (6V)	1.56pf (3.0V)	1.03pf (6V)
FBW=14.3%	2.17pf (8V)	1.03pf (6.0V)	1.46pf (3.5V)

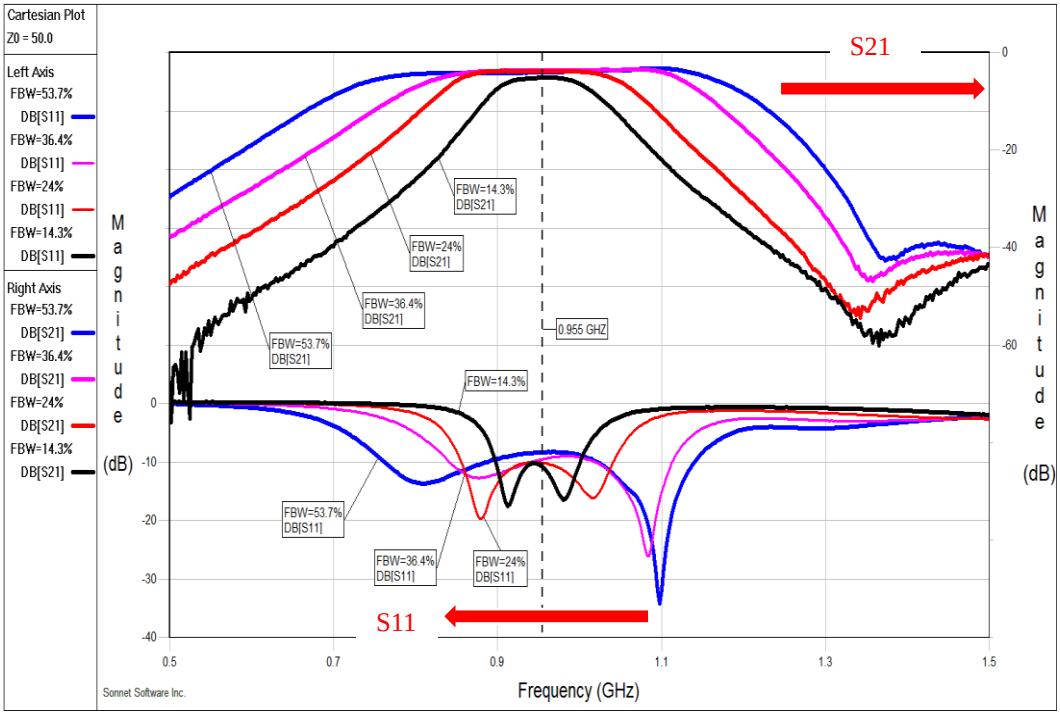

Figure 5.11: Measurement results of the proposed tunable bandpass lossy filter.

The measurement response of this tunable bandpass lossy filter is shown in Figure 5.11 and the values of tuning varactors are also given in Table 5.2.The measurement results show a good agreement with the simulation results. It has four FBW states (14.3%, 24%, 36.4% and 53.7%) centred at 0.955 GHz with a flat passband. The insertion loss variations for each state are 0.3 dB, 0.62 dB, 0.94dB and 1.12 dB respectively, which is can be told that lossy technology has a better result in narrow band.

In this part, tunable bandpass lossy filter with resistor loading is presented to control the bandwidth at a fixed centre frequency. By combining this resistor loading and cross coupling, a new method to introduce loss to make the insertion loss flat will be proposed in the next section.

5.4 Tunable Lossy Filter with Combining Resistor Loading and Cross Coupling

In the previous section, resistor loading is used to introduce the loss in the tunable bandpass filter to achieve flat passband. By extending this resistor loading, a new method combining cross coupling and resistor loading can also achieve the loss

introduction. A 5-pole tunable bandpass lossy filter is demonstrated in detail.

The fix structure of this 5-pole filter is centred at 1.1 GHz and the EM simulation layout with dimensions is shown in Figure 5.12. The novelty of this filter is use a cross coupling to connect with the source and the resistor loading of the fourth resonator, which can generate a transmission zero at the higher side to improve the selectivity, compared to the 3-pole tunable bandpass lossy filter described in the second part of this chapter. This type of tunable filter is still tuned in symmetric, which reduce the numbers of dc bias circuit to half to simplify the filter complexity.

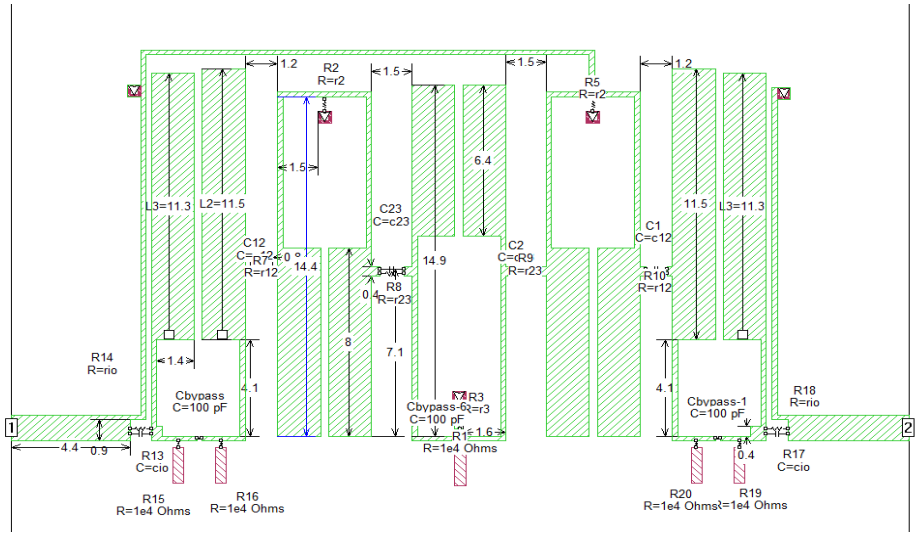

Figure 5.12: EM simulation layout of 5-pole tunable bandpass lossy filter.

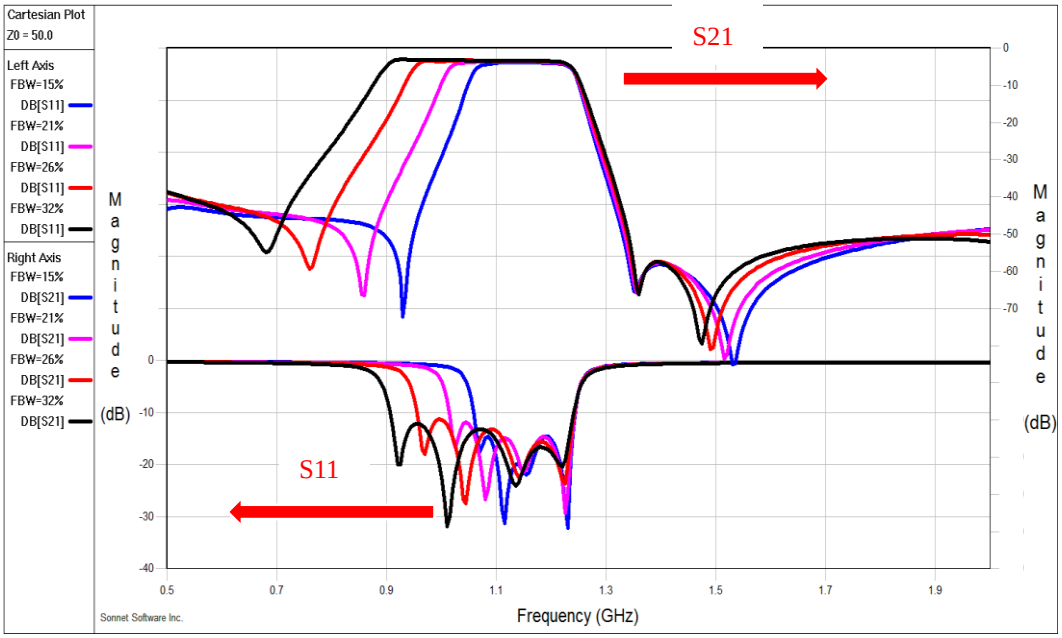

Figure 5.13: Simulation tuning response of the 5-pole tunable filter.

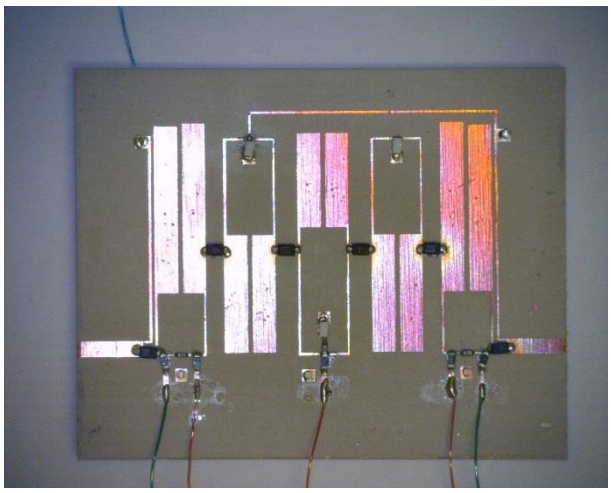

Figure 5.14: Fabrication Photograph of 5-pole tunable bandpass lossy filter.

The simulation tuning response is given in Figure 5.13. Because the tuning part does not include the resonators' resonated frequencies, this filter can only show the characteristic of controlling bandwidth and selectivity at the higher side of passband edge. Four different 3dB FBWs (15%, 21%, 26% and 32%) with the proper positions of higher side transmission zero are displayed. What's more, for each state, the passband insertion loss is quite flat to verify that this new method also can employ additional loss to make the passband flat.

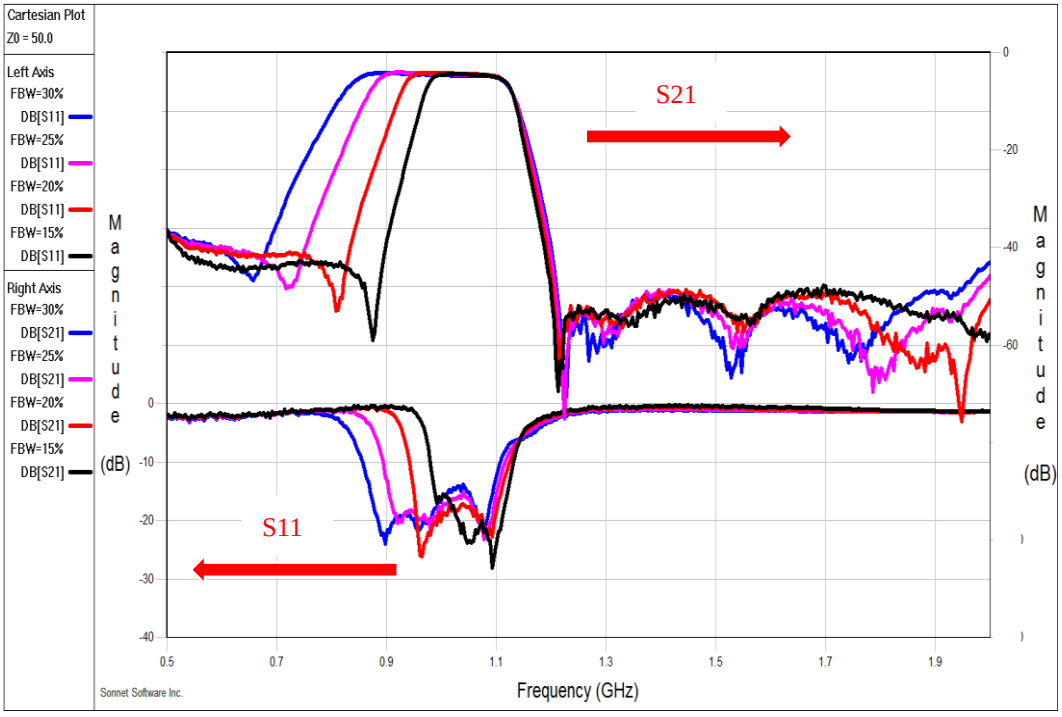

Figure 5.15: Measurement response of 5-pole tunable bandpass lossy filter.

Table 5.3: Reverse voltage values of tuning varactors.

Tuning values	External Coupling (Cio)	Side coupling coefficients (C12=C45)	Inner coupling coefficients (C23=C34)
Varactor type	SMV1800-079LF	SMV2020-079LF	SMV2020-079LF
FBW=30%	3V	4V	5V
FBW=26%	4V	6V	7V
FBW=21%	5V	8V	10V
FBW=15%	6V	12V	16V

The 5-pole tunable bandpass lossy filter is fabricated on the RT/Duriod 6010 with dielectric constant 10.2 and 1.27mm thickness (loss $\tan\delta = 0.0023$). The fabricated photo is displayed in Figure 5.14. SMV1800-079LF varactors are used to tune the external couplings, while SMV2020-079LF varactors are employed to tune the coupling coefficients. The values of the resistor used to load to the ground is 100 Ω. The tuning method is also symmetric so that the numbers of dc bias circuit required is only three. The physical size of the filter is $35\text{ mm} \times 20\text{ mm}$ ($0.32\lambda_g \times 0.24\lambda_g$ at fix centre frequency 1.1 GHz), which is very compact and easily to be tuned.

The measurement response of this proposed filter is shown in Figure 5.15 and the reverse voltage values of tuning varactors are also given in Table 5.3. The high side transmission zero is located at 1.22GHz, generated by the cross coupling to improve the selectivity. There are four different 3dB FBW states (30%, 26%, 21% and 15%), which slightly smaller than that of simulated response due to the fabrication tolerance (in this case, the filter circuit is over etched to make the couplings among resonators weak). The passband insertion loss variations for each state is 0.22 dB, 0.31 dB, 0.43 dB and 0.55 dB respectively. Therefore, this new method can not only introduce the additional loss to make passband flat, but also generate a transmission zero to improve the selectivity without affecting the performance of passband, compared with conventional resistor loading.

5.5 Summary

Based on the tunable filter literature review mentioned in Chapter 4, this chapter introduce my contributions to the tunable lossy filter works focusing on combining lossy technology and tunable bandpass filter under symmetric tuning. Firstly, a three-pole tunable bandpass lossy filter with resistor loading to control the bandwidth and selectively is presented. Although its fixed structure is a traditional 3-pole Chebyshev filter, its tunable structure with bias scheme still have two transmission zeros at each band edge, which is due to the tuning external coupling structure. Then to enhance the performance of this filter, its resonators are also extended to be tuned to achieve the goal of controlling the bandwidth at a fixed centre frequency. Finally, by combining the resistor loading and cross coupling, a new type of 5-pole tunable lossy filter is proposed with a flat passband and good improved selectivity, contributed by the cross coupling. Even though this structure is asymmetric, the tuning method is still symmetric.

The symmetric tuning can reduce the required number of dc bias circuit to half, however, in practical applications, the requirement of the filter is not symmetric tuning which can achieve a better performance at the cost of increasing the numbers of dc bias circuit. In the following chapter, asymmetric tunable bandpass lossy filter will be described in detail.

Reference

[1] A. R. Brown and G. M. Rebeiz, "A varactor-tuned RF filter," *IEEE Trans. Microw. Theory Techn.*, vol. 48, no. 7, pp. 1157–1160, Jul. 2000.

[2] J. Nath, D. Ghosh, J.-P. Maria, A. I. Kingon, W. Fathelbab, P. D. Franzon, and M. B. Steer, "An electronically tunable microstrip bandpass filter using thin-film barium–strontium–titanate (BST) Varactors," *IEEE Trans. Microw. Theory Tech*., vol. 53, no. 9, pp. 2707–2712, Sep. 2005.

[3] M. A. El-Tanani and G. M. Rebeiz, "High performance 1.5–2.5 GHz RF MEMS tunable filters for wireless applications," *IEEE Trans. Microw. Theory Tech*., vol. 58, no. 6, pp. 1629–1637, Jun. 2010.

[4] J. Ni and J.-S Hong, "Compact varactor-tuned microstrip high-pass filter with a quasi-elliptic function response," *IEEE Trans. Microw. Theory Tech*., vol. 61, no. 11, pp. 3853–3859, Nov. 2013.

[5] W.-X. Tang and J.-S. Hong, "Varactor-tuned dual mode bandpass fiiters,"*IEEE Trans. Microw. Theory Tech*., vol. 58, no. 8, pp. 2213-2219, Apr. 2010.

[6] C. H. Kim and K. Chang, "Ring resonator bandpass filter with switchable bandwidth using stepped-impedance stubs," *IEEE Trans. Microw. Theory Techn*., vol. 58, no. 12, pp. 3936–3944, Dec. 2010.

[7] A. Miller and J. S. Hong, "Reconfigurable cascaded coupled line filter with four distinct bandwidth states," *IET Microwave Antennas Propagat*., vol. 5, no. 14, pp. 1730–1737, Nov. 2011

[8] A. Miller and J. S. Hong, "Cascaded coupled line filter with reconfigurable bandwidths using LCP multilayer circuit technology," *IEEE Trans. Microwave Theory Tech.*, vol. 60, no. 6, pp. 1577–1586, June 2012.

[9] J. Ni and J. S. Hong, "Varactor-tuned microstrip bandpass filters with different passband characteristics," *IET Microwave Antennas Propagat.*, vol. 8, no. 6, pp. 415–422, 2014.

[10] X. Luo, S. Sun, and R. B Staszewski, "Tunable bandpass filter with two adjustable transmission poles and compensable coupling," *IEEE Trans. Microw. Theory Tech.*, vol. 62, no. 9, pp. 2003–2013, Sep. 2014.

[11] T. Yang and G. M. Rebeiz, "Tunable 1.25–2.1-GHz 4-pole bandpass filter with intrinsic transmission zero tuning," *IEEE Trans. Microw. Theory Techn*., vol. 63, no. 5, pp. 1569–1578, May 2015.

[12] B. F. Zong, G. M. Wang, J. G. Liang, and C. Zhou, “Compact bandpass filter with two tunable transmission zeros using hybrid resonators,” *IEEE Microw. Wireless Compon. Lett.*, vol. 25, no. 2, pp. 88–90, Feb. 2015.

[13] J.-R. Mao, W.-W. Choi, and K.-W. Tam, “Tunable bandpass filter design based on external quality factor tuning and multiple mode resonators for wideband applications,” *IEEE Trans. Microw. Theory Tech*, vol. 61, no. 7, pp. 2574–2584, Jul. 2013.

[14] Y.-C. Chiou and G. M. Rebeiz, “A tunable 3-Pole 1.5–2.2 GHz bandpass filter with bandwidth and transmission zero control,” *IEEE Trans. Microw. Theory Tech*., vol. 59, no. 11, pp. 2872–2878, Nov. 2011.

[15] Y.-C. Chiou and G. M. Rebeiz, “A quasi elliptic function 1.75–2.25 GHz 3-pole bandpass filter with bandwidth control,” *IEEE Trans. Microw. Theory Tech*., vol. 60, no. 2, pp. 244–249, Feb. 2012.

[16] Y.-C. Chiou and G. M. Rebeiz, “Tunable 1.55–2.1 GHz 4-pole elliptic bandpass filter with bandwidth control and 50 dB rejection for wireless systems,” *IEEE Trans. Microw. Theory Techn.*, vol. 61, no. 1, pp. 117–124, Jan. 2013.

[17] H.-J. Tsai, N.-W. Chen, and S.-K. Jeng, “Centre frequency and bandwidth controllable microstrip bandpass filter design using loop-shaped dual-mode resonator,” *IEEE Trans. Microw. Theory Tech*., vol. 61, no. 10, pp. 3590–3600, Oct. 2013.

[18] A. L. C. Serrano, F. S. Correra, T.-P. Vuong, and P. Ferrari, “Synthesis methodology applied to a tunable patch filter with independent frequency and bandwidth control,” *IEEE Trans. Microw. Theory Tech*., vol. 60, no. 3, pp. 484–493, Mar. 2012.

[19] E. Pistono, M. Robert, L. Duvillaret, J.-M. Duchamp, A. Vilcot, and P. Ferrari, “Compact fixed and tune-all bandpass filters based on coupled slow-wave resonators,” *IEEE Trans. Microw. Theory Tech*., vol. 54, no. 6, pp. 2790–2799, Jun. 2006.

[20] Y.-H. Cho and G. Rebeiz, “Two- and four-pole tunable 0.7–1.1-GHz bandpass-to-bandstop filters with bandwidth control,” *IEEE Trans. Microw. Theory Techn*., vol. 62, no. 3, pp. 457–463, Mar. 2014.

[21] Jiasheng Hong, Jia Ni, Petronilo Martin, “New Method for Improving the Passband Flatness in a Microwave Planar Filter”, ESA PAT 694

[22] SMV2020-079LF datasheet.

CHAPTER 6

Asymmetric Varactor-Tuned Microstrip Bandpass Lossy Filter with Extracted-Pole Technology

6.1 Introduction

Previously, we have discussed the designs of tunable bandpass lossy filter with resistor loading by using symmetric tuning to achieve bandwidth controlling. In this chapter, we focus on combining lossy technology and extracted-pole technology to realize tunable bandpass lossy filter with controlling bandwidth and selectivity characteristics by using asymmetric tuning, since this type of tunable filter is close to practical applications in the wireless systems.

In general, an ideal tunable bandpass filter requires a filter topology with a wide tuning centre frequency range, bandwidth controlling capability and high selectivity. In the open literature, typical coupled resonators filters are very popular because of their wide stopband performance and compact physical size [1]-[6]. However, the big challenge for them is that they highly relay on proper coupling controlling schemes to achieve good response performance over the whole tuning range [2]-[5]. Most of tunable filters' fix structures are designed by second-order coupled resonators, which don't have a sharp band edge. Moreover, most of the published tunable bandpass filters are concentrated on lower filter order (no more than 4th order), while very few works have been done for high order, which can be a way to improve the selectivity at the cost of filter circuit complexity.

In this chapter, based on the discussion in Chapter 3, three different tunable bandpass lossy filters with various bandwidth characteristic are presented with theory analysis and experimental demonstration. This type of filters can have not only good selectivity, but also flat passband with controlling bandwidth over the entire tuning range. The highly

selectivity is contributed by extracted-pole technology while the flatness passband is resulted by using resistor cross couplings. It has been found that the selectivity can be tuned independently with a slightly affection on the passband, which can be ignored. In the following sections, these three filters will be described in detail.

6.2 Controlling Bandwidth and Selectivity with Tuning one Extracted-Pole

In this part, a 6-pole tunable bandpass lossy filter with resistive cross coupling to control bandwidth and selectivity is designed. Apart from the conventional lower order tunable filter, this higher order filter has a centre frequency tuning range from 1.73 to 1.86 GHz with 3dB FBW tuning range from 12% to 30% and flat passband by tuning the lower side extracted-pole.

6.2.1 Filter Design and Analysis

The equivalent circuit model in AWR is shown in Figure 6.1.Two shunt series LC elements represent two extracted-poles and four parallel LC elements represent four resonators in the inline network. Two transmission lines are used for external couplings and three J-inverters are employed for coupling coefficients. Moreover, two crossing resistors are regarded as the resistive cross couplings to introduce the extra loss in the passband.

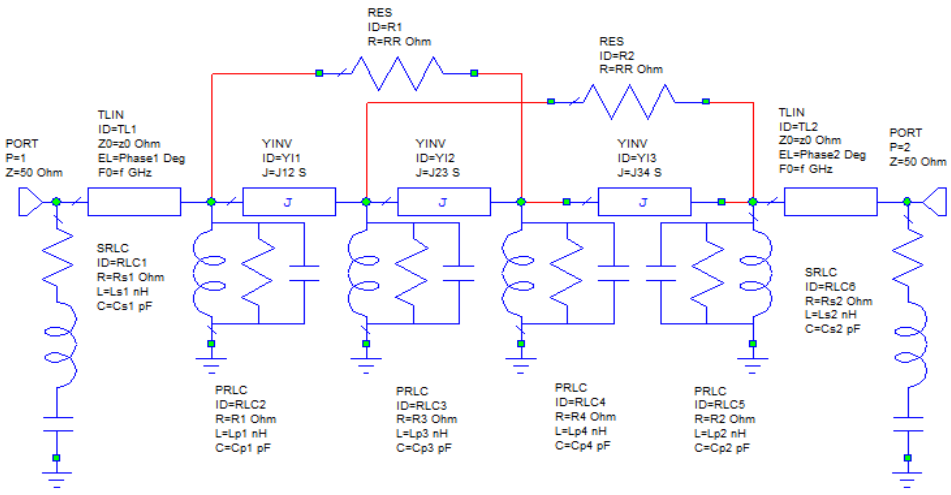

Figure 6.1: Equivalent circuit model of the proposed tunable filter.

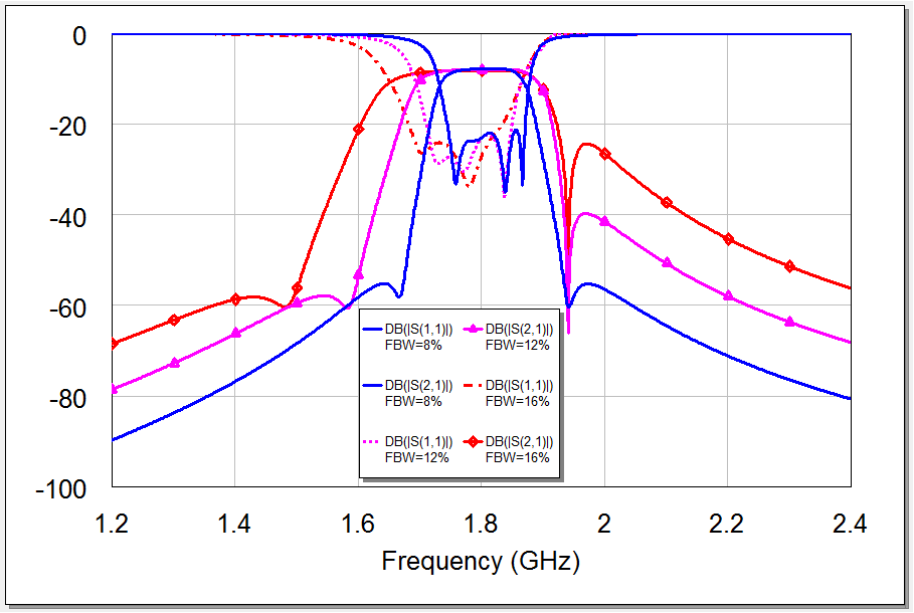

Figure 6.2: Simulation results of the equivalent circuit model.

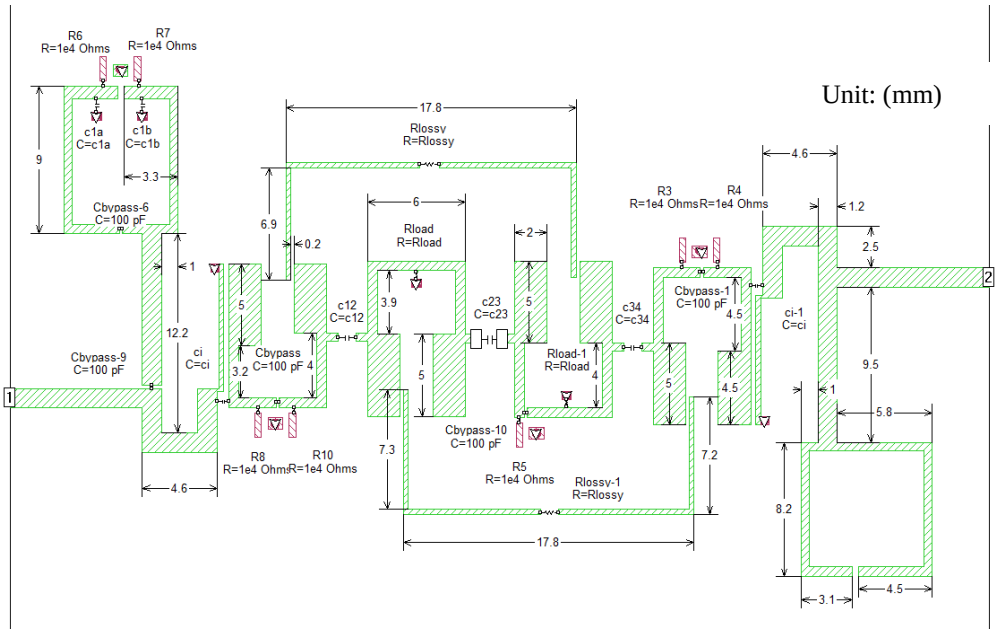

Figure 6.3: EM simulation layout of the propose filter.

The simulation results with three tuning states is given in Figure 6.2. It can be seen that this filter has flat passband and FBWs tuning characteristics (8%, 12% and 16%) with tuning the external couplings, coupling coefficients and lower side extracted-pole. The higher side transmission zero is fixed but still has some changes, which is due to the matchings of mix couplings.

By following the filter implementation method discussed in Chapter 3, this equivalent circuit model can be converted to EM simulation model. The layout of EM

simulation with dimensions is displayed in Figure 6.3. As we can see, the external couplings, coupling coefficients and the lower side extracted-pole are tuned by the varactors, while the higher side extracted-pole is fixed, which may cause some mismatching during the tuning and can be seen in the simulation results of Figure 6.2.

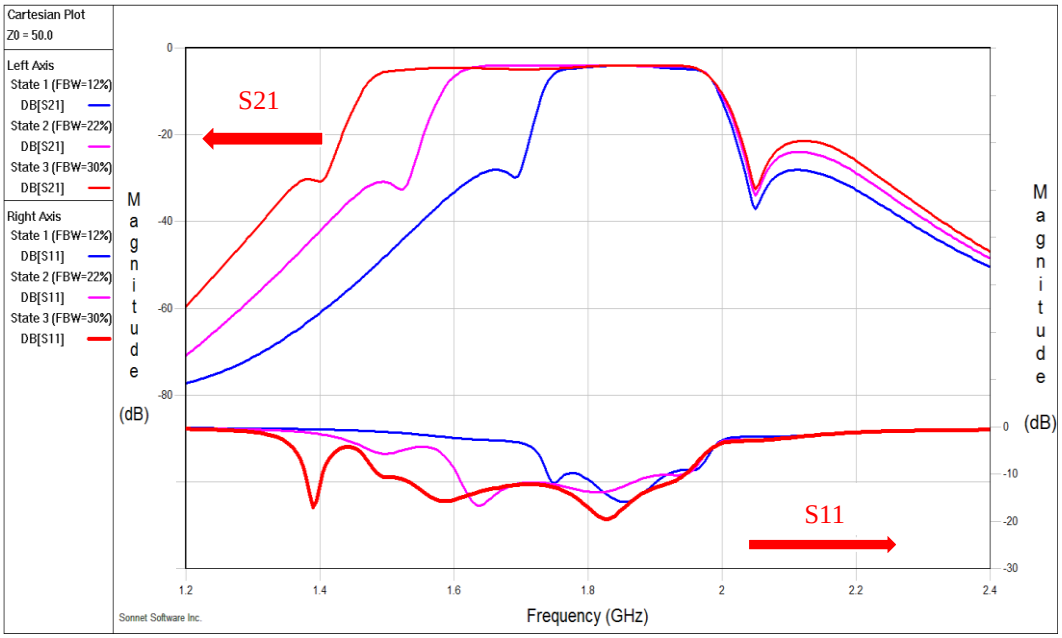

(a)

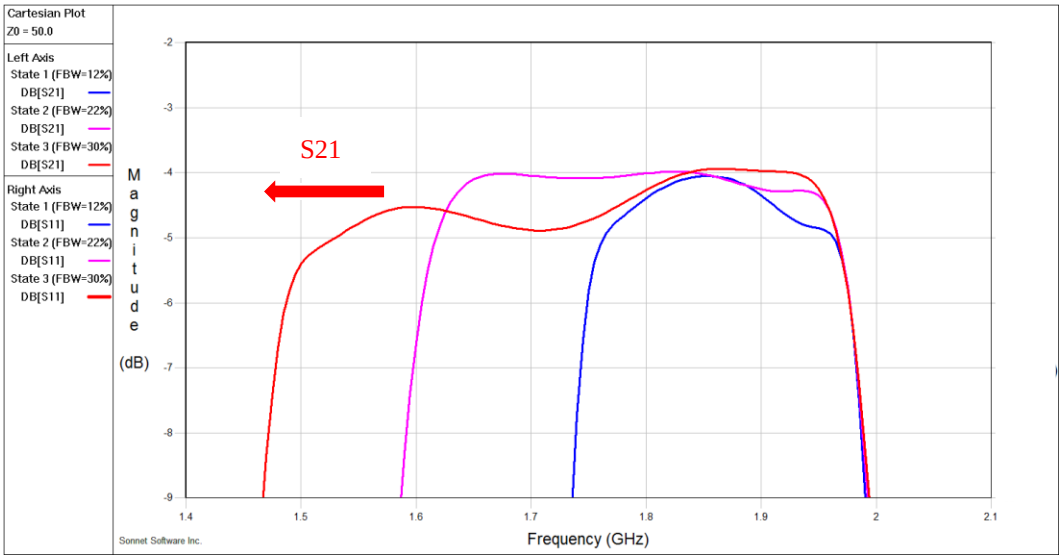

(b)

Figure 6.4: (a) Simulation results of EM model. (b) Zoom in view.

The simulation results of the EM model are shown in Figure 6.4. From the results, there are three different FBWs states (12%, 22% and 30%) with a fixed position of higher side transmission zero and a tunable lower sider transmission zero. The high selectivity has been realized as well as the flat passband (0.9dB, 0.5dB and 1.2dB insertion loss variation), which can be seen from the zoom in view.

6.2.2 Filter Implementation and Measurement

The proposed 6-pole tunable filter is fabricated on the RT/Duriod 6010 substrate with 1.27 mm thickness and dielectric constant 10.2 (loss $\tan\delta = 0.0023$). The detail fabrication photograph of the filter with bias scheme is shown in Figure 6.5. The filter size is $60\text{ mm} \times 40\text{ mm}$ ($1.15\lambda_g \times 0.77\lambda_g$ at fix centre frequency 1.8 GHz) . SMV2020-079LF varactors are employed to tune the external couplings and coupling coefficients, while SMV2019-040LF varactors are used to tune the lower side extracted pole ratio. Panasonic resistor 10k ohm resistors are used to reduce the RF signal leakage in the dc bias circuits and the Murata 0402 GRM 100pF capacitors are used to block the dc voltages. Panasonic resistor 100 ohm resistors are used in the two resistive cross couplings to contribute the loss. Noted that there are very small gaps between the resistive cross couplings and the resonators, which are very sensitive to the results because of its controlling the level of the additional loss.

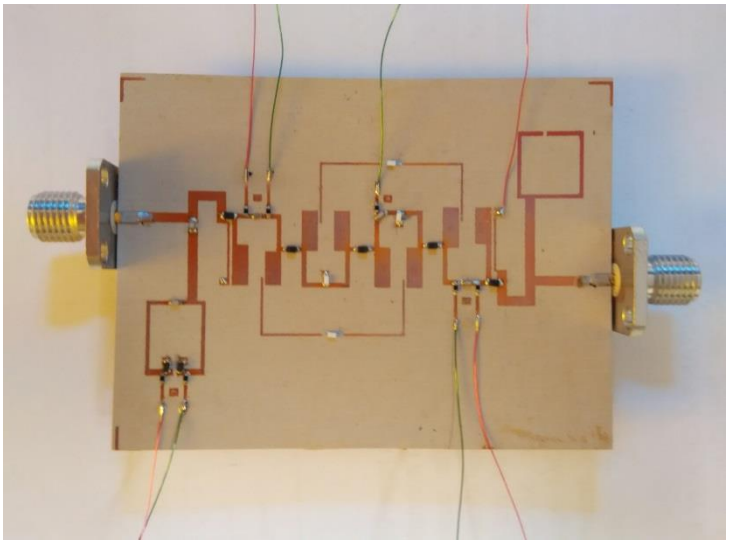

Figure 6.5: Fabrication photo of 6-pole tunable bandpass lossy filter.

Table 6.1: Values of tuning elements.

Tuning values	External coupling (Ci)	Side coupling coefficient (C12=C34)	Inner coupling coefficient (C23)	Extracted-pole ratio (C1a)	Extracted-pole ratio (C1b)
Varactor type	SMV2020-079LF	SMV2020-079LF	SMV2020-079LF	SMV2019-040LF	SMV2019-040LF
State 1	8V	14V	20V	8V	20V
State 2	6V	10V	12V	6V	10V
State 3	4V	8V	7V	2V	3V

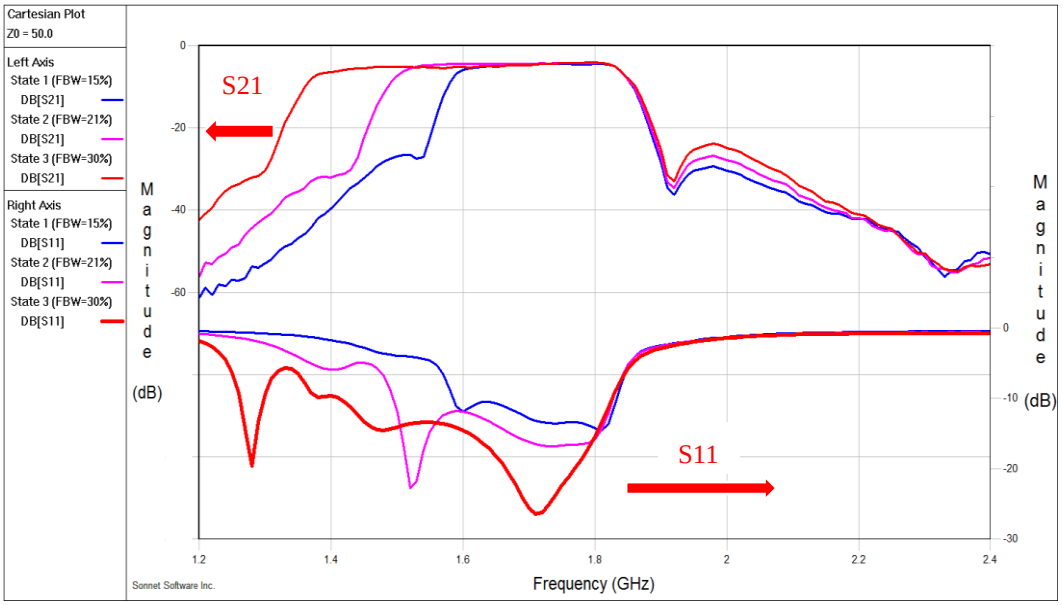

(a)

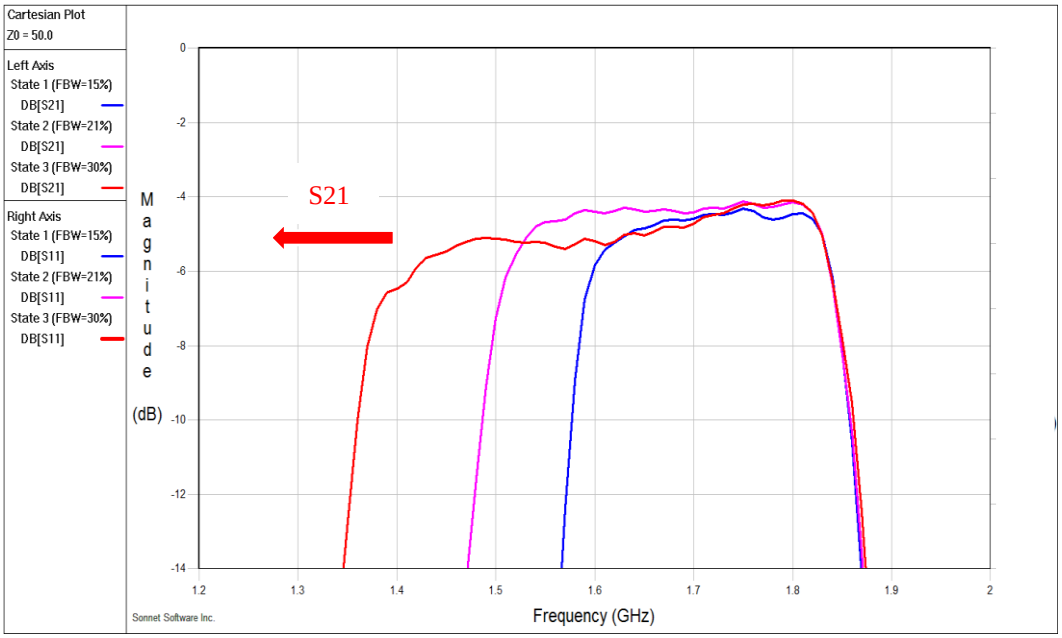

(b)

Figure 6.6: (a) Measurement results of fabricated filter. (b) Zoom in view.

The measurement results of the fabricated filter is illustrated in Figure 6.6, which shows a good agreement with the simulation results. Due to the fabrication tolerance, the measurement results have 120 MHz frequency shift to the lower frequency domain. And this fabricated circuit is under etched resulted in more strong couplings than that of simulation, which we can see from the comparison of state 1 between simulation (FBW=12%) and measurement (FBW=15%). The insertion loss variations for each state are 1.2dB, 0.8dB and 1.9dB respectively, which are also close to the simulation results. The values of tuning elements for each state is shown in Table 6.1.

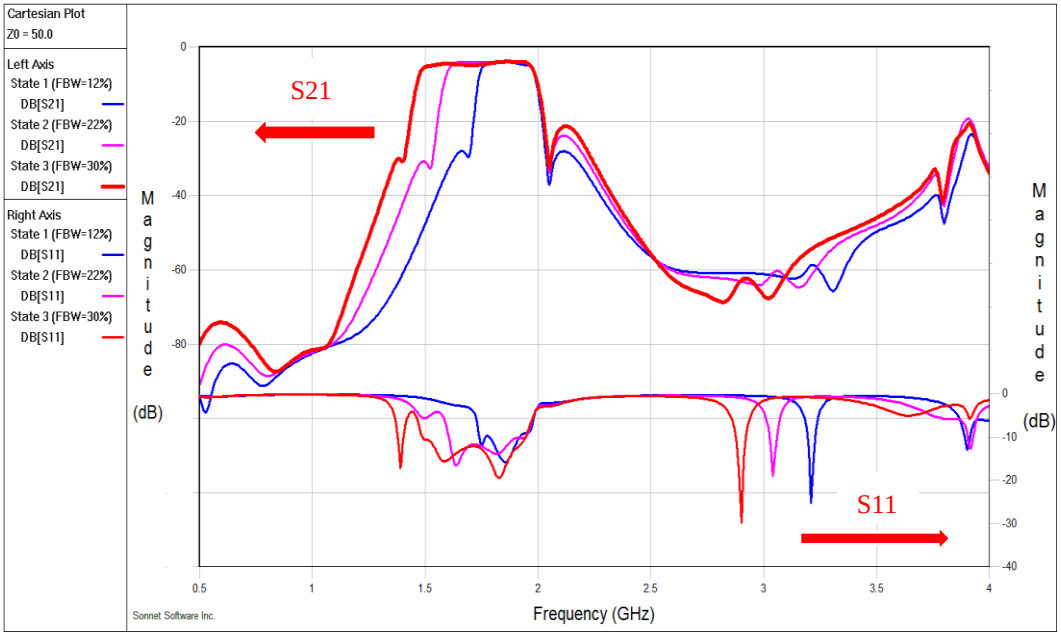

(a)

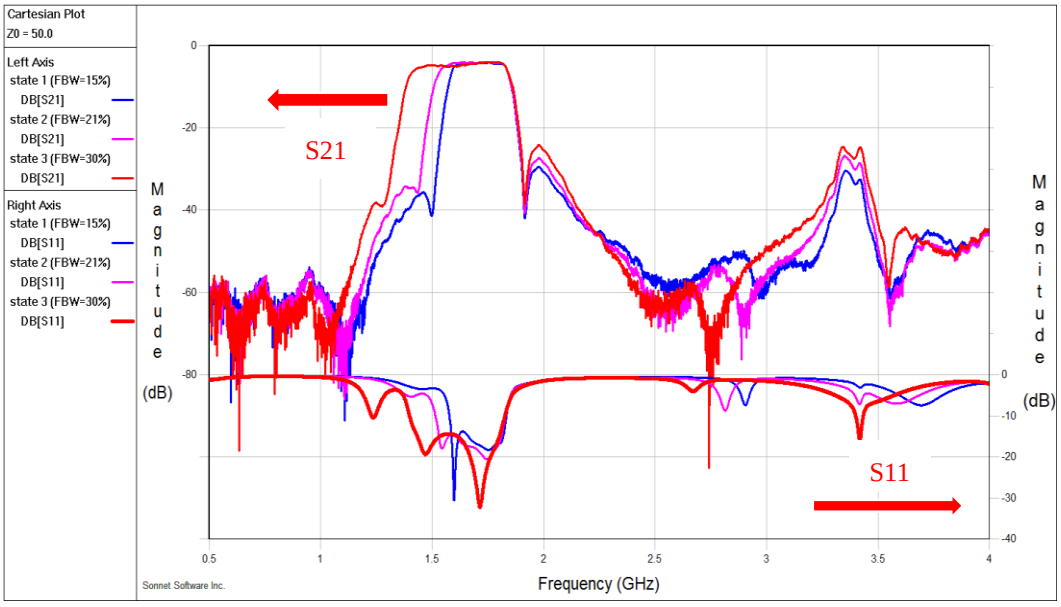

(b)

Figure 6.7: Comparison of wideband results. (a) Simulation. (b) Measurement.

In terms of the performance in the wideband, the comparison between simulation results and measurement results is given in Figure 6.7. This type of filter has a very good stopband rejection at 2.2 times of centre frequency under -40dB according to the measurement results, which is due to the employed step-impedance hairpin resonators.

This tunable filter only tunes the lower side extracted-pole with the fixed higher side extracted-pole, which could cause some mismatching in the performance. In the following section, the higher side extracted-pole will be also tuned. But when the tuning scheme increases, the performance may not be good as expected, since the extra tuning elements can affect the performance because of the loss of these elements.

6.3 Controlling Bandwidth and Selectivity with Tuning a Pair of Extracted-Poles

In the previous section, the higher side extracted-pole is fix structure and the lower side one is tuned. To investigate how the higher side extracted-pole can affect the filter performance, both of these two extracted-poles are tuned in this part.

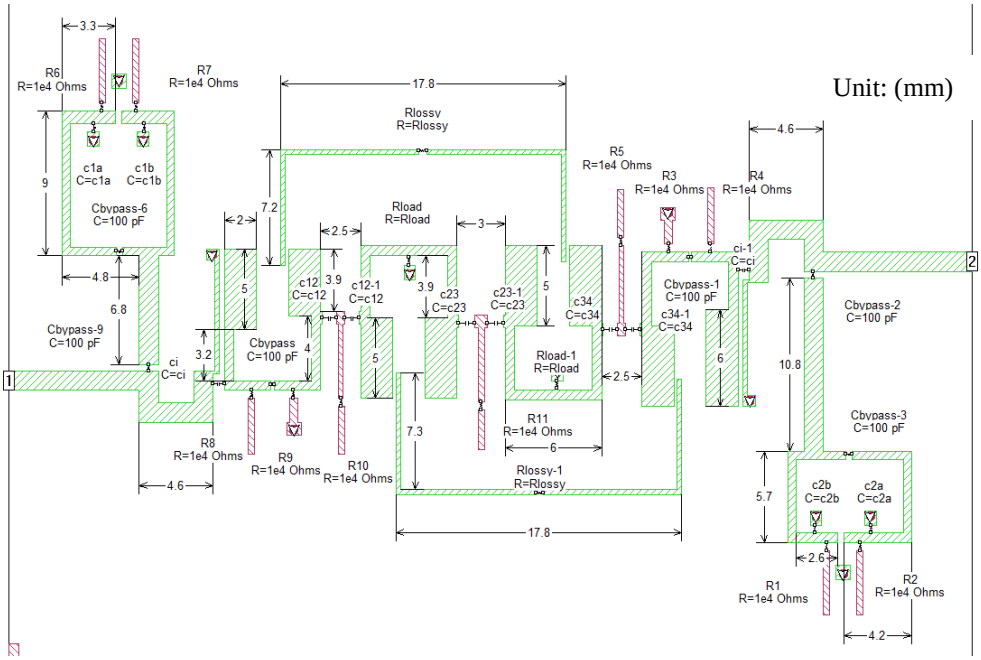

Figure 6.8: EM simulation layout of the presented tunable filter.

The EM simulation layout of this presented tunable filter with detail dimensions is given in Figure 6.8. The asymmetric structure and tuning method increases the

complexity of the filter circuit. This EM model combines resistor loading and resistive cross couplings to achieve the flat passband, which increases the complexity of the filter circuit. The four inline resonators have been redesigned to meet the requirement of tuning the higher side extracted-pole to improve the response performance. Different from the previous tunable filter, this uses back-to-back varactors to tune the coupling coefficients to achieve narrower bandwidth controlling.

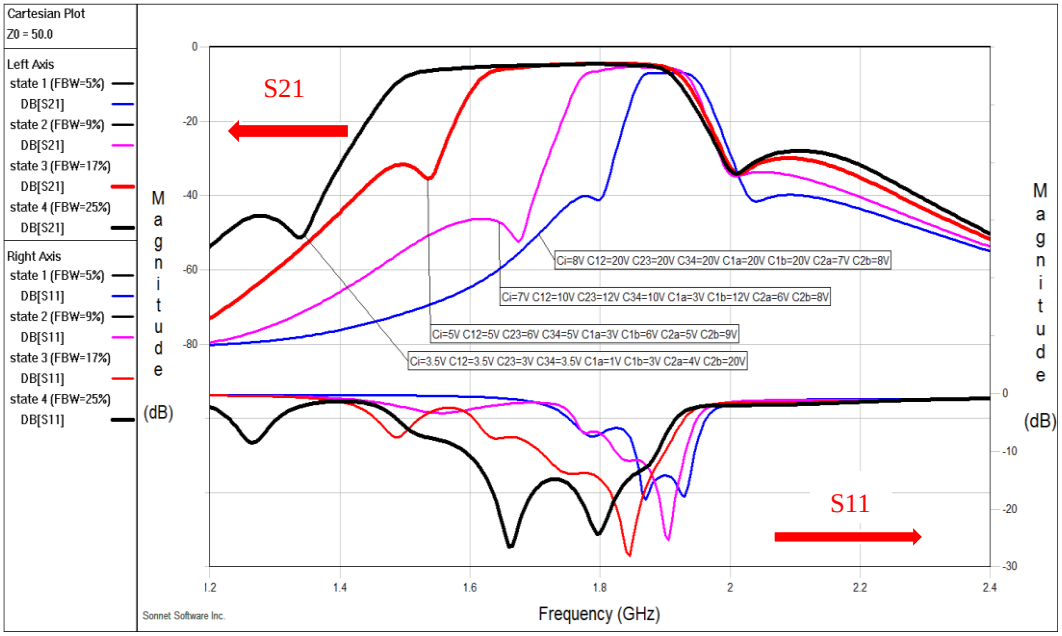

(a)

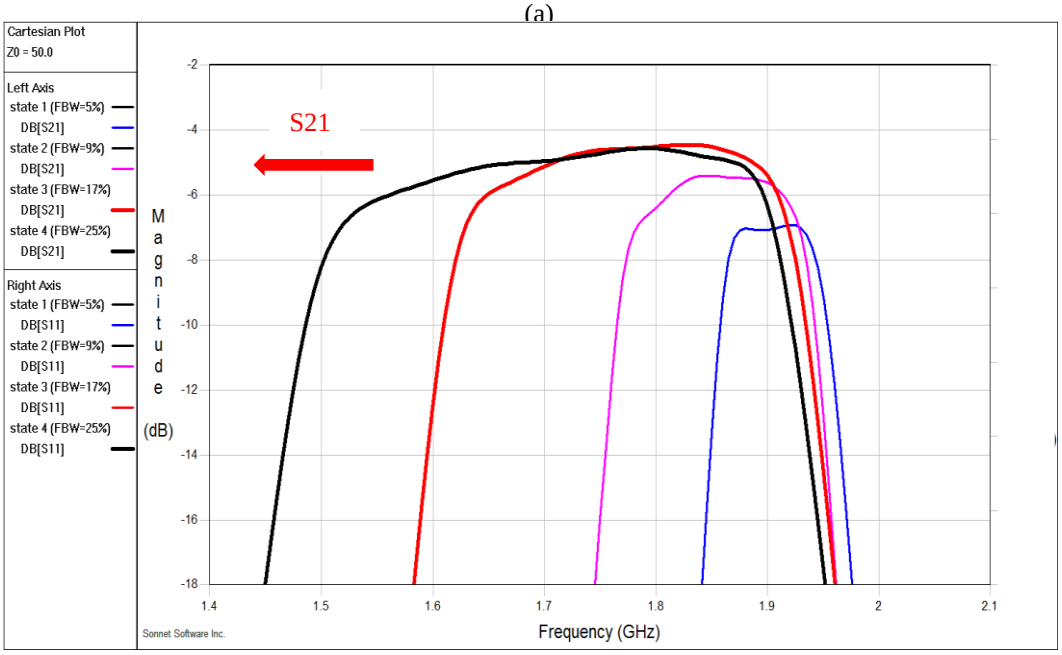

(b)

Figure 6.9: (a) EM simulation results. (b) Zoom in view.

The EM simulation results and detail passband view are shown in Figure 6.9. There are four FBWs' tuning states (5%, 9%, 17% and 25%) with flat passband (0.4dB, 0.9dB, 1.8dB and 2.2 dB insertion loss variations). The lower side transmission zero is tuned obviously, while the higher side transmission zero is tuned in a small range. The values of tuning elements in this simulation results is given in Table 6.2.

Table 6.2: Values of tuning elements for each state.

Tuning values	External coupling (Ci)	Side coupling coefficient (C12=C34)	Inner coupling coefficient (C23)	Lower side extracted-pole ratio (C1a)	Lower side extracted-pole ratio (C1b)	Higher side extracted-pole ratio (C2a)	Higher side extracted-pole ratio (C2b)
Varactor type	SMV2020-079LF	SMV2020-079LF	SMV2020-079LF	SMV2019-040LF	SMV2019-040LF	SMV2019-040LF	SMV2019-040LF
State 1	8V	20V	20V	20V	20V	7V	8V
State 2	7V	10V	12V	3V	12V	6V	8V
State 3	5V	5V	6V	3V	6V	5V	9V
State 4	3.5V	3.5V	3V	1V	3V	4V	20V

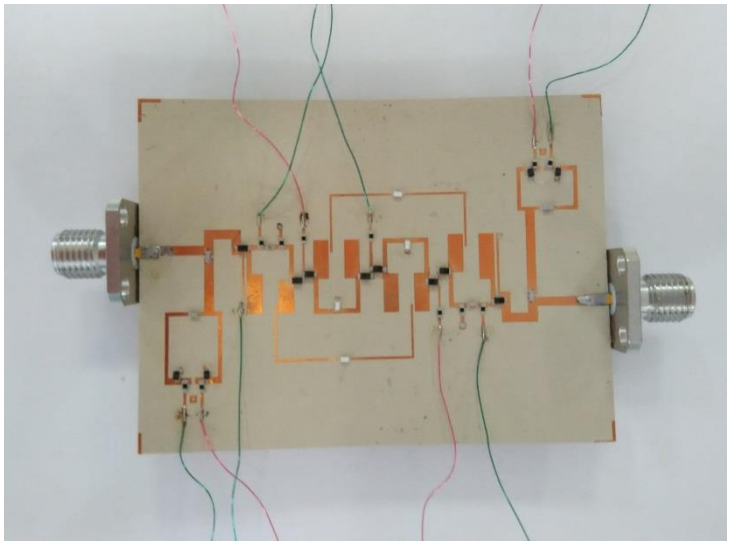

Figure 6.10: Fabrication photo the presented tunable filter.

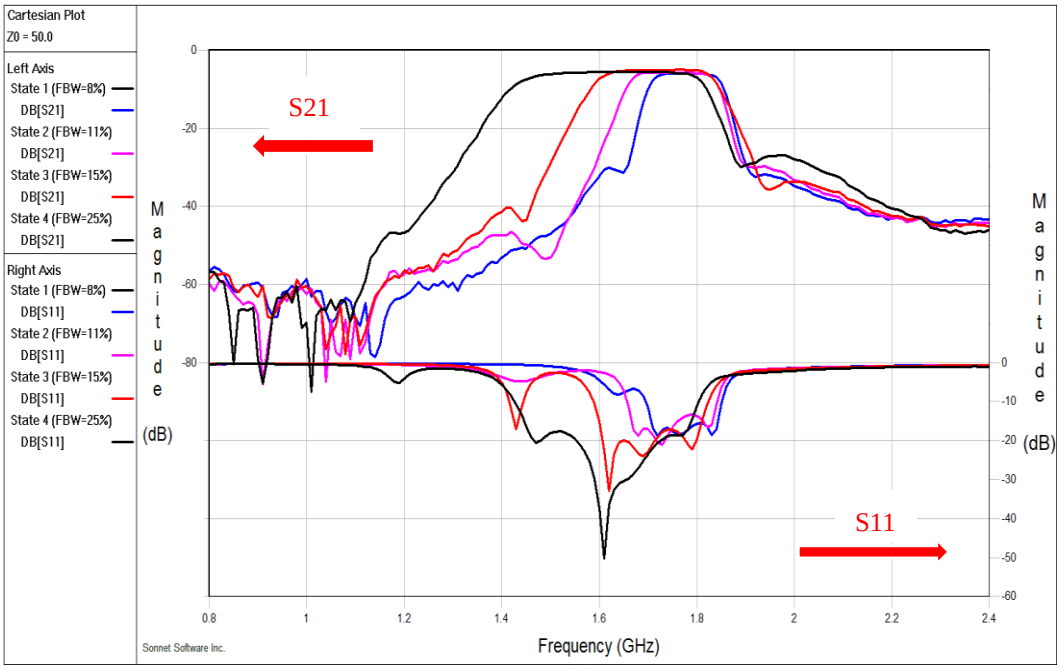

(a)

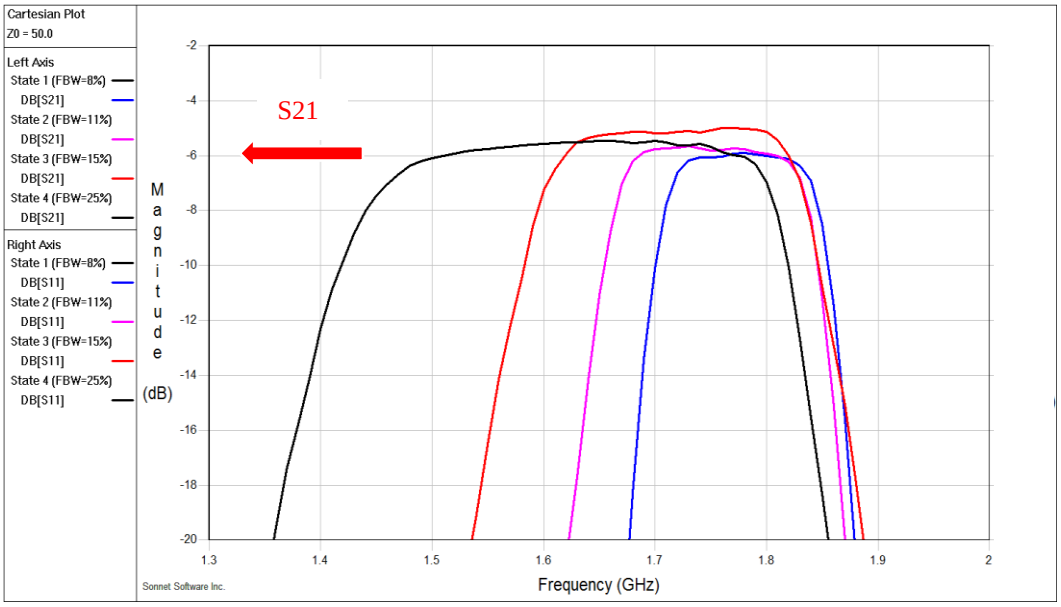

(b)

Figure 6.11: (a) Measurement results of fine tuning. (b) Zoom in view.

Table 6.3: Fine tuning values of tuning elements.

Fine tuning values	External coupling (Ci)	Side coupling coefficient (C12=C34)	Inner coupling coefficient (C23)	Lower side extracted-pole ratio (C1a)	Lower side extracted-pole ratio (C1b)	Higher side extracted-pole ratio (C2a)	Higher side extracted-pole ratio (C2b)
State 1	8V	12.5V	10V	20V	20V	7.3V	8V
State 2	7V	10V	8V	3V	12V	6.5V	8V
State 3	6V	7.5V	6.5V	4.5V	5V	7V	12V
State 4	3.5V	3.5V	4V	1V	3V	4V	20V

The proposed 6-pole tunable filter is fabricated on the RT/Duriod 6010 substrate with 1.27 mm thickness and dielectric constant 10.2 (loss $\tan\delta = 0.0023$). The detail fabrication photograph of the filter with bias scheme is shown in Figure 6.10. The filter size is $60\text{ mm} \times 40\text{ mm}$ ($1.20\lambda_g \times 0.85\lambda_g$ at fix centre frequency 1.9 GHz) . SMV2020-079LF varactors are used to tune the external couplings and coupling coefficients, while SMV2019-040LF varactors are employed to tune the two extracted-poles. Panasonic resistor 10k ohm resistors are used to reduce the RF signal leakage in the dc bias circuits and the Murata 0402 GRM 100pF capacitors are used to block the dc voltages. Panasonic resistor 100 ohm resistors are used in the two resistive cross couplings to contribute the loss. Noted that there are very small gaps between the resistive cross couplings and the resonators, which are very sensitive to the results because of its controlling the level of the additional loss. With the increasing numbers of elements, the expected response has many uncontrolled factors such as the packaging technologies of varactors and resistors.

The measurement results are given in Figure 6.11 and the fine tuning values of the tuning elements are also shown in Table 6.3. The fine tuning measurement results show a good agreement with the EM simulation results. Due to the fabrication tolerance, the measurement results have 100MHz shift to the lower frequency domain. Moreover, this fabricated filter is under etched, which makes the couplings strong to result in wide bandwidth, compared with simulation results in each state. There are four tuning 3dB FBWs states (8%, 11%, 15% and 25%) with flat passband (0.5dB, 0.8dB, 1.2dB and 1.7dB insertion loss variation). The higher side transmission zero is also not tuned obviously while the lower side transmission zero changes as the FBW changes. The measurement results' passband insertion loss level is around -5.2dB, compared to -4.5dB of simulation results', which is because the s2p files of tuning elements in EM simulation has a different with practical products.

In the previous section and this part, we have investigated how the couplings (external coupling and coupling coefficients) and transmission zeros affect the filter response performance when they are tuned. In the next section, resonators' resonated

frequencies will be tuned as well, since they are also the important parts of tunable filters.

6.4 Controlling Bandwidth at Fixed Centre Frequency

By extending the previous section tunable filter to control bandwidth at fixed centre frequency, resonators' resonated frequencies need to be tuned as well. In this part, a tunable bandpass lossy filter with controlling bandwidth at fixed centre frequency is proposed. The equivalent circuit model is still the same with Figure 6.1. The ideal circuit model response is shown in Figure 6.12. As we can see, the responses have four different 3dB FBWs (6%, 10%, 15% and 20%) operated at 2.0GHz with high selectivity at both sides of passband edges.

By following the filter implementation method discussed in Chapter 3, this equivalent circuit model can be converted to EM simulation model. The layout of EM simulation with dimensions is displayed in Figure 6.13 with general view and detail view. It can be seen that there are around 75 components used for tuning, which means that these components may also introduce the loss from themselves resulted that the expected response is hard to control. Noted that the s2p files of tuning components used in the EM simulation may also be different with the actual products, which also can't be controlled to avoid. Moreover, the response results got from AWR in Figure 6.12 can't be trust, because that it is impossible for those four states to have the same level of insertion loss, noted that the narrow band always have more loss than wideband.

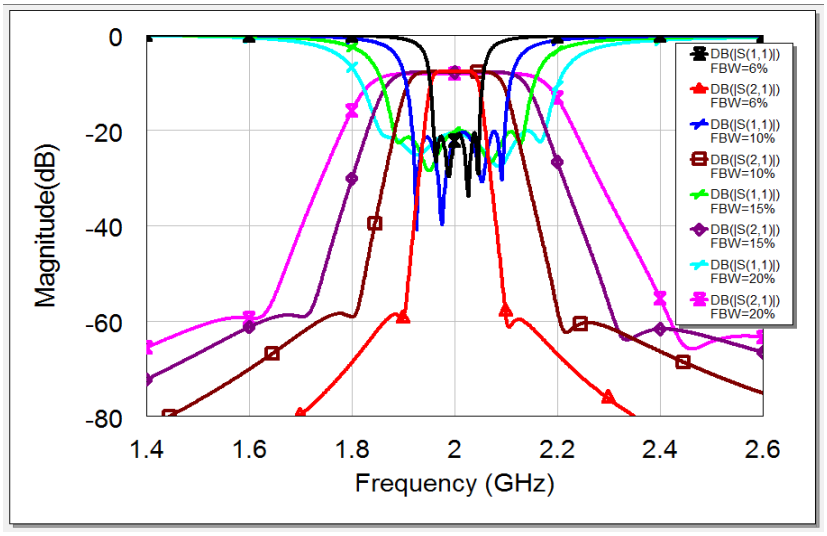

Figure 6.12: Response of circuit model with different FBWs centred at 2GHz.

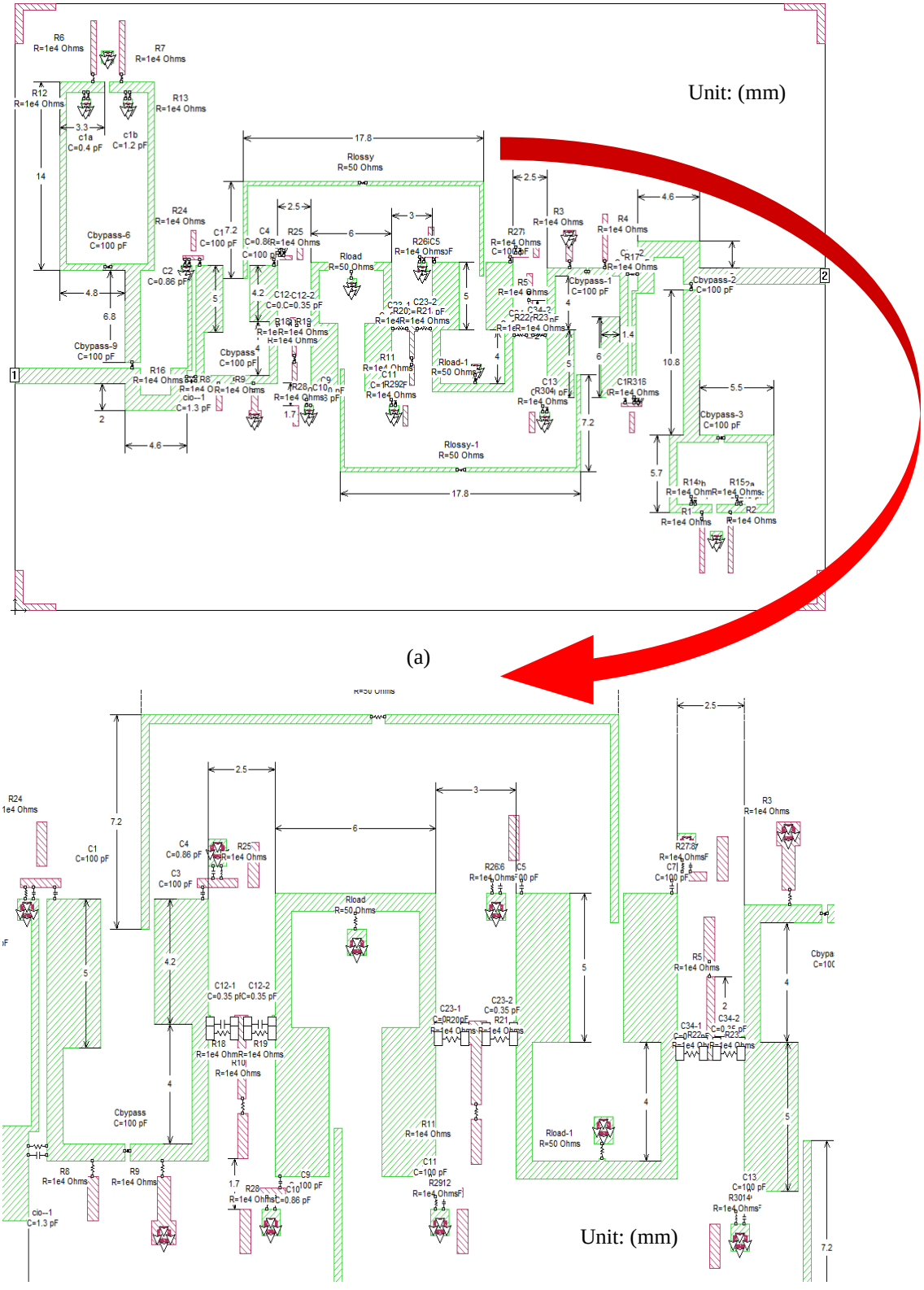

Figure 6.13: Layout of EM simulation. (a) General view. (b) Zoom in view.

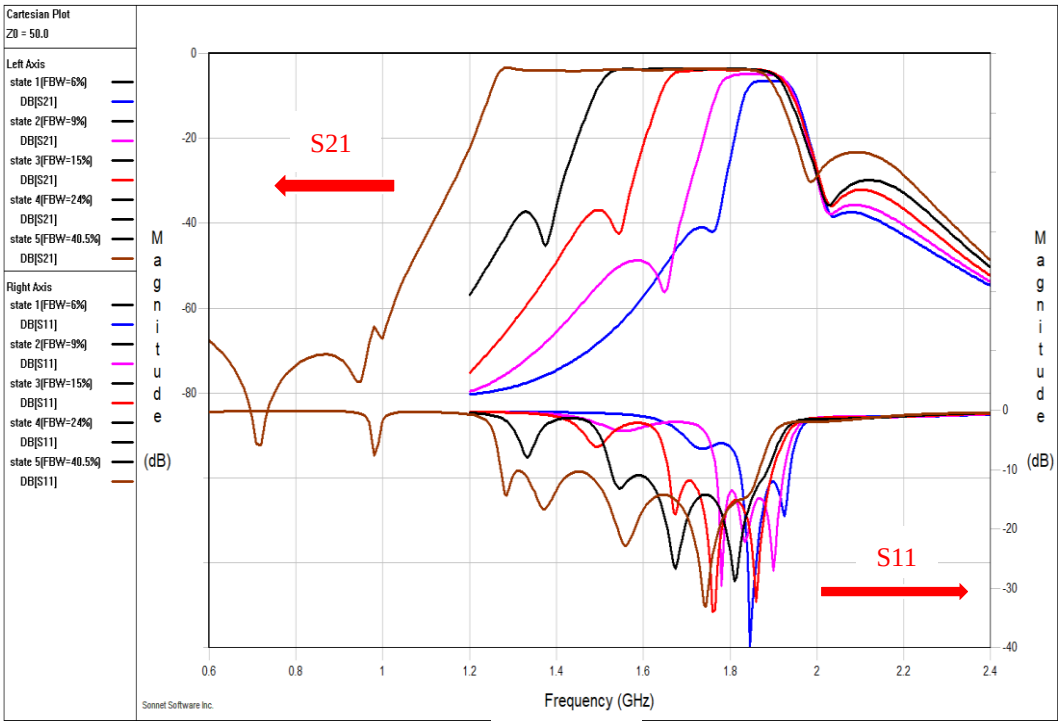

(a)

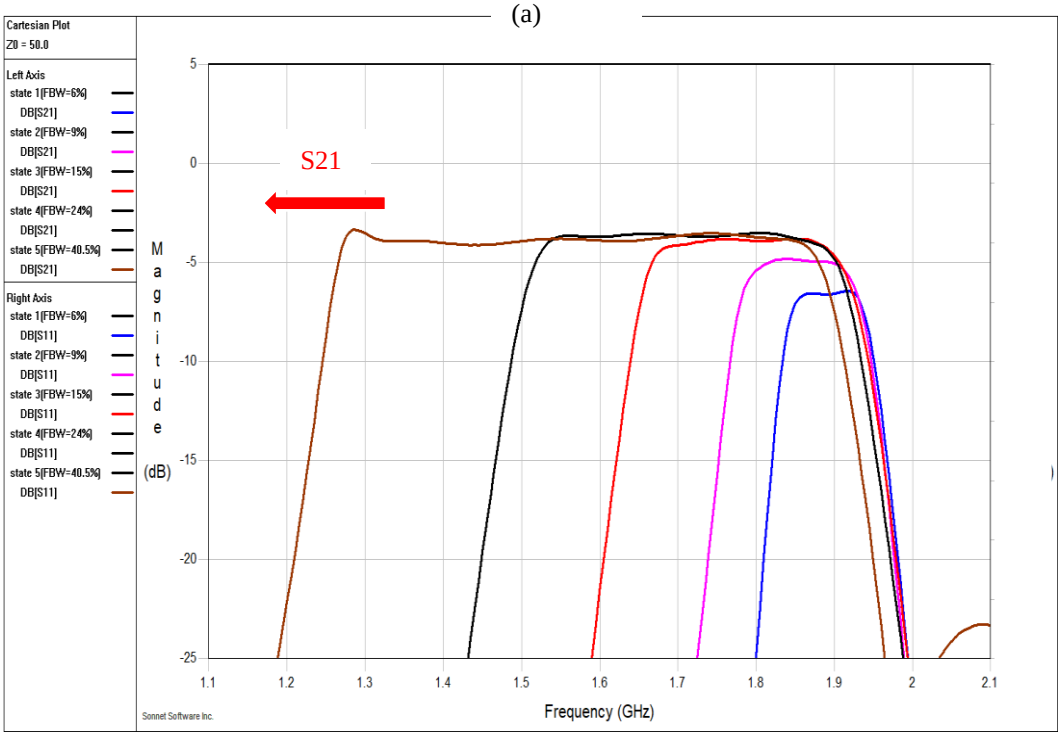

(b)

Figure 6.14: (a) Simulation results with bandwidth controlling. (b) Zoom in view.

In the zoom view of Figure 6.13, we can see that two back-to-back varactors are used to tune the coupling coefficients instead of one. This is because that the capacitance of this back-to-back varactors is only a half of conventional one varactor, which is good to achieve desired narrow band. What's more, resistor loadings and resistive cross couplings are combined to introduce the additional loss to achieve flat passband.

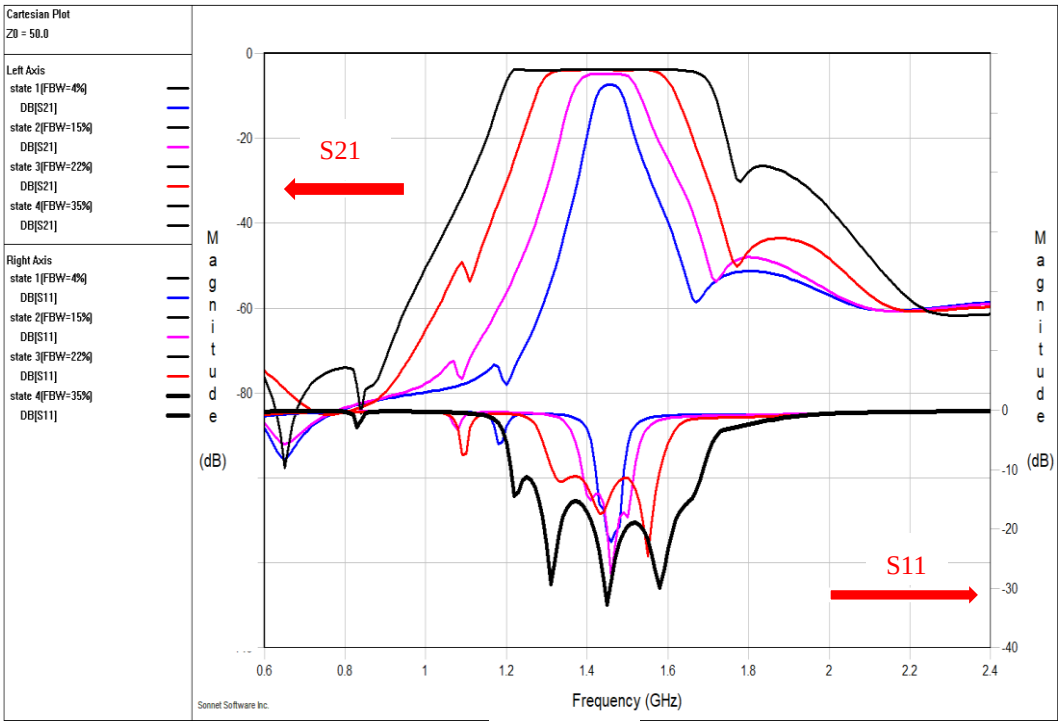

(a)

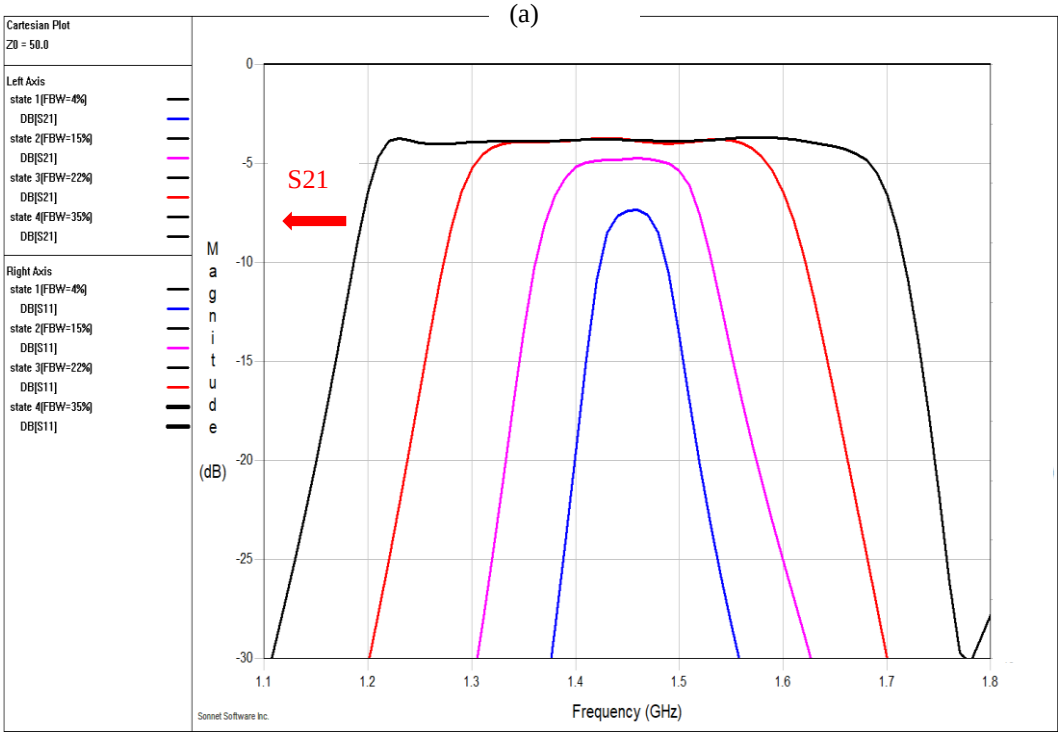

(b)

Figure 6.15: (a) Simulation results of controlling bandwidth at fixed centre frequency. (b) Zoom in view.

Figure 6.14 shows the simulation results with bandwidth controlling, which is similar with last section proposed tunable filter's response to test the tuning bandwidth range. There are five different 3dB FBWs states: 6% centred at 1.89GHz; 9% centred at 1.86GHz; 15% operated at 1.8GHz; 24% operated at 1.7GHz and 40.5% centred at

1.58GHz. From the zoom in view of Figure 6.14, the insertion loss variations in the pass for each state are 0.4dB, 0.8dB, 1.1dB, 1.2dB and 1.9dB respectively. Apart from this, the selectivity for each state is quite good as well, due to the tuning of two extracted-poles. The higher side transmission zero is adjusted very lightly while the lower side one can move as required by the FBW tuning.

Figure 6.15 shows the simulation response of controlling bandwidth at fixed centre frequency. This is realized by tuning the resonated frequencies to shift the whole filter function shape in the frequency domain. So this results actually have a close relationship with the ones in Figure 6.14. It can be seen that there are four different 3dB FBWs operated at 1.45GHz: 4%, 15%, 22% and 35%. The insertion loss variations for each state are 1.2dB, 0.84dB, 0.92dB and 1.0dB respectively. The reason why state 1 has so big insertion loss 1.2dB is that due to the very narrow band 4%, the loss introduced by the resistor loadings and resistive cross couplings is not main loss compared with the loss of tuning components so that the mid-band can't be compensated with extra loss to be flat with band edges.

The proposed 6-pole tunable filter is fabricated on the RT/Duriod 6010 substrate with 1.27 mm thickness and dielectric constant 10.2 (loss $\tan\delta = 0.0023$). The detail fabrication photograph of the filter with bias scheme is shown in Figure 6.16. The filter size is 70 mm × 40 mm ($1.04\lambda_g \times 0.6\lambda_g$ at fix centre frequency 1.4 GHz). SMV2020-079LF varactors are used to tune the external couplings and coupling coefficients, while SMV2019-040LF varactors are employed to tune the two extracted-poles. Panasonic resistor 10k ohm resistors are used to reduce the RF signal leakage in the dc bias circuits and the Murata 0402 GRM 100pF capacitors are used to block the dc voltages. Panasonic resistor 100 ohm resistors are used in the two resistive cross couplings to contribute the loss. Noted that there are very small gaps between the resistive cross couplings and the resonators, which are very sensitive to the results because of its controlling the level of the additional loss. With the increasing numbers of elements, the expected response has many uncontrolled factors such as the packaging technologies of varactors and resistors.

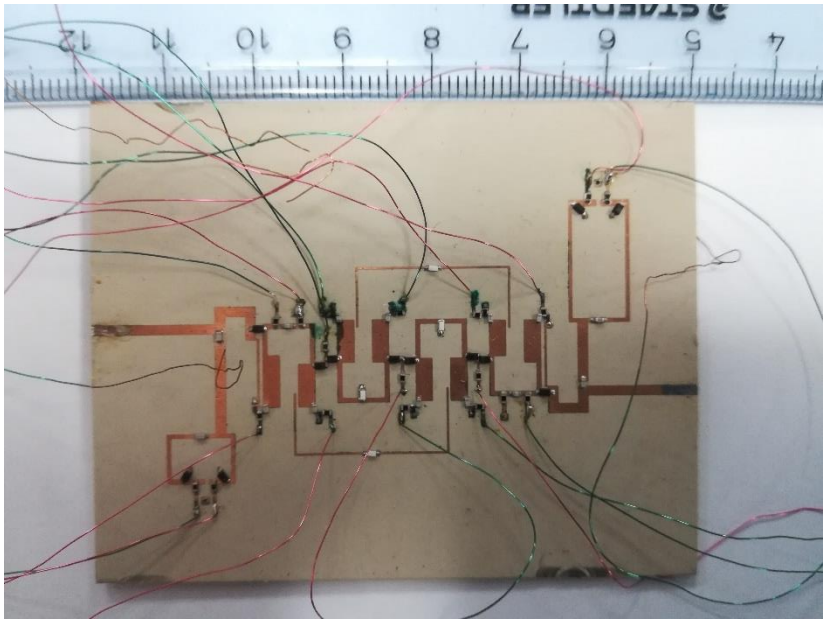

Figure 6.16: Fabrication photograph of the proposed tunable filter.

Table 6.4: Values of tuning elements.

Tuning elements	External coupling (Cio) (pF)	Side coupling coefficient (C12=C34) (pF)	Inner coupling coefficient (C23) (pF)	Lower side extracted-pole ratio (C1a) (pF)	Lower side extracted-pole ratio (C1b) (pF)	Higher side extracted-pole ratio (C2a) (pF)	Higher side extracted-pole ratio (C2b) (pF)
Varactor types	SMV2020-079LF	SMV2020-079LF	SMV2020-079LF	SMV2019-040LF	SMV2019-040LF	SMV2019-040LF	SMV2019-040LF
State 1	0.9	0.35	0.35	0.42	0.3	0.45	0.5
State 2	1.0	0.57	0.48	0.98	0.35	0.55	0.44
State 3	1.2	0.95	0.9	1.0	0.6	0.6	0.4
State 4	1.55	1.5	1.5	1.51	0.98	0.98	0.3
State 5	2.5	2.8	2.8	3.2	2.8	2.8	0.3

Figure 6.17 shows the measurement results with bandwidth controlling and the values of tuning elements for each state is given in Table 6.4. There are five different 3dB FBWs states: 6% centred at 1.79GHz; 8.5% centred at 1.78GHz; 12% operated at 1.74GHz; 24% operated at 1.63GHz and 32% centred at 1.59GHz. From the zoom in view of Figure 6.18, the insertion loss variations in the pass for each state are 0.4dB, 0.6dB, 1.2dB, 1.9dB and 2.4dB respectively. Compared with a small tuning range of higher side transmission zero,

the lower transmission zero has a much wider tuning range to meet the requirement of FBW tuning. However, due to the fabrication tolerance, the measurement results have 95MHz shift to the lower side frequency domain. The controlling of selectivity for lower side transmission zero is also not as good as the simulation results, which is mainly because of the differences between the used simulation s2p files of varactors and their actually performances.

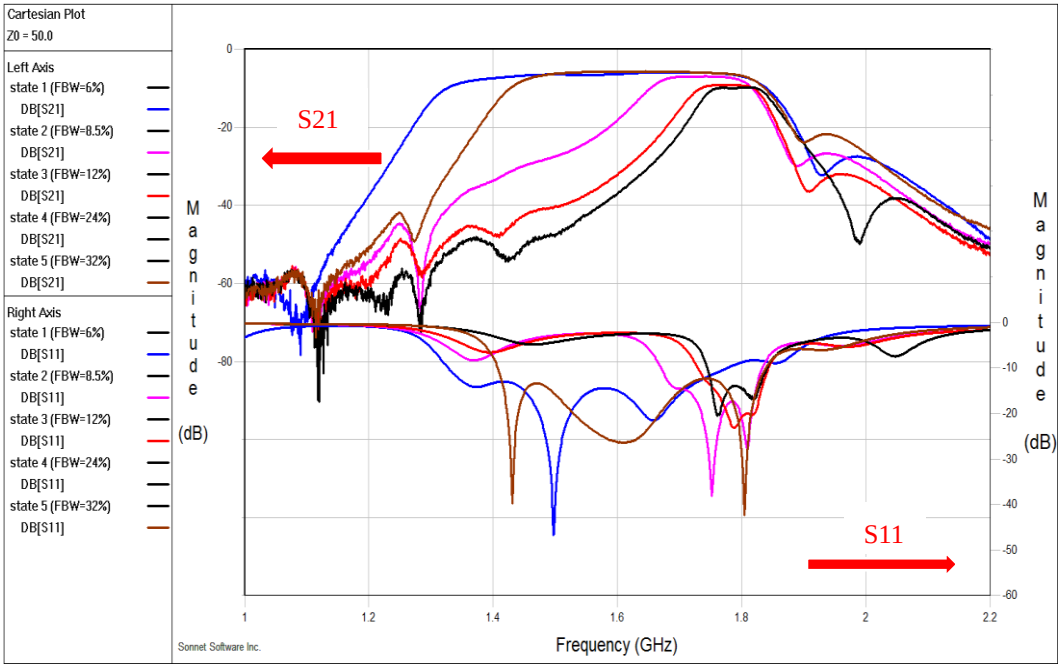

(a)

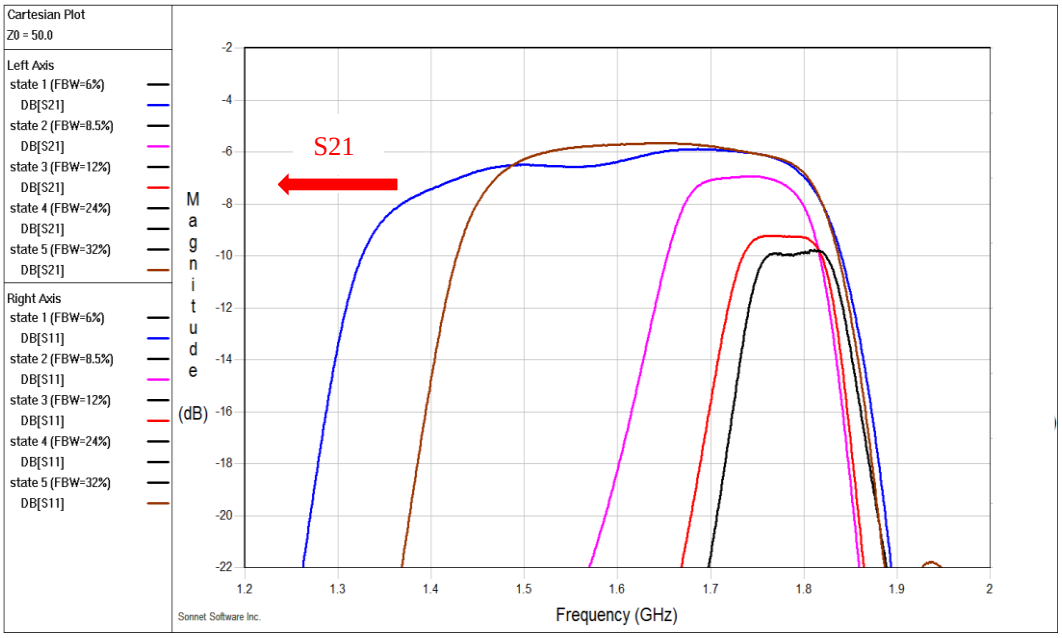

(b)

Figure 6.17: (a) Measurement results with bandwidth control. (b) Zoom in view.

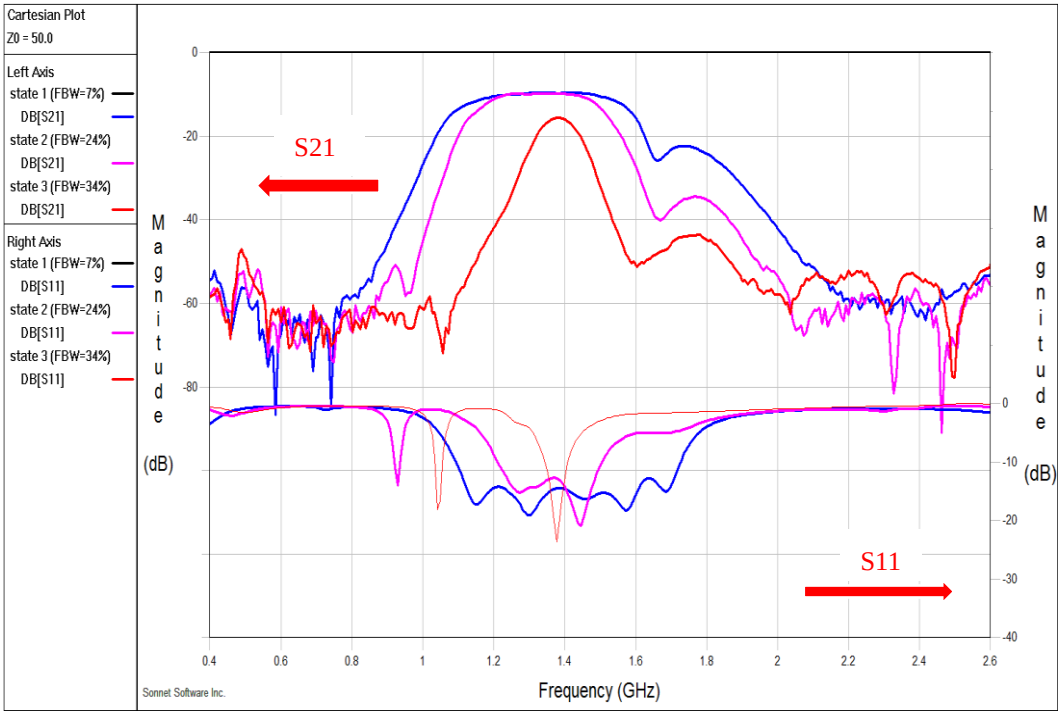

(a)

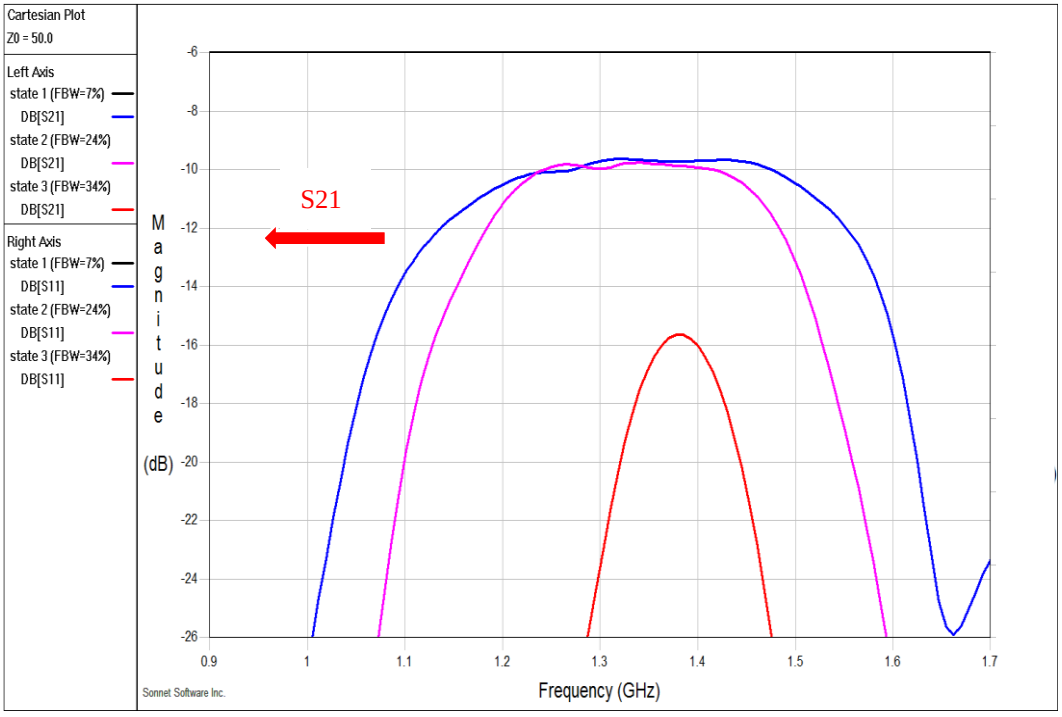

(b)

Figure 6.18: (a) Measurement results of controlling bandwidth at fixed centre frequency. (b) Zoom in view.

Table 6.5: Values of tuning elements.

Tuning elements	External coupling (Cio) (pF)	Coupling coefficient (C12=C23=C34) (pF)	Lower side extracted-pole ratio (C1a) (pF)	Lower side extracted-pole ratio (C1b) (pF)	Higher side extracted-pole ratio (C2a) (pF)	Higher side extracted-pole ratio (C2b) (pF)
Varactor types	SMV2020-079LF	SMV2020-079LF	SMV2019-040LF	SMV2019-040LF	SMV2019-040LF	SMV2019-040LF
State 1	1.4	0.9	0.8	1.6	1.2	0.8
State 2	2.0	1.8	1.2	1.0	1.8	0.5
State 3	2.5	2.8	2.8	2.6	1.4	0.6

Figure 6.18 shows the simulation response of controlling bandwidth at fixed centre frequency and the values of tuning elements for each state is given in Table 6.5. It can be seen that there are three different 3dB FBWs operated at 1.36GHz: 7%, 24%, and 34%. The insertion loss variations for each state are 1.2dB, 2.4dB and 3.0dB respectively. This measurement results show an agreement with simulation results, but the flatness of the passband and the selectivity are not good enough as simulation results, which is mainly because that: 1. The performance of the used s2p files of varactors in simulations is different with their practical products performance; 2. The number of the components is 78 and too many components are used to introduce many uncontrolled factors such as affecting the loss contributed by the resistor loadings and resistive cross couplings; 3. The three coupling coefficients C12,C23,C34 are connected to the same dc supplier, which is not right under the condition of this asymmetric tuning structure, while it is a trade-off between reducing the number of dc circuits and improving performance response. Moreover, this research work highly relays on the package technology of varactors, resistors and capacitors, which is because the insertion loss at narrow band has a high loss. This can be seen in the zoom in view of Figure 6.18 that the insertion loss of state 1 is -15.8dB with only 7% 3dB FBW. More investigations are still needed for asymmetric high order tunable bandpass lossy filter.

6.5 Summary

In this Chapter, asymmetric high order tunable bandpass lossy filters have been proposed. This type of filter can control the bandwidth at fixed centre frequency with flat passband and high selectivity. The flat passband is contributed by combining resistor loadings and resistive cross couplings to introduce additional loss in the mid-band to make the insertion loss flat, while the high selectivity is achieved by tuning two extracted-poles to adjust the positions of the introduced two transmission zeros at each side of passband edges. Through the analysis of the equivalent circuit model and EM simulation model, this type of filter has been investigated step by step. In theory, this proposed tunable filter can be tuned from vary narrow band (4% 3dB FBW) to wide band (40%) at a fix centre frequency 1.8 GHz with a flatness passband and good skirt selectivity. However, due to the fabrication tolerance and too many used components, this fabricated filter can be reconfigured from 7% to 34% FBW operated at 1.35GHz. Even though the measurement results show an agreement with the simulation results, the flatness of the passband and the selectivity can still be improved which need to make further investigations.

Reference

[1] M. A. El-Tanani and G. M. Rebeiz, "High performance 1.5–2.5 GHz RF MEMS tunable filters for wireless applications," *IEEE Trans. Microw. Theory Tech.*, vol. 58, no. 6, pp. 1629–1637, Jun. 2010.

[2] I. C. Hunter and J. D. Rhodes, "Electronically tunable microwave bandpass filters," *IEEE Trans. Microw. Theory Tech.*, vol. 30, no. 9, pp. 1354–1360, Sep. 1982.

[3] S.-J. Park and G. M. Rebeiz, "Low-loss two-pole tunable filters with three different predefined bandwidth characteristics," *IEEE Trans. Microw. Theory Tech.*, vol. 56, no. 5, pp. 1137–1148, May. 2008.

[4] X. Y. Zhang, Q. Xue, C. H. Chan, and B.-J. Hu, "Low-loss frequency-agile bandpass filters with controllable bandwidth and suppressed second harmonic," *IEEE Trans. Microw. Theory Tech.*, vol. 58, no. 6, pp. 1557–1564, Jun. 2010.

[5] M. Sanchez-Renedo, R. Gomez-Garcia, J. I. Alonso, and C. Briso-Rodriguez, "Tunable combline filter with continuous control of centre frequency and bandwidth," *IEEE Trans. Microw. Theory Tech.*, vol. 53, no. 1, pp. 191–199, Jan. 2005

[6] Y.-C. Chiou and G. M. Rebeiz, "Tunable 1.55–2.1 GHz 4-Pole elliptic bandpass filter with bandwidth control and >50 db rejection for wireless systems," *IEEE Trans. Microw. Theory Tech.*, vol. 61, no. 1, pp. 117-124, Jan. 2013.

CHAPTER 7

Conclusions and Future Work

7.1 Conclusions and Contributions

This dissertation focuses on two main types of filter designs: one is to realize miniaturized microstrip filter based on multilayer LCP technology and the other is to combine microstrip tunable bandpass filter with lossy technology to achieve multi-functions. For miniature filter part, the topic is to concentrate on the stopband rejection performance to suppress the harmonic standing wave by using the advantage of broadside couplings of multilayer LCP technology rather than focus on the passband performance. In terms of tunable bandpass lossy filter, the goal needs to be achieved is to control the bandwidth from narrow band to wide band at fixed centre frequency with a flat passband insertion loss and high selectivity at both sides of passband edges in the entire tuning range.

In detail, the major contributions of the research proposed in this dissertation are summarized as below:

In Chapter 2, a novel microwave bandpass filter using microstrip slow-wave open-loop resonators and multilayer LCP technology has been presented. The new filter has not only very compact size due to the slow-wave effect, but also exhibits a wider upper stopband resulting from the dispersion property. A five-pole microstrip filter of this type, i.e., a bandpass filter centred at f_c=1.18 GHz with -3dB fractional bandwidth of 17%, has been designed and fabricated. No spurious response, which are at least 30-dB rejection, occurs for the frequency up to 10 GHz. Moreover, the fabricated filter also has the compact size of $0.102\lambda_g \times 0.081\lambda_g$ (λ_g is the guided wavelength) and the light weight less than one gram by using multilayer LCP circuit technology. Good agreement can be observed between the simulation and measurement.

In Chapter 3, the design of microstrip lossy filters combining lossy synthesis and extracted-pole technique has been proposed. This type of proposed filter has both of high selectivity and flat passband not only in narrowband but also in wideband. The high selectivity is contributed by using extracted-pole technique and the flat passband is achieved by introducing RCCs in the inline network. Two six-pole filters has been fabricated and analysed to demonstrate the response performance in narrowband and wideband respectively. Good agreements between experimental and theoretical results have been achieved. This proposed filter also has a good upper stopband rejection. This kind of proposed lossy microstrip filter is promising to increase to high order and extend to the tunable filter. Based on this Chapter, the fix structure of microstrip bandpass lossy filters are extended to tunable filter.

In Chapter 4, a literature review of tunable/reconfigurable filter from tuning technologies, conventional tuning structures to recent related tunable works has been given. Different tuning technologies can be used to realize tunable filters, such as mechanically tunable filters, YIG filters, BST filters, RF MEMS switches filters, and Varactor-diode-based filters. Since tunable bandpass filter is the main topic in this thesis, conventional tuning resonator structures, like varactor-loaded $\lambda/4$ and $\lambda/2$ resonators and dual-mode resonators, have been described. Moreover, three classical types of tunable bandpass filter (controlling centre frequency, controlling bandwidth at fixed centre frequency and simultaneously controlling bandwidth and centre frequency) with a new type (controlling filter order) have been introduced in detail with typical research works comparisons. In the following chapters, based on this literature review, my own tunable filter works with lossy technology will be presented.

Based on the investigations in Chapter 3 and 4, my own research works on tunable bandpass lossy filter are described in Chapter 5 and 6. Chapter 5 focuses on symmetric varactor-tuned microstrip bandpass lossy filter, while Chapter 6 concentrates on asymmetric varactor-tuned microstrip bandpass lossy filter with extracted-pole technology.

In Chapter 5, firstly, a three-pole tunable bandpass lossy filter with resistor loading to control the bandwidth and selectively is presented. Although its fixed structure is a traditional 3-pole Chebyshev filter, its tunable structure with bias scheme still have two transmission zeros at each band edge, which is due to the tuning external coupling structure. Then to enhance the performance of this filter, its resonators are also extended to be tuned to achieve the goal of controlling the bandwidth at a fixed centre frequency. Finally, by combining the resistor loading and cross coupling, a new type of 5-pole tunable lossy filter is proposed with a flat passband and good improved selectivity, contributed by the cross coupling. Even though this structure is asymmetric, the tuning method is still symmetric.

In Chapter 6, asymmetric high order tunable bandpass lossy filters have been presented. This type of filter can control the bandwidth at fixed centre frequency with flat passband and high selectivity. The flat passband is contributed by combining resistor loadings and resistive cross couplings to introduce additional loss in the mid-band to make the insertion loss flat, while the high selectivity is achieved by tuning two extracted-poles to adjust the positions of the introduced two transmission zeros at each side of passband edges. Through the analysis of the equivalent circuit model and EM simulation model, this type of filter has been investigated step by step. In theory, this proposed tunable filter can be tuned from vary narrow band (4% 3dB FBW) to wide band (40%) at a fix centre frequency 1.8 GHz with a flatness passband and good skirt selectivity. However, due to the fabrication tolerance and too many used components, this fabricated filter can be reconfigured from 7% to 34% FBW operated at 1.35GHz. Even though the measurement results show an agreement with the simulation results, the flatness of the passband and the selectivity can still be improved which need to make further investigations.

7.2 Future Work

The following are suggestions to expand upon the research presented in this dissertation:

1. The miniature slow-wave open-loop resonator presented in Chapter 2 can be further investigated to improve the passband performance and is promising to extend to tunable bandpass filter with controlling the centre frequency due to the fix couplings.

2. The fix microstrip lossy bandpass filter with extracted-pole technology proposed in Chapter 3 can be realized to use multilayer LCP technology to find a another way to improve selectivity instead of using extracted-pole technology, like cross couplings, which can make the physical size compact and improve the performance.

3. For the tunable bandpass lossy filter in Chapter 5 and 6, a better fix filter structure needs to be found to break current limitations of tunable bandpass filter by combining the lossy technology. It should be possible to merge these two technologies, not a way to regard them as two separated technology. Because that the development of tunable filter is quiet limited by the packaging technology of tuning elements.